Geochemical evidence for weathering in northwestern European loess on a sub-millennial scale during the last Ice Age

By

Terence Charles Hill

A thesis submitted to the University of Gloucestershire in accordance with the requirements of the degree of Doctor of Philosophy in the Faculty of Environment and Leisure

University of Gloucestershire

May 2005

ABSTRACT

This study seeks to determine the extent to which chemostratigraphy can supplement other stratigraphic tools in determining the effects of climate change in loess-palaeosol sequences. Geochemical change has been used to illuminate the effects of glacial/interglacial climate change in Chinese loess-palaeosol sequences; less work has been done to examine the effects of stadial/interstadial climate change and little work has been carried out in Europe on either aspect.

Two loess-palaeosol sites were selected in northwestern Europe that were known to provide good records of the last ice age. This study has produced detailed descriptions of variation in concentrations of the major, minor and rare-earth elements. These are compared with variation in the standard sedimentological parameters (grain size, organic carbon content and carbonate content) and in enviromagnetic characteristics, which are accepted as palaeoclimate proxies. The existing polymineral-based luminescence chronology at each site has been enhanced using a quartz-based approach, which broadly confirms the accuracy of previous ages and generates estimates of increased precision.

That chronology facilitates comparison of these analyses with evidence for palaeoclimatic change in the wider record, including GRIP ice-core data. Grain size is shown to be a strong proxy for variation in mean wind strength and in accumulation rates which can be correlated in detail with GRIP.

The study has established that geochemical heterogeneity now apparent at the sites has been imposed by weathering. Carbonate weathering is a reliable indication of major pedogenic episodes but its detailed interpretation is tempered by carbonate mobility. Silicate weathering occurs at lower intensity than carbonate weathering but is a permanent record since silicates are not subject to reprecipitation under these conditions. The study concludes that chemostratigraphy is a climatological proxy, detecting periods of significant amelioration. It is not a replacement for conventional proxies, it complements them and provides additional evidence upon which climatic reconstructions can be made.

I declare that the work in this thesis was carried out in accordance with the regulations of the University of Gloucestershire and is original except where indicated by specific reference in the text. No part of the thesis has been submitted as part of any other academic award. The thesis has not been presented to any other education institution in the United Kingdom or overseas.

Any views expressed in the thesis are those of the author and in no way represent those of the University

Signed ..... Date 21-3-06

'the more that I have studied the subject [Rhine loess], the more difficult I have found it to form a satisfactory theory.' (Lyell, 1834)

LIST OF CONTENTS

FIGURES

LIST OF TABLES

List of abbreviations and symbols

AMS	Accelerator mass spectrometry
ARM	Anhysteric remanent magnetism
BP	before present
c.	circa
c.c.	correlation coefficient
CIA	Chemical Index of Alteration
CCRMP	Canadian Certified Reference Materials Project
cm	centimetre
CRPG	Centre de Recherches Petrographique et Geochimiques
D_e	equivalent dose
D-O	Dansgaard-Oeschger
d.u.	dimensionless unit
g	gramme
GI	Greenland Interstadial
GSJ	Geological Survey of Japan
GRIP	Greenland Ice Core Project
Gy	gray
HIRM	Hysteresis Induced Remanent Magnetism
HREE	heavy REE
ICP-OES	Inductively-Coupled Plasma Optical Emission Spectroscope
INQUA	International Union for Quaternary Research
IRM	Induced Remanent Magnetism
IRSL	Infra-Red Stimulated Luminescence
k	Kelvin
ka	thousand years
K_{lf} and K_{hf}	volume-specific low- and high frequency magnetic susceptibility
km	kilometre
LGM	Last Glacial Maximum
LREE	light REE
LOI	loss-on-ignition
m	metre
M	molar solution
Ma	million years
MD	multidomain

MIS	Marine Isotope Stages
ml	millilitre
mm	millimeter
MS	magnetic susceptibility
$mWcm^{-2}$	milliwatts per square cm
nm	nanometre
NGRIP	North Greenland Ice Core Project core
org. C	organic carbon
OSL	optically stimulated luminescence
ppm	parts per million
PSD	pseudo-single-domain
REE	rare-earth elements
s	second
SABS	South African Bureau of Standards
SD	stable single domain
SIRM	Saturation Induced Remanent Magnetism
SMOW	Standard Mean Ocean Water
SP	superparamagnetic
TL	thermoluminescence
USGS	United States Geological Service
UCC	upper continental crust
%RSD	percentage relative standard deviation

μm	micrometre
χ	mass-specific magnetic susceptibility
χ_{ARM}	susceptibility of Anhysteric Remanent Magnetism
χ_{fd}	mass-specific, frequency-dependent magnetic susceptibility
χ_{lf} and χ_{hf}	mass-specific low- and high frequency magnetic susceptibility

Acknowledgements

I am indebted to many people who have helped in the preparation of this thesis, and the research work that has preceded it. Special thanks are due to my supervisors Dr Phil Toms, Dr John Hunt and Dr Mike Fowler for their patience, help, advice and support, and to Prof. Hugh Rollinson and Dr Manfred Frechen for their work as supervisors during the early stages of this project.

Fieldwork at Harmignies was significantly enhanced by the presence of Dr Brigitte van Vliet-Lanoë (University of Lille). Research papers that would otherwise been inaccessible were provided by Dr Manfred Frechen, Prof. Wolfgang Schirmer (Heinrich Heine University, Düsseldorf), Dr. Etienne Juvigné (Université de Liège) and Prof. Jean-Pierre Lautridou (Centre de Géomophologie du C.N.R.S, Caen). Invaluable laboratory support, advice and training was also given by Dr Ian Foster (Coventry University) and Dr Sarah James (Royal Holloway, University of London).

Diagram preparation by Trudi James and laboratory assistance by Paul Kimber, Julia Newbury and Alison Bennett has been invaluable, and encouragement from fellow post-graduates and friends – too many to name – has helped me to stay focussed and motivated.

I am grateful to Mr Alain Canivet at Crayeres, Cimenterie et Fours a Chaux d'Harmignies for permission to work in Harmignies quarry, to Professor W. Boenigk, Head of the Geological Institute, University of Cologne, for permission to work on the nationally-protected Koblenz-Metternich site and to the Flöch family for their hospitality and permission to dig up their garden. Generous funding for a field trip was provided by the Quaternary Research Association.

Above all, thanks are due to Chris, my wife, for her unfailing belief in me throughout these seven years of BSc and PhD studies.

Thank you, all.

Chapter 1: Quaternary climate change and this study

1.1 The study of Quaternary climate change

1.1.1 The climate system

The Earth's climate system is intimately connected with everything that happens on the Earth's surface from the highest levels of the atmosphere to the ocean depths; it maintains and is modified by life and in the very long term it affects even the formation and composition of land masses. The system appears to operate in a series of quasi-stable states, which are acted on by a multitude of forcing factors. External forcing factors involve agents acting outside the climate system, such as astronomical and geological change. These generally operate on timescales which can extend to tens of millions of years. Internal forcing mechanisms, such as changes in atmospheric and oceanic circulation patterns, are generated within the climate system but can be driven by external forcing agents. They can respond rapidly to change and operate on shorter timescales.

This inherent complexity and interdependency makes the climate system highly sensitive to minor changes in initial conditions (the 'butterfly effect' (Lorenz, 1972)). This generates a substantial degree of random behaviour which accounts for much of the short-term climate variation and may be responsible for aspects of climate change by amplifying weak but cyclic forcing mechanisms through stochastic resonance (Alley *et al.*, 2001). One consequence of this randomness is that a large proportion of shorter-term climate variation cannot be predicted, another is that the longer-term climate record contains background 'noise' caused by that short-term variation (Lorenz, 1991).

1.1.2 Tertiary and Quaternary climate change

The Earth has undergone long-term, major cooling since the late Tertiary, amounting to a global temperature reduction of approximately 20°C (Fig. 1.1). The causes are unclear but are likely to be 'external forcing factors' that may include the raising of the Rocky Mountains, the Himalayas and the Tibetan Plateau by plate tectonics (Ruddiman and Kutzbach, 1991; Raymo and Ruddiman, 1992), the presence of continents at or close to the poles (Barron, 1985), the closure of seaways (Beaty, 1978) and the long-term reduction in atmospheric CO_2 caused by the chemical weathering of silicate rocks (Raymo *et al.*, 1988; Raymo, 1991).

Glaciation began on Antarctica *c.* 34 Ma (e.g. Zachos *et al.*, 2001) and by *c.* 15 Ma large ice sheets were being formed there (Shackleton and Kennet, 1975), with rapid changes occurring in sea levels (Haq *et al.*, 1987).

Figure 1.1 Global temperature since the early Tertiary (after Zachos *et al.*, 2001).

Glaciation in the Northern Hemisphere started between 10 and 6 Ma (e.g. Wolf-Welling *et al.*, 1995). Continued long-term cooling led to the Late Miocene glaciation of Greenland and the Arctic, with major increases in global ice volume occurring *c.* 2.5 Ma (Maslin *et al.*, 1998). Between then and 1.5 Ma ice ages recurred with a periodicity *c.* 40 ka but around 750 ka the periodicity changed to *c.* 100 ka, accompanied by an increase in the indicated glacial/interglacial temperature range (Hays *et al.*, 1976, Lisiecki and Raymo, 2005) (Fig. 1.2)

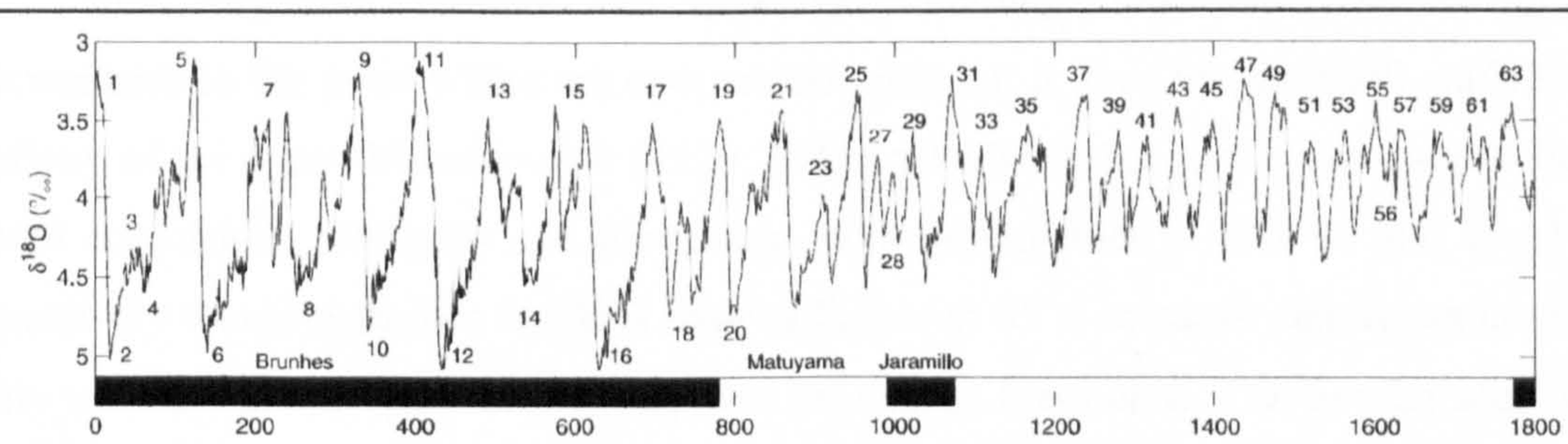

Figure 1.2 Glacial (odd-numbered) and interglacial (even-numbered) periods for the last 1800 ka (identified by $\delta^{18}O$ variation in marine cores), showing the change in cycle periodicity. The plot also shows the Brunhes and Jamarillo periods of 'normal' magnetic polarity and the Matuyama period of reversed magnetic polarity (from Lisiecki and Raymo, 2005) .

Mudelsee and Stattegger (1997) and Paillard (1998) suggest that at this time, the Earth's climate changed from a 'two-state solution' ('interglacial' and 'moderate glacial'

conditions) to a 'three-state solution' (interglacial, moderate glacial and maximum glacial conditions) (Fig. 1.3), and moved into a phase of stronger and longer cyclicity.

These recent ice ages have all featured a rapid cooling phase to full glacial conditions, followed by a period of alternating warm and cold phases with a general trend towards progressively more intense cooling which culminates in a glacial maximum period with extremely large Northern Hemisphere continental ice caps and major reductions in sea levels. At the Last Glacial Maximum (LGM) one third of the Earth's land surface was covered by ice (Williams *et al.*, 1993) and half the area of the world's ocean was covered in icebergs and pack ice (Erickson, 1990). Each glacial maximum has been followed by very rapid warming and disintegration of the ice sheets, these terminations marking the commencement of a relatively brief interglacial period (Fig. 1.3).

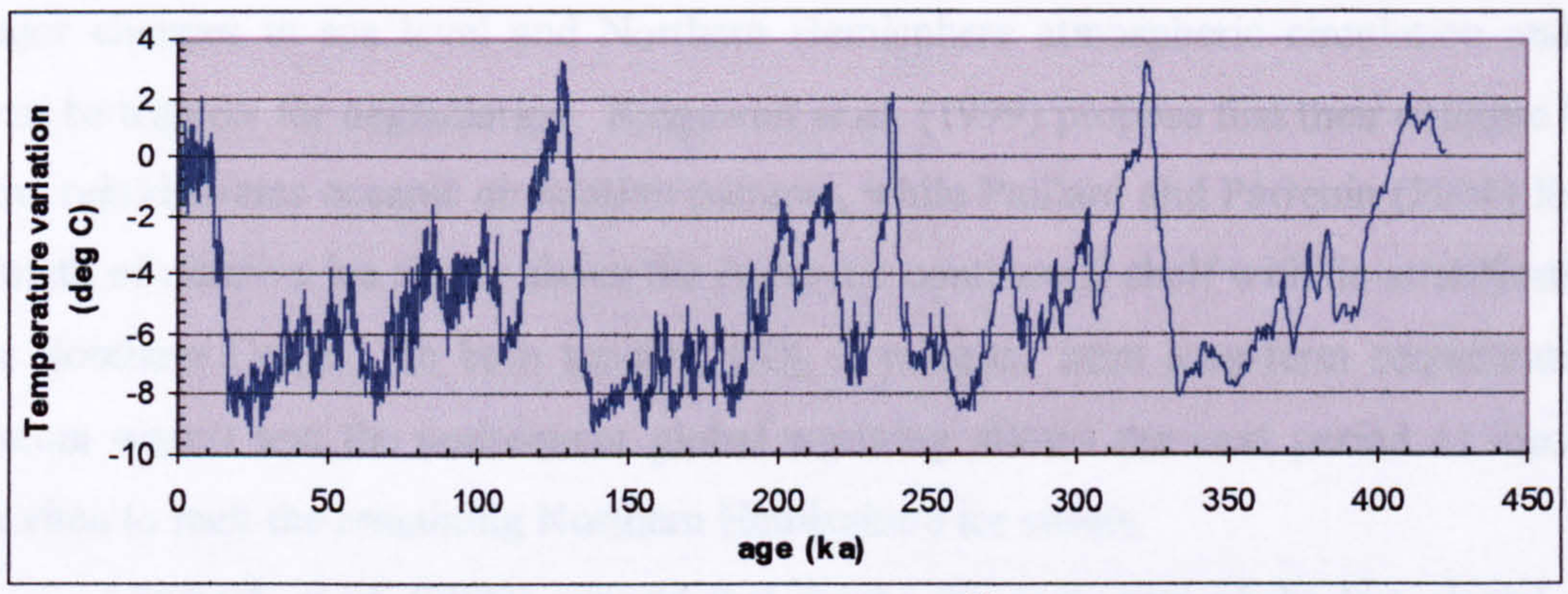

Figure 1.3 Temperature variation over the last 420 ka, from $\delta^{18}O$ variation in the Vostok ice core (Petit *et al*, 1999). This shows the brief nature of interglacials, compared to glacial periods. Each glacial period proceeds as a series of successively-colder episodes, culminating in a glacial maximum which is followed by rapid warming into the next interglacial period.

1.1.3 Astronomical climate forcing

The long-term Tertiary and Quaternary cooling may have lowered global temperatures to the point where ice ages are possible but it does not, in itself, explain the cyclicity of ice ages. Milankovitch (1920, 1941) calculated that cyclic variation in Earth orbital eccentricity, obliquity and precession, with periodicities *c.* 100, 41 and 19-23 ka respectively would modulate incident solar radiation at 65°N to cause significant cooling, likely to cause an ice age. This theory was proved by Hays *et al.* (1976) who identified these periodicities in marine cores; they are now accepted to be the pacemakers for ice ages. Imbrie (1982) suggests that summer insolation at 65°N is the key factor controlling glacial climate: strong insolation maxima limit ice build-up, weak insolation maxima allow massive Northern Hemisphere ice sheets to form.

These periodicities are a constant factor in the Earth's orbit; they have subsequently been identified in a range of records, extending to the Jurassic (albeit tempered by a lack of chronological control) (Hinnov and Park, 1999).

1.1.4 Internal climate forcing

The physical mechanisms that convert minor, orbitally-induced variation in incident radiation into major climatic changes remain unclear (Paillard and Parrenin, 2004). They are likely to include albedo variations caused by cloud, snow and airborne dust, changes in the atmospheric content of the greenhouse gases CO_2 and CH_4, and changes in the ocean-atmosphere circulation system. The ice sheets that initially develop in response to insolation changes cause regional adjustments in albedo and radiation balance, and become responsive to internal forcing factors (Clark *et al.*, 1999). They cause major changes in sea level and Northern Hemisphere atmospheric circulation and may even be triggers for deglaciation. Ridgewell *et al.* (1999) propose that their collapse by ice flow reinvigorates oceanic circulation patterns, while Paillard and Parrenin (2004) link the growth of massive ice sheets above the Antarctic continental shelf with de-stratification of the Southern Ocean. In both models, CO_2 is released from long-term sequestration in bottom waters and the consequent global warming allows the next period of insolation maxima to melt the remaining Northern Hemisphere ice sheets.

Lambeck *et al.* (2002) suggest that during the early part of the last glacial cycle, astronomically-forced insolation changes drove the system but climate-driven feedback mechanisms became increasingly important until the climate system became unstable and responded to the interplay between these different factors with relatively high-frequency change. Greenland ice cores show that the local climate, particularly during MIS 3 and 4, was characterised by an alternation of cold and warmer periods (stadials/interstadials), termed Dansgaard-Oeschger (D-O) cycles (Dansgaard *et al.*, 1993). Local temperatures rose by 5-10°C within a few years or decades, followed by much longer cooling phases that lasted up to 3000 years and culminated in a return to full glacial conditions (*ibid*, Johnsen *et al.*, 1995). This is shown in Fig. 1.4, together with the Greenland Interstadial (GI) numbering scheme.

Alley *et al.* (2001) suggest that the 'preferred spacing' of 1500 years shown by D-O cycles (for some, 3000 or 4500 years) may be due to the effects of stochastic resonance in conjunction with a weak forcing factor, possibly a 1500-year weak solar cycle. This same cyclicity is present in the Holocene (Campbell *et al.*, 1998; Bond *et al.*, 2001) and in earlier glacial and interglacial stages (Oppo *et al.*, 1998); it may be a fundamental climate feature (Bond *et al.*, 2001).

D-O cycles are attributed to variations in the vigour of the North Atlantic thermohaline circulation which illustrate the climatic sensitivity of the ocean/ice/atmosphere system and its rapid response to perturbations. Under moderate ice age conditions (i.e. interstadials), the North Atlantic thermohaline circulation system delivered warm water northwards in surface currents and removed dense, cold and highly saline water southwards by deep water formation. The atmospheric humidity that accompanies relatively warm water led to rapid growth of the Laurentian and Fennoscandian ice sheets, which resulted in a general trend towards cooling, increased aridity and sea level fall (e.g. Broecker *et al.*, 1990; Stocker *et al.*, 1992). Periodically, at *c.* 1000 to 1500-year intervals, these ice sheets released pulses of meltwater and icebergs into the North Atlantic. This reduced the strength of the thermohaline system. Circulation slowed and for a period of time, the normal flow of warm water northwards was diverted westwards, causing further cooling in the northern areas (i.e. stadials). After the freshwater influx ceased, the thermohaline system was able to return to its northern circulation pattern, the North Atlantic regions warmed rapidly and the ice sheets began to grow again (Broecker *et al.*, 1990; Stocker *et al.*, 1992). The release of icebergs during part of the D-O cycle did not significantly reduce the size of ice sheets; the net effect was continued growth.

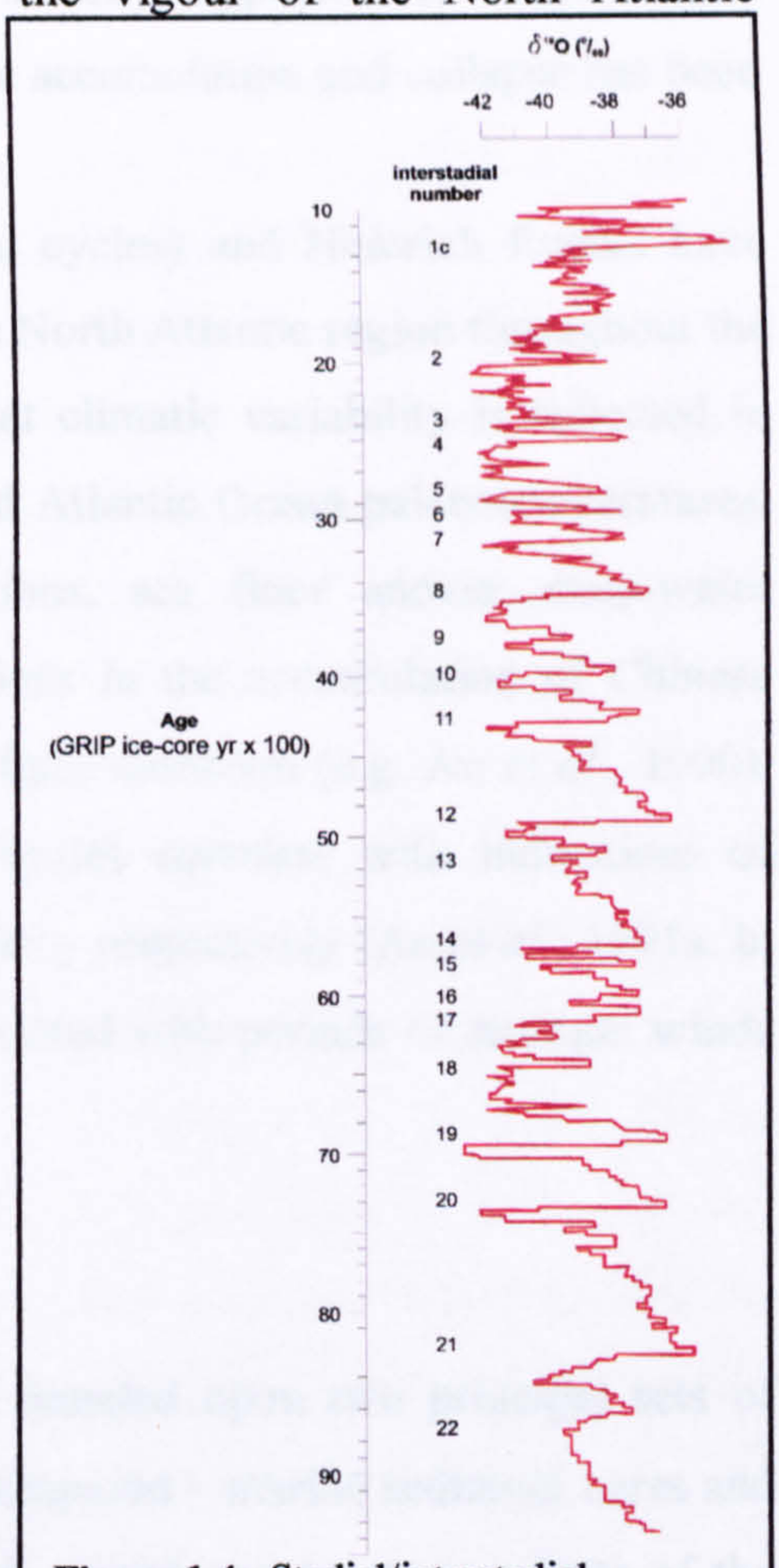

Figure 1.4 Stadial/interstadial alternation over the last 90 ka, plus interstadial identification numbers (after Bond *et al.*, 1993).

Groups of progressively-cooler D-O cycles led to the formation of massive, unstable ice sheets which periodically underwent major collapse. They discharged armadas of icebergs into the North Atlantic, releasing large volumes of fresh water and detrital carbonate rock particles carried in the ice (the marine sediment 'signature' of Heinrich Events (Heinrich, 1988)). That massive freshwater cap brought the North Atlantic circulation system to a halt, causing intense cooling in the North Atlantic region (Broecker, 1994) while the central Atlantic and South Atlantic Ocean grew warmer (Vidal *et al.*, 1999). Eventually ice sheet collapse ceased, the meltwater cap became homogenised, the thermohaline system returned to its previous state, stored-up warm water was moved northwards and the North Atlantic region warmed by as much as 10°C in a few

years (Broecker, 1994). The accompanying rise in humidity supported renewed ice sheet growth and the cycle restarted (*ibid.*). This cycle of ice accumulation and collapse has been termed 'binge-purge' (Alley and MacAyeal, 1994).

Together, D-O cycles (i.e. stadial/interstadial cycles) and Heinrich Events have been the dominant signal of climatic variability in the North Atlantic region throughout the last ice age (Lueschner and Sirocko, 2000), and that climatic variability is reflected in world-wide records (*ibid.*). These include Pacific and Atlantic Ocean palaeotemperatures, rates of glacier growth, lake sediment compositions, sea floor anoxia, deep-water ventilation, and the Arabian Sea monsoon. Variations in the accumulation of Chinese loess are related to the strength of the East Asian winter monsoon (e.g. An *et al.*, 1990). Within that overall variability, stadial/interstadial cycles correlate with indications of stronger/weaker winds and decreased/increased humidity respectively (An *et al.*, 1991a, b; Chen *et al.*, 1996). Heinrich events have been correlated with periods of stronger winds and increased aridity (Porter and An, 1995);

1.2 The Nature of the Evidence

The study of Quaternary climate change is founded upon two principal sets of evidence, against which other lines of evidence are compared – marine sediment cores and ice cores. These contain a range of variables which record one or more aspects of the climate system.

1.2.1 Marine cores

Marine sediment cores can contain a wide range of variables that can be interpreted as climate proxies. A major line of research has focussed on carbonate foraminifera shells which record the isotopic composition of the seawater-derived oxygen used to build their shells (Emiliani, 1954). Seawater contains both ^{16}O and ^{18}O but (a) temperature, and (b) variation in the amount of polar ice modulate the $^{18}O/^{16}O$ ratio (conventionally expressed as $\delta^{18}O$) in the preserved foraminifera fossil shells. Analysis of selected foraminifera species (selected to reduce the temperature effect) is measured relative to an accurately-known standard termed 'Standard Mean Ocean Water' (SMOW) (Coplen, 1996). The $\delta^{18}O$ record in marine cores is, therefore, a proxy record of global ice volume and of the glacial cycle (Shackleton, 1967).

The succession of relatively warm and relatively cold periods indicated by changes in this $\delta^{18}O$ value were numbered by Emiliani (1955) as Marine Isotope Stages (MIS), starting at 1 for the current interglacial (Fig. 1.4).

Other marine core information comes from the analysis of floral and faunal abundances, the changing proportions of species sensitive to specific conditions and morphological change (e.g. temperature-controlled left/right-handed spiral forms). These provide information on palaeoconditions such as surface-water and deep-water temperatures, salinity, oceanic stratification, dissolved oxygen content and nutrient availability. The sediment also records non-biological signals such as atmospheric dust content, changes in the type and amount of terrestrial debris delivered by rivers or icebergs and the orientation of the earth's palaeomagnetic field (e.g. Farrell *et al*, 1995; Harris and Mix, 1999).

These cores can extend back for millions of years (e.g. Jansen *et al.*, 1988). However, direct dating control is problematic since cores contain insufficient material suitable in mass or age for the application of any single geochronometric method. Chronologies can be constructed indirectly by assuming that there is a direct and unvarying relationship between the orbital parameters and the $\delta^{18}O$ record, and then using those orbital parameters to adjust the $\delta^{18}O$ chronology in a process known as 'orbital tuning' (Imbrie *et al.*, 1984). Marine core chronologies can also be crosschecked against the climate signal preserved in ice cores (see below) and events such as the Brunhes/Matuyama magnetic reversal *c.* 778 ka (Tauxe *et al.*, 1996) (Fig. 1.2).

1.2.2 Ice cores

Ice cores are unique archives of information on past climates and the mechanisms of glaciation. They can contain proxy information on palaeotemperatures and precipitation rates, and aerosol fluxes of marine, volcanic, terrestrial, cosmogenic and anthropogenic origin; trapped air bubbles provide direct records of the earth's atmosphere (Petit *et al*, 1999: McManus, 2004).

Since ice layers accumulate at much higher rates than marine sediments, ice cores have finer resolution, although they cannot provide the extreme long-term coverage that marine cores can achieve. Chronologies of deposition are achieved through a range of methods such as counting visible annual ice layers and using very-high-precision techniques to measure, for example, the seasonal enrichment of snow in sodium ions. This can provide better than annual resolution, potentially extending back to 100 ka (e.g. Hammer *et al.*, 1978, 1985; Röthlisberger *et al.*, 2000).

Snow has a temperature-modulated $^{16}O/^{18}O$ content, with colder temperatures leading to more negative $\delta^{18}O$ values (relative to SMOW) (Grootes *et al*, 1993; Dansgaard *et al*, 1993). Under suitable conditions, snow accumulations are converted to ice, which can preserve this $\delta^{18}O$ record and so down-core variation can be used as a proxy for

relative change in surface temperature when the snow fell (Dansgaard *et al.*, 1973). The Greenland Ice Core Project (GRIP) core has provided a record of the last 250 ka (Dansgaard *et al.*, 1993) (the last 110 ka are shown in Fig. 1.5), reinforced by the 123 ka record of the North Greenland Ice Core Project core (NGRIP members, 2004). The GRIP ice core record has been accepted by the Palaeoclimate Commission of the International Union for Quaternary Research (INQUA) as an arbitrary but consistent standard for climate change studies (Lowe, 2001).

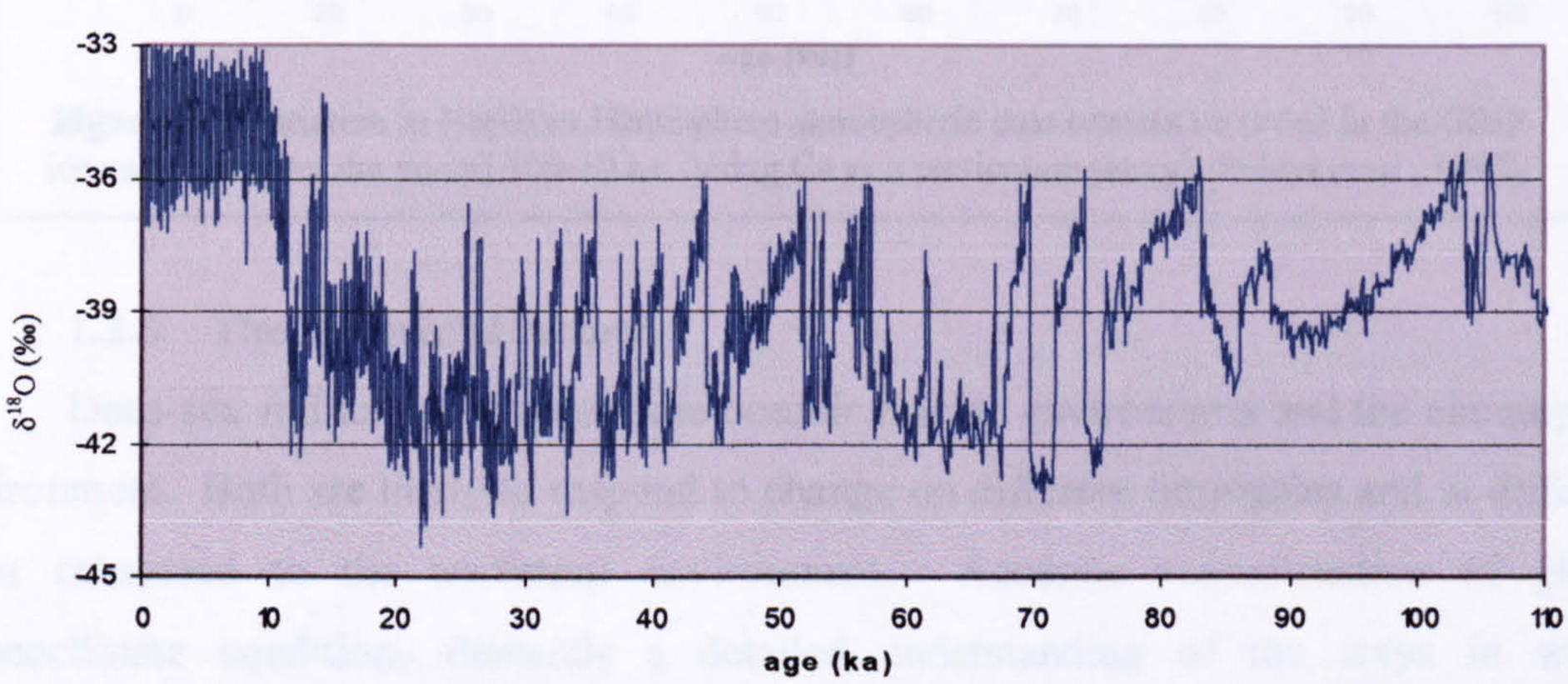

Figure 1.5 High-amplitude and rapid climatic variation over the last 110 ka recorded in the GRIP ice core (using $\delta^{18}O$ as a climatic proxy) (Dansgaard *et al.* (1993).

The presence in the core of very fine mineral dust particles, transported long distances by high-altitude winds is particularly relevant to this study. Variations in particulate concentration (Fig. 1.6) reflect variations in the vigour of the atmospheric system and the availability of fine sediment, and correlate with the $\delta^{18}O$ record of temperature change (Fig. 1.5): atmospheric dust loading was greatest during glacial periods, and within that, was greatest during stadials. Low atmospheric dust concentrations occur during interglacial and interstadial periods (e.g. Thompson and Mosley-Thompson, 1981; Petit *et al.*, 1981; Petit, 1990; Fuhrer *et al.*, 1993). Loess is deposited most rapidly during stadials (e.g. Frechen *et al.*, 2003) which correlates with that increased atmospheric dust loading. In consequence, dust in Greenland ice cores and loess deposition are expressions of the same climatic conditions.

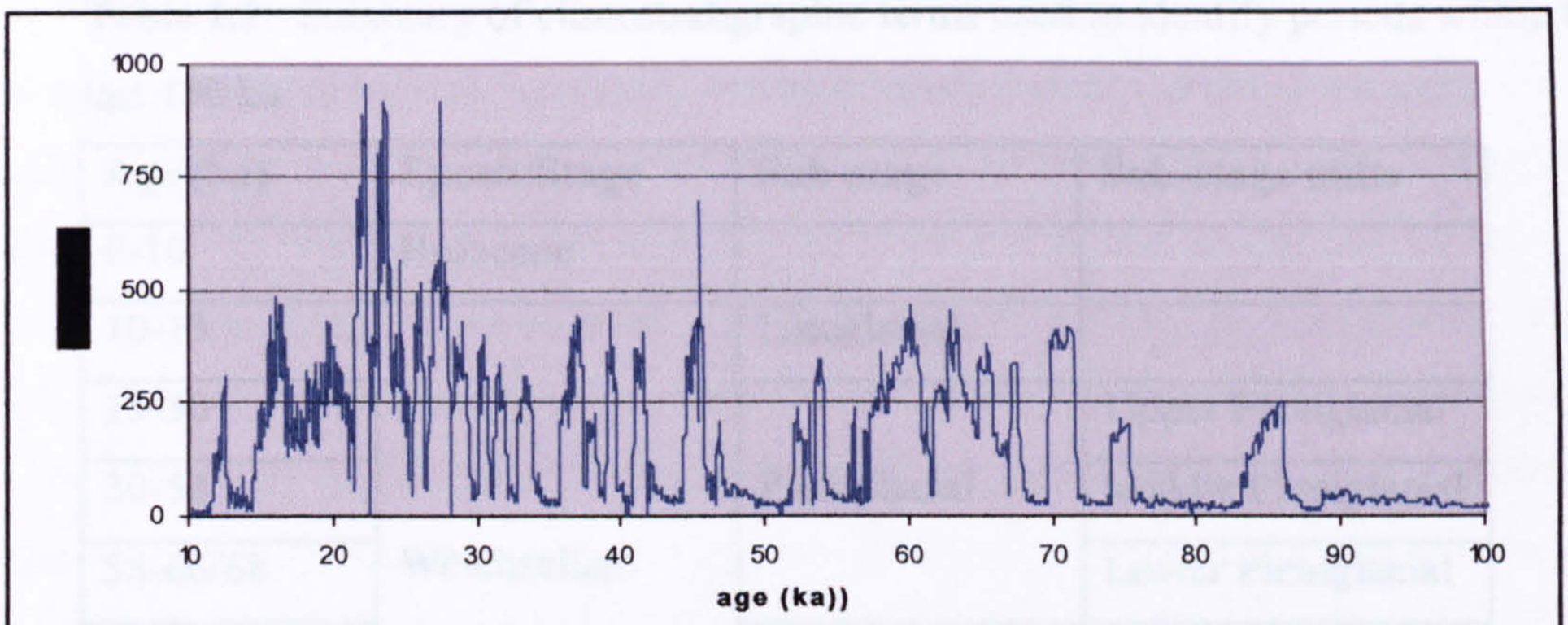

Figure 1.6 Variation in Northern Hemisphere atmospheric dust content recorded in the GRIP ice core, covering the period 100-10 ka, (using Ca as a particulate proxy) (Fuhrer *et al.*, 1993).

1.2.3 The terrestrial record

Deep-sea and ice cores record the oceanic marine environment and the circumpolar environment. Both are likely to respond to change on different timescales and in different ways compared to the terrestrial environment. Accurate reconstruction of global palaeoclimate conditions demands a detailed understanding of the ways in which continental climates have changed, and this has to be accurately correlated with the polar and oceanic record to understand how these different components of the world climate system interact. However, there are few high-resolution, long, and continuous records of terrestrial climates since land surfaces are primarily zones of erosion and most terrestrial depositional zones are relatively temporary (e.g. lakes, peat bogs etc.). Loess-palaeosol sequences have been proved to be a paramount record of terrestrial climate. They have become the subject of intense research, focussed mainly on the Chinese loess record which extends back at least 2.5 million years (Rutter *et al.*, 1991, Ding *et al.*, 1993) and which has been compared in quality to the marine core record (Kukla, 1987, Kemp and Derbyshire, 1998, Derbyshire *et al.*, 1997).

1.2.4 The terminology and timescale of the last interglacial/glacial cycle

In western Europe, the last interglacial (defined by the presence of tree pollen; van Kolfschoten and Gibbard, 2000) has been assigned the stage name 'Eemian' (Van der Vlerk and Florschütz, 1950); the last glacial period is the 'Weichselian' (Woldstedt, 1950). The Weichselian is divided into Early Glacial, Pleniglacial and Lateglacial stages. The Pleniglacial is further subdivided into the Lower, Middle and Upper Pleniglacial (Table 1.1). The Weichselian is followed by the Holocene Epoch, starting at 10,000 radiocarbon years BP (Mangerud *et al*, 1974).

Table 1.1. Summary of climostratigraphic terms used to identify periods within the last 130 ka.

Age (ka)	Epoch/Stage	Sub-stage	Sub-stage units
0-10	Holocene		
10-13	Weichselian	Lateglacial	
13-30		Pleniglacial	Upper Pleniglacial
30-58			Middle Pleniglacial
58-66/68			Lower Pleniglacial
66/68-107		Early Glacial	
107-130	Eemian		

Antoine *et al.* (2003) propose that the Early Glacial/Pleniglacial boundary should be placed at 68-66 ka and the Middle/Upper Pleniglacial should be at 30 ka (used in Table 1.1). The start of the Upper Pleniglacial was marked by the very rapid growth of major ice sheets (Lambeck *et al.*, 2000, Yokoyama *et al.*, 2000). It continued through the LGM (*c.* 22-19 ka (Yokoyama *et al.*, 2000)) until *c.* 13 ka. The Lateglacial period contains the final stages of deglaciation.

The Eemian, Weichselian and Holocene stages/Epoch fall within the MIS 5 to MIS 1 group. Shackleton (1969) and Imbrie *et al.* (1984) subdivided MIS 5 into the series 5e-5a, with the interglacial period MIS 5e occurring between 130-117 ka. However, the timings and durations of western European climate states differ from the MIS chronology: pollen data show that in southwestern Europe the Eemian lasted until 107 ka, when deciduous forests were abruptly replaced by steppe vegetation (Kukla, 2000; Sánchez-Goñi *et al.*, 2000). MIS 5d to 5a equate to the early Weichselian. The Weichselian period is covered by MIS 4 (75-59 ka), 3 (59-25 ka) and 2 (24-10 ka) (chronology from Imbrie *et al.*, 1984). MIS 1 equates to the Holocene.

1.3 Is the past the key to the future?

The rise of modern man and our technological civilisation has occurred entirely within the current interglacial, yet the projected duration of this warm period is unclear. Loutre and Berger (2003) use predicted insolation variations to suggest that for the next 60 ka, a glacial period is unlikely but Ruddiman *et al.* (2005) and Ruddiman (2005) suggest that pre-industrial anthropogenic production of CO_2 and CH_4, occurring over the last several thousand years, has prevented global temperatures falling. They predict that without this factor, the Earth would now be 2°C cooler, about one third of the way to full glacial conditions, and that the next glaciation is, therefore, overdue.

However, the modern intensive use of fossil fuels has raised the atmospheric CO_2 concentration beyond any value naturally reached during the last 400 ka (Petit *et al.*, 1999) and after a millennium in which the global average temperature fell slowly, it has risen rapidly in the last 100 years and is now higher than at any time in the last 1000 years (Crowley, 2000). In the world of minor insolation change proposed by Loutre and Berger (2000), greenhouse gas concentrations may play a very important role in climate change, and the International Climate Change Taskforce (2005) considers that continued greenhouse gas emission may trigger rapid and potentially catastrophic climate change within a decade.

Some of the climate system linkages are obvious, and some are very poorly understood, with the result that current climate change predictions are very imprecise: however, predictions that are accepted to be reliable and accurate are essential if we are to obtain widespread agreement on the extent of any necessary adjustments (e.g. management of fossil fuel usage and of CO_2 production) and the methodologies for implementing them. Mayewski and Bender (1995), speaking for the American Geophysical Union, consider that 'understanding the Earth system and, in particular, its climate, remains one of the major intellectual challenges faced by science. The processes influencing climate, the mechanisms through which they act, and the responses they generate are, in general, as complex and poorly understood as they are important'. Drummond *et al.* (1995) propose that 'a fundamental goal of earth science is to develop a more complete understanding of mechanisms and rates of climate change so that credible estimates of past global conditions can be constructed'.

Loess-palaeosol sequences can provide an extremely wide range of palaeoclimatic data, which has its highest resolution when glacial climates are most severe. That climatic information must be established in a reliable chronostratigraphic framework that will allow different types of record to be correlated accurately across different environmental zones. This will support that aim of constructing 'credible estimates of past global conditions'.

1.4 The aims and objectives of this study

Geochemical analysis has proved to be of major value in examining the effects of climate change in the Chinese loess province. It has shown how the composition of loess is affected by weathering and has helped to illuminate long-term variability in the Asian monsoon and the variable strength of the monsoon system in different regions of China (e.g. Yang *et al.*, 2004). It has been less strongly applied to European loess-palaeosol sequences; Juvigné and Moors (1995) pointed to a dearth of research into the composition of western European loess.

This study seeks to evaluate the potential use of geochemical variation as a loess-palaeosol stratigraphic tool within the last ice age. It examines variation in geochemical composition that may have been caused by post-depositional processes, notably element mobilization linked to weathering. Standard sedimentological and enviromagnetic methodologies are known to be valid indicators of millennial-scale climate change in loess-palaeosol sequences, including weathering, and the study examines the degree to which geochemical alteration can be correlated with the climate change signals contained in those other parameters. The existing luminescence chronology is enhanced through the application of new techniques that may provide increased accuracy.

The study examines two locations selected from the wide range of potential Weichselian loess-palaeosol study sites across western Europe: Harmignies (southern Belgium) and Koblenz-Metternich (Germany, close to the Rhine valley). These were never glaciated and were on the southern margin of the continuous permafrost zone during the coldest stages of the Weichselian. They have been examined by other researchers (e.g. Frechen *et al.*, 1995, 2001; Boenigk and Frechen, 2001) who consider that they both contain good histories of Weichselian loess deposition. The presence of ice segregation features in some horizons at Harmignies suggests periods of significant humidity (van Vliet, 1975) while Metternich lacks such features and appears to have been drier. This may contrast an 'Atlantic maritime' climate with one showing increased continentality and these climatic differences may manifest themselves in variations in the degree of geochemical weathering at the two sites.

The study's aim is to determine the extent to which chemostratigraphy can supplement other stratigraphic tools in determining the effects of climate change in loess-palaeosol sequences. This is examined through the consideration of five hypotheses:

a) that heterogeneity in geochemical, sedimentological and enviromagnetic parameters in the vertical profile at both sites has been imposed on originally-homogeneous compositions,
b) that patterns of heterogeneity correlate,
c) that these correlated patterns represent the sites' response to climate change,
d) that these local responses to climate change can be correlated with the known patterns and chronology of Weichselian climate change in the western Europe/N. Atlantic region, and,
e) that geochemical variation in loess-palaeosol sequences can be used as a chemostratigraphic tool in north-west Europe.

These hypotheses are examined through the following objectives:

a) for each site, the production of detailed descriptions of major, minor and rare-earth element concentrations,
b) for each site, the production of detailed descriptions of standard sedimentological parameters (grain size, organic carbon content, $CaCO_3$ content) and mineral magnetic properties,
c) determination of the extent to which variations in these geochemical and sedimentological parameters reflect homogeneity in the original sediment and heterogeneity imposed by climatic and other aspects of change,
d) the application of new luminescence dating methodologies to enhance the rigour of the established chronology at each site, thus increasing confidence in correlations between loess-palaeosol sites and to other records of climate change, and,
e) the comparison of the geochemical evidence for palaeoclimatic change shown in these techniques with the wider palaeoclimate record.

1.5 Thesis structure

This thesis is presented in eight chapters. This chapter has introduced the subject, defined the study's aim and outlined the approached used to reach that aim. Chapter 2 defines loess and describes its distribution world-wide. Chapter 3 describes the relationship of loess and palaeoclimate, and details the climate-induced loess characteristics to be addressed in this study. Chapter 4 explains the ways in which loess has been deposited in two areas of northwestern Europe and describes the study sites in each of those areas. Chapter 5 defines the sample collection methodology and the laboratory techniques used to examine the samples. Chapter 6 presents the analytical results for each technique and offers critiques of some methods and techniques based on the results and the experience gained in obtaining them. Chapter 7 interprets the results, synthesises them to determine how each site responded to climate change and compares those responses. Chapter 8 compares these findings with the northern hemisphere record, draws conclusions about the extent to which chemostratigraphy can supplement other stratigraphic tools to determine the effects of climate change in loess-palaeosol sequences and offers suggestions for further research work.

Chapter 2: Loess and its distribution

2.1 Loess and its history

Loess is an extremely widespread terrestrial sediment; it covers up to 10% of the world's land surface area (Pécsi, 1968). It has been defined as "a terrestrial clastic sediment, composed predominantly of silt-sized particles, which is formed essentially by the accumulation of wind-blown dust" (Pye, 1995). Most loess is pale yellow-grey or yellow-brown, formed from silt-sized detrital mineral grains, mainly quartz and feldspar, with a small proportion of other mineral grains. Some loess is calcareous, containing a mix of detrital and authogenic carbonates. It is extremely porous and is poorly cemented. This gives it a metastable character – it can form steep cliffs, especially when dry, but is prone to sudden collapse when wet.

The term 'loess' (in German: Löss, translated as 'loose' or 'crumbly') was first used by the mineral trader von Leonhard (1823/24) to describe deposits in the Rhine valley. Virlet d'Aroust (1857) proposed the aeolian-origin hypothesis, but von Richtofen (1882) was responsible for popularizing it in his writings on China.

Swineford and Frye (1955) consider that although loess in different regions shows strong similarities in field appearance, topography, soil profile development, texture and stratigraphy, it possesses strong differences in mineralogy. Smalley and Leach (1978) consider that loess deposits worldwide have undergone differing methods of formation. They suggest that the similarities have been over-valued and the distinctions overlooked.

2.1.1 The formation of loess

Hardcastle (1890) identified four fundamental requirements for the production of 'a massive sub-aerial formation of dust' (i.e. loess deposit). These are:

a) a source of wind-blown dust,
b) winds to transport the dust,
c) vegetation to reduce wind speeds and trap the dust, and,
d) sufficient time for its accumulation.

This definition is very close to that used by Pye (1995), who pointed out that the source has to be exposed, at least episodically, for periods of thousands to tens of thousands of years, and that the deposition site could feature topographic traps as well as vegetation. Loessic particles can also be trapped by surface moisture (van Vliet-Lanoë, pers. comm.).

The silt grains can be produced from parent rocks by a range of processes including glacial grinding, frost action and abrasion. Smalley (1995) divides silt production into 'major' and 'minor' processes and Smalley (1966) argues that glacial grinding is the only realistic major silt production method. Assalay *et al.* (1998) suggest that the major mode size of silt grains - the 20-60 μm fraction - may be controlled by 'Moss defects' present within the parent quartz crystals. These defects focus stress such that high-energy breakage (typical of glacial grinding) tends preferentially to produce grains of that size. Further crushing and grinding can reduce some of these grains to the comminution limit of 3-5 μm. Experiments by Smalley *et al.* (2004) show that the mechanical application of comminution stress to natural quartz sand grains, as an analogue of glacial grinding, does indeed produce abundant silt. However, the production mechanism for 'mountain loess' grains in High Asia (which lacks extensive glaciers) is unclear though tectonic activity and high-altitude weathering must be significantly involved (Smalley, 1995).

Although 'primary loess' is deposited mainly from airborne suspension, the constituent particles are not transported directly from their point of formation to their final deposition site, they are initially contained within glacial debris of all sizes and recycled sedimentary material which is transported away from the glacial region generally by fluvial processes. Repetitive, major river-valley floods or glacio-eustatic sea-level fall can both lead to the formation of large, unvegetated and unstable land surfaces covered in non-cohesive, quartz-rich, silt-rich sediment (Pye, 1987). This provides the source material for the final, aeolian, stage of transport.

Winds during the last glacial period were not only stronger than present, due to a steeper meridional surface temperature gradient but also very variable (Ruth, 2002). These powerful and turbulent winds could easily deflate large volumes of fine grains from dry, unstable land surfaces and at the LGM the atmosphere contained up to 20 times the modern dust flux (Steffenson, 1997; Petit *et al.*, 1999). Most particles settle relatively quickly by dry deposition and by precipitation scavenging ('wet deposition') (Prodi and Fea, 1979). Dry deposition is controlled by factors that encourage concentrated deposition, including gravitational settling relatively close to the source, topography (especially where topographical traps act to reduce wind speeds abruptly), vegetation cover and surface wetness. Precipitation scavenging removes particles by trapping them in snow and rainfall (*ibid.*) and so produces more random deposition patterns. Very fine grains (< 2.5 μm) can be transported high in the atmosphere and remain suspended for extended periods (Pye, 1987).

According to Pécsi (1990), a process of 'loessification' takes place after deposition. Cilek (2001) has identified a key element of this process to be the rapid formation of inter-

grain cementation bonds composed primarily of clay, sometimes impregnated by calcium carbonate and aluminium-silicon hydroxides. This is attributed to capillary water movement and repeated cycles of condensation in pore spaces. Balescu (1988) considers these 'buttresses' to be diagnostic of primary loess. Loess deposits can be modified by processes such as rainfall, sheet wash, cryoturbation and solifluction which, at their extremes, convert primary loess into loessic alluvium. Loess deposits can further be modified by pedogenesis, bioturbation and carbonate mobility, and loess geochemistry can be substantially altered by the effects of weathering. The result of these processes is that no loess deposit is in the same condition that it was when the grains were first deposited, it has all undergone some modification.

2.1.2 Loess classification

According to Pye (1995), Quaternary loess can be fitted into three main classes: periglacial (formed in mid-continental shield areas beyond the limits of ice sheets), perimontane (formed on the margins of high mountain ranges) and peridesert (formed on the semi-arid margins of some lowland deserts). Smalley and Krinsley (1978) proposed, and Sun (2002) proved, that the Central Asian and Chinese loess deposits, which appear to be desert loess, have been derived from silt grains produced in the mountains of High Asia and simply stored in desert regions during a multi-stage transport history. At least some of the northwestern loess deposits do not correspond with either the periglacial or perimontane definition; this is discussed further in Section 4.1.

2.2 The main loess provinces world-wide

Loess deposits are found worldwide, with substantial deposits in central North America, South America, Europe, Siberia, central Asia, and China (Fig. 2.1). Smaller amounts are present in Alaska, New Zealand and southern Britain.

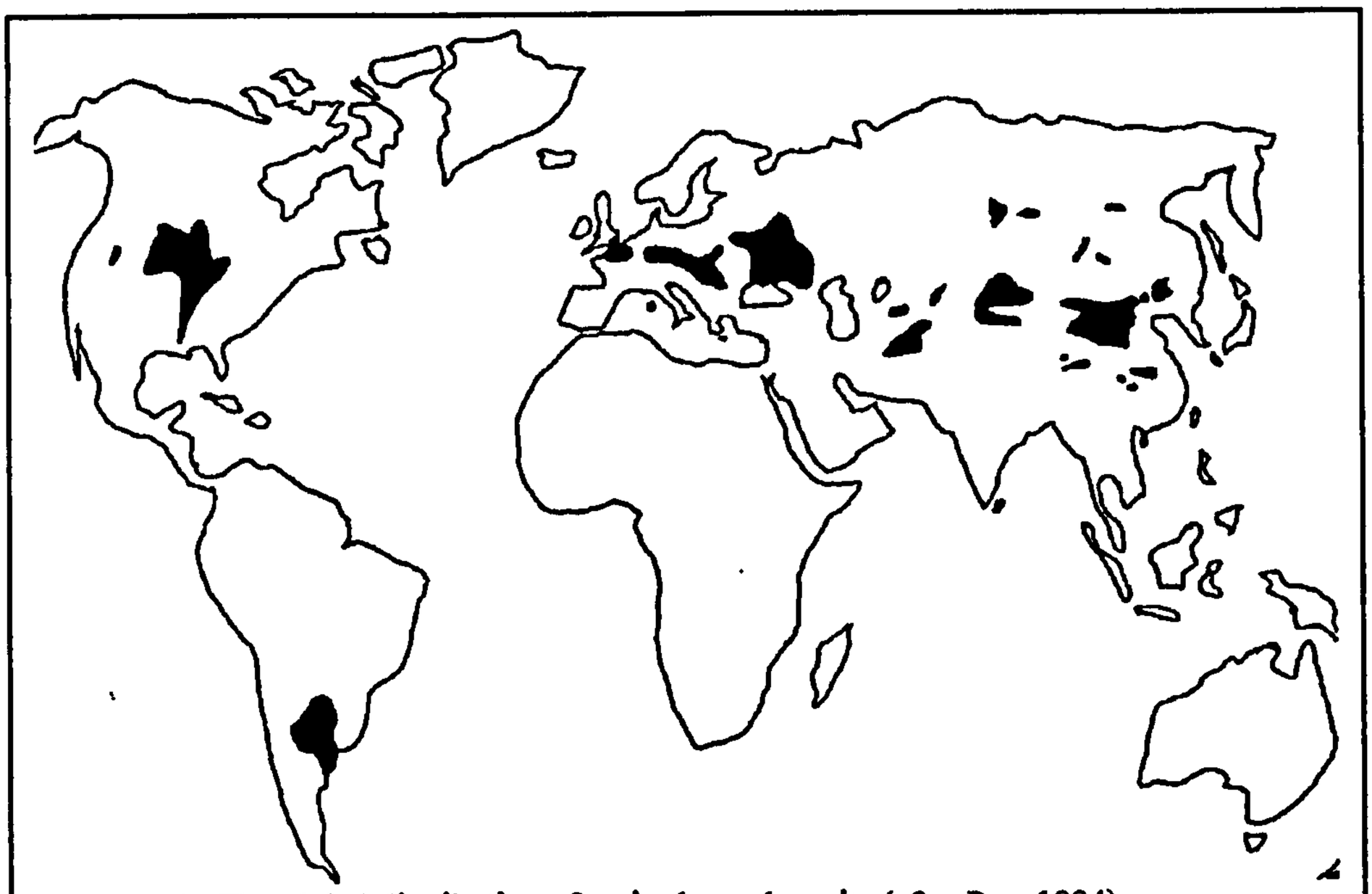

Figure 2.1. The global distribution of major loess deposits (after Pye, 1984).

2.2.1 China

The Chinese loess plateau lies between 30°N and 40°N and covers an area of about 300,000 km^2 with a thickness varying from 100 to 200 m (Liu, 1991). The loess-palaeosol sequences preserved here provide the most complete terrestrial record anywhere in the world of Quaternary environmental change.

The loessic material is derived from weathering in 'High Asia' (Smalley and Krinsley, 1978; Sun, 2002). The source rocks are heterogeneous but the particles undergo mixing, first in the eastern desert regions where they accumulate, and then again in transit to the final deposition zones (Honda and Shimizu, 1998). As a result, Chinese loess is geochemically homogeneous (Ishii *et al.*, 1995, Matsuhisa *et al.*, 1996).

An accurate chronology has been developed using variation in grain size distributions that can be equated to reduction in mean interglacial wind strength, and in magnetic characteristics that equate to interglacial pedogenesis reinforced by analysis of the prevailing orientation of the Earth's magnetic field at deposition (Heslop *et al.*, 2000). The Loess Formation extends back 2.6 Ma and records at least 56 major climatic cycles (e.g. Heller and Liu, 1982; ; Kukla and An, 1989; Rutter *et al.*, 1991; Ding *et al*, 1995). The underlying Red Clay Formation (also aeolian) extends this to 7 Ma (Ding *et al*, 1998).

Loess and palaeosol units are designated by the prefix 'L' (loess) or 'S' (soil). The Holocene soil is S0 and the last glacial period loess (the Malan loess) is designated L1; within that, the LGM is represented by substage L1-1 (Liu *et al.*, 1986). Deposition of aeolian silt has continued in the Holocene (Ding *et al.*, 2001).

As a consequence of the age of this record, and its detailed resolution of glacial/interglacial stages, Chinese loess has been intensively studied to determine how the regional climate has changed and how those changes correlate with the wider record. Many of these studies have compared glacial and interglacial climates using standard sedimentological parameters such as grain size (Porter and Zhisheng, 1995, Xiao *et al.*, 1995) and magnetic susceptibility (Bloemendal *et al.*, 1995).

2.2.2 North America

North America contains two significant loess provinces – Alaska and the central plains. Loess in Alaska has been deposited mainly in river valleys (Muhs *et al.*, 2004), showing the importance of fluvial transport. It contains a long record of climate change: fission-track dating of volcanic glass shards, allied to the development of tephro- and magneto-stratigraphies, indicate that loess deposition began three million years ago, during the late Pliocene (Westgate *et al.*, 1990, Preece *et al.*, 1999). The Alaskan loess record contains multiple local unconformities but these tephra beds can be used to link separate deposits and create a comprehensive and reliable stratigraphic record (Preece *et al.*, 1999).

Loess continues to be deposited in Alaska, providing a modern analogue for past climate change (Begét, 1996). Muhs *et al.* (2004) have used this to demonstrate down-wind fining, depositional episodicity and variation in pedogenesis that is controlled by the depositional rate, not by climate. Accumulation rates are relatively high close to the source area and the mean grain size is coarse. This rapid build-up of sediment allows insufficient time for strong soil formation and little geochemical weathering occurs (measured by the ratios of elements that are relatively mobile to those that are relatively immobile). Further away (*c.* 10-25 km), accumulation rates are lower and deposits are thinner and finer-grained. These contain morphologically well-developed soils and higher rates of geochemical weathering occur. Thus aeolian deposition and pedogenesis can co-exist under the same set of climatic conditions as competing processes; they are not mutually exclusive (*ibid.*). A similar interpretation has been placed on palaeosols in China, concluding that the presence of a palaeosol simply indicates that at that time, pedogenesis dominated aeolian deposition (Verosub *et al.*, 1993).

Loess deposits in central North America are extremely widespread and locally thick (up to 50 m). They do not have the long history that Alaskan and Chinese loess offers.

The lower part of the Roxana Silt was deposited 75-55 ka (Follmer, 1983; Hansel and Johnson, 1996), the upper part from 55-28 ka (Currey and Follmer, 1992). The Preoria Silt was deposited 25-12.5 ^{14}C ka BP (Hansel and Johnson, 1996). The deposits were formed south of the Laurentide ice sheet, in what is now the Great Plains region, and follow the regional drainage pattern south to the Gulf of Mexico (Blum *et al.*, 2000; Muhs and Bettis, 2000). That drainage was an important factor in loess distribution; accumulation rates were highest east of the Mississippi River, deflated from river flood deposits by predominantly west winds (Muhs and Bettis, 2000).

Some loessic material was derived from the Laurentide ice sheet, notably from the Superior and Lake Michigan lobes (Grimley *et al.*, 1998); some (at least in Kansas) is derived from Rocky Mountain glacial outwash, dune sands and eroded arenaceous bedrocks (Welch and Hale, 1987).

2.3.3 South America

South America contains a major loess province, located east of the Andes between 20°S and 40°S, covering 1,100 km^2 of the Argentinean pampas and parts of Paraguay (Teruggi 1957). It contains two main types of loess: the Pampean Loess between 40-30°S and sub-tropical loess between 30-20°S (Sayago *et al.* 2001). Teruggi (1957) suggested that these were derived from a single source but more recent analysis of sedimentological characteristics suggest that they have multiple sources (e.g. Bidart 1996). This is reinforced by a small number of geochemical studies (e.g. Morrás 1995, 1999). The latter paper suggested that multi-source provenance appears to have operated throughout the Quaternary. Loess-palaeosol sequences have been identified as early as the Pliocene (Kemp and Zárate 2000) and production of the source sediments may have been initiated by late Miocene orogenesis (Zárate, 2003). Smith (2001) identified geochemical mixing trends between different Argentinean loess sources and also examined element mobility under weathering.

These loess-palaeosol sequences provide one of the most detailed archives of Quaternary environmental change in the Southern Hemisphere (Muhs and Zárate 2001) but analysis has been hampered by the lack of a comprehensive lithostratigraphic and chronostratigraphic framework (Toms *et al.*, 2004). The sequences contain several geochemically-distinct tephra layers that may support the development of such a framework, aided by luminescence chronologies (*ibid.*).

According to Iriondo and Kröhling (2004), other loess deposits of varying kinds are present elsewhere on the continent. Dark red, aeolian and fine-grained 'tropical loess' sediments mantle large areas in tropical South America. Volcanic loess, termed

'cangahua' is a loose aeolian sediment formed from reworked silt and very fine sand-sized andesitic particles, fixed by minor silica reprecipitation in a humid prairie climate. It is present in the Andes and adjacent slopes in northern Ecuador and in southern Colombia (Iriondo 1994).

2.2.4 Russia and Central Asia

Loess is extremely widespread in Russia and the post-Soviet independent states but its study has been hindered by accessibility and language (Jefferson *et al.*, 2003). Loess deposits on the Russian Plain cover over one million square kilometres (Velichko, 1990). derived from the northern alluvial and lacustrine plains that formed in front of Pleistocene ice sheets (*ibid.*). Further extensive deposits are present in central Russia and central Asia as far east as Lake Baikal (Jefferson *et al.*, 2003).

2.2.5 Europe

The small-scale and fragmented deposits found in Europe have been less intensively studied than the Chinese loess and many of the research papers obtained by personal communication for this study have not been published in mainstream journals. The development of regional stratigraphic schemes has been tempered by the treatment of many sites in relative isolation, by a lack of chronological control and by a lack of obvious regional lithostratigraphic or climatostratigraphic markers. However, the development of detailed chronologies for many key sites (e.g. Frechen *et al.*, 1995, 2001) has supported inter-site correlation and some researchers (e.g. Huijzer and Vandenberghe, 1998; Ikinger and Schirmer, 2002) have used a range of multi-proxy studies to synthesise regional depositional histories and detailed climatic reconstructions of the Weichselian in northwestern Europe.

During Quaternary glaciations, loess has been deposited in Europe in a series of discontinuous patches from southern Britain, Belgium and northern France across central Europe to Ukraine and Siberia[1] (Fig. 2.2) In western Europe, this belt was bounded by the Scandinavian ice sheet to the north and the Alpine glaciers to the south.

[1] The loess deposits that form the Belgium/northern France complex, and Rhine valley loess are discussed in detail in Section 4.1.1 and 4.1.2.

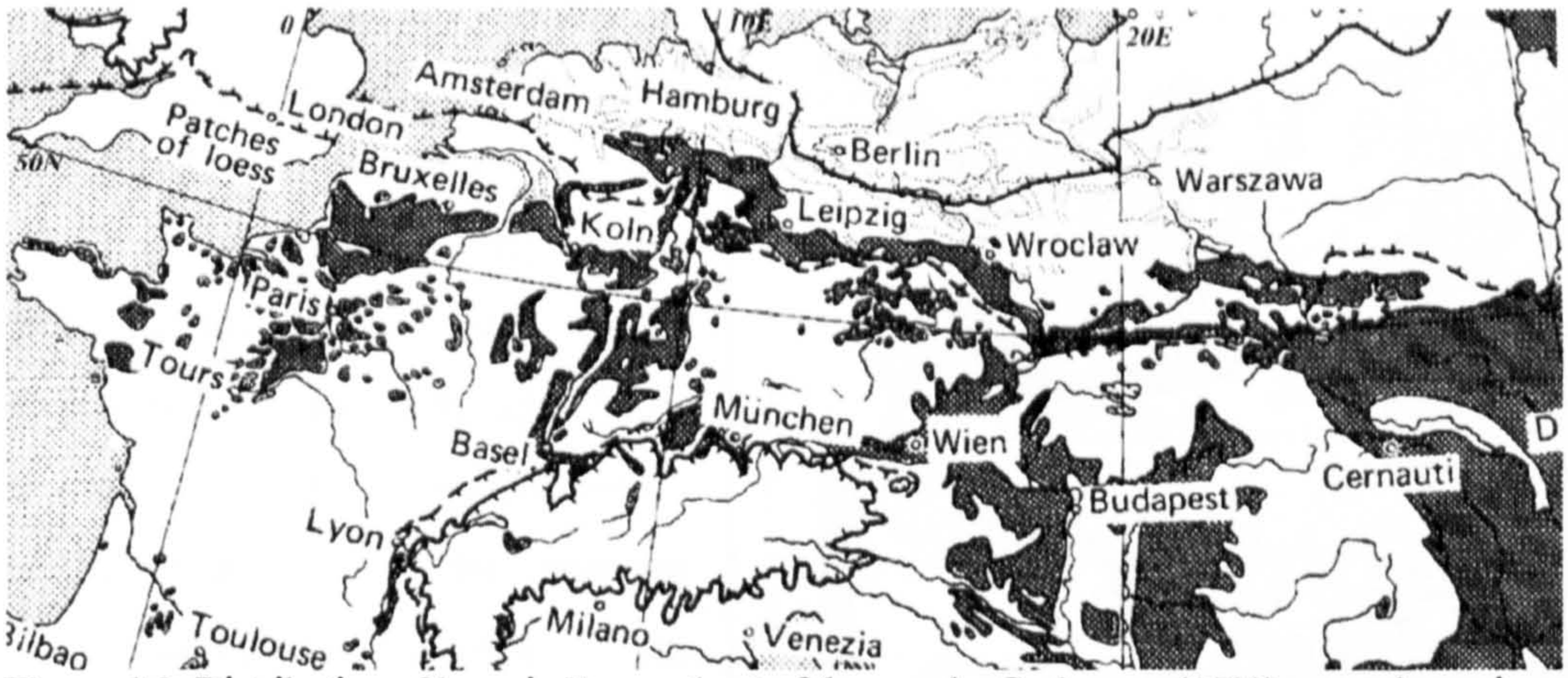

Figure 2.2 Distribution of loess in Europe (part of the map by Grahmann (1932), as re-drawn in Flint (1971)).

The European loess belt does not have the deep, accretionary nature of Chinese loess, nor the same relatively simple stratigraphy and sedimentology. The different loess provinces are limited in extent, they have been derived from different sources, they have been deposited in regions with differing climatic regimes and they have undergone periods of non-deposition and erosion.

Unlike loess deposits elsewhere, loess in western Europe has a direct, causal link with sea-level changes. The cyclic growth and decay of the Laurentide and Fennoscandian ice-caps during the Weichselian early and mid-glacial periods caused sea-levels to fluctuate between drops of 20-30 m and 40-60 m, compared to modern levels (Lambeck and Chappell, 2001). This exposed large areas of off-shore sediment deposits around the coastlines of Britain and western Europe (Huijzer and Vandenberghe, 1998). At the LGM, global sea-levels were up to 140 m lower than today (Lambeck and Chappell, 2001), exposing most of the North Sea basin and the whole of the English Channel (Huijzer and Vandenberghe, 1998). During these periods, the palaeo-Thames, Rhine, Meuse and other rivers in this area fed the Fleuve Manche ('Channel River') which transported part of their sediment discharge through complexes of anastomosing palaeo-valleys to abyssal depositionary fans on the western edge of the continental shelf (Bourillet *et al.*, 2003; Lericolais e*t al.*, 2003). The pre-existing sediment deposits, augmented by Fleuve Manche flood deposits, would have provided an extremely large source area for silt deflation.

Climate model simulations of the LGM (Rousseau *et al.*, 2002) show that the North Sea source area would have been in the path of very strong westerly winds, with the major northwestern European loess sites lying down-wind (Fig. 2.3). Local easterlies were superimposed by the summer glacial anticyclone over the Fennoscandian ice sheet.

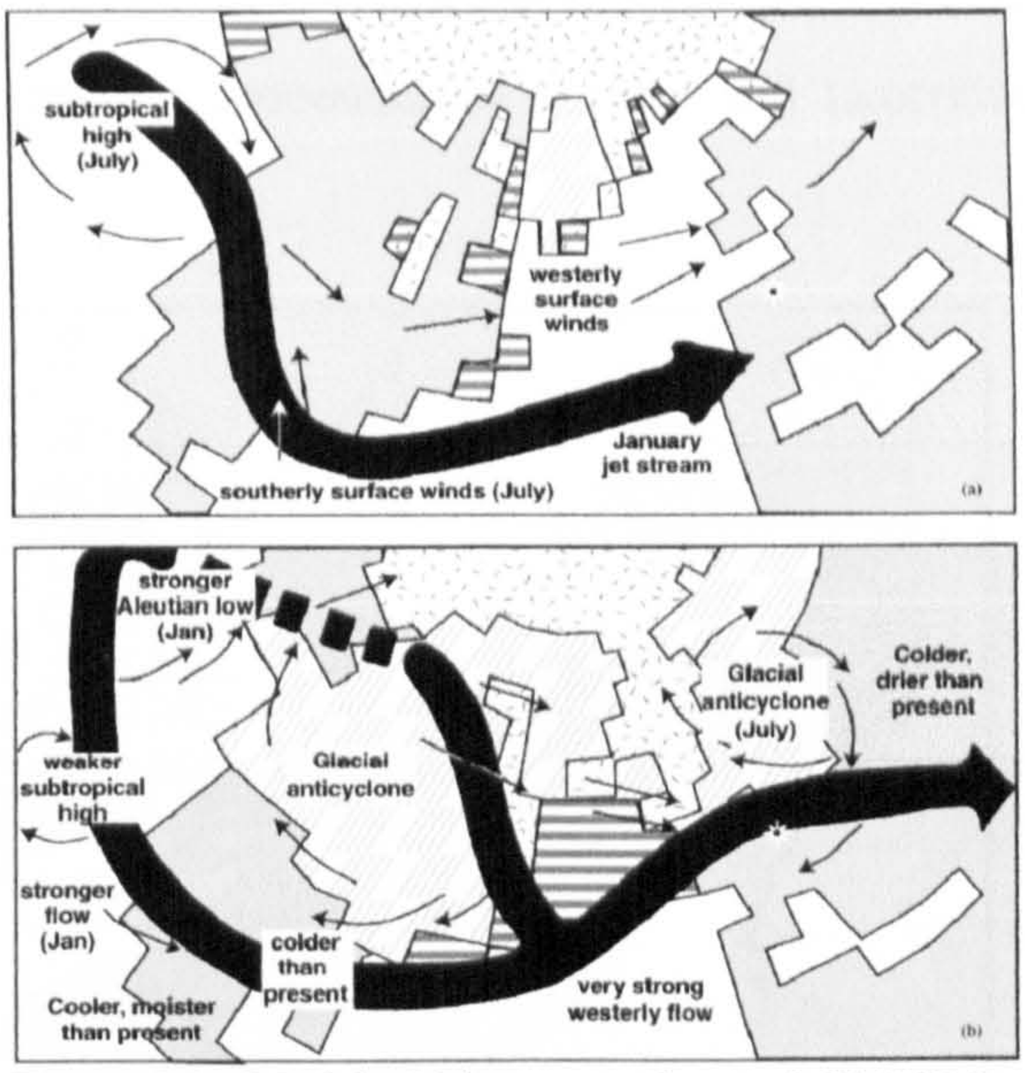

Figure 2.3. Model of (a) present-day, and (b) LGM climate dynamics over the Northern Hemisphere (from Rousseau *et al*. 2002, after COHMAP members, 1988). The star identifies the general location of the two study sites.

2.2.5.1 Britain

Regions of eastern and southern Britain have been overlain by a thin blanket of loess and cover-sand deposits up to 4 m thick (Catt, 1985), mainly deposited after the LGM (e.g. Wintle, 1981) (Fig. 2.4). There are also a few localised patches of older (mainly OIS 6 and 12) loess, which are the dissected remnants of originally more extensive covers (Antoine *et al.*, 2003). The grain size gradient and mineralogy of the recent loess suggest that some may have been derived from glacial outwash created by the North Sea lobe of the Late Devensian ice-sheet and transported by north-easterly winds (Catt, 1978). It has been heavily eroded and altered by soil-forming processes (*ibid.*). Deposits of sandy loess in Cornwall may have been derived from outwash of the glacier that occupied the Irish Sea basin (Catt and Staines, 1982).

2.2.5.2 The French Channel coast

Lautridou (1985) proposed that the discontinuous patches of loess on the French coast of the western English Channel (Fig. 2.4) might be derived from off-shore Channel sediments exposed during marine lowstands. Balescu (1988), Lautridou (1990) and Lebret and Lautridou (1991) used thermoluminescence characteristics, heavy mineral content, grain size gradients and deposit morphology to suggest that these coastal loess deposits have been derived from a combination of (a) Armorican marine sediment that has gradually migrated eastwards and (b) from calcareous detrital sediments deposited in the palaeoestuaries of the Somme and other rivers, exposed by glacio-eustatic sea level fall.

These sediments were deflated by north to north-westerly winds and redeposited relatively nearby, in the valleys of the rivers feeding those palaeoestuaries (Lebret and Lautridou, 1991).

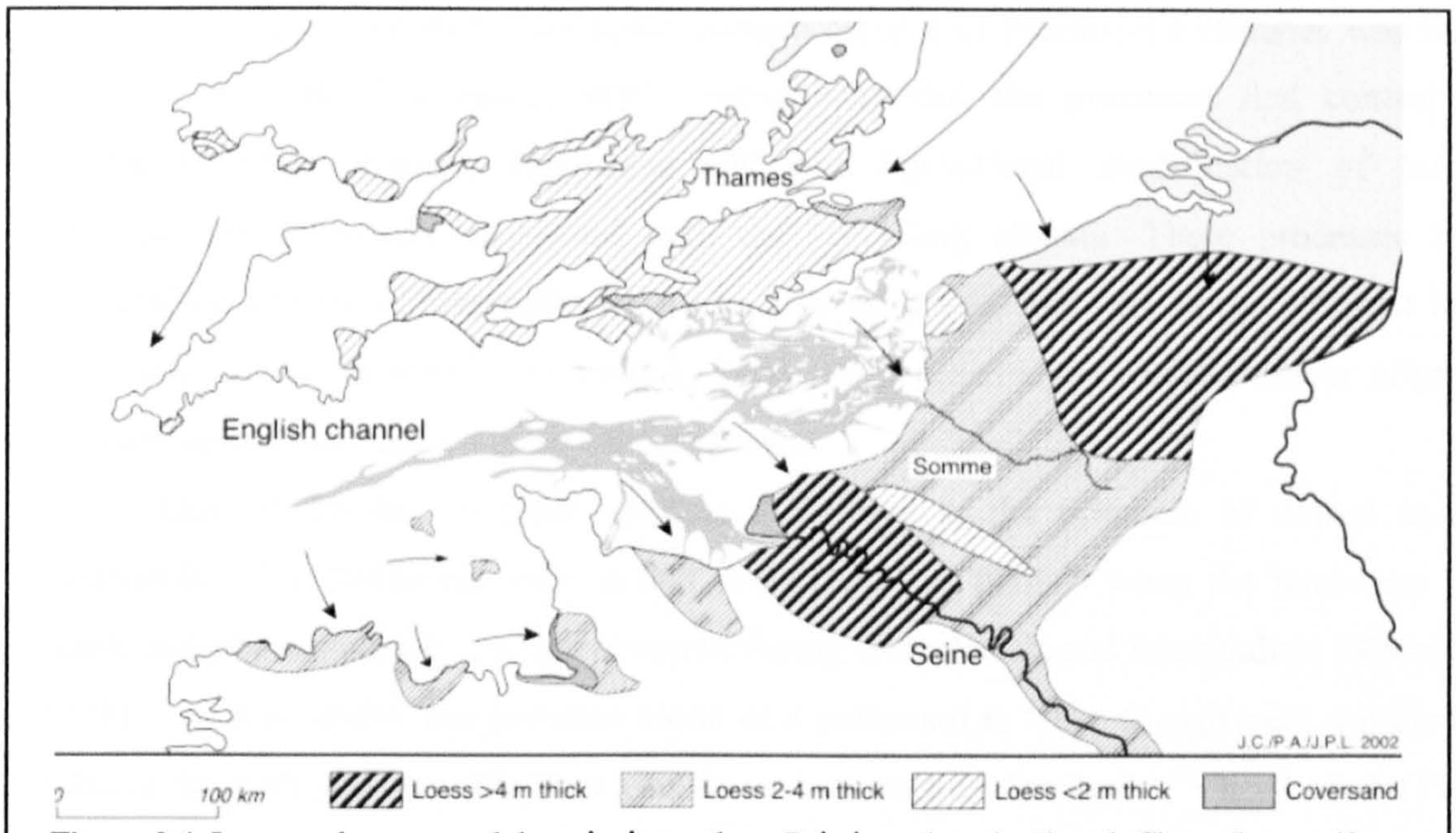

Figure 2.4 Loess and cover-sand deposits in southern Britain and on the French Channel coast (from Antoine *et al.*, 2003).

Chapter 3: Loess, climate and time

3.1 Loess as a palaeoclimate archive

The suggestion that loess could contain records of Pleistocene climates was made as early as 1890 (Hardcastle, 1890), recognising that the processes that control the formation, transportation, deposition and post-depositional modification of loessic sediment are intimately connected with the prevailing climate. These processes have operated on a range of timescales from annual to millennial and vary in the different loess provinces across the world. As a result, loess sequences contain a large number of proxy climate signals recorded on different timescales.

One of the key climatic indicators in loess is the presence of buried soils - palaeosols. The traditional view is that these represent periods when the landscape was stable and vegetated, and that this occurred during interglacials and interstadials (Morrison, 1978). In this model, the presence alone of a palaeosol is taken to represent a period of relative warmth and humidity but this is not necessarily the case. Vliet-Lanoë (1988) found that in the current climate of Spitzbergen, cryosols (arctic soils) can develop under prostrate tundra vegetation in a few hundred years.

Soils are classified by (*inter alia*) vertical segregation into a series of horizons from the upper surface to the unaltered parent material (Fig. 3.1).

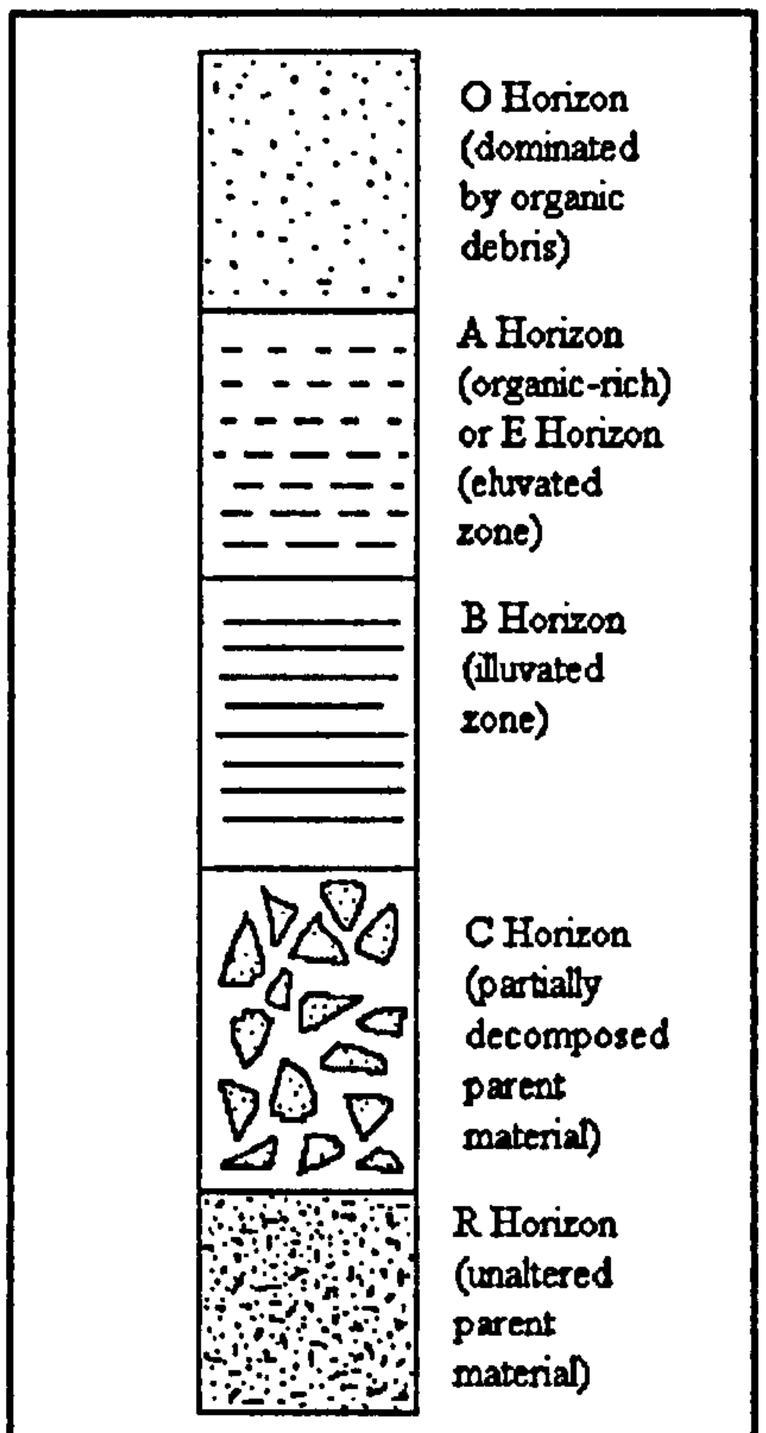

Figure 3.1. The vertical classification of soil horizons (after Food and Agriculture Organisation of the United Nations, 1998)

Jenny (1941) demonstrated that soil formation is controlled by a variety of interlinked processes. These include humidity levels and temperatures, the action of vegetation and soil organisms (responding to humidity, temperature, soil chemistry, pH, availability of nutrients etc.), surface stability, the nature of the parent material (e.g. texture, moisture retention, aeration, chemistry) and time. Catt (1991) suggested that since loess was a relatively uniform sediment, the types of soils formed in it could be compared directly to modern analogues and thus provide a reliable indicator of the palaeoclimate that formed that soil. However, there are several areas of uncertainty that inhibit the apparent simplicity of this approach. It is unclear whether the soil development rate responds in a linear, proportional form to change in one or more of the controlling parameters or whether some aspects respond as step functions

when certain thresholds are exceeded (Muhs, 1984). In addition, fundamental diagnostic features in those modern analogues may actually have been formed much earlier under different conditions (Van Vliet-Lanoë, 1990). In many loess-palaeosol sequences, erosion between the end of soil formation and the recommencement of loess deposition has almost invariably removed O horizons, part or all of the A horizon and sometimes part of the B horizon. In addition, pedogenic carbonate loss can be masked by subsequent carbonate mobility (e.g. Kemp, 2001). Nevertheless, provided assumptions and constraints are taken into account, palaeosols can be used as climatic indicators (*ibid.*).

Kemp (2001) and Muhs *et al.* (2004) have also suggested that that the formation of many loess-palaeosol sequences is not an either/or process. Instead, they are competing processes governed by changes in climate. Loess deposition takes place mainly during stadials, when cold and arid conditions allow pedogenesis to proceed only slowly. This leads to the formation of loess beds, which closely resemble the source material. Pedogenesis is accelerated during the periods of climatic amelioration that mark interglacials and interstadials, accompanied by a reduction in the supply of fresh loess grains.

During interglacials, including the Holocene, the source regions for some loess provinces have continued to deliver significant amounts of silt grains produced by high-altitude cold weathering (Kemp and Derbyshire, 1998, Begét, 1996). This is not the case in Europe and central North America, where the production of loessic silt grains has been confined to glacial periods.

3.2 Sedimentological and enviromagnetic metrics of climate change

The deposition and subsequent modification of loess-palaeosol sequences has been controlled by multiple climatic factors. As a result, these sediment complexes contain many different types of proxy signals. Sedimentological and enviromagnetic characteristics have been established to be robust and reliable tools in the interpretation of some of these climate change proxy signals; they are used in this study to provide a 'calibration standard' against which geochemical variation can be compared, showing the extent to which geochemical variation, as a proxy for climate change, correlates with indications of climate change shown by these other proxies. This will allow the utility of geochemical change as a climate proxy to be assessed.

3.2.1 Particle shape and size

Particle shape, size and particle-size distribution are among the fundamental physical properties of sediments. The determination of those properties and analysis of

how they vary in time or space can provide important clues to the source of the sediment grains, the transport mechanisms, the conditions under which they were deposited and, in some cases, the effects of post-depositional processes.

Wind moves mineral grains through a combination of creep (rolling/sliding), saltation (briefly airborne, in bounces) and airborne suspension (Fig. 3.2). There is no sharp distinction between saltation and suspension (Tsoar and Pye, 1987). These different transport modes are not simply controlled by wind strength: atmospheric turbulence, the wetness and roughness of the deflationary surface and the size, shape and density of the grains are also strongly relevant. Typically, quartz grains larger than 0.5 mm (coarse sand) move by creep, grains between 0.5-0.05 mm (medium to very fine sand) move by saltation and short-term suspension, grains finer than 0.05 mm (silt) can be transported in suspension as a mineral aerosol (Bagnold, 1941, Tsoar and Pye, 1987).

Within that suspension fraction, silt particles >20 μm are transported mainly in relatively brief suspension episodes at lower levels in the atmosphere by surface winds, and accumulate in the adjacent areas downwind of the source area to form loess deposits (Sun *et al.*, 2002). Very fine grains (<2.5 μm) can be transported thousands of kilometers in high-altitude suspension (Tsoar and Pye, 1987; Pye, 1987, 1995).

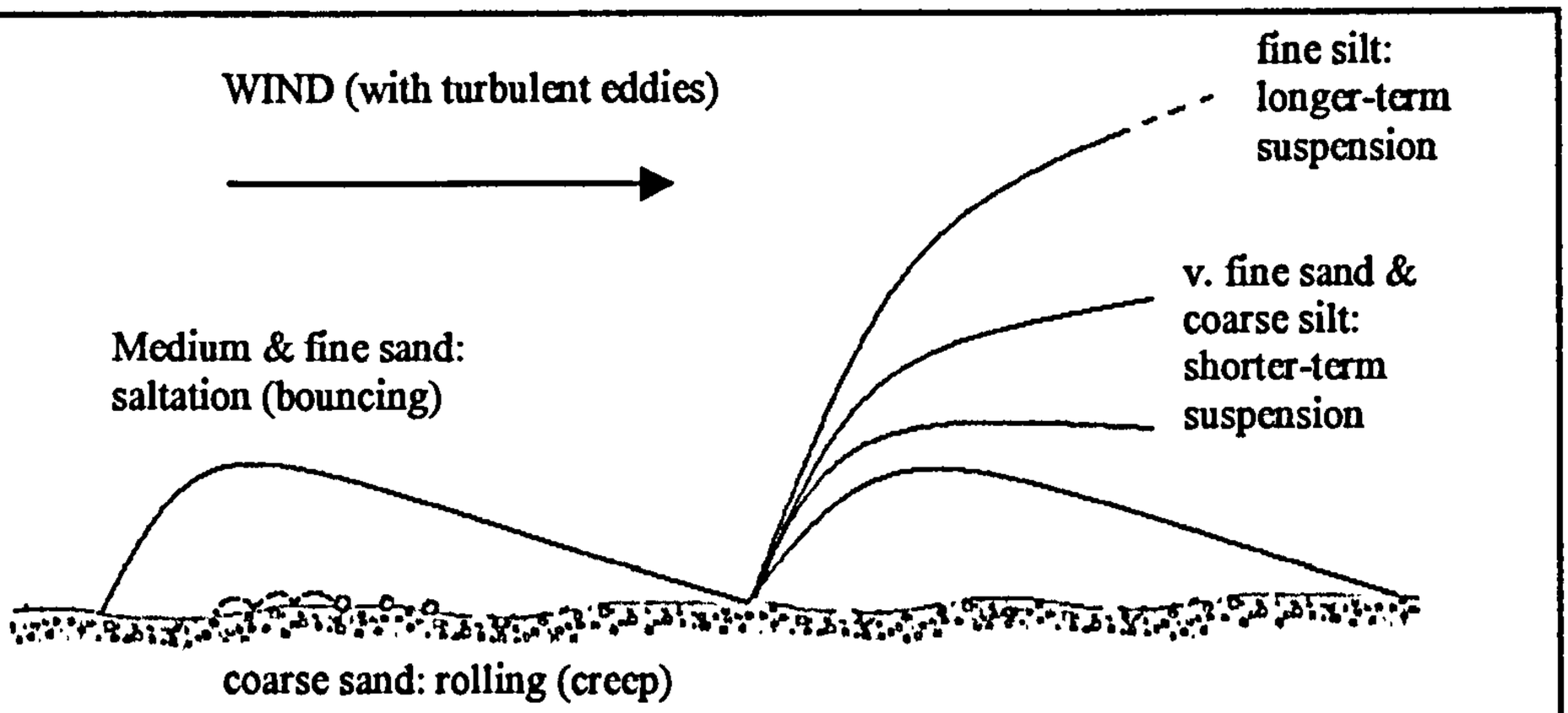

Figure 3.2. Summary diagram showing the principal modes of aeolian sediment transport (after Pye, 1995).

The model commonly used to describe palaeowind control of transported grain size (e.g. Pye, 1995) assumes, implicitly, that all factors other than variation in wind strength remain constant, that the source sediment surface contains an abundant population of representative and homogeneous grains in a range of sizes from ultra-fine to very coarse and that deposition occurs progressively throughout transportation episodes, not as a single event. Within those limitations, variation in the grain size distribution through the vertical

profile of an aeolian deposit at a single site can be considered as a temporal proxy for wind strength variation. Under conditions of approximately-constant wind direction, gravitational sedimentation during sub-aerial transport phases is likely to impose a down-wind fining trend, which may illuminate the source/site relationship or indicate prevailing wind directions (Pye, 1987). However, there are multiple ways in which a particular grain size distribution can be obtained and so it should be considered indicative rather than conclusive (McTainsh and Walker, 1982; Pye, 1992).

These temporal and spatial trends are apparent in Chinese loess. At individual loess sites, down-profile variation in grain-size reflects medium- and long-term change in the strength of the East Asian Monsoon system (e.g. Porter and An, 1995, Lu et al., 2004). Coarser-grained sediments were deposited in dynamic climatic conditions of cold, aridity and strong winds; finer-grained sediments were deposited in conditions of climatic amelioration, increased humidity and weaker winds (e.g. Liu et al., 1985). Overall, Chinese loess grain size distributions show a fining trend from northwest to southeast (Liu, 1966), down-wind of the eastern desert regions which act as temporary 'holding areas' for loessic grains (see Section 2.2.1).

Western Europe shows similar trends, imposed by predominantly west winds (Fig. 2.3). Cover-sand and loess deposits along the French Channel coast and in the Netherlands/Belgium/northern France region are deposited east and south of their assessed source areas (see Section 2.2.5) and Rhine loess thins east of its river valley source (Smalley, 1975). Grain size variation at individual sites can be related to the climatic conditions prevailing at the time of deposition (Vandenberghe et al., 1998). For example, Rousseau et al. (2002) identified a 1500-year periodicity in loess grain-size variation in the southern Rhine valley, related to wider climatic changes.

3.2.2 Carbonate content

Loess is frequently calcareous, typically with a carbonate content in the range 15-25%. Carbonates are highly mobile and, as a result, the carbonate content will include not only silt-sized fragments of the source rocks but also calcitic cement formed by in-situ processes. In addition, some may be derived from the local bedrock, as is the case at the Harmignies site in Belgium, used in this study (see Section 4.2.1). Controlling factors include:

a) the source(s), nature and chemical compositions of carbonate particles delivered during loess deposition,
b) carbonate dissolution by meteoric water containing CO_2 and plant acids, typically during pedogenesis, and,

c) calcite re-precipitation from groundwater enriched in bicarbonate and calcium ions when the microenvironment becomes alkaline, typically during pedogenesis.

Dissolution and reprecipitation often result in a net downwards migration of carbonates in the loess sequence. This mix of source and mobility factors means that the amount of carbonate present in any single loess sample cannot be used as a direct climate proxy. However, variation in the carbonate profile can reveal episodes of depletion and reprecipitation and it is especially indicative of soil-forming episodes.

3.2.3 Organic carbon content

Loess sediments contain variable amounts of organic carbon debris, derived from vegetation, which grew on the original loess surface. Low amounts of organic carbon are associated with cold, arid conditions; higher amounts are linked with episodes of warmer, more humid conditions and commonly correlate with palaeosol horizons (e.g. Muhs *et al.*, 2003). This organic content is, therefore, a climate proxy signal. It is present in the form of very fine organic debris. Recognisable plant fragments (e.g. roots etc.) are very unlikely to be original; samples containing such material may give inaccurate analytical results. The fine, disseminated organic material present even in primary loess has also been used for radiocarbon dating (e.g. Hatté *et al.*, 1999) and its isotopic composition has been used as a proxy for palaeoprecipitation (Hatté *et al.*, 2001).

3.2.4 Enviromagnetism

Enviromagnetism, also known as mineral magnetism, examines the non-directional magnetic properties of natural iron-bearing minerals in the natural environment - primarily in sediments. This includes the pre-existing magnetic properties of the mineral and its remanent response to applied magnetic fields (Thompson and Oldfield, 1986).

The magnetic minerals found in loess-palaeosol sequences have complex histories. The primary iron-rich minerals crystallise in igneous rocks, from which they are released by erosion and weathering. Some crystals, released by erosion, may become directly incorporated in sedimentary rocks and unlithified deposits. Other crystals and weathered compounds may be recycled through the geological environment to form assemblages of new iron-rich minerals in sedimentary rocks and unlithified deposits (Evans and Heller, 2003). Those minerals may be further modified by the dynamic and large-scale processes that create and transport loess particles and post-depositional changes can continue this recycling process, destroying pre-existing iron-rich mineral particles and creating new ones with different properties.

Magnetic minerals are only a small proportion of the total iron content in loess; most is contained in detrital silicate mineral grains (Fine *et al.*, 1993), which have paramagnetic behaviour (i.e. a weak response to imposed magnetic fields). The enviromagnetic properties of loess-palaeosol sequences are commonly controlled by four magnetic minerals (Maher *et al.*, 1999). Magnetite (Fe_3O_4) and its fully oxidised form maghemite[1] (γ-Fe_2O_3) are ferrimagnetic. They have low coercivity (i.e. they become magnetised to saturation in relatively low field strengths), are strongly magnetic and will often dominate the magnetic properties of a sample even when present in relatively small amounts (Evans and Heller, 2003). Haematite (α-Fe_2O_3) and goethite (α-FeOOH) respectively have 'canted antiferromagnetic' and 'imperfect antiferromagnetic' properties[2]. This gives them low susceptibility and high coercivity (i.e. they require higher field strengths to reach saturation magnetisation). The effects of low- and high-coercivity properties on the acquisition of remanence properties are shown in Fig. 3.3, and illustrate how magnetite is magnetised to saturation at low field strengths while haematite remains unsaturated even at relatively high field strengths.

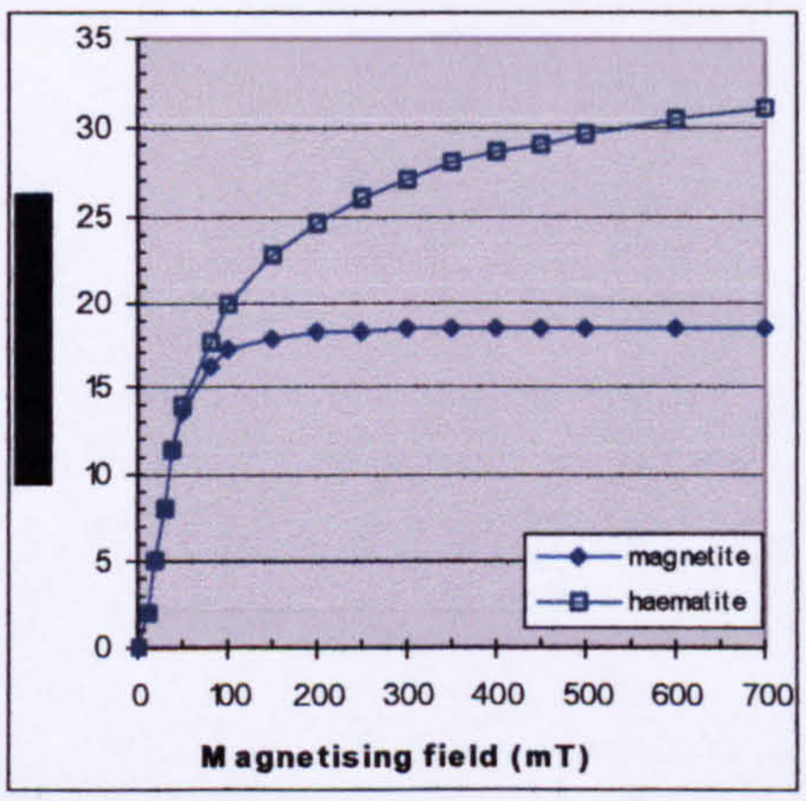

Figure 3.3 Typical IRM acquisition curves for pure magnetite and haematite (Butler, 1982), showing their different response to increasing field strengths.

In enviromagnetic studies, the term 'grain' is not synonymous with 'particle'; it has specific relevance to the way that magnetism is organised in magnetic domains - small, self-organising regions of uniform magnetisation. Domain size is governed by the coercivity of the mineral involved and is closely linked to magnetic remanence (where the application of a magnetic field permanently alters the magnetic properties). The domain/size relationships for magnetite are complex and vary with grain shape (Evans and Heller, 2003). Assuming equant morphology, ultra-fine grains, below *c.* 0.5 μm, are too small to support even one domain. They are magnetically unstable with no remanence or coercivity but the magnetization of these grains can align very quickly with an external magnetic field, giving them high susceptibility. This is known as superparamagnetic (SP) behaviour. Fine grains between 0.5-1.0 μm can support a stable single domain (SD), have high remanence and low coercivity (*ibid.*). Grains at the SP/SD boundary (*c.* 0.1 μm) are magnetically metastable; they have high remanence but some grains will undergo spontaneous relaxation of their individual magnetic moments, leading

---

[1] Maghemite is metastable and is normally present only as ultra-fine grains since grains >1 μm are likely to convert to the more stable haematite (De Boer, 1999).

[2] Like maghemite, haematite and goethite can both be produced by the oxidation of magnetite.

to an exponential decrease in sample remanence, slowing as the metastable population reaches stability. This is also known as viscous loss (Butler and Banerjee 1975).

Grains larger than 1 μm can contain a small number of domains and possess many of the attributes of SD grains. These are termed pseudo-single-domain (PSD). With increasing grain size, domain structure becomes increasingly complex, forming multiple domains that act independently (multidomain - MD). Magnetite grains larger than 20 μm are invariably MD. Due to this independence, MD grains have higher coercivity and are less able to carry stable remanence than SD and PSD grains (Peters and Dekkers, 2003). Thus domain state is a function of grain size. Haematite has higher coercivity than magnetite and grains can remain as single domain up to 15 μm (Butler and Bannerjee, 1975).

This range of magnetic characteristics can be examined in a range of tests (see Section 5.7) and the results can identify the enviromagnetic response to processes accompanying climate change. One of the main enviromagnetic responses to climatic amelioration is the formation of ultra-fine-grain magnetite; this is discussed in Section 3.3.5.

3.2.5 The causes of magnetic variation between loess and palaeosols

Le Borgne (1955) first identified that topsoils have enhanced magnetic susceptibility (MS), compared to their subsoil horizons. The same phenomenon is present in Chinese loessic palaeosols (Heller and Liu, 1982) and it is now known that MS variation in these sequences correlates closely with the marine $\delta^{18}O$ record of ice volume (Kukla *et al.*, 1988). It is, therefore, a climatic proxy. MS has been widely used in Chinese loess-palaeosol sequences as a climatostratigraphic indicator, proving the presence of successive interglacial palaeosol horizons and contributing strongly to the development of long chronologies (see Section 2.2.1).

Chinese 'primary loess' is dominated by a mixture of PSD and MD magnetite grains but palaeosols and weathered horizons contain an increased proportion of fine and ultra-fine magnetite and maghemite grains with SD and SP characteristics which contribute to the observed magnetic enhancement (Zhou *et al.*, 1990; Maher and Thompson, 1995; Van Velzen and Dekkers, 1999). These ultra-fine grains have been studied closely and there appear to be two major theories for their formation.

The first is that they are the result of weathering during periods of increased warmth and humidity. Magnetite can oxidise to maghemite or haematite, with the mineral phase being size-dependent. Coarse magnetite particles can develop haematite surface films while smaller particles (with large surface area to volume ratios) may undergo

complete oxidation (Xie *et al.*, 2004). In this latter process, particles larger than 1-2 μm oxidise to haematite (De Boer, 1999), with low susceptibility. However, smaller particles oxidise to stable, nano-scale, multicrystalline maghemite with very high susceptibility (Xie *et al.*, 2004).

The second[1] relates to life processes during soil formation episodes. Under cyclic wetting/drying conditions, bacterially-mediated Fe reduction processes can efficiently produce ultra-fine magnetite crystals from non-magnetic available iron, as can the life processes of magnetotactic bacteria (Blakemore, 1982; Lovley *et al.*, 1987; Zhou *et al.*, 1990; Maher and Thompson, 1991). This occurs mainly in the biologically-active O and A soil horizons which are generally missing from loessic palaeosols (by erosion etc.) but Fine *et al.* (1989) suggest that these newly-formed crystals may be transported to deeper horizons by eluvation.

Either process – whether induced by weathering or by pedogenesis – is linked to humidity, temperature and time and so magnetic enhancement can be considered as a climate proxy signal (e.g. Maher and Thompson, 1995). However, Tang *et al.* (2003) consider that enhanced MS in Chinese palaeosols is the result of a complex mix of climatic, environmental, physical, geochemical and other factors that are not fully understood.

Similar palaeosol MS enhancement has been observed in central Asia, eastern Europe (Forster and Heller, 1997; Shi *et al.*, 2003) and France (Rousseau and Puisségur, 1990). Sartori *et al.* (1999) attributed the observed MS enhancement in Hungarian loessic palaeosols mainly to weathering processes, including the oxidation of detrital magnetite to haematite and the conversion of pre-existing minerals into new, fine-grained magnetic minerals.

Elsewhere in the world, the processes that lead to magnetic variation between loess and palaeosols appear to differ. In Alaskan and Siberian loess deposits, the primary loess has relatively high susceptibility and the palaeosols show relative MS depletion (Begét *et al.*, 1990; Chlachula *et al.*, 1998; Zhu *et al.*, 2000). Begét *et al.* (1990) conclude that the strong winds that result in loess deposition are able to transport dense magnetic particles; weaker winds, characteristic of interstadial or interglacial conditions, cannot. Evans (2001) suggests that this is applicable when sites are close to their source regions; sites remote from their source are likely to be dominated by Chinese-type patterns.

---

[1] Other suggested pathways for MS enhancement have included: concentration by pedogenic carbonate loss and soil compaction (Heller and Liu, 1984); the alteration by frequent natural fires of weakly-magnetic soil minerals to strongly-magnetic (Kletetschka and Bannerjee, 1995), the formation of ultra-fine magnetic crystals in redox conditions linked to decomposing vegetation (Meng *et al.*, 1997); the dilution by rapid dust accumulation in cold phases of a near-constant rain of ultra-fine magnetite (Kukla *et al.*, 1988).

A consideration applicable to specific topographic conditions rather than climate or region, is that in waterlogged, anaerobic, gleying conditions, magnetotactic bacterial fail to thrive and pre-existing iron minerals - especially magnetite/maghemite - may be removed by redox processes (Nawrocki *et al.*, 1996; Maher, 1999; Zhu *et al.*, 2003). This may be specific to individual sites, areas within sites or even the same site under different conditions (Liu *et al.*, 2001).

In Germany, different loess sequences appear to contain 'normal' and 'reversed' MS signatures. A well-developed Eemian palaeosol near Mainz had decreased mineral magnetic content, compared to its parent loess (Bibus *et al.*, 1996) but similar palaeosols elsewhere showed MS enhancement (Terhorst *et al.*, 2001). This affected interglacial and interstadial soils, though the latter were only weakly developed and the magnetite present in these interstadial soils may be abiotic, produced relatively rapidly by weathering (*ibid.*). Hus and Geeraerts (1999) were unable to identify magnetic enhancement in Belgian loess sections except in the Eemian 'Sol de Rocourt' palaeosol, which may have been caused by volcanic mineral particles (*ibid.*).

This evidence proves that the mineral magnetic record in loess-palaeosol sequences is sensitive: it is not a simple 'magnetic change equals climate change' proxy signal but is instead a complex response to a range of variable conditions which include the nature of the source material, the source/site relationship, the depositionary environment and the nature of post-depositional modification, including the effects of climate and time. That sensitivity will be an important consideration when using the mineral magnetic record as a proxy paleoclimatic indicator in the present study. Variations in single magnetic parameters are ambiguous and cannot be considered in isolation; the body of enviromagnetic data must be placed in the wider context to understand how each site has responded to climatic change.

3.3 Loess geochemistry

3.3.1 Geochemical characteristics

Loess contains all the major rock-forming elements - silicon (Si), titanium (Ti), aluminium (Al), iron (Fe), manganese (Mn), magnesium (Mg), calcium (Ca), sodium (Na), potassium (K) and phosphorous (P). By convention, they are reported in geochemical analyses (including this study) as oxides as percentage weight units (SiO_2, TiO_2, Al_2O_3, $Fe_2O_{3\,(tot)}$[1], MnO, MgO, CaO, Na_2O, K_2O and P_2O_5). Na and K are classed as 'alkali metals'; Ca and Mg are 'alkaline earth metals'.

[1] The $Fe_2O_{3\,(tot)}$ value in ICP analysis represents total iron, not just the specific Fe_2O_3 abundance.

Si is present mainly as quartz, with a smaller contribution carried in feldspars, micas and other silicate minerals common in loess. It will, therefore, invariably comprise a high percentage of any loess geochemical composition. Ti is carried in minerals such as rutile (TiO_2) and titanite/sphene ($CaTiSiO_5$), and it can form solid-solution series with iron in minerals such as magnetite. The majority of the Al content is likely to be present in feldspars: anorthite ($CaAl_2Si_2O_8$), albite ($NaAlSi_3O_8$;) and microcline/orthoclase ($KAlSi_3O_8$). Solid solution variation between anorthite and albite is classed as plagioclase feldspars $(Ca,Na)AlSi_3O_8$); between albite and microcline/orthoclase is classed as alkali feldspars $((K,Na)AlSi_3O_8)$. Al is also carried in micas (muscovite: $KAl_2(Si_3Al)O_{10}(OH)_2$; biotite: $K(Mg,Fe)_3(AlSi_3O_{10})(OH)_2$).

Fe is present in the magnetic minerals, as weakly magnetic oxides and hydroxides (including the oxide staining on quartz particles that gives loess its predominant buff colour) and in silicate minerals. Mn is generally present in low concentrations and can be concentrated into nodules under waterlogged conditions. Ca is the dominant constituent of limestone (as $CaCO_3$). Ca and Mg, in variable proportion, are the dominant constituents of dolomite ($CaMg(CO_3)_2$). Na and K are carried in feldspars and micas (see above). P is present mainly as phosphate minerals such as apatite ($Ca_5(PO_4)_3(F,Cl,OH)$). Most of these elements are also present in clay minerals, which have complex silicate compositions.

Loess also contains a multitude of trace elements, incorporated in a wide range of accessory minerals and as substitute atoms in rock-forming crystal lattices. They are conventionally reported as elements, in parts per million (ppm). This study examined barium (Ba), cobalt (Co), copper (Cu), gallium (Ga), niobium (Nb), nickel (Ni), lead (Pb), scandium (Sc), strontium (Sr), vanadium (V), yttrium (Y) and zinc (Zn). These are important in rock-forming processes and can also reflect some effects of weathering. Ba and Sr are 'alkaline earth metals'.

The rare-earth elements (REE) are part of the trace element population and are carried in a wide range of minerals. They are similarly reported as elements in ppm but are conventionally treated separately. They are: lanthanum (La), cerium (Ce), praesodymium (Pr), neodymium (Nd), promethium (Pm), samarium (Sm), europium (Eu), gadolinium (Gd), terbium (Te), dysprosium (Dy), holmium (Ho), erbium (Er), thulium (Tl), ytterbium (Yb), and lutetium (Lu). Pm is radioactive and has decayed to undetectable levels in geological materials. They are divided into the light REE (LREE) (La to Eu) and the heavy REE (HREE) (Gd to Lu). To equalise the relative abundance of atoms with even atomic numbers (the Oddo-Harkins rule of element abundances) and make graphical plots more informative, REE analytical results are conventionally normalised against known

standards; this study has used the Taylor and Mclennan (1985) carbonaceous chondrite composition.

The REE are regarded as being among the least soluble trace elements and are relatively immobile under weathering conditions (Nesbitt, 1979), though some co-illuvation may occur with clay particles (Aide and Smith-Aide, 2003). They are frequently used as benchmarks for the behaviour of more mobile elements (e.g. Gallet *et al.*, 1998) and as provenance indicators (e.g. Bhatia and Taylor, 1981; Taylor and McLennan, 1985).

3.3.2 Loess as a proxy for the average upper crust

Taylor, McLennan and McCulloch (1983) analysed loess as a proxy for the upper continental crust (UCC). The composition of 12 loess samples from sites in America, China, Europe and New Zealand was generally uniform (excluding variations in carbonates) and close to UCC composition. Silica was enriched relative to the UCC due to the processes of silt formation and the sorting imposed by transportation, and this caused a relative depletion in the other major elements. REE patterns were strikingly similar to those in shales, confirming from this set of worldwide samples that loess is a very homogeneous material, as representative of the UCC as shale is.

This work was amplified by Gallet *et al.* (1998), using loess from a range of sites in western Europe plus Argentina and Spitzbergen. Their findings reinforce that earlier work and show that loess deposits are extremely well mixed. There is a consistent pattern of enriched light REE and relatively flat heavy REE, with a restricted range of La/Yb and Eu/Eu* ratios. Gallet *et al.* use this constancy, plus evidence from other trace element ratios, to argue that these loess samples must be derived from multi-recycled and well-mixed ancient sediments (excluding Argentinean loess which contains particles derived from Cainozoic Andean volcanic rocks). Gallet *et al.* further state that these loess samples cannot have been derived by direct glacial grinding of igneous or meta-igneous bedrocks, since this would generate distinctive geochemical signatures. By implication, this appears to preclude much of Scandinavia as a major, direct source of western European loess, since the exposed rocks in that area are primarily igneous and meta-igneous, part of the Fennoscandian Shield.

3.4 Geochemical effects of weathering

3.4.1 Geochemical change

Physical and chemical weathering together play a crucial part in the rock cycle, converting rock into sediments, colluvium and soils. Physical weathering converts rock materials into smaller fragments, mainly by stress-induced fracturing, and so causes a reduction in mean grain size (e.g. Bartlett, 1832). However, silt-sized loess particles are relatively unaffected and it has no effect on the bulk geochemical properties. In contrast, chemical weathering is the result of a complex and variable range of factors which include temperature, humidity, the presence of dissolved CO_2 in meteoric water, the pH of soil solutions, the redox state at different soil horizons, the susceptibility of different minerals to different forms of chemical attack, the nature of secondary minerals formed by chemical alteration and the extent to which cations are removed by groundwater flow. It produces significant changes in the bulk geochemical properties of loessic sediment by the progressive removal of mobile elements, with the degree of loss dependant on both the intensity and the duration of weathering episodes. As a general trend, the alkali metals and alkaline earth elements are relatively mobile; Al, Ti and the REE are relatively immobile.

According to Welch and McPhail (2003) chemical weathering in soils is heavily mediated by biological processes. Micro-organisms have profound effects on silicate mineral weathering rates by changing the soil solution pH, by producing organic acids and other compounds which complex with ions on the mineral surface, and by changing reduction/oxygenation conditions (*ibid.*). Linell and Tedrow (1981) demonstrated that under arid, cold conditions, biological processes are restricted and pedogenesis is weak, though some biological activity occurs even in frozen soils (Tedrow, 1977). Rogers *et al.* (1998) showed that in anoxic groundwater conditions with limited micro-nutrient availability, microbial attack could destroy feldspars and form secondary clay minerals 'at rates orders of magnitude faster than predicted based on laboratory rates'.

The early stages of weathering are dominated by the degradation of primary minerals and the release of elements in solution (e.g. loss of Ca from carbonates) (Nesbitt *et al.*, 1980). In more advanced stages of weathering, feldspars (widely present in loess) undergo hydrolysis which converts the crystal surface into clay micro-coatings (Berner and Holdren, 1977). Theoretical concepts of mineral stability, such as the Goldich stability series (Birkeland, 1999) and studies of rock weathering (Colman, 1982) suggest that potassium feldspar is stable under moderate weathering attack, as is muscovite mica, but plagioclase and biotite are susceptible, weathering to produce secondary clays (Wilson, 2004). These clays retain the original Al content and remain in the weathering column but

the relatively soluble elements Mg, Ca, Na and K are lost to solution (Nesbitt *et al.*, 1980). The equation for the breakdown of potassium feldspar is:

$$\underset{\text{K-feldspar}}{2KAlSi_3O_8} + \underset{\substack{\text{acid from}\\ \text{atmosphere}\\ \text{and biosphere}}}{2H^* + 9H_2O} \longrightarrow \underset{\substack{\text{kaolinite}\\ \text{(clay mineral)}}}{Al_2Si_2O_5(OH)_4} + \underset{\substack{\text{silica \& potassium}\\ \text{(in solution)}}}{4H_4SiO_4 + 2K}$$

Since Ba can substitute for K, it is commonly carried in biotite and K-feldspar. Unlike K, it tends to be retained in the secondary clays by absorption (Nesbitt *et al.*, 1980).

Salm *et al.* (1998) conducted acid attack 'accelerated weathering' tests on clay and loess samples and confirmed that these soluble metals were preferentially removed. High-Na feldspars decomposed faster than K-feldspars and overall, clays (which have large surface areas to volume ratios per particle) showed the fastest decomposition loss; sands, the slowest.

The homogeneity of Chinese loess (see Section 2.2.1) has allowed researchers there to examine palaeosol geochemical heterogeneity with confidence that the observed variations are likely to be climatically induced rather than being a function of source change. Gallet *et al.* (1996) examined element mobility during pedogenesis. They found that interglacial palaeosols are severely depleted in Ca and Sr, and moderately depleted in Mg as a result of carbonate dissolution by meteoric water. Ca and Sr were reprecipitated as calcite lower in the profile. K and Na were lost due to the partial destruction of feldspars. Other elements were relatively invariant, especially Al and Ti. Diao and Wen (1999) showed an weathering mobility sequence of $CaCO_3$>FeO>MgO>Na_2O>K_2O>SiO_2>Al_2O_3>TiO_2>Fe_2O_3. Smith (2001) showed the same general geochemical trends in Argentinean loess, with weathering-induced changes identifiable in the ratios of mobile/relatively immobile elements such as Rb/Sr and Na_2O/Al_2O_3. Juvigné and Moors (1995) used XRD techniques to examine European loess and concluded that like China, carbonates were highly mobile in weathering conditions.

This range of research work shows that loessic sediments undergo systematic geochemical change during weathering and that the degree of change is linked to the duration and intensity of the weathering event: moderate weathering results in the loss of elements carried in easily-weathered minerals, more intense weathering causes elements to be lost from less-susceptible minerals. Geochemical change induced by weathering is, therefore, a climate proxy signal.

3.4.2 Chemical weathering indices

That consistency of geochemical response to weathering has been used to create 'chemical weathering indices', sometimes referred to as indices of alteration. They characterise weathering profiles by comparing the ratios of mobile and immobile elements and reduce weathering complexity to a single figure. Price and Vebel (2003) recommend that weathering indices should be appropriate to the weathering environment: under intense weathering the most mobile elements will be lost relatively early in the process; under weak weathering even moderately-mobile elements may be unaffected. Nesbitt *et al.* (1980) and other workers suggest that the Chemical Index of Alteration (CIA; Nesbitt and Young, 1982) is most suitable for analysing the response by loess-palaeosol sequences to moderate weathering. The CIA examines the weathering of, primarily, biotite and plagioclase feldspar by comparing the retention in the weathering column of the original Al content with the loss of the relatively mobile K, Na and Ca content (removed in solution - see Section 3.4.1). The Ca content must be determined only from silicate minerals.

Since indices such as the CIA will only act as valid indicators of change when applied against profiles with constant original compositions, one of the fundamental objectives of this study is to determine the extent to which the original sediment was homogeneous and the extent to which heterogeneity now present has been imposed by climatic and other aspects of change (see Section 1.4).

The CIA has another unavoidable limitation, related to the homogeneity of the aeolian sediment. Loessic sediment stripped of any clay content during its transportation phase would produce CIA values equivalent to fresh rock, with any subsequent weathering generating autochthonous clays that contribute to the weathering signal. However, the presence of allochthonous clays (e.g. delivered as clay skins or as silt-sized aggregates) would generate a raised Al content and might thus indicate weathering where none had occurred.

3.5 Chronological controls

3.5.1 The datable event

The establishment of precise and accurate chronologies for continental sedimentary sequences is a key problem in correlating terrestrial, marine and ice sheet climatic records and in understanding the global processes of climate change (e.g. Lang *et al.*, 2003). However, the chronological 'age' of a loess-palaeosol record could describe the age of the constituent crystals, the time they were converted into silt grains, the time they underwent final deposition or the time they were last modified (e.g. by pedogenic processes). These

different ages would encompass extremely different periods of geological time and could not be dated by a single technique. All of these different ages would provide useful evidence in identifying the source area and in reconstructing the processes that have produced the loess-palaeosol sequence as observed today. For climate change purposes, an accurate chronology of both deposition and pedogenic modification would be most useful but no single method can date both, and independent methods will return chronologies that cannot be accurately correlated. Fig. 3.4 provides an outline of the different dating techniques applicable to Quaternary records, and the periods of time they cover. Table 3.1 shows the applicability of these different techniques to different materials that may occur in conjunction with loess.

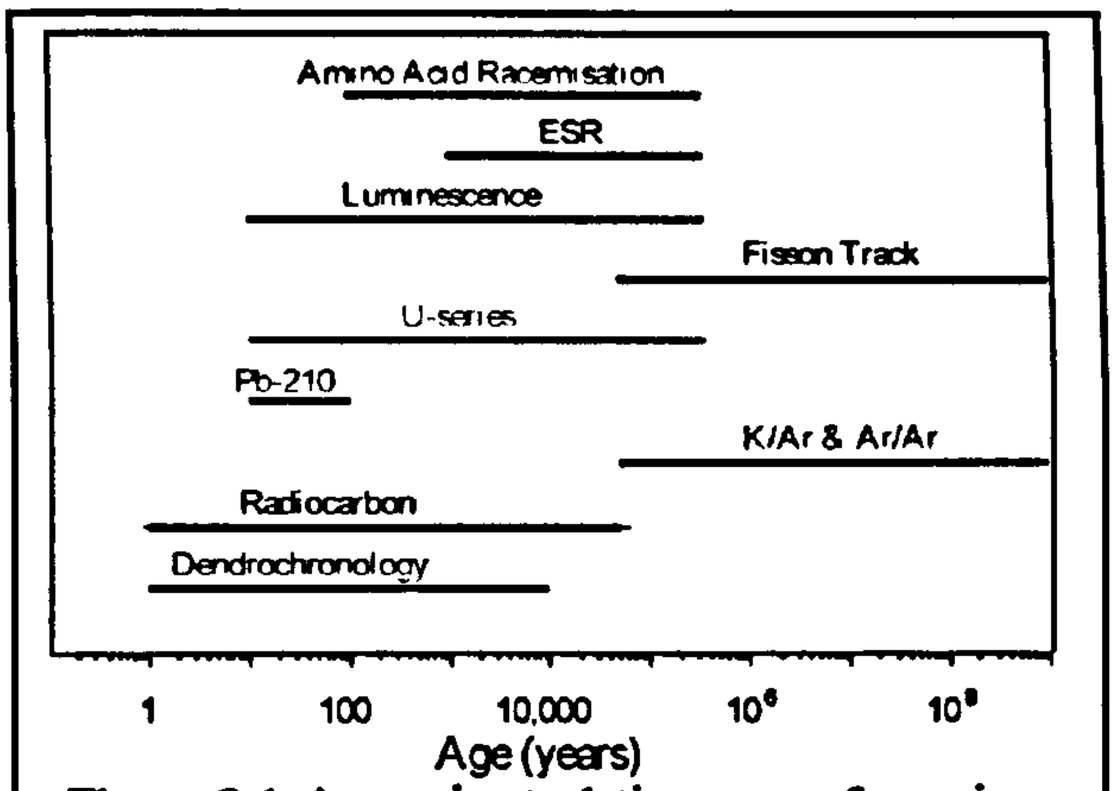

Figure 3.4. Approximate dating ranges for various Quaternary dating methods (after Colman & Pierce, 2000; Colman *et al.*, 1987).

Table 3.1. Applicability of Quaternary dating methods to sediments and related materials (modified from Aitken, 1990).

Dating method	Wood/ plants	Bones	Tooth enamel	Shells	Sedi- ments	Surfaces	Obsidian & glass	Volcanic minerals
Radicarbon	●	●	○	●	⊖			
K/Ar, $^{40}Ar/^{39}Ar$								●
U-series		⊖	⊖	○	○			●
Fission tracks							●	●
Luminescence					●			○
ESR			⊖	⊖				●
Amino Acid		○	○	●				
Hydration							●	
Cosmogenic isotopes					●	●		

●: well-suited materials ⊖: results may sometimes be unreliable ○: results often unreliable.

Timescales derived from stratigraphic evidence alone (e.g. magnetic susceptibility, grain size variation or organic carbon content) rest on assumptions and can create circular arguments. The measurement of amino-acid racemisation in fossil gastropod shells (relatively common and often well-preserved in loess) is a stratigraphic correlation technique which, at its best, can identify single isotope stages (Moore and Oches, 2002). Oches *et al.* (2004) have combined racemisation rates for different amino-acids in single shells with radiocarbon and luminescence dates to calculate mean soil palaeotemperature

post-burial. Fission-track dating can be used only where loess contains tephra (e.g. Westgate *et al.*, 2000). U-Th disequilibrium dating is unsuitable for pedogenic carbonate nodules ('loesskindl') due to open system behaviour (Stirling *et al.*, 2000). Radiocarbon dating, using Accelerator Mass Spectrometry (AMS), can directly measure ^{14}C in finely-disseminated organic debris in loess (Hatté *et al.* 1999, 2001) with errors limited to ±100 years *c.* 12 ka BP, rising to ±1200 years *c.* 35-40 ka BP (Lang *et al.* (2003). However, this only covers part of the last ice age; to cover the whole, luminescence dating is used, which can provides dates to at least 100 ka. Beyond then, magnetic susceptibility variation has been used to provide chronological control in the deep, continuous loess-palaeosol deposits of the Chinese Loess Plateau. MS variation can respond to climate change (see Section 3.4.5) and has been shown to parallel the ocean $\delta^{18}O$ record (see Section 1.2.1). This correlation technique is reinforced by analysis of the periodic (and well-dated) reversals of the Earth's magnetic polarity, preserved in these same sediments (An *et al.*, 1990).

3.5.2 Luminescence age determination

Luminescence dating was first used to date pottery (Kennedy and Knopf, 1960) but is extremely suitable for loess dating since it uses material that loess contains in abundance and it can potentially provide a depositional chronology for the whole of the last glacial-interglacial cycle. The technique measures the concentration of electrons held in 'electron traps' within the atomic lattices of feldspar and quartz crystals. If these crystals are exposed to light during their aeolian transport phase, the photon flux purges the traps and any latent luminescence signal is reduced to near-zero ('bleaching'). After burial the crystals are subject to continuous alpha, beta and gamma radiation from the decay of radionuclides (^{238}U, ^{232}Th and ^{40}K) naturally present in the sediment (plus a minor contribution from cosmic rays). This radiation can force electrons from their stable orbits into the traps and the crystals begin to acquire a trapped-charge population, in effect acting as local dosimeters. This trapped-charge population increases proportionally with burial time provided that the radionuclide concentration remains invariant. As a result, the time elapsed since burial can be determined by measuring the sample's sensitivity and the size of its luminescence signal and by estimating the flux of ionising radiation to which it has been exposed since burial (the 'dose rate') (Murray and Olley, 2002).

The emission of this stored signal can be stimulated in two ways: by heating the sample to *c.* 500°C (thermoluminescence - TL), and by exposing the sample to light of a specific wavelength (optically stimulated luminescence - OSL). Infra-Red Stimulated Luminescence (IRSL, a form of OSL) stimulates the luminescence signal from feldspars and zircon, but not quartz.

Luminescence dating contains intrinsic means of examining accuracy, including the comparison of ages obtained from the same sediment grains using different forms of luminescence stimulation. This was undertaken in some previous studies by using TL and IRSL multiple-aliquot additive and regenerative-dose protocols on fine silt polymineral fractions (Harmignies: Frechen *et al.*, 2001; Metternich: Frechen *et al.*, 1995). Each technique gave age estimates with relative errors of the order ±10-20%, and mean estimates made with different methodologies varied by as much as 70% for the same sample. The overestimation of TL ages, compared to IRSL ages on the same samples (apparent in the Koblenz-Metternich results) may indicate the existence of partial bleaching, which leads to the supposition that these IRSL ages are overestimates and represent only maximum ages. However, since (a) most of the luminescence signal emitted by polymineral fractions emanates from feldspars and (b) the datable signal within those feldspars may have suffered anomalous fading over the sample's burial period (Wintle, 1973), there is also the possibility that these 'maximum' ages may in fact be age underestimates.

In addition, the multiple-aliquot protocols used by Frechen *et al.* (1995) and Frechen *et al.* (2001) to evaluate the total dose exposure (from which luminescence ages are derived) can generate inaccurate and imprecise ages due to inherent complications arising from inter-aliquot normalisation and sensitivity change. These factors make it difficult convincingly to equate climatic change episodes dated by those chronologies with other records. There appears to be a requirement for an alternative chronological control for the study sites to assess the accuracy of the original chronology. This is sought in this study through recent developments in luminescence dating. These include the elimination of feldspars by acid digestion (Berger *et al.*, 1980; Jackson *et al.*, 1976) and improved protocols for determining the burial dose in quartz (Murray and Wintle, 2000)

3.6 Problems in interpreting the climate signal in loess-palaeosol sequences

Despite the detailed climatic information available from loess-palaeosol sequences, there are several aspects of their interpretation, especially in the European context, which present difficulties. The first problem is that the history of deposition in most loess sites is episodic, with periods of rapid deposition interrupted by long periods of non-deposition (e.g. Frechen *et al.*, 2001; Muhs *et al.*, 2004).

The second problem is that, as intimated above, it is impossible to develop an accurate loess chronology which comprehensively dates major, climatically-important events throughout the Weichselian. Luminescence ages developed for palaeosol horizons can only provide a chronology of deposition, not of pedogenic modification. The existing luminescence chronologies have relatively large errors which preclude the quantification of periods of rapid change.

The third problem is that loess and palaeosols are prone to erosion. Increases in rainfall or meltwater runoff are likely to remove surface layers. Palaeosols appear to be especially prone to erosion during the period between the end of the soil-forming episode and the re-start of loess deposition, which results in the loss of the A horizon and at least parts of the upper B horizons (e.g. lower Rhine valley loess sequences (Ikinger and Schirmer, 2002)). The loess record may also be affected by cryoturbation, solifluction and the deflation of existing loess sediment. These processes impose a lack of continuity on the loess-palaeosol record which cannot be resolved by even a detailed and accurate bed-by-bed chronology – missing evidence cannot be dated. This raises a fundamental problem: the datasets developed from the vertical profiles at the study sites are not continuous chronological sequences; they represent a series of stratigraphic 'islands', each ill-defined, of unknown duration and separated from the next by unknown periods of missing evidence. However, since the hiatus periods are unknown and largely unidentifiable, there is no alternative except to plot these datasets as seen.

Chapter 4. Loess in western Europe, and the study sites

4.1 Distribution and provenance

4.1.1 The loess of Belgium and northern France

This loess province was probably derived from sediment deposited in the southern North Sea basin. De Ploey (1964) found the same commonality of garnet, epidote and hornblende in Weichselian cover-sand deposits in northern Belgium that Baak (1936) identified in southeastern North Sea sediment and in Rhine fluvial sediments. Baak suggested that these North Sea sediments were deposited when the Rhine flowed southwards through the Straits of Dover. De Ploey concluded that these glacial cover-sand deposits had been formed from those North Sea sediments, remobilised by north-west winds. Lebret and Lautridou (1991) developed this argument to propose that North Sea sediment, exposed during glacial lowstands, provided the sand and silt for a major depositionary sequence which extends south-west from the southern Netherlands and Belgian coast, across central and southern Belgium and into northern France. They identified a diminishing grain-size gradient from the modern coast inland which they attributed to the effects of predominantly north-western palaeowinds transporting grains southeastwards from those deflation areas (Figs. 2.3, 2.4). However, this gradient cannot be taken entirely at face value: at least some major sand sheets formed in north-west Europe during a late Weichselian arid phase between 14-12.4 ka (Kasse, 1997) and so this gradient may be diachronous.

Fluvial sediment has been deposited in the southern North Sea basin as deltas and off-shore fans since at least MIS 22 (Lericolais *et al.*, 2003); during glacial low-stands fresh sediment must have been deposited sub-aerially by strongly seasonal Rhine and Meuse outflows. In consequence, the sediments present in source area are likely to be complex and to have a wide range of ages

Balescu (1988) showed that quartz grains from Belgian coastal marine sediments of Eemian age have luminescence characteristics similar to those of the Belgian and northern French loess while quartz grains from a North Sea source close to the outwash zone of the Scandinavian ice-cap have different luminescence characteristics. Balescu's measurements were made on multi-grain aliquots and so represent an average of the grains present. However, they reinforce the 'fluvial sediment' argument and suggest that material of directly glacial, Fennoscandian origin does not contribute significantly to the northwestern European loess story.

4.1.2 Rhine Valley loess

The Rhine originates in the Central Alps of Switzerland and flows northward to the North Sea through a series of grabens that extend to the complex tectonic area of the North Sea basin (Fig. 4.1). It has a total length of 1360 km and a drainage area of 225,000 km^2 (Allen 1997). During the Weichselian, the lower Rhine was a braided river system but it is now channelised and controlled (Lang *et al.*, 2003).

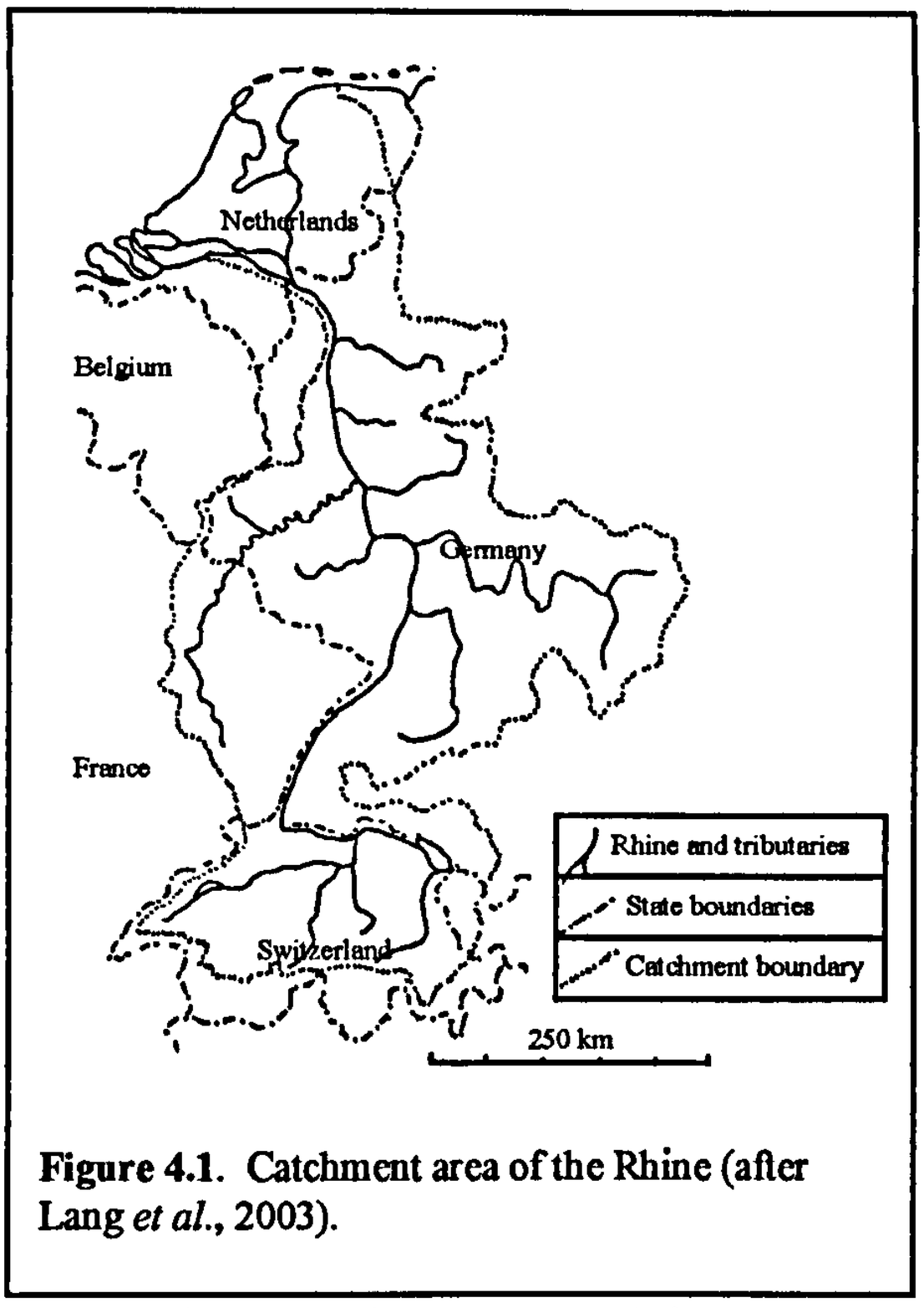

Figure 4.1. Catchment area of the Rhine (after Lang *et al.*, 2003).

The Alpine part of the Rhine is formed by the Reuss and Aare tributaries in the west and the Rhine in the east (*ibid.*) This area makes up only 4% of the drainage, but it has the highest topography and fastest erosion, producing half of the long-term sediment yield of the Rhine (Bernet *et al.*, 2004). The rocks here have been heavily tectonised by the Alpine orogeny; they include granite, continental basement, metamorphic and sedimentary rocks which include calcitic and dolomitic limestone (Ramsay, 1963). The remaining Rhine sediment fraction is derived from complex and varied geological environments downstream and some is also supplied by tributaries. Rock types in those areas include basement rocks, Mesozoic and Cenozoic sediments, metamorphosed Devonian mudstones/sandstones and volcanoclastic deposits (Bernet *et al.*, 2004).

During ice ages, intensive high-altitude weathering and glacial action in the Alpine drainage area must have produced immense volumes of clastic debris. This must then have been transported northwards along the Rhine valley by summer meltwater floods, supplemented by tributary contributions. As a result, the grabens now contain beds of Tertiary and Quaternary fluvial sands and gravels several hundred metres thick (Lang *et al.*, 2003). As each annual floodwater pulse receded, large areas of fine-grained sediments – clay-poor, moderately sorted, unconsolidated and unfrozen – would have been exposed to deflation, resulting in the deposition of loess in beds on both sides of the river (Smalley, 1975). However, only some of these areas would have suitable topographic and other conditions to support long-term accumulation. Elsewhere, these new sediments would be washed down-slope and probably back into the Rhine. The grains forming Rhine valley

loess may thus have undergone multiple cycles of fluvial and aeolian transport before their final deposition, which is likely to have resulted in strong homogenisation. Balescu (1988) used a combination of heavy mineral content and thermoluminescence characteristics to show that Rhine loess (at Ariendorf) closely resembles Rhine fluvial sediment.

Rhine loess, at least from the Moselle confluence onwards, probably contains volcanic mineral particles derived from the abundant and extensive Tertiary and Quaternary volcanism of the Eifel region. This produced potassium-rich, silica-poor scoria cones, which are typical for intraplate, continental settings (Ritter *et al.*, 2001; Bogaard, 1995). Hand specimens obtained locally contained large biotite crystals. There is also evidence from this study that loess at Metternich contains material eroded from the Rhenish massif and sedimentary rocks south of that massif.

4.1.3 Mineralogical composition

Swineford and Frye (1955) compared samples of, *inter alia*, Rhine Valley and Belgian loess with Kansas loess using microscope, chemical and X-ray diffraction techniques. The size distribution quoted in that paper suggests that Swineford and Frye did not consistently sample 'primary loess'; their Rhine valley samples contained coarse lithic fragments and particles larger than 250 μm. The main constituent of the sand/silt fraction was angular to well-rounded clay-coated quartz grains with some iron oxide staining, plus feldspar, calcite and small amounts of other mineral grains. The clay fraction contained calcite, quartz, illite and kaolinite.

The Belgian loess sand/silt fraction contained angular to sub-rounded quartz grains stained with iron oxides, less feldspar than the Rhine valley loess, plus muscovite and biotite. The clay fraction contained substantial amounts of montmorillonite, plus kaolinite, calcite and quartz (*ibid.*). It was suggested that (a) at least some of this loess was derived from a 'deeply weathered region', not from glacially-abraded crystalline rocks, and (b) that the mineralogy of both the coarse and the fine fractions was controlled by the source; the variation between samples could be attributed to the difference in source areas (*ibid.*).

Other mineralogical examinations of European loess reveal a wider range of minerals. Doeglas (1949) summarised earlier studies to demonstrate that the heavy mineral fraction of loess in the southern Netherlands contains a mix of igneous and metamorphic minerals. Epidote, garnet, zircon, rutile and hornblende each contribute 10-30%, and tourmaline, brookite (titanium oxide), titanite, kyanite, staurolite and andelusite are below 5%. 'Opaques' contribute more than 30%. Garnet, hornblende, pyroxene, tourmaline and zircon are Rhine valley loess components (Boenigk *et al.*, 1994). This

range of igneous and metamorphic minerals can be attributed to the variety of source rocks in the Rhine catchment area.

4.2 The study sites

4.2.1 Harmignies

The Harmignies site is located in the aeolian belt that stretches from the Netherlands coast south-east into northern France (Fig. 2.4). Haesaerts and van Vliet-Lanoë, both major researchers in western European loess, consider it to be one of the most important sites for loess research in Belgium and northern France (e.g. Haesaerts and van Vliet, 1973). Apart from one horizon which was heavily gullied, Frechen *et al.* (2001) consider that the site shows little evidence for reworking by sheetwash or solifluction compared to many others in this general area.

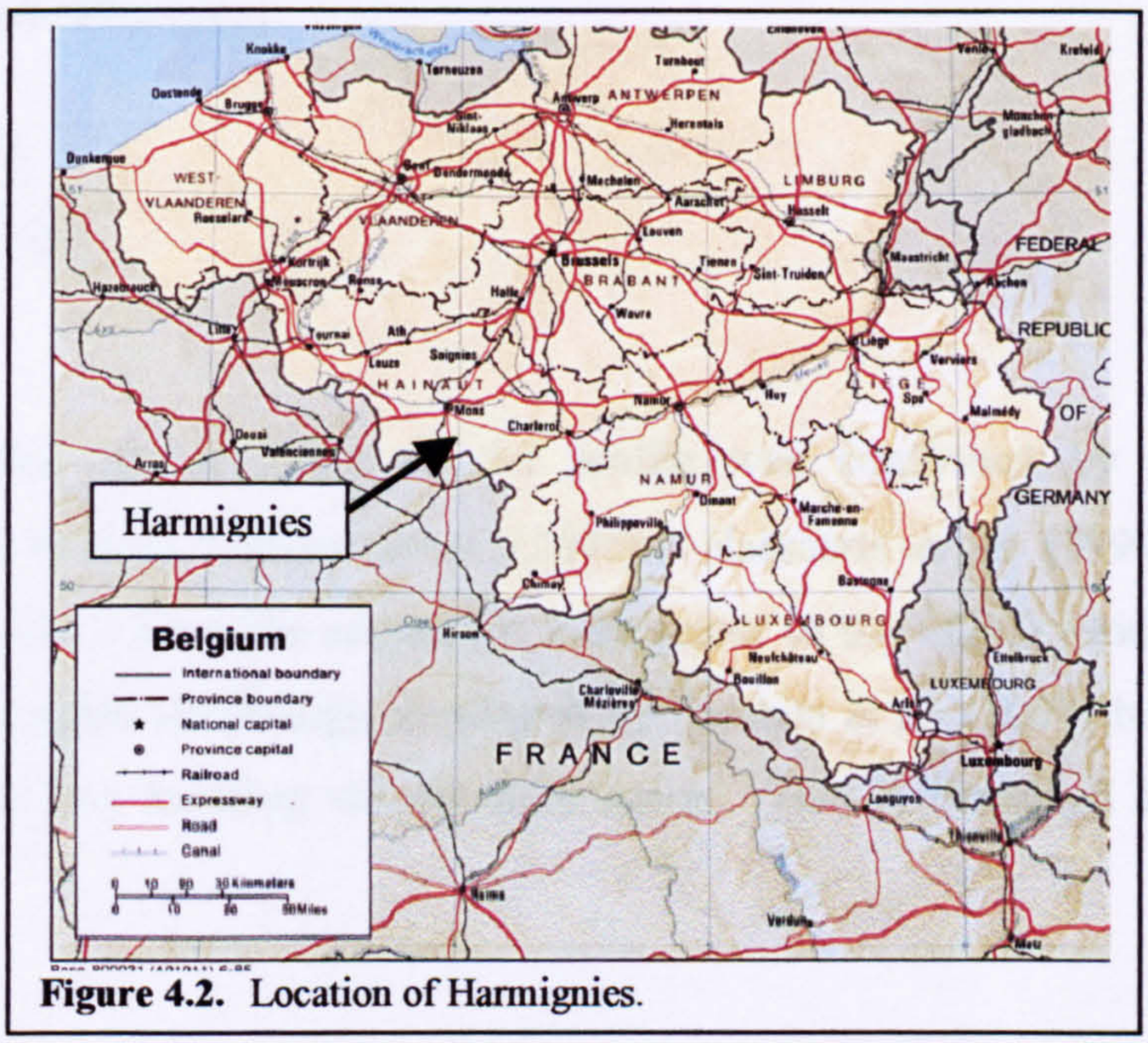

Figure 4.2. Location of Harmignies.

It is located in southern Belgium, at 5041N 0402E (Fig. 4.2). The topography is subdued and is controlled by the underlying Cretaceous chalk. At the 'Cuesta D'Harmignies', a low ridge oriented ENE-WSW falls steeply to the SSE. This is being heavily quarried from the south for cement production. As quarrying operations progressively cut northwards into the ridge, the loess and topsoil overburden in a strip 10-20 m wide along the quarry edge is regularly bulldozed clear, down to bedrock, to prevent it slumping into the quarry working area. This planar face, approximately 12 m high, formed the research working area.

The site was periodically within the European permafrost zone and contains a range of ice segregation features, including ice lenses, cracks and large ice wedge formations with polygonal distributions (van Vliet, 1975). This indicates that the local climate was at least periodically humid and van Vliet-Lanoë (pers. comm.) suggests that loess deposition here was not controlled primarily by topography, as appears to be the case at Metternich, but by surface wetness, with grains trapped as they hit the surface. This could explain why deposition here is on the upwind slope and ridge top. The limited exposures visible on the

lee slope suggest that much less loess was deposited there, although lee-slope deposition might be expected as a consequence of a slowing airflow. However, this apparent thinning may be an artefact of mass wasting, agricultural erosion and other forces.

This study uses the stratigraphic assignments developed in Haesaerts (1973) and in van Vliet's (1975) detailed pedological study of the site (Fig. 4.3). Due to the site's topography when fieldwork was in progress, it was not possible to examine the full vertical sequence as a single profile. With the field assistance of van Vliet-Lanoë, the major stratigraphic units were identified in three separate, overlapping sections. This provided the maximum vertical continuity but as a result, the vertical profile shown in this study is composite. The three profile sub-units cover:

(a) bedrock to top of Unit D,
(b) Unit D to top of Unit F, and,
(c) Unit F to Unit L.

The general Weichselian age of most of the profile was confirmed by a luminescence chronology presented in Frechen *et al.* (2001). Haesaerts *et al.* (1999) assigned a date of approximately 23 ka to the uppermost loess (close to the LGM) which accords with the luminescence-based chronology developed by Frechen *et al.* (2001) but dates and attributions for other key horizons do not fully agree. This is examined in Section 6.8.1.

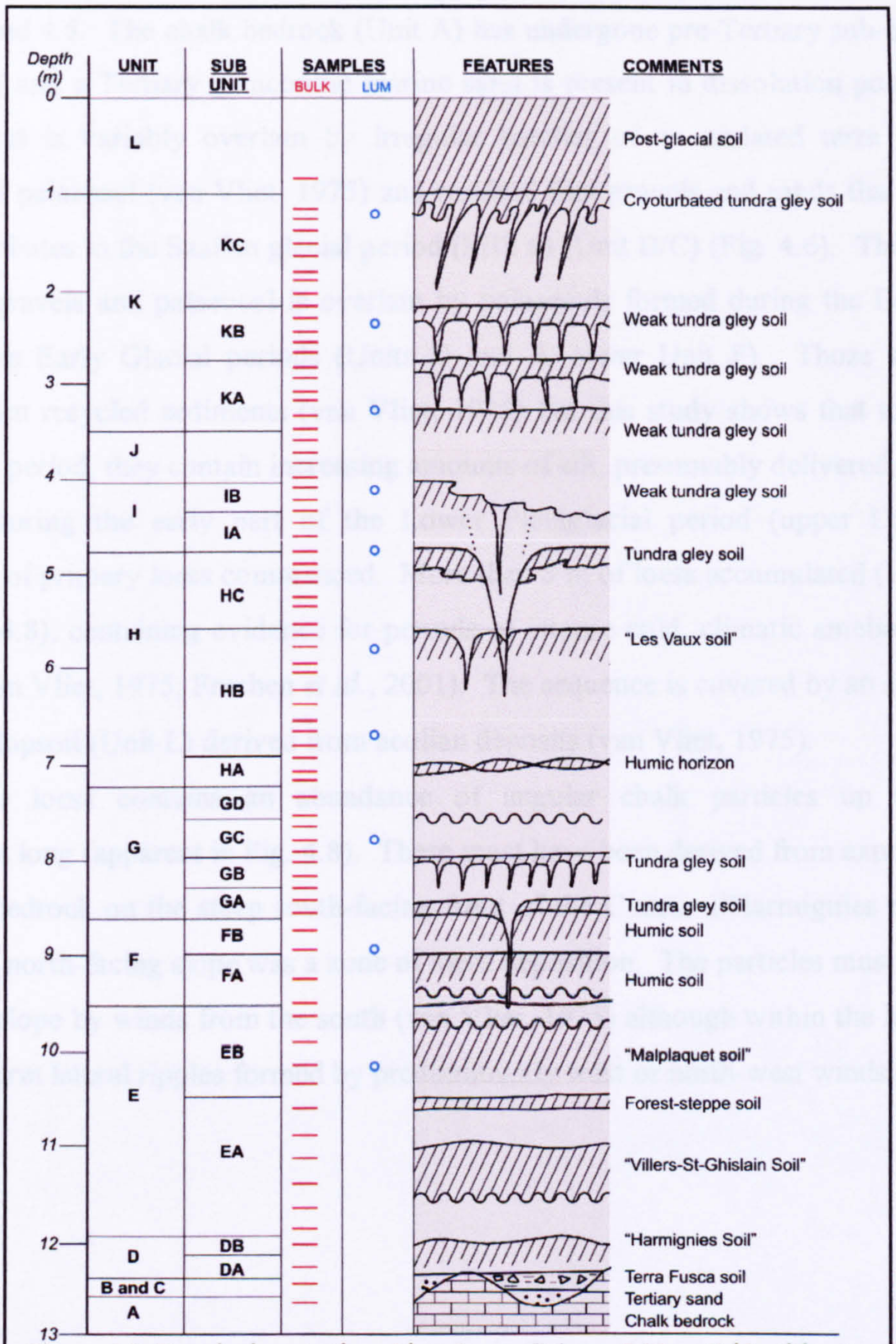

Figure 4.3. Harmignies: stratigraphic column. Column 5 ('Lum') identifies the locations of luminescence samples. Column 6 shows soil horizons, together with indications of large and small ice wedges and cryogenic involutions. (after van Vliet 1975; Haesaerts *et al.*, 1999; Frechen *et al.*, 2001).

A general view of the quarry and the relative location of the loess face is shown in Figs. 4.4 and 4.5. The chalk bedrock (Unit A) has undergone pre-Tertiary sub-aerial karst weathering and a Tertiary glauconitic marine sand is present in dissolution pockets (Unit B/C). That is variably overlain by irregular patches of an undated terra fusca-type interglacial palaeosol (van Vliet, 1975) and residual flint gravels and sands that Haesaerts (1998) attributes to the Saalian glacial period (MIS 6) (Unit B/C) (Fig. 4.6). This complex of sands, gravels and palaeosol is overlain by palaeosols formed during the Eemian and Weichselian Early Glacial periods (Units D and E, lower Unit F). Those are mainly formed from recycled sediments (van Vliet, 1975) but this study shows that towards the end of this period, they contain increasing amounts of silt, presumably delivered by aeolian action. During the early part of the Lower Pleniglacial period (upper Unit F) the deposition of primary loess commenced. More than 8 m of loess accumulated (Units G-K) (Figs 4.7, 4.8), containing evidence for periods of intense cold, climatic amelioration and erosion (van Vliet, 1975; Frechen *et al.*, 2001). The sequence is covered by an agricultural Holocene topsoil (Unit L) derived from aeolian deposits (van Vliet, 1975).

The loess contains an abundance of angular chalk particles up to several millimetres long (apparent in Fig. 4.8). These must have been derived from exposed, frost-shattered bedrock on the steep south-facing front of the Cuesta d'Harmignies ridge since the gentle, north-facing slope was a zone of loess deposition. The particles must have been blown up-slope by winds from the south (van Vliet, 1975) although within the loess, some particles form lateral ripples formed by predominantly west or north-west winds (*ibid.*).

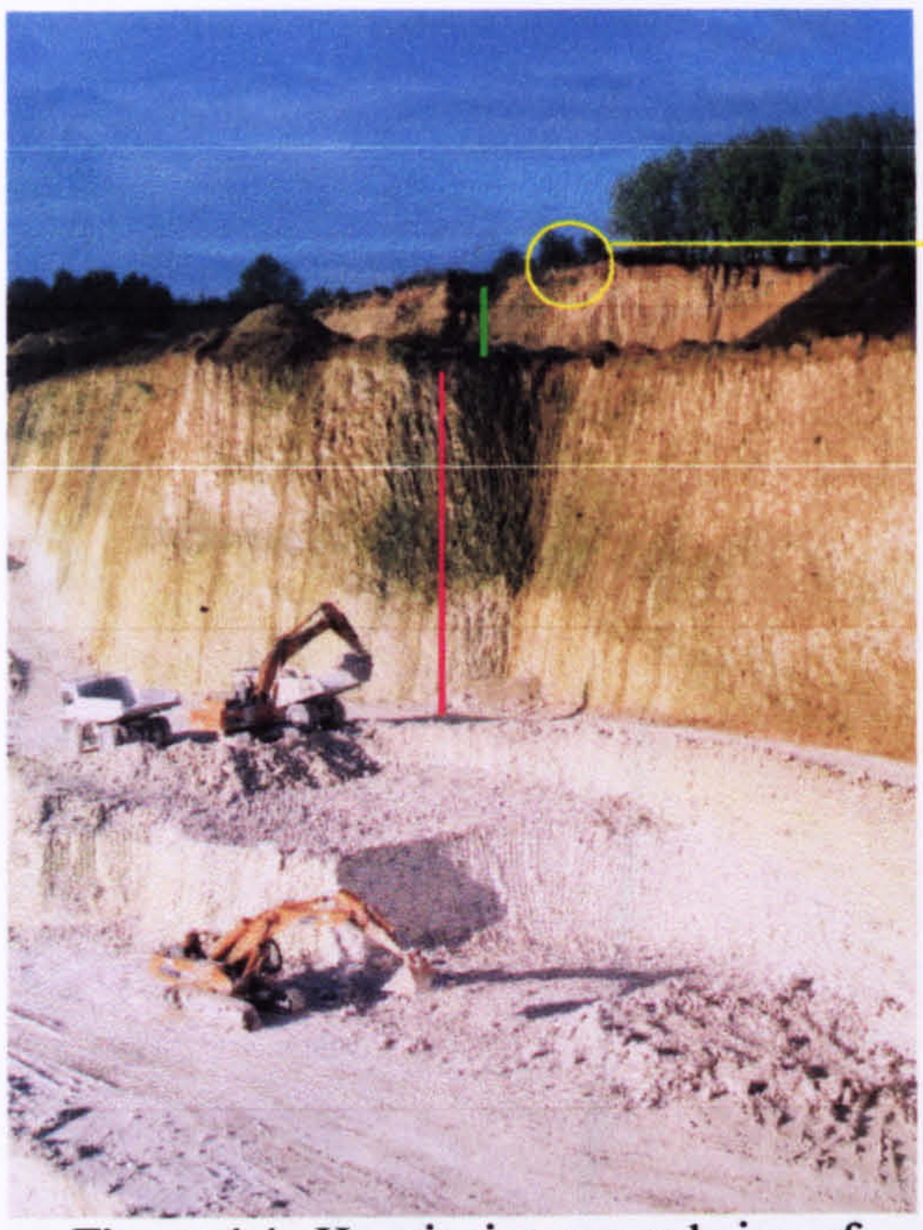

Figure 4.4. Harmignies: general view of quarry, showing chalk (red), stained by soil and algae, and loess (green). The post-glacial soil is circled.

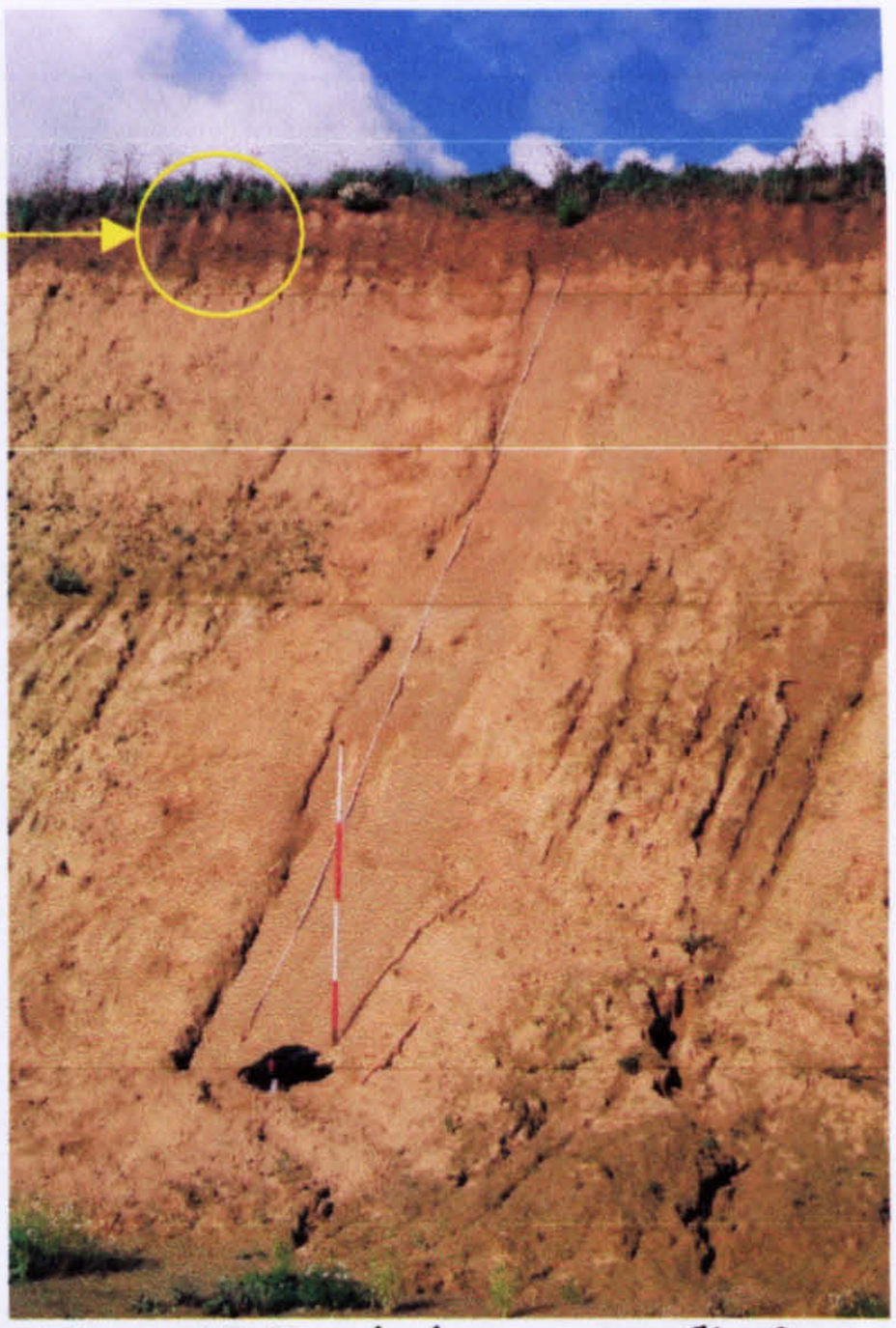

Figure 4.5. Harmignies: upper profile, from Unit F to Unit L (post-glacial soil) (2 m survey pole for scale).

Figure 4.6. Harmignies: lower profile, showing karst chalk bedrock and lowermost palaeosol units (2 m survey pole).

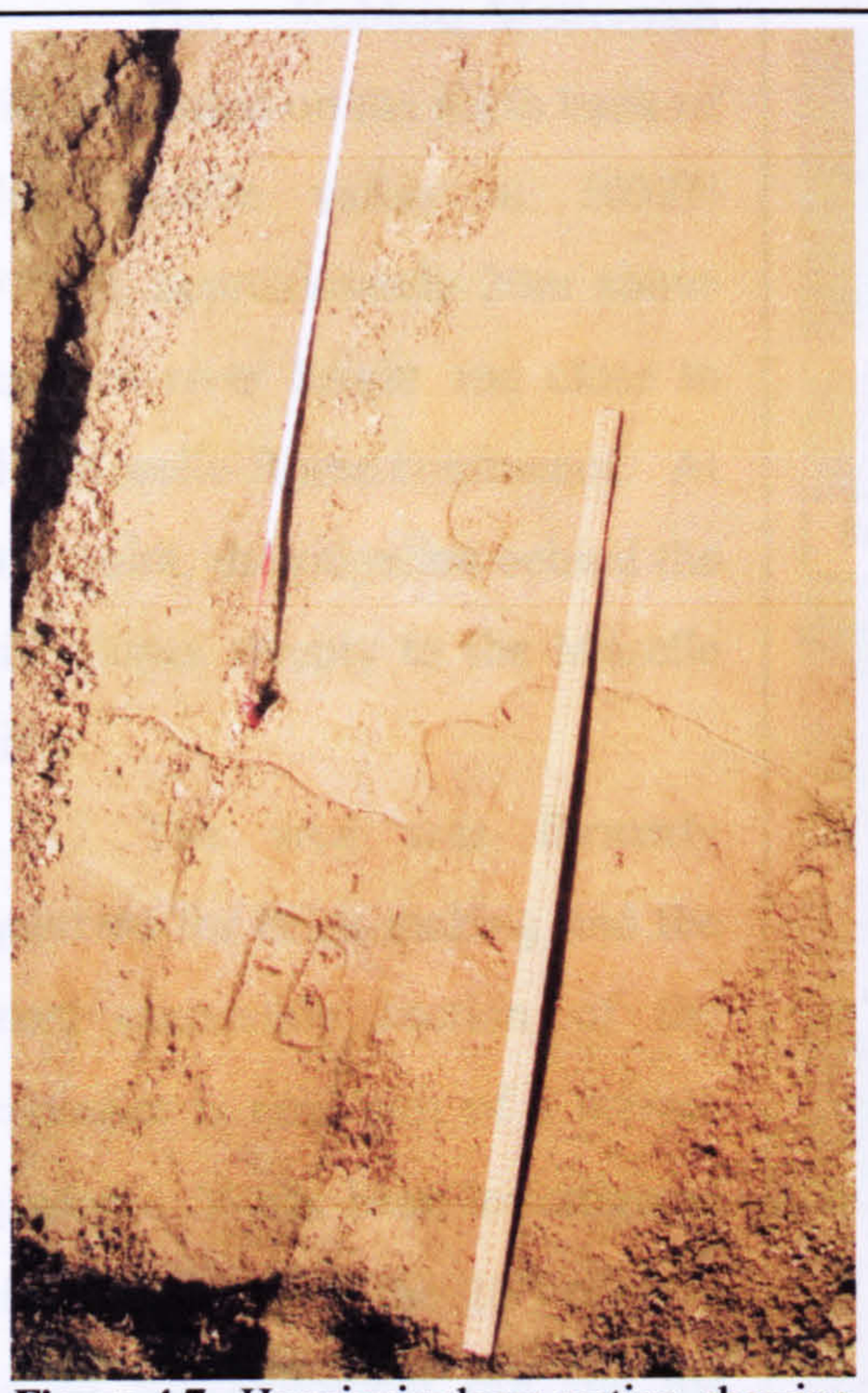

Figure 4.7. Harmignies loess section, showing upper Unit F (cryoturbated) and lower Unit G. 1 m ruler at right

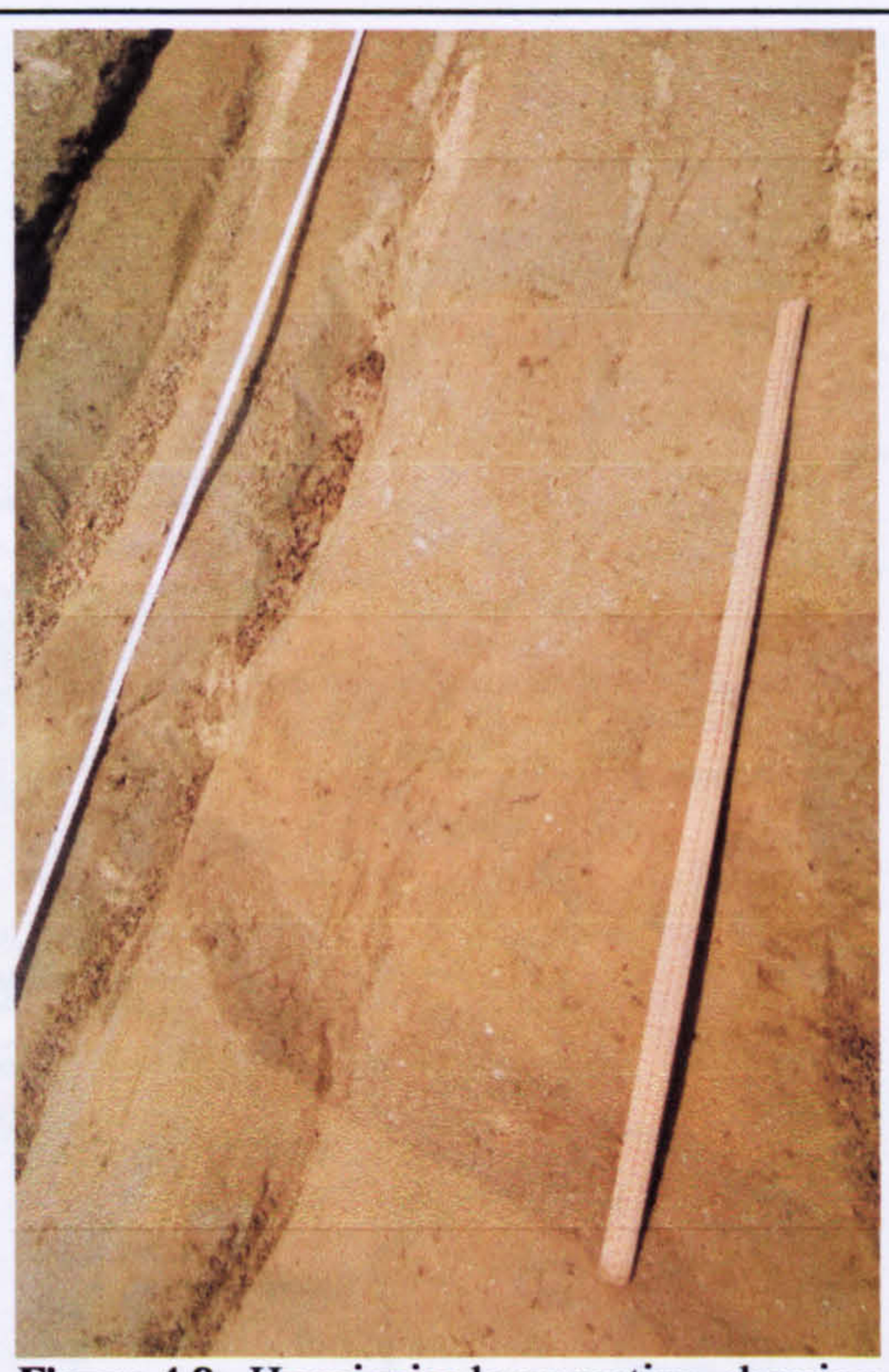

Figure 4.8. Harmignies loess section, showing upper Unit G, a cryoturbated humic horizon at the base of Unit H and part of Unit H. The white speckles are large chalk particles. 1 m ruler at right.

4.2.2 Koblenz-Metternich

The Koblenz-Metternich site is located on the north bank of the Moselle valley at 5037N 0755E, approximately 20m above modern river height and close to the Moselle-Rhine confluence. At this point, the ridgeline behind the site slopes steeply to the Moselle river.

Figure 4.9 Location of Koblenz-Metternich.
Map courtesy of www.theodora.com/maps, used with permission.

The area was formerly quarried for brick-making and the most accessible section of the exposure is now part of a private garden . It has been investigated since the start of the 20th century as an archaeological site and for its stratigraphy, and is a protected 'natural monument' (Boenigk and Frechen, 2001). It is considered to contain a fully-representative history of loess deposition in the central Rhine valley during the Weichselian (Frechen, pers. comm.). The former working face of the quarry is wooded and forms near-vertical, east-facing cliffs approximately 20-25m high, against the steep bedrock slope up to the ridgeline. These cliffs extends south-westwards (upstream) for a few hundred metres and appear to thin and vanish against a steepening valley slope. Within fifty metres north-eastwards, it thins to a few metres in thickness where a valley must have carried surface water down from the ridge. The vertical profile is not accessible in one continuous sequence; previous workers have cut a series of ledges that provide moderate support for ladders. In consequence, the Metternich vertical profile used in this study is, like that for Harmignies, composite.

A luminescence chronology by Frechen *et al.* (1995) proved that most of the profile is Weichselian; units below the current ground level extend to the Eemian.

The profile has not previously been divided into a series of well-defined units and so an arbitrary, simplified stratigraphy has been developed here, based partly on stratigraphic variation and partly on depth (Fig. 4.10). Unit 1 is pre-MIS 5a loess; Unit 2 is the early Weichselian palaeosol complex; Unit 3 starts with the loess marker horizon and continues up to 16 m depth; it includes the transition to primary loess deposition. Unit 4

extends from 16 to 12 m and Unit 5 from 12 to 1 m depth. Both contain primary and reworked loess, with gravel horizons. Unit 6 is the overlying post-glacial soil.

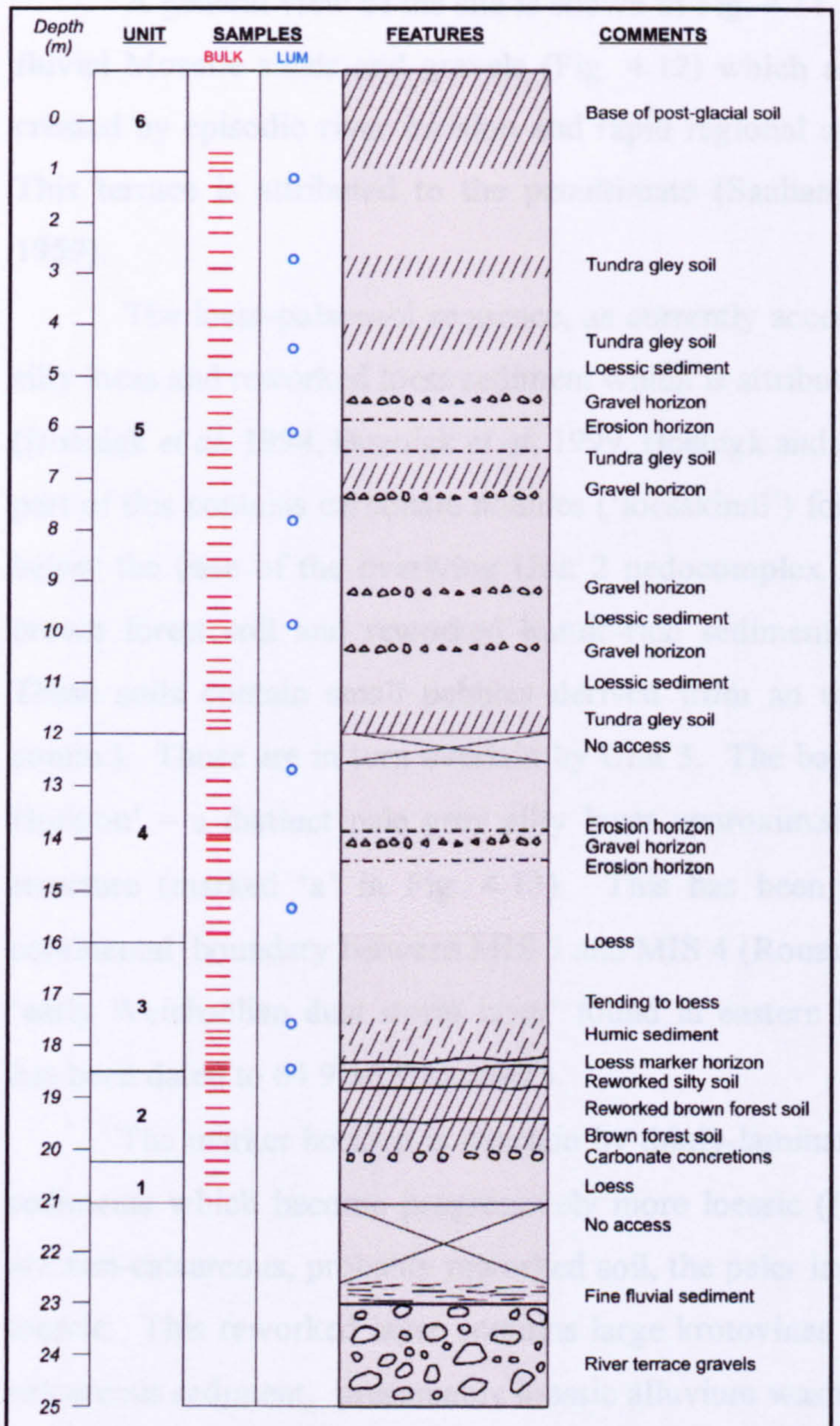

Figure 4.10 Metternich: stratigraphic log. Column 4 ('Lum') identifies the locations of luminescence samples. Column 5 shows soil horizons, together with indications of gravel and eroded horizons (after Boenigk *et al.* 1994; Boenigk *et al*, 1999; Boenigk and Frechen, 2001).

A general view of the site is shown in Fig. 4.11. The base of the sequence rests on fluvial Moselle sands and gravels (Fig. 4.12) which are part of a river terrace complex created by episodic river incision and rapid regional uplift (e.g. Meyer and Stets, 2002). This terrace is attributed to the penultimate (Saalian) glacial period (Remy and Paas, 1959).

The loess-palaeosol sequence, as currently accessible, begins with a layer of grey, silty loess and reworked loess sediment which is attributed to a glacial stage before MIS 5a (Boenigk *et al*, 1994, Boenigk *et al*, 1999, Boenigk and Frechen, 2001) (Unit 1). The upper part of this contains carbonate nodules ('loesskindl') formed by calcite reprecipitation just below the base of the overlying Unit 2 pedocomplex. This includes the B Horizon of a brown forest soil and reworked humic-rich sediments attributed to MIS 5d-5a (*ibid.*). These soils contain small pebbles derived from an upper terrace level (Frechen, pers. comm.). Those are in turn overlain by Unit 3. The base of this unit is the 'Marker Loess Horizon' – a distinct pale grey silty layer approximately 3-6 cm thick without internal structure (marked 'a' in Fig. 4.13). This has been suggested to mark the European continental boundary between MIS 5 and MIS 4 (Rousseau *et al.*, 1998). It equates to the 'early Weichselian dust storm layer' found in eastern France and eastern Europe, which has been dated to 64.9 ±6.9 ka (*ibid.*).

The marker horizon is overlain by thinly-laminated brown and grey-buff reworked sediments which become progressively more loessic (Fig. 4.13). The darker laminations are non-calcareous, probably reworked soil, the paler laminations are calcareous and more loessic. This reworked layer contains large krotovinas (animal burrows) filled with pale, calcareous sediment, presumably loessic alluvium washed into the burrow (marked 'b' on Fig. 4.13). Within approximately 2 m these sediments become homogeneous buff-grey calcareous loess and the remainder of the vertical section (upper Unit 3, Unit 4 and 5) continues as homogeneous loess which lacks obvious palaeosol layers (Figs. 4.14-4.16). It contains infrequent lenses and thin layers of fine gravel with angular schist fragments and rounded, weathered, quartz pebbles up to *c.* 2 cm. These were not sampled. Boenigk *et al.* (1994) also identified several tundra gley soils ('Nassboden') in this part of the profile (Fig. 4.9): these could not be detected during this study's fieldwork. At the top of the section, the loess merges rapidly into the Unit 6 post-glacial soil and appears to have provided the parent material for at least that soil's C horizon.

Evidence for modification by surface flow is present elsewhere in the loess profile, including erosion surfaces and thin, wedge-shaped beds of loessic alluvium. Although those particular features were not observed at the study section, it is likely that coarse material was washed down-slope from older river terraces higher on the valley side.

Figure 4.11. Metternich: general view of the loess profile, showing approximately 15 m of the total 21 m vertical profile examined in this study .

Figure 4.12 Metternich: fluvial gravels marking the basal river terrace, overlain by fine fluvial sediment.

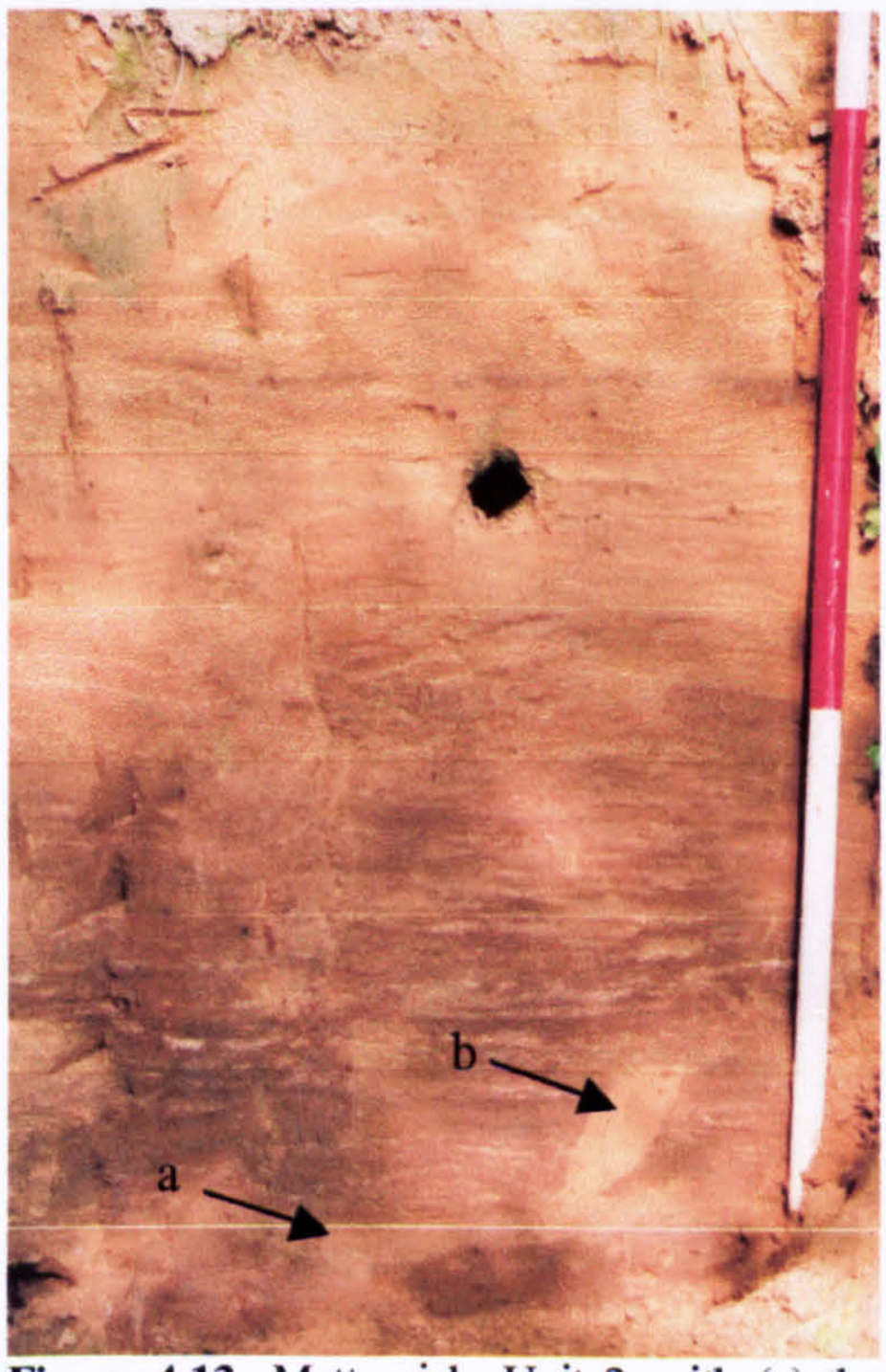

Figure 4.13 Metternich: Unit 3, with (a) the loess marker horizon , and (b) a prominent animal burrow (krotovina). The reworked dark soil and paler loessic sediment becomes more loessic upwards (hole in upper centre is from previous luminescence sampling).

Figure 4.14 Metternich: mid- and upper sections of the profile, showing successive sampling levels.

Figure 4.15 Metternich: limited access to profile mid-section.

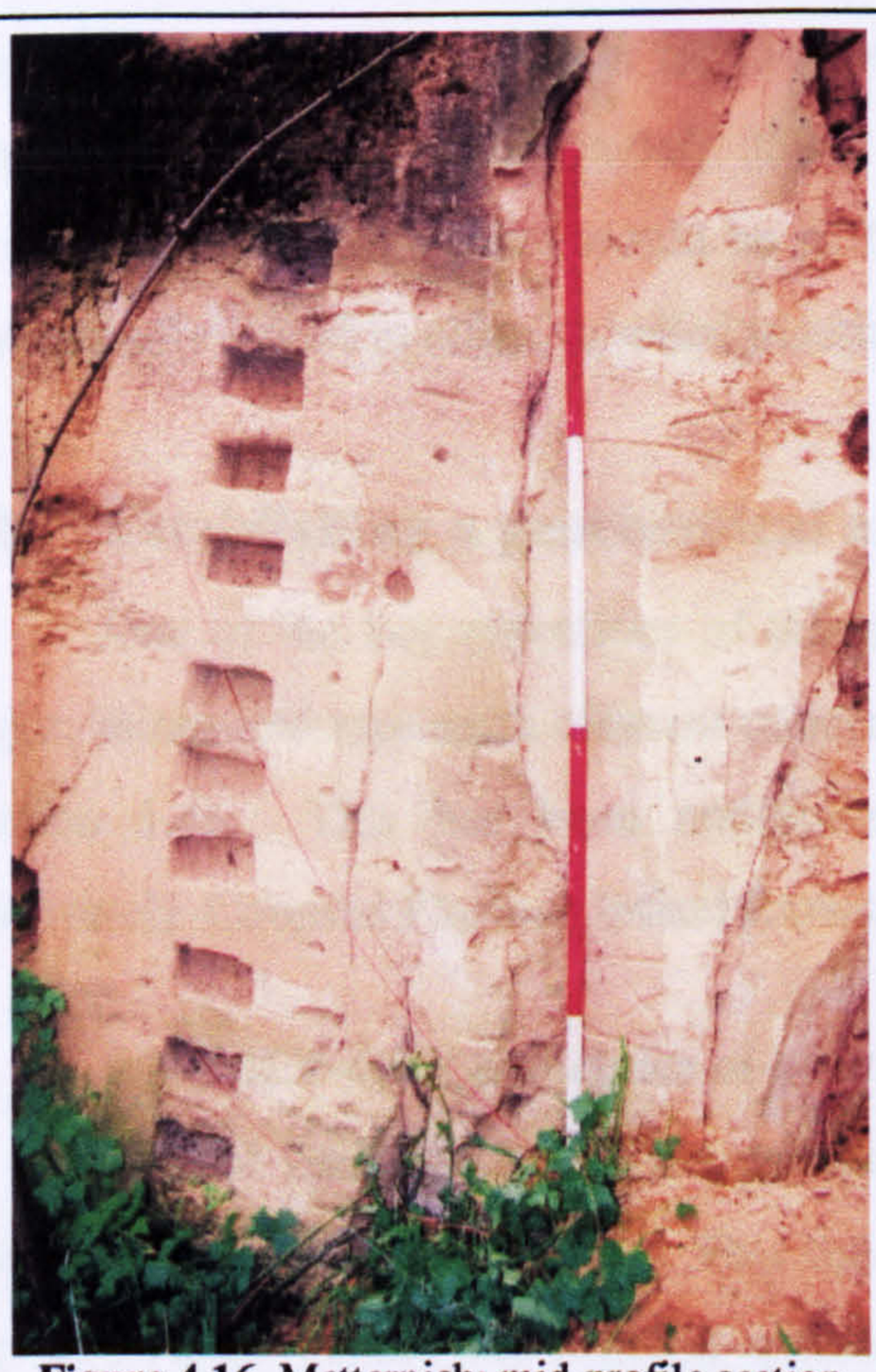

Figure 4.16 Metternich: mid-profile section showing sample collection slots. The 'X' symbols engraved in the face mark gravel horizons (not sampled).

Chapter 5: Field and Laboratory methodologies

Double, double toil and trouble;
Fire burn and cauldron bubble....
[Macbeth: 4.1, Shakespeare, W.]

5.1 Sample collection methodology

Individual samples, approximately 50 mm thick, were collected at intervals which would return approximately 80 samples from each site. Only one sample was taken at any one horizon: it is accepted that single-point sampling cannot fully represent the lateral variation that is likely to be present.

Samples were collected from the 12 m vertical profile at Harmignies at approximately 150 mm intervals, and from the 21 m profile at Metternich at approximately 350 mm intervals. Samples were cut parallel to any visible laminations and where observable changes in lithostratigraphy occurred, sample spacing was modified to ensure proper representation. The existing chronologies (Frechen *et al.*, 1995; Frechen *et al.*, 2001) give an average of approximately 700 years between samples, and substantially less than this during periods of rapid loess deposition. The thin gravel horizons at Metternich were examined in the field but not sampled. The condition of the loess faces, especially at the latter site where parts of the long-exposed face were extremely dry and hard, precluded the use of Teflon® tools to clear the face and to extract samples; clean stainless steel tools were used instead. Approximately 350 g of sediment were collected from each sample location to ensure that there would be sufficient material for the analyses. Samples were immediately stored in clean, labelled plastic bags.

5.2 Establishing a geochemical analytical methodology

One of the key objectives of this study is to produce detailed descriptions of the major, minor and rare earth element concentrations of the full sample set for each site (see Section 1.4). This has been undertaken using the PerkinElmer® Optima 4300DV Inductively-Coupled Plasma Optical Emission Spectroscope (ICP-OES).

5.2.1 ICP-OES principles of operation

Optical emission spectroscopy measures the light produced by atoms that have been stimulated to high energies. This light is emitted at element-specific wavelengths in the ultra-violet, visible and infrared spectrum. The complex spectrum of light emitted by multi-element samples can be reduced to specific spectral lines of interest and quantified,

allowing the elemental concentration in the sample to be measured precisely and accurately.

The Optima 4300 is capable of analyzing tens of elements simultaneously; additional analytes do not require additional measurement time. This instrument has a dual-view optical system which examines light emitted from the side of the plasma (radial view) or along the plasma axis (axial view). Axial viewing provides higher light intensities than radial, allowing low-emission and high-emission elements to be measured simultaneously. Each analytical result has been automatically averaged from three replicate measurements taken in rapid sequence.

The Optima 4300 instrument has a highly stable radio frequency generator which induces intense, oscillating magnetic and electric fields within the torch. Those fields maintain an extremely stable argon plasma at approximately 7000-8000K (PerkinElmer, 2000).

The liquid samples are converted to a fine aerosol in a cross-flow nebuliser, with argon as the shear gas, and delivered to the heart of the plasma. At this point the droplets vapourise into a molecular gas which is then dissociated into its component atoms. These atoms move vigorously in the intensely-hot plasma field; they collide with other particles and absorb electromagnetic energy in a process of 'excitation' which either promotes some of their component electrons from stable ground state orbitals into higher energy states, or which liberates electrons from their atoms (ionization). Atoms have a residence time in the plasma of about 2 milliseconds and as these unstable atoms move forward in the argon stream, they decay back to stability either by re-absorbing free, high-energy electrons or by transferring electrons from high-energy orbitals back to stable ground state orbitals. In either case, the quantum energy loss is achieved by emitting photons with elementally-characteristic wavelengths and the light intensity for each element is governed by the fraction of atoms excited to the higher energy state. The potential number and wavelengths of spectral lines for any one element depends on the number of electrons in the atom and the number of energy steps involved in electron shell movement. Under the intense excitation conditions found in an inductively-coupled plasma, some elements (e.g. iron and cobalt) generate many spectral lines, others (e.g. boron) generate very few. This does allow the user to select from a range of spectral lines for any one element but it also increases potential spectral interference. Elements have differing excitation energy requirements and so will produce widely-differing emission counts for the same sample concentrations (Boss and Fredeen, 1999).

In the Optima 4300, the total emission spectrum is spread by an echelle grating and, for visible light, a prism, before being directed to the segmented-array charge-coupled-

device detectors. Two hundred and thirtyfive sub-arrays on the detectors are automatically positioned at the physical locations of the pre-selected emission lines as generated by the optical system (PerkinElmer, 2000). They measure the incident radiation and produce intensity readings. Comparison of these values against previously-determined intensities for standards of known composition then provides elemental concentrations (see Section 5.2.2). The PerkinElmer software provides a list of available spectral lines for each element, ranked by a range of performance characteristics. Experimentation proved that the 'default' recommendations were the most suitable for analysis of loessic flux-fusion samples.

5.2.2 ICP-OES Calibration

ICP-OES is a comparative analytical technique: the signal intensity must be calibrated against standards in which the concentrations of the various elements of interest are known. There are two main calibration methods: using synthetically-prepared calibration standard solutions or using standard natural reference materials. It is vital for ICP stability that all solutions passing through it should be as closely-matched as possible, in terms of composition, the total dissolved solids content and the acid concentration of both the analyte solution and the wash solution. Although the lithologies of commercial rock standards differ from loess, the composition of the prepared sample is dominated by lithium and boron from the flux and effectively, the calibration standard solutions and the analytes are compositionally matched (Murray et al., 2000). The rock standards used for calibration must be prepared with the same reagents as the samples, from the same batches. In addition, a 'calibration blank', prepared with the same batches of reagents, is used to correct for any systematic contamination introduced by the sample preparation process.

The samples were analysed against a wide range of commercial silicate rock standards (Table 5.1), which were diluted by varying amounts to ensure that they covered the full range of sample element concentrations.

Compositional values were taken from Potts *et al.* (2000). Most of the major element values and some of the minor element values quoted for these standards have 'precision .... established to be better than 10% relative (two sigma)'; precision values for the remainder are unquantified. The calibration curves achieved towards the latter end of the process of developing a satisfactory operational methodology had quality of fit better than .999.

Table 5.1. Rock standards used as ICP calibration standards

Reference standard	Rock type	Source
AGV-1	Andesite	United States Geological Service (USGS)
BR	Basalt	Centre de Recherches Petrographique et Geochimiques (CRPG)
DNC-1	Diabase	USGS
GA	Granite	CRPG
G-2	Granite	USGS
JB-1	Alkali Basalt	Geological Survey of Japan (GSJ)
JG-1a	Granodiorite	GSJ
SARM-1	Granite	South African Bureau of Standards (SABS)
SCo-1	Cody Shale	USGS
SY-3	Syenite	Canadian Certified Reference Materials Project (CCRMP)
W-2	Diabase	USGS

5.2.3 Problems in developing a reliable ICP-OES methodology for major element analysis

The major element compositions of rock samples are conventionally expected to total 100±1%. ICP-OES instruments have inherent levels of variation that make this a demanding target (Walsh, 1992).

The procedures for major element preparation and analysis were developed from an initial low level of understanding and underwent successive evolutionary stages to identify the conditions that provided suitable levels of stability and accuracy. During the initial stages of this study, the Optima 4300 produced unacceptable results, with significant sample-to-sample variation and long-term drift. This necessitated a complex and prolonged method development process.

In attempts to minimise problems that might have been induced by the Optima 4300 system, the peristaltic pump tubing was replaced ahead of schedule, the axial and radial windows were replaced and the ceramic injector tube was replaced. PerkinElmer advised (pers. comm.) that Si was persistent and could remain in the system. Accordingly, the flow of auxiliary argon was increased, 0.8 M nitric acid was substituted for distilled water as the wash fluid and the inter-sample wash time was increased.

Despite this, successive analyses of single, representative loessic sample solutions continued to show short-term variation exceeding 10% and drift of several percent per hour. In contrast, analyses of water and acid leach samples for other applications returned

extremely precise and accurate results with virtually no drift, suggesting that the observed lack of precision related more to the nature of loessic samples than the Optima 4300 itself.

This problem was not unique: Walsh (1992) considered that although many factors contribute to the sample-to-sample inaccuracy widely observed in ICP-OES measurement of geological samples, the main cause is short-term change in nebuliser efficiency, and recommended the use of 'internal standards' to improve precision. These are high-purity solutions of one or more elements that are present in the original sample at negligible concentrations, added to each sample solution in precise and consistent amounts. The analysis run includes the internal standard as an analyte. If there are no system-induced errors, the concentration value for the internal standard should be the same in all samples. If there are system-induced errors, then successive internal standard concentration values will vary. However, since each successive reading relates to the same concentration value, the fluctuation is quantifiable and correctable. If all the measured elements were to co-vary with the internal standard, then this compensation factor could be applied uniformly to those readings, thus compensating for sample-to-sample variation and for long-term drift throughout that run. However, Walsh (1992) proved that elements do not all co-vary with these system-induced variations: different elements respond in different ways and must be referenced against different internal standards. Si, Al and Mg should be referenced against Ga, Fe and Ca against Cd, and the other alkali elements against Li.

With the support of ICP-OES users at Royal Holloway University of London, this study experimented with the use of Ga and Li as internal standards. A Ga stock solution was used as one internal standard and since Li was already present in the precisely-measured amounts of flux, this was used as the second. An extensive suite of experiments with bulk and individual sample solutions under varying operating conditions showed that Ga did co-vary with Si, Al and Mg but Li proved extremely variable. During some runs it appeared to co-vary closely with K and Na but during other runs Na, in particular, showed no covariance, and this could not be explained by changes in any machine or methodological parameters.

Further experiments were made at increasing sample dilutions, revealing that at a 2% sample concentration (i.e. a 50x dilution of the 'standard' sample, with a total dissolved solids value of 0.012%) the system produced stable and consistent results. Successive analyses of a representative bulk sample produced major oxides totals that varied within approximately ±1% of the 100% target, with minor sample-to-sample variation and little long-term drift, and successive single samples consistently produced totals within ±2% of the target 100%. This surprising but welcome improvement in performance negated any requirement for internal standards and this high-dilution flux-

fusion method was adopted for this study. Results that produced major oxide totals of 100 ±1.5% were accepted as valid. Those that did not were re-analysed and, where necessary, re-processed. This low sample concentration, combined with the poor detection limits for Na in the ICP system, meant that in some samples K, Na and P results were below the 'quantitative' threshold. However, concentrations were higher in samples that had been prepared by acid digest processes for minor element analysis, and prior Optima 4300 analysis of those samples were comparable with those achieved by flux-fusion. It is, therefore, possible to combine these results.

5.3 Sample preparation procedures for major, minor and rare earth element analysis

The major, minor and rare-earth elements analysed in this study are defined in Section 3.3.1. All chemicals were analytical grade and deionised water was used for all dilutions and final rinse operations. All utensils, glassware etc. used in sample preparation were pre-cleaned in 10% HNO_3 and rinsed in deionised water.

Minor element analysis was carried out using original sample material. Major element and REE analysis was carried out using the ignited samples remaining after loss-on-ignition tests. This ensured that the sample:flux ratio remained constant. To avoid rehydration, these calcined samples were stored in a dessicator until they were needed.

5.3.1 Sample preparation for major element analysis

Samples prepared by HF digest were unsuitable for major element analysis since silica is lost; instead, the Totland *et al.* (1992) lithium metaborate ($LiBO_2$) flux-fusion method was used. This process is rapid, cost-effective and relatively safe but volatile minor elements are lost (including Pb, Sn, Sb, Zn, plus structural water and CO_2). The process creates high concentrations of total dissolved solids (TDS) in sample solutions and the procedural blanks, leading to high detection levels.

Sub-samples were ground to a fine powder in an agate pestle and mortar and 0.25 g (± 0.0002 g) was measured into a ceramic crucible. This was mixed to an homogeneous powder with 1.25 g (± 0.001 g) of SpexCertiPrep® granular lithium metaborate flux, transferred to a graphite crucible and heated in an electric muffle furnace at 1050°C for 20 minutes. An intermittent problem in which some samples underwent only partial fusion was resolved by changing to Spectroflux® 100B flux (a coarse powder mix of 80% lithium metaborate and 20% lithium tetraborate ($Li_2B_4O_7$)). The liquid borate glass bead was tipped from the hot crucible into approximately 100 ml of 0.8 M nitric acid at room temperature and placed on a heated magnetic stirrer plate. Samples that failed fully to

dissolve after 20 minutes were discarded and re-processed, as were those that precipitated polysilicic acid gels. This latter problem was found to be caused by slow transfer to the stirrer plate and was easily resolved. Samples were filtered using glass microfibre filters, made up to 200 ml with 0.8 M HNO_3 and stored in non-reactive plastic bottles. Each batch of samples was accompanied by a procedural blank and three rock standards, produced to the same procedure and with the same reagents. Aliquots of these solutions were further diluted with 0.8 M HNO_3 to achieve the 50x dilution described above.

5.3.2 Sample preparation for minor element analysis

Samples were prepared using the Totland *et al.* (1992) acid dissolution methodology. This produces samples with low levels of total dissolved solids but is time-intensive and presents significant health and safety risks. Most of the common rock-forming minerals dissolve readily under this acid attack; some minerals such as chromite, zircon and rutile are resistant but this was not considered to be significant in the context of this study. Silica is lost as the volatile compound SiF_4.

Sub-samples of 0.5 g (±0.0002 g) of ignited, finely-ground sample (see above) were ground to fine powder in an agate pestle and mortar and subjected to acid attack in 20 ml PTFE beakers. Processing was carried out in specialist fume cabinets with water washdown capability to remove any explosive perchlorate and perchloride deposits.

Each sample was treated with 2 ml of 70% HNO_3 to remove organic material and carbonates, 5 ml of 40% HF and 2 ml of 60% $HClO_4$. The beakers were heated on a hotplate and allowed to fume to incipient dryness (evaporation to complete dryness can produce insoluble fluoride residues; Croudace, 1980). The acid attack was repeated twice using 10 ml of HF and 4 ml of $HClO_4$, each time allowing the sample to fume to incipient dryness. A final attack with 4 ml of $HClO_4$ was again evaporated to incipient dryness to convert any remaining fluorides to soluble perchlorates. The crystalline end-product was dissolved in 10 ml HNO_3, filtered and made up to 50 ml with deionised water.

Each batch of samples was processed with a procedural blank and three rock standards (GA, JG-1 and AGV-1), produced to the same procedure and with the same reagents. Samples that produced insoluble residues were re-processed.

5.3.3 Sample preparation for REE analysis

In ICP-OES analysis, the REE emit extremely complex spectra with a proliferation of strong emission lines and extensive spectral overlap from major element lines. The complexities of these emission lines, the low levels at which the REE are originally present (often ppb levels) and the potential for spectral interference make it necessary to remove

most of the major elements from the sample and to produce high-concentration REE sample solutions.

REE elements are generally trivalent, which allows them to be separated from elements with other valencies by ion-exchange resins. Samples were prepared using the Watkins and Nolan (1992) methodology: 1.0 ± 0.0002 g of ignited, finely-ground sample was weighed into a clean ceramic crucible, gently mixed to a homogeneous powder with 2.0 ± 0.0004 g of Spectroflux 100B flux and transferred to a clean graphite crucible. Crucibles were heated to 1050°C for 20 minutes and the borate bead was quenched in approximately 100 ml of 1.27 M HCl at room temperature. During dissolution, each solution was continuously stirred to prevent the formation of polysilicic acid gels and filtered to remove graphite particles. Samples were prepared in batches which included one procedural blank, one rock standard (SY-3, which has substantial REE concentrations) and 6 loess unknowns.

The separation procedure was performed using Bio-Rad AG 50W-8X (200-400 mesh) resin, loaded into ion exchange columns to a depth of 100 mm. The speed of each step was governed by the rate at which solutions percolated through this resin. The resin was pre-washed with 200 ml of deionised water and 100 ml of 1 M HCl. The samples were loaded into the columns and allowed to drain through. The resin was then eluted with 200 ml of 1.75 M HCL and 200 ml of 1.75 M HNO_3 which removed the major elements and most of the trace elements in the solution. The REE, which are quantitatively retained on this resin, were then eluted by washing with 100 ml of 6 M HNO_3, containing $5x10^{-3}$ oxalic acid ($C_2H_2O_4$), followed by a further 100 ml of 6 M HNO_3. This was evaporated to final dryness in 25 ml beakers. Immediately before analysis, the dried sample residue was redissolved in 5 ml 1.5 M HNO_3. This limited sample volume precluded use of the standard autosampler system but by using a short length of narrow-bore nylon tubing to feed the solution directly from the preparation beaker to the ICP peristaltic pump, it was possible to analyse as little as 1.5 ml of sample solution.

Eleven samples from each site were analysed for REE. Samples were selected to be fully representative of the range of loess and palaeosol units present at each site. Results have been corrected for the high and variable carbonate content using CaO values derived from ICP-OES major-element analysis and normalised against standard chondrite values (see Section 3.3.1), except where stated.

5.4 ICP precision and accuracy

5.4.1 ICP Detection limits

Detection limit is defined as the analyte concentration equivalent to three times the standard deviation of the background beneath the analyte line. (Skogerboe and Grant, 1970). PerkinElmer (1997) quote detection limits at 3 σ of 0.05-4 ppm for many of the elements measured in this study. For accurate quantitification, the concentration should be greater than 100 times the detection limit (Boss and Fredeen, 1999).

5.4.2 Precision and accuracy of major element determination

In this study, the extreme dilution needed to ensure stability in Optima 4300 analysis of flux-fusion samples forced the low-concentration elements K, Na and P below the detection limit in some samples. The K and Na results from successful flux-fusion analyses correlated strongly, with a correlation coefficient[1] (c.c.) >0.9) with those from the previously-measured acid-digest minor-element datasets, where concentrations were higher. Accordingly, the more complete acid-digest data for Na, K and P have been converted to % oxide values and used in this study.

A representative acid-digest sample was generated by amalgamating aliquots from several loess samples and was used to maintain a continuous quality control check on reproducibility and instantaneous precision during analytical runs. Fig. 5.1 shows the degree of precision achieved for K, Na and P from one long-duration run, in which this sample was measured a total of 21 times (after approximately every fourth analytical sample). As demonstrated, there is only minor short-term variation and no long-term drift throughout the run. The summary statistics for these elements are shown in Table 5.2.

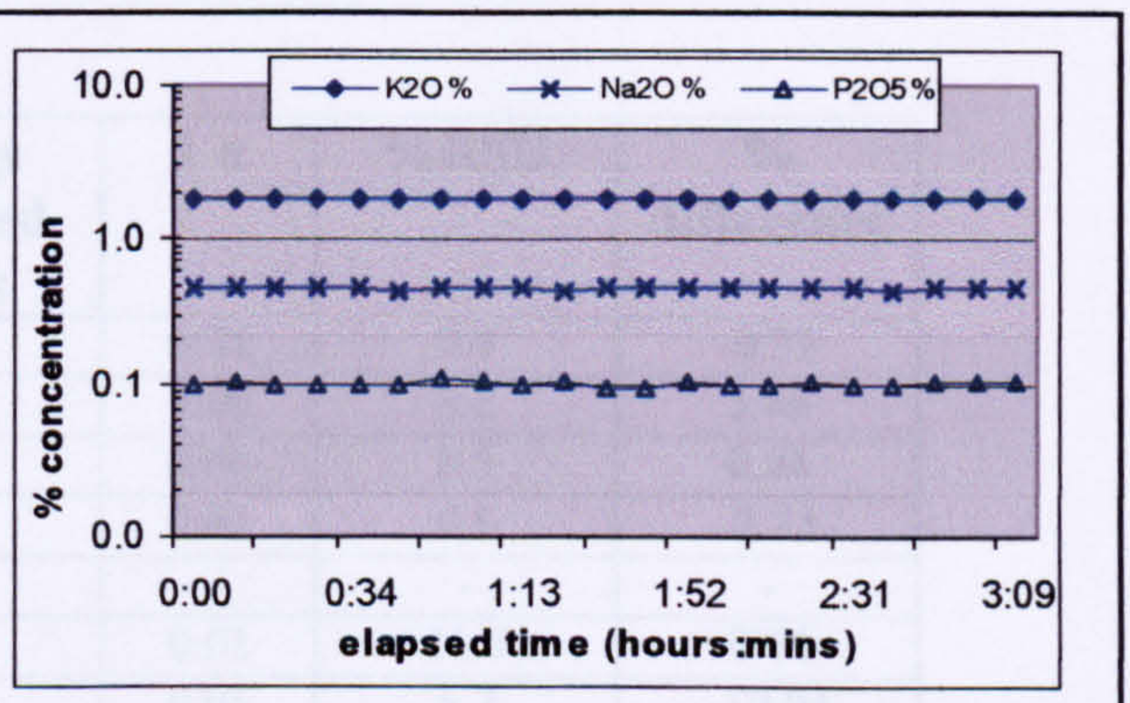

Figure 5.1 Stability of K, Na and P measurement during an extended run, measured from a single quality control solution.

Table 5.2. Variation in K, Na and P values during a 3-hour run.

	Mean conc. (%)	1 σ	%RSD
Na_2O	0.456	0.007	1.5
K_2O	1.779	0.013	0.7
P_2O_5	0.103	0.004	3.5

[1] The correlation coefficient is the covariance of two data sets divided by the product of their standard deviations.

Measurement accuracy for these elements was checked using granite rock standard GA (Table 5.3). Measured K and Na values were slightly higher than the reference values, P was slightly lower. However, no confidence limits are provided for these reference values (Potts et al., 2000) and so it is not possible to test statistical concordance.

Table 5.3 Accuracy and precision of major element measurement (Na_2O, K_2O, P_2O_5)

	GA reference values (%)	measured value (%)	% difference
Na_2O	3.55	3.69	3.68
K_2O	4.03	4.15	2.90
P_2O_5	0.12	0.11	-6.11

A similar continuous quality control check on system precision during analytical runs with flux-fusion solutions was made using a single bulk sample of granite rock standard SARM-1 (Table 5.1). Twenty-seven measurements made on major elements (excluding Na_2O, K_2O, P_2O_5) during an extended run returned the levels of precision shown in Table 5.4.

Table 5.4 Accuracy and precision of major element measurement (excluding Na_2O, K_2O, P_2O_5)

	SARM-1 reference values	average measured values	1 σ	%RSD	% difference
SiO_2	75.70	75.95	0.71	0.9	-0.32
TiO_2	0.10	0.09	0.00	3.8	5.46
Al_2O_3	12.08	11.98	0.06	0.5	0.84
Fe_2O_3	1.90	1.96	0.02	0.9	-3.33
MnO	0.02	0	-	-	-
MgO	0.06	0.05	0.01	11.7	8.64
CaO	0.78	0.86	0.05	5.7	-10.04

Two σ confidence levels of 'better than 10% relative' are provided for SiO_2 and Al_2O_3 (Potts *et al.*, 2000); no confidence levels are provided for the remainder. The measured SiO_2 and Al_2O_3 values are statistically concordant. MgO is concordant with the reference value and the closeness of the remaining measurements to the unquantified reference values suggest that Optima 4300 major element measurements made on samples dissolved by acid digest and flux-fusion are accurate and precise.

5.4.3 Precision and accuracy of minor element determination

The summary statistics for a precision test, measured by eleven successive measurements upon a representative sample solution, are listed in Table 5.5. The results of an extended stability test, using a single quality control sample, are also shown in Table 5.5

and graphically in Fig 5.2. The precision test demonstrates that for most elements, precision is better than 1%RSD, and the extended-duration test demonstrates the extreme stability of the Optima 4300.

Table 5.5 Precision and stability of minor element analysis

	Precision test			**Extended stability test**		
	Mean	**1 σ**	**%RSD**	**Mean**	**1 σ**	**%RSD**
Ba	301.20	0.92	0.31	299.71	2.76	0.92
Co	11.97	0.08	0.69	11.84	0.12	1.02
Cu	4.35	0.05	1.21	4.30	0.11	2.49
Ga	6.05	0.13	2.10	5.93	0.19	3.21
Nb	15.43	0.16	1.02	15.07	0.53	3.53
Ni	17.87	0.13	0.70	17.68	0.21	1.17
Pb	8.18	0.61	7.40	8.10	0.59	7.26
Sc	6.38	0.04	0.66	6.34	0.10	1.54
Sr	189.90	1.20	0.63	184.71	1.62	0.88
Th	16.61	0.11	0.66	16.47	0.23	1.38
V	48.95	0.18	0.36	48.79	0.42	0.85
Y	15.88	0.08	0.50	15.87	0.13	0.85
Zn	31.52	0.23	0.74	30.96	0.37	1.18

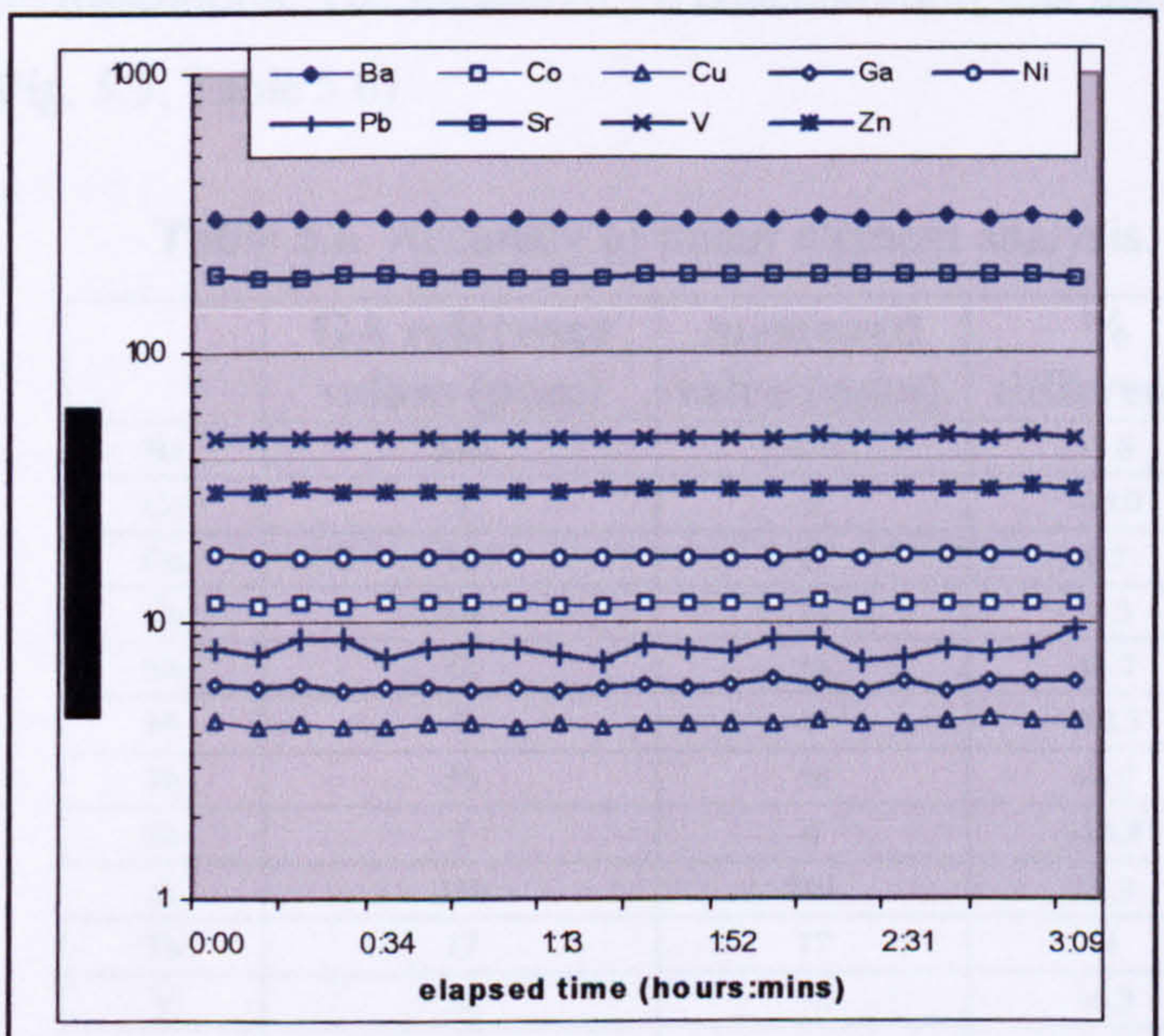

Figure 5.2 Stability during minor element analysis, with concentrations measured repetitively from a single bulk sample (Nb, Sc, Th, Y omitted for clarity).

Accuracy was checked using the granite rock standard GA as an unknown. No confidence levels are provided for any of the reference values (Potts *et al.*, 2000). Using %RSD values based on 1 σ values from the precision test, Cu and Th were statistically concordant. Ba, Ga, Sr, V and Y were all close to the reference values with the discrepancies concentrated at the lower concentration values. Co, Nb, Ni, Sc and Zn were all present in solution at values significantly below their reference values. It is possible that they were carried in mineral phases that did not undergo complete dissolution. The measured Pb concentration was higher than the reference value (Fig. 5.3, Table 5.6).

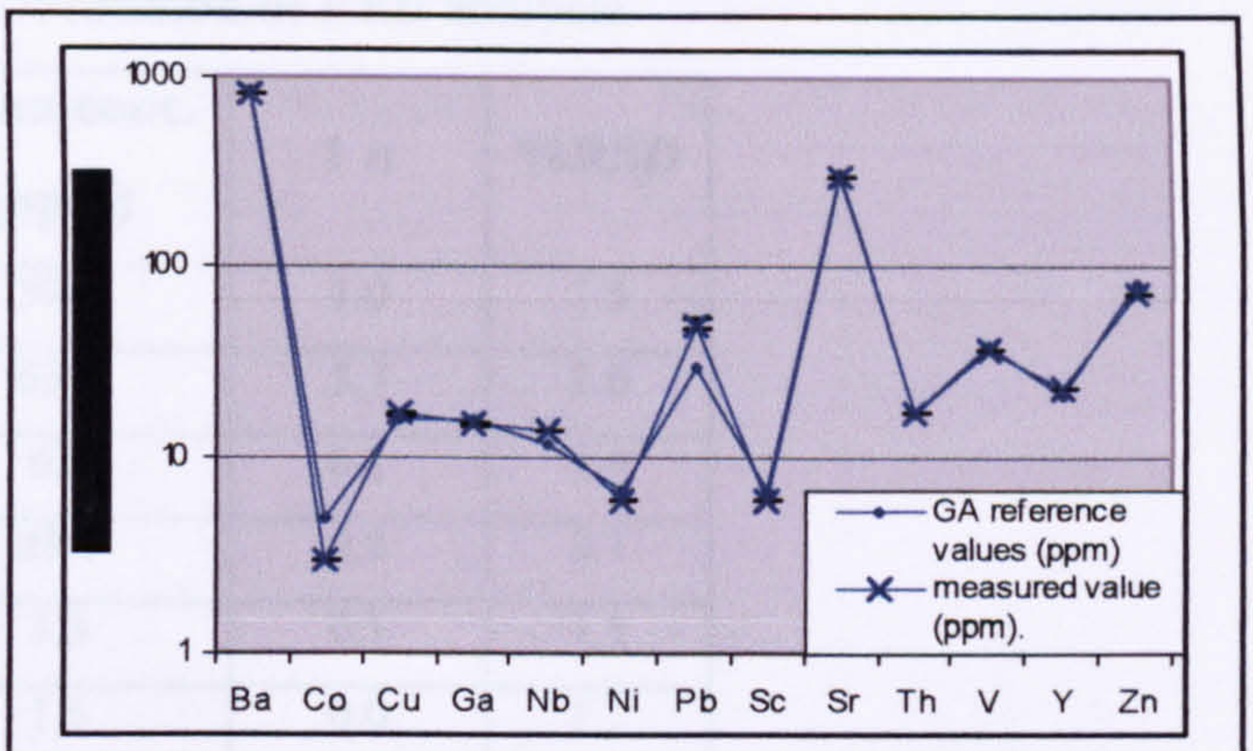

Figure 5.3 Comparison of measured and reference minor element concentrations, using GA as an 'unknown'.

Table 5.6. Accuracy of minor element analysis.

	GA reference values (ppm)	measured value (ppm).	% difference
Ba	840	810	-3.6
Co	5	3	-40.0
Cu	16	17	6.3
Ga	16	15	-6.3
Nb	12	14	16.7
Ni	7	6	-14.3
Pb	30	50	66.7
Sc	7	6	-14.3
Sr	310	301	-2.9
Th	17	17	0
V	38	36	-5.3
Y	21	23	9.5
Zn	80	71	-11.3

5.4.4 Precision and accuracy of REE determination

A precision test was carried out using the rock standard AGV-1 as an 'unknown'. Only three successive tests could be carried out, due to the small amounts of sample solution (5 ml, see Section 5.3.3). As shown in Table 5.7, they returned an average error of 2% RSD, reaching a maximum of 3.4%.

Table 5.7. Precision of REE analysis.

	Mean conc. (ppm)	**1 σ**	**%RSD**
La	39.4	1.0	2.5
Ce	65.9	1.7	2.6
Pr	6.6	0.1	0.9
Nd	28.1	0.8	2.7
Sm	5.3	0.1	1.5
Eu	1.5	0.0	1.7
Gd	4.1	0.1	1.6
Tb	0.7	0.0	0.9
Dy	3.2	0.1	2.3
Ho	0.7	0.0	3.4
Er	1.6	0.0	2.1
Tm	0.3	0.0	2.1
Yb	1.5	0.0	2.6
Lu	0.3	0.0	3.3

Accuracy was checked using AGV-1 as an unknown to examine REE measurement accuracy. Two σ confidence levels of 'better than 10% relative' are provided for Ce, Sm, Dy and Yb; the remainder are unquantified (Potts *et al.*, 2000). Using the %RSD value based on 1 σ levels from the precision test, Ce, Pr, Sm, Tb, Ho, Er, Tm, Yb and Lu are statistically concordant. La and Eu are close to the reference values, Nd, Gd and Dy show apparent under-estimations against the reference values (shown graphically in Fig. 5.4 and listed in Table 5.8).

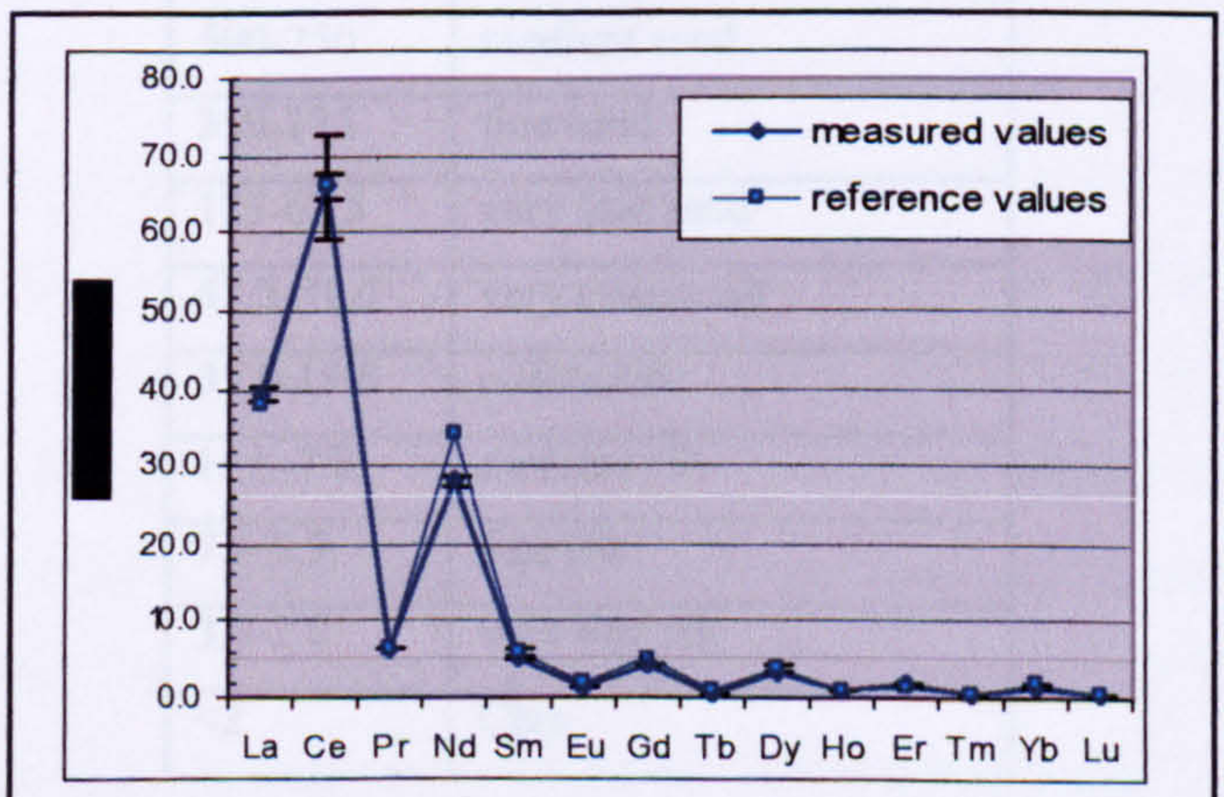

Figure 5.4 Comparison of measured and reference REE concentrations, using AGV-1 as an 'unknown'.

Table 5.8. Comparison of measured REE concentrations with AGV-1 rock standard

	Measured value (ppm)	Reference value (ppm)	% difference
La	39.4	38.0	3.7
Ce	65.9	66.0	-0.1
Pr	6.6	6.5	1.0
Nd	28.1	34.0	-17.3
Sm	5.3	5.9	-11.0
Eu	1.5	1.7	-12.4
Gd	4.1	5.2	-21.3
Tb	0.7	0.7	-5.2
Dy	3.2	3.8	-16.6
Ho	0.7	0.7	0.9
Er	1.6	1.6	2.3
Tm	0.3	0.3	-13.5
Yb	1.5	1.7	-8.2
Lu	0.3	0.3	7.1

5.5 Particle description and size measurement

The sediment class size terminology used in this study conforms to Friedman and Sanders (1978), and is based on the Wentworth scale (Wentworth, 1922) (Table 5.9).

Table 5.9. Size categories and terminology for sediments.

Size (μm)	Descriptive terminology
2000-1000	very coarse sand
1000-500	coarse sand
500-250	medium sand
250-125	fine sand
125-62.5	very fine sand
62.5-31.0	very coarse silt
31.0-15.6	coarse silt
15.6-7.8	medium silt
7.8-3.9	fine silt
3.9-2.0	very fine silt
<2	Clay

The grain size data produced in this study have been further analysed by means of the 'GRADISTAT' statistics package (Blott and Pye, 2001) to determine the mean, mode, sorting, skewness and kurtosis. GRADISTAT uses Folk and Ward (1957) graphical methods and descriptive terms, modified by Blott and Pye (2001).

5.5.1 Sample preparation for optical microscopy

A representative sample of primary loess from each site, formed by combining aliquots from several different samples, was used to examine variation in grain shape, roundness, mineralogy and homogeneity within the loess coarse-grain population. The two samples were decalcified using 10% HCl and then washed to remove the fine fraction (< *c.* 30 μm) since this could not be viewed clearly and was likely to obscure features of interest in the coarse-grain fraction. The prepared samples were viewed with a reflected-light Nikon® SMZ800 binocular microscope and images were captured with an integral digital camera, using Microsoft® Eclipse Net software. Scale bars were added during subsequent image processing.

5.5.2 Size measurement techniques

A range of methods could have been used in this study to determine the particle size distribution of sediment samples, including sieving, X-ray diffraction granulometry and laser granulometry. These methods examine widely different aspects of 'size', influenced by variations in particle shape, density, optical properties and methodology. Sieving, for example, sorts by shape as well as size; results are skewed towards the two shorter dimensions of the measured particles. X-ray diffraction granulometry assumes that the sample material is homogeneous and spherical. It measures the changing X-ray transparency of a sample as its constituent particles settle under gravity. This provides the settling velocity and since a sphere's terminal velocity is proportional to its cross-sectional area, the size of the particles can be determined. Laser granulometry results are also based on 'homogeneous and spherical' assumptions and are skewed towards the longest dimension. This particularly affects the clay fraction; the platy nature of clay particles ensures that some are reported as very fine silt particles (Konert and Vandenberghe, 1997).

In addition, results are reported in different ways: the series of size fractions obtained by sieving and by X-ray diffraction granulometry are both '% mass' while laser granulometry results are '% volume'. Thus results obtained using different methods are not directly comparable, making it important fully to define the method used.

This study used the Malvern Instruments® Mastersizer2000 laser granulometer because this can measure the full grain size distributions of loessic samples in a single operation. The Malvern 'default' size categories provide the finest resolution; the use of broader size categories (permitted by the Malvern software) would produce different '% volume' results though the shape of the size distribution graph would be identical.

5.5.3 Sample preparation for size measurement

Samples were removed from the sample bags as coherent lumps to avoid sorting effects and were wet-sieved at 500 μm to remove rhyzoliths, root fragments and clasts. The sediment was then dried and treated with 10% HCl to remove small chalk particles and other carbonates so that (a) only aeolian grains were measured and (b) grains were measured individually, not as cemented aggregates. Optical microscopy of crushed but untreated samples showed that they contained abundant sand-sized cemented aggregates; these were not present after acid treatment. This acid attack also removed detrital carbonate grains but Pye (1983) showed that in Rhine loess, calcite and dolomite grains were similar in size to silicate grains; their loss is not considered to affect the particle size distribution. This accords with the initial stages of the loess grain-size preparation technique proposed by Sun *et al.* (2000) but that technique continued with highly aggressive treatments to isolate the quartz grain fraction. The decarbonated, acidic sub-samples were carefully rinsed with distilled water and centrifuged before being stored as moist, thick and homogenous slurry. This was re-homogenised immediately before use and fractions of each sample were added to the measurement system incrementally by spatula to reach the required concentration.

The potential influence of soil organic matter was examined by treating a representative range of prepared sub-samples with 30% H_2O_2 for 72 hours at room temperature. This made no difference to the measured grain size distribution and so this factor can be discounted.

5.5.4 Malvern operating conditions

The Mastersizer2000 laser granulometer is a laser diffraction system that uses red and blue lasers (wavelengths 632 and 466 nm) to illuminate sample material held in liquid suspension in a recirculating flow which is controlled by the Hydro Malvern2000MU sample introduction unit. For all samples, the 'obscuration factor' (a measure of sample concentration) was maintained at 14-18%, within the Malvern 'recommended' range.

A standard agitation speed of 2500 rpm was used to maintain coarse grains in suspension. At higher speeds, fine bubbles were generated which the Malvern system may interpret as a proliferation of coarse grains. Immediately before analysis, ultrasonic energy was applied for 60 seconds with a probe displacement of 20 μm, to ensure that grains were fully disaggregated. The rising obscuration factor showed that disaggregation occurred rapidly in the first 30 seconds but slowed to a halt by the end of that minute. Sperazza *et*

al. (2004) found that the application of ultrasonic energy beyond 1 minute could lead to clay flocculation or grain fracturing.

Laser light diffraction is inversely size-dependent: the smaller the particle, the greater the degree of diffraction. The diffraction pattern generated by any one sample contains the total scattering effect of every particle present; it is detected by a sensor array and the resulting signals are analysed against Mie theory (Mie, 1908) which describes the scattering of light by particles. This theory assumes that the sample grains are homogeneous and spherical, that the dispersant is homogeneous and it requires the indices of refraction and absorption for the grains and the dispersant. For each measurement result, the system carried out three replicate 12-second runs, providing a total of 36,000 readings which were automatically converted into the average particle size distribution in 100 size fraction classes (0 to 2000 μm) as % volume.

For this study, the refractive index value 1.544 (pure quartz) was used for samples and 1.330 for the dispersant (water), with an absorption factor of 0.1, appropriate for grains that are semi-opaque. The Malvern software allows diffraction data to be reprocessed with altered optical settings; experimental recalculations using an absorption factor of 0.5 were close to the 0.1 data but a factor of 0.001 resulted in apparent under-reporting of the fine-grain spectrum below 1 μm and over-reporting at the mode (Fig. 5.5). This matches the findings of Sperazza *et al.* (2004).

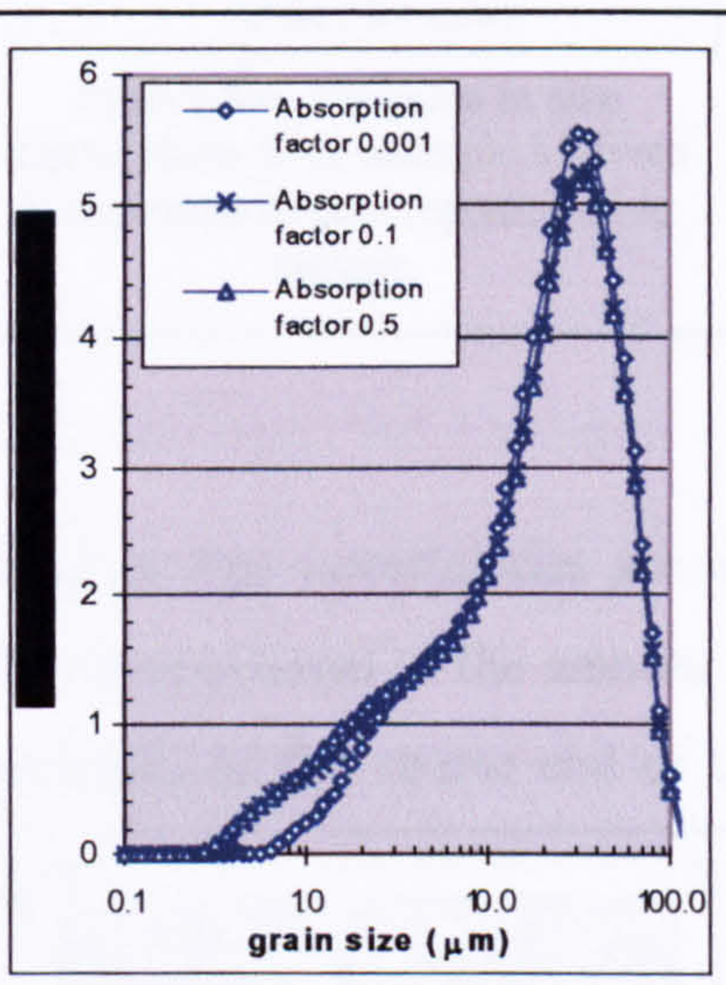

Figure 5.5 Effect of different 'absorption factors' on the measured grain size distribution.

5.5.5 Precision of grain size measurement

It was considered possible that samples prepared as slurries might not be homogeneous and that using a spatula to add successive sample aliquots to reach the required concentration might induce errors. A precision test was carried out by eleven successive analyses of a single, bulk sample prepared as a slurry and added by spatula. These tests returned extremely consistent results with c.c. values >0.99 (Fig. 5.6). This suggests that the selected methodology provides high precision and reproducibility. This agrees with previous studies (e.g. Hall, 1988; Loizeau *et al.*, 1994) which have stated that laser diffraction size analysis is precise and generally accurate, especially when compared to methods based on the measurement of size rather than gravitational settling rates.

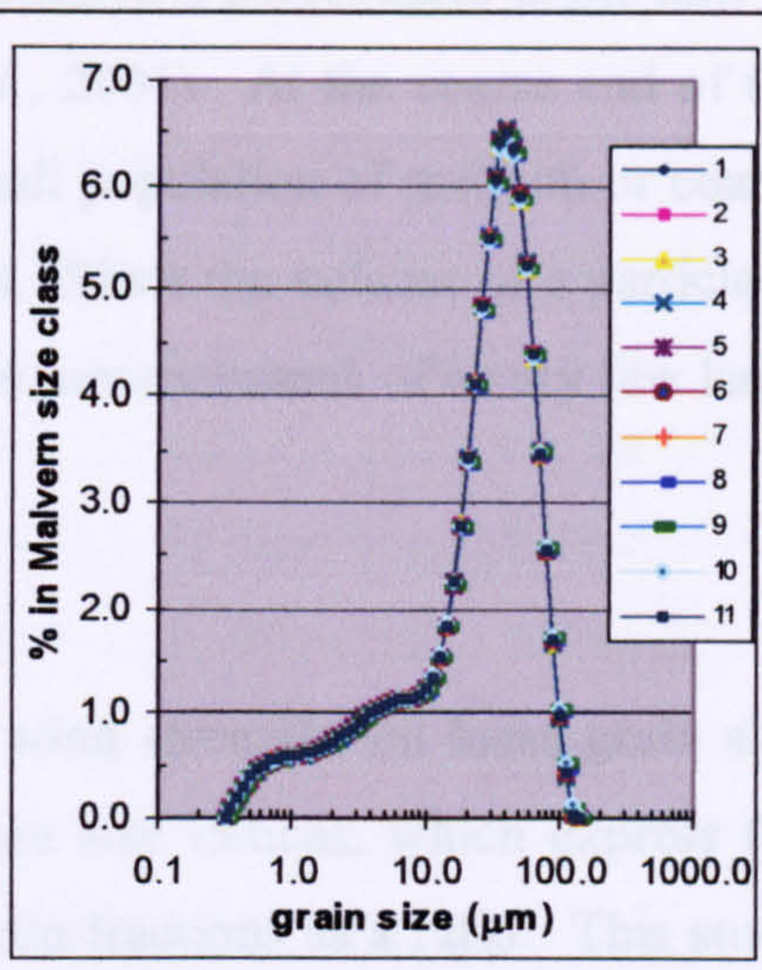

Figure 5.6 Variation in size distributions from multiple Malvern measurements on a representative sample.

The %RSD values for the 11 sets of results both show that uncertainties are not evenly distributed across the size spectrum but are inversely proportional to the amount of sample present in each Malvern size category, heavily weighted to the coarse end of the spectrum (Fig. 5.7). At the extreme fine end of that spectrum, size categories which each contain less than 0.4% of the sample content (below 0.56 μm) produce uncertainty values that reach a maximum of 4.5%. As the sample content in each size category rises to 0.5% (0.63 μm and larger), uncertainty values reduce to approximately 1% and continue to reduce to *c.* 0.4% about the mode (20-70 μm), where size category content values are in the range 3-6.5%.

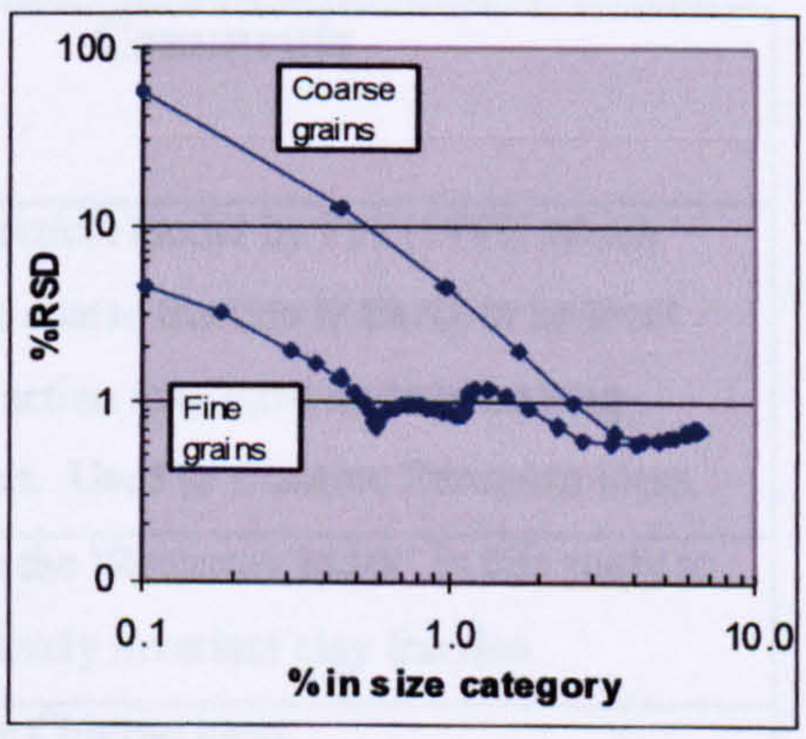

Figure 5.7 Comparison of %RSD with % content in each Malvern size category.

At the coarse end of the spectrum, size categories containing less than 1.0% content return increasingly-large uncertainty values which rise to more than 50%. Thus the high-uncertainty size fractions are heavily localised and affect only a small proportion of the sample, below 0.5 μm and above 90 μm. In this test-sample dataset, 97.5% of the inter-sample %RSD values are lower than 1.5%. Those fine-fraction size categories, which

contain less than 0.2% of the sample mass, and those coarse-fraction categories which contain less than 1.0% are likely to contain significant uncertainties.

These uncertainties are partly induced by low volumetric percentages in the tails of skewed non-Gaussian size distributions (Sperazza *et al.*, 2004). At the coarse end of the spectrum, they may also be caused in part by a very small population of medium or coarse grains, present in some measurements and not in others. Since the volume of a particle is proportional to its radius cubed, it is possible for random measurements of a very few large particles to induce high uncertainties.

5.5.6 Grain size indices

Section 3.3.1 described the effects of variable wind strengths on loess grain size distributions. These effects can be investigated by grain size indices, which express the relationship between defined sets of fine and coarse grain fractions as a ratio. This study compares two indices developed by researchers working with Chinese and European loess sequences, which compare different fine and coarse fractions, and has modified one to remove the relatively invariant clay fraction (Table 5.10). Grain size indices are valid as wind speed indicators only in primary loess: the fundamental grain size distribution in palaeosols was established prior to the pedogenic event and may have been modified by reworking or by clay formation during strong pedogenesis.

Table 5.10. Grain size indices examined in this study.

Grain size index	Grain size fractions (μm)	Comments
'Rousseau index' (Rousseau *et al.*, 2002)	20-50 /<20	Based on a theoretical model by Pye (1995) which suggests that the coarse fraction is likely to be local while the fine fraction may have undergone long-distance transport. Used to examine European loess.
'modified Rousseau index'	20-50/3.8-20	Developed from the 'Rousseau index' in this study to remove the relatively invariant clay fraction.
U-ratio (Vandenberghe *et al.*, 1993)	16–44/5.5-16	Used to examine Chinese loess.

5.6 Carbonate content measurement

The carbonate content of sediment samples can be determined by measuring the volume of CO_2 evolved by acid decomposition of carbonates from a known weight of sample under known conditions, and by measuring the weight loss caused by the reduction of carbonates to oxides by heating. Gasometry was the prime method used in this study, but since the study was already using loss-on-ignition to measure the organic carbon

content (see Section 5.6), sequential loss-on-ignition was used to derive a parallel carbonate measurement.

5.6.1 Gasometric carbonate determination

The gasometric method and its associated calculations are described in Gale and Hoare (1991). The volume of CO_2 is actually derived from all the carbonates present (at the study sites, this includes calcium and magnesium carbonates, see Section 6.5.2) but the calculations treat this volume as being produced only by $CaCO_3$. Results are, therefore, quoted as 'calcium carbonate equivalent', and are expressed as % mass. The Bascombe Calcimeter used in this study had a 50 ml calibrated chamber, in comparison to the 250 ml version described by Gale and Hoare (1991), which restricts the weight of high-carbonate samples to less than 2 g. In such cases (the majority of samples), multiple sub-samples were analysed and the mean was calculated. The mean %RSD on these sequential analyses was better than 3%.

Samples were oven-dried to constant weight and were weighed to an accuracy of 0.001 g. Room temperature was measured to an accuracy of 0.5°C and air pressure was determined by an aneroid barometer regularly calibrated against local aviation meteorological data (Staverton, 2003). Results were calculated using Gale and Hoare's formula:

$$\% \ CaCO_3 \text{ equivalent} = {}^{VpC}/_{MT}$$

where V = CO_2 volume in ml, p = pressure in mm Hg, C = 0.1605, M = sample mass in g, T = temperature in K. System checks were carried out using pure calcium carbonate at the start of each run, with results within the tolerances quoted by Gale and Hoare (1991) (100% ± 2%).

Many of the Harmignies samples from mid-Unit F (above *c.* 9 m depth) contained substantial amounts of chalk particles derived from the local chalk bedrock. To examine the influence of the larger granules on the carbonate content, two sets of carbonate determinations were carried out, one on the full sample and one on a sub-sample sieved at 300 μm. The 'full sample' tests used raw samples weighing *c.* 40 g. These were oven-dried at 105°C for 24 hours, cooled in a desiccation chamber, crushed gently in an agate mortar and homogenised. The 'sieved sample' tests used a second set of 40 g raw samples, uncrushed and wet-sieved at 300 μm using distilled water. The sieved fraction and the wash water was then oven-dried, gently crushed to powder, homogenised and cooled in a dessication chamber before measurement in the calcimeter.

5.7 Measurement of the organic carbon and carbonate contents by sequential loss-on-ignition

5.7.1. LOI methodology

The sequential loss-on-ignition (LOI) method is used to estimate the residual organic matter and carbonate contents of sediments. It measures the weight loss caused by:

(a) the medium-temperature oxidation of organic material ('ashing'), and,

(b) the evolution of CO_2 during the high-temperature reduction of $CaCO_3$ and $MgCO_3$ to CaO and MgO.

During the first stage, carbohydrate organic matter such as cellulose and lignin is converted to ash and the resultant CO_2 and H_2O is lost to atmosphere. The relative weight loss provides the percentage of organic matter present in the sample. For this study, this has been converted to the commonly-used 'percentage organic carbon' (% org. C) by using the empirical correction factor of 2.13 devised by Dean (1974).

There are conflicting assessments of the validity of the second stage as a determinant for carbonate content, due at least in part to the fact that this degree of heating can drive off structural water, as is present in clays. Bengtsson and Enall (1986) claim that it gives a 'rough indication' but Dean (1974) concluded that for clay-poor calcareous sediments, it can provide accurate results. Heiri *et al.* (2001) used batches of homogeneous lake sediments with varying carbonate and organic content to examine combinations of sample weight, oven temperature and heating time. They recommended that samples should be of approximately constant weight and the first stage (ashing) should be carried out at 550°C. The duration should vary with the amount of organic matter present: 2 hours for low-organic samples, 4 hours for high-organic samples. The second stage (calcination) should be carried out at 950°C for 2 hours.

This study used those Heiri *et al.* (2001) findings as the basis of an LOI methodology suitable for loess, with its low clay and low organic content. Samples weighing approximately 40 g were gently crushed and homogenised. Samples and crucibles were oven-dried to constant weight (approximately 24 hours at 105°C). Sub-samples of approximately 20 g were weighed to an accuracy of 0.001 g and heated for 2 hours at 550°C in a muffle furnace. The furnace cooled naturally and the samples were removed as soon as possible. Final cooling to room temperature was carried out in dessicator vessels and samples were reweighed immediately they were cold. They were

then reheated to 950°C for a further 2 hours to decompose carbonates to oxides, and the same cooling and reweighing procedures were followed. The ignited and calcined samples were later used to prepare sample solutions for major-element analysis.

5.7.2 Assessment of methodological precision and accuracy

Using the organic carbon content as a proxy for palaeoclimatic conditions demands that the samples are not contaminated by more recent organic material. The exposed faces at both study sites have supported recent vegetation growth (annual herbs at Harmignies, shrubs and trees at Metternich) and thus may contain recent root fragments. Care was taken to avoid sampling areas that contained obvious plant debris.

The reliability of LOI carbonate determination was checked using chalk bedrock and pure $CaCO_3$ samples. After LOI at 950°C the chalk samples had lost between 42.4% and 43.3%, giving a carbonate content of 96.3-98.4%. The pure $CaCO_3$ sample lost 43.9% (the theoretical LOI loss factor is 44.02%; Heiri *et al.*, 2001), giving a carbonate content value of 99.7%. These results prove that this methodology gives accurate results and confirm the Dean (1974) assessment that LOI is an accurate method of determining the carbonate content.

Comparison of gasometric against LOI methods of measuring the carbonate content shows that the two methods produced results that were consistent. For both sites, LOI and gasometry correlate strongly (c.c. 0.99), illustrated in Fig. 5.8. However, for very-low-carbonate samples, gasometric and LOI measurements differed. At both sites, where gasometric carbonate results were below 2%, LOI consistently indicated that the carbonate content was 1-2% higher.

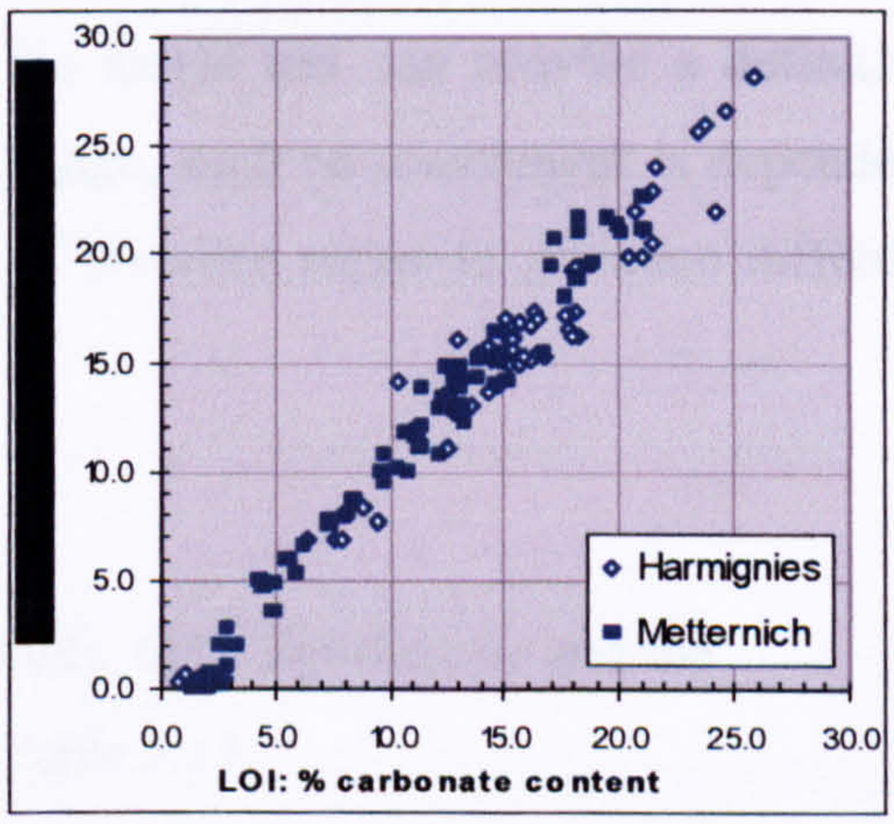

Figure 5.8. Comparison of gasometric and LOI carbonate content results at both sites.

The identification of dolomite as part of the carbonate content (see Section 6.5.1) raises the possibility of LOI methodological errors since the magnesium carbonate component of dolomite can begin to disassociate at temperatures as low as 425°C (Heiri *et al.*, 2001). In samples with high dolomite content, weight loss from the first, medium-temperature stage (considered to represent only the ashing of organic carbon debris) could also include some CO_2 loss from magnesium carbonate reduction, and so be an overestimate. Conversely, the weight loess from the second, high-temperature stage could be a small underestimate since some carbonate reduction has already occurred.

5.8 Determination of enviromagnetic characteristics

Evans and Heller (2001) consider that while low-field magnetic susceptibility (MS) is the most commonly-investigated magnetic property, the wider range of magnetic tests now available offers a powerful tool for the investigation of loess-palaeosol sequences, especially when combined with other proxies such as particle size and carbonate content. Verosub and Roberts (1995) proposed that a series of ambient-temperature tests of magnetic susceptibility and remanence properties can provide information on:

(a) the concentration of magnetic particles in the sample,

(b) the range of magnetic grain sizes present, and,

(c) the magnetic mineralogy.

This information can be used to identify the enviromagnetic response to palaeoenvironmental change. These enviromagnetic characteristics, and others, have been examined using the range of tests and statistical comparisons listed in Tables 5.11-5.14) against the full sample sets from both sites. A magnetically-separated fraction was also subjected to optical microscopy examination.

Natural samples will show variability in all of these magnetic characteristics, driven by complex responses to changing conditions. No single test can provide a definitive statement about the enviromagnetic response to change, such an assessment is dependent on the comparison of several tests and the use of bivariate ratios to compare different magnetic parameters.

5.8.1 The magnetic properties

The magnetic properties examined in this study, their significance and the techniques used to measure them are described in Table 5.11.

Table 5.11 The magnetic properties examined in this study

Magnetic property	**Measurement techniques and significance**
Magnetic susceptibility (MS, 10^{-3}, d.u.)	Magnetic susceptibility is controlled primarily by the concentration of magnetic minerals present; over the range of grain sizes found in natural sediments it is largely independent of the magnetic grain size (Heider *et al.*, 1996). It is the best parameter for assessing magnetic concentration (Peters and Dekkers, 2003). Values are expressed in dimensionless units (d.u.). Measurement at low and high frequencies can identify the presence of ultra-fine ferrimagnetic grains (approximately 0.02 μm) because these grains respond differently at these two frequencies (Evans and Heller, 2003). Measured in the field with the Bartington® MS2F probe head at 0.58 kHz. Measured in the laboratory with the MS2B dual-frequency sensor at 0.465 kHz and 4.650 kHz in a magnetic field of 0.1 mT, to give the volume susceptibility parameters K_{lf} and K_{hf}.
Anhysteric remanent magnetism (ARM)	SD ferrimagnetic grains acquire ARM much more efficiently than larger grains, and so ARM is approximately proportional to the concentration of magnetite/maghemite grains in the 0.02-0.5 μm range (Hounslow and Morton, 2004). ARM was induced using a Molspin Variac with a DC bias field of 100 mT and a superimposed peak alternating field of 40 mT, measured on a Molspin fluxgate magnetometer and normalized to the sample weight.
χ_{ARM} (um^3/kg)	χ_{ARM} signifies ARM normalized to the DC bias field, necessary for comparison against other research work, which may have used different bias fields, (Maher, 1988). For the reasons shown above, χ_{ARM} is strongly grain-size dependent.
Isothermal Remanent Magnetism (IRM)	Variation in IRM (and SIRM – below) are related to the coercivity spectrum of a sample and so can be used to examine the relative concentrations of magnetite and haematite. Magnetite can dominate IRM acquisition even when haematite forms half of the magnetic assemblage (Lowrie, 1990). Incremental IRM acquisition curves were produced using the Molspin pulse magnetizer and Molspin fluxgate magnetometer to examine the sample response to increasing magnetic fields in 10 steps from 10 mT to 880 mT, approximately equal on a log scale. Normalized to the sample weight (m^2/kg). Since remanence decayed rapidly in some samples due to viscous loss (see below), care was taken to measure the remanence signal consistently, immediately after magnetisation.
Saturation IRM (SIRM)	SIRM is the highest amount of magnetic remanence that can be produced

	in a sample by applying a large forward magnetic field (here 880 mT; assumed to be saturation). It is controlled by the magnetic concentration, mineralogy and grain size. SIRM was measured with a Molspin fluxgate magnetometer immediately after acquisition, and normalized to the sample weight.
Viscous remanent magnetism.	Viscous remanent magnetism is attributable to the progressive randomisation of the individual magnetic moments linked with every grain. Metastable SD magnetite grains near the SP/SSD threshold grain-size show rapid loss of remanence (also known as viscous loss) (Butler and Banerjee 1975). In this study, it is expressed as the percentage loss of remanence from the initial SIRM value after 24 hours. Its general tendency compares to the more customary, but less sensitive, frequency-dependent susceptibility χ_{fd}, which is commonly used to quantify the ultra-fine magnetite fraction in environmental materials (Dearing *et al.*, 1996).

5.8.2 Determination of magnetic characteristics

These tests provided data on a wide range of magnetic characteristics. Some measurements can be examined as individual enviromagnetic indicators and some can also be combined in ratios of variable and relatively invariable characteristics to clarify aspects of enviromagnetic behaviour. Tables 5.12, 5.13 and 5.14 explain the measurement parameters used to determine the magnetic mineral concentration, the magnetic grain size and the magnetic mineralogy, respectively.

Table 5.12 The measurement parameters used to determine the magnetic mineral concentration.

Magnetic parameter	Interpretation
MS (field measurement)	Each field measurement is the average of 5 replicates, rounded to the nearest 0.05.
MS (laboratory measurement)	MS values measured on prepared samples at 0.465 and 4.65 kHz (K_{lf} and K_{hf}). Expressed as X_{lf} and X_{hf}, when normalised to the sample weight (mass-specific magnetic susceptibility) (units μm^3 kg). Each measurement is the average of 3 replicates, rounded to the nearest 0.05.

Table 5.13 The measurement parameters used to determine the magnetic grain size

Magnetic parameter	Interpretation
χ_{fd} Frequency-dependent magnetic susceptibility (%)	χ_{fd} is a magnetic granulometry proxy that indicates the presence of SP/SD grains. It is calculated on the difference between χ_{lf} and χ_{hf}, which is controlled by the presence of ultra-fine ferrimagnetic (magnetite/ maghemite) grains probably formed by *in situ* pedogenic processes (Maher, 1988); Dearing *et al.* 1996). A significant population of SP/SD grains will return χ_{fd} values in the range 7-15%, while for MD grains χ_{fd} is <5-6% (as measured in natural samples, Maher, 1988).
χ_{ARM}/χ_{lf} χ_{ARM}/SIRM SIRM/χ_{lf}	For magnetic mineral assemblages dominated by magnetite, these ratios are widely used as granulometry proxies within the magnetically-stable fraction from SD to MD grain size (Evans and Heller, 2003). Ultra-fine magnetite grains are more efficient at acquiring remanence, particularly ARM, while SIRM is size-dependent (*ibid.*). Samples that contain increasing abundances of SD and PSD grains, compared to MD grains, will yield higher ARM/SIRM ratios (King *et al.*, 1982). Here, χ_{ARM} has been used. However, SIRM is also affected by mineralogy; in multi-mineral assemblages dominated by magnetite, the SIRM/χ_{lf} ratio is low. For haematite-dominated sediments, it is high (Opdyke and Channell, 1996). Relative to ARM and SIRM, χ_{lf} is relatively size-independent (Evans and Heller, 2003) and so the ratios χ_{ARM}/χ_{lf} and SIRM/χ_{lf} similarly reflect magnetite grain size within that magnetically stable fraction, with higher values indicating an increasing contribution by SD and PSD grains (King *et al.*, 1982; Opdyke and Channell, 1996).
χ_{ARM}/χ_{lf}	For sediments dominated by magnetite, this ratio reflects two magnetic parameters – concentration and grain size (King *et al*, 1982). In plotting these parameters, changes along a line of constant slope identify changes in concentration; changes in slope indicate variation in the abundance of ultra-fine SD and PSD magnetite grains, relative to MD grains. Samples that plot above or below the line of slope are magnetically finer- or coarser-grained than those which plot along the line of slope (ibid.).
Viscous loss (%)	The rate at which samples lose remanence (in this study, measured after 24 hours) is an indication of the population of metastable magnetite grains near the SP/SD threshold (Butler and Banerjee 1975).

Table 5.14 The measurement parameters used to determine the magnetic mineralogy

Magnetic parameter	Interpretation
S-ratio	This ratio (derived from the SIRM response to an IRM backfield of -100 mT) indicates the relative proportions of 'soft', low-coercivity components (magnetite/maghemite) and 'hard', high-coercivity components (haematite/ goethite) (Bloemendal *et al.*, 1992). S-ratio values close to 1 indicate a strong dominance by magnetite/ maghemite, lower values indicate an increasing contribution by haematite/ goethite.
Incremental IRM acquisition (mAm^2/kg)	This is controlled by the coercivity of the magnetic minerals present. Magnetite can become magnetically saturated by IRM fields of less than 300 mT; haematite can remain unsaturated in fields exceeding the maximum available to this study (880 mT). IRM values that do not reach saturation by 300 mT and which continue to rise with increasing field strengths indicate the presence of both magnetite and haematite (Butler, 1982). However, this may over-simplify complex magnetic behaviour (Kruiver and Passicra, 2001).
'Forward S ratio'	This represents the percentage IRM saturation at 300 mT in the incremental IRM acquisition sequence (see above), and is controlled by the proportions of low- and high-coercivity components. Pure magnetite would return a value of 100%.

5.8.3 Methodology for field measurement of magnetic properties

A Bartington MS2® meter was used for the field MS measurements, with the MS2F® sensor which operates at 0.58 kHz. The meter was zeroed in air after each reading to reduce the effects of thermal drift. Each measurement is the average of 5 successive readings, rounded to the nearest 0.05. At both sites, measurements were made at each sample collection point and within the topsoil profile. The loess face was cleaned and levelled using stainless steel implements prior to measurement and care was taken to ensure that the relationship of the probe head and sample surface remained constant for all readings.

5.8.4 Methodology for laboratory measurement of magnetic properties

Sub-samples were taken from each sample in the full Harmignies and Metternich sample sets, air-dried, gently crushed and packed tightly in 10 ml plastic pots. Each sample weighed approximately 13-15 g, measured to an accuracy of .001 g. These pots remained unopened for the full sequence of measurements. A lug on the pot lid engaged with a cutout in the sample holder to ensure that sample orientation remained constant. These were then subjected to a uniform set of environmental magnetic measurements,

shown in Table 5.11. Measurements were made at room temperature and a standard correction was made for the diamagnetic signature of the plastic pots.

These sub-samples were prepared from the original samples and thus have high and variable carbonate content. Because carbonates are diamagnetic (i.e. they are composed of atoms which have no collective magnetic interactions and are not magnetically ordered), they act as a variable 'dilution factor'. This has been removed by recalculating the sample weight to a 'carbonate-free' value, using the % carbonate content determined by the gasometric method. Thus all mass-specific values are carbonate-free values.

5.8.5 Precision of enviromagnetic measurements

For both sites, the field MS measurements correlate strongly with the laboratory measurements (Harmignies, c.c. 0.9; Metternich, c.c. 1.0).

The precision of laboratory MS determination was tested by sets of ten successive measurements made on three samples with widely-differing low-frequency volume-specific MS values (K_{lf}) (12, 24 and 109 10^{-3}d.u.). Each result is the average of three replicates, rounded to the nearest 0.05. The results are shown in Table 5.15 and demonstrate that K_{lf} measurements (and, by implication, K_{hf} since this is measured with the same equipment under the same conditions) have uncertainty values better than 1% of the measured values; these measurements are, therefore, precise and reproducible.

Table 5.15. Precision of magnetic susceptibility measurement.

Sample ref.	Mean (10^{-3} d.u.)	1 σ	%RSD
a (low-range)	11.70	0.09	0.75
b (mid-range)	24.00	0.05	0.23
c (high-range)	108.75	0.14	0.13

By normalization to sample weight, K_{lf} and K_{hf} values are converted to the MS parameters χ_{lf} and $\chi_{hf.}$, and the % difference between those parameters is the frequency-dependent parameter χ_{fd}. According to Maher (1988), χ_{fd} has significance at values between 7-15% (see Table 5.13). Many of the samples used in this study have low concentrations of magnetic minerals, and have very small differences between their K_{lf} and K_{hf} values (Fig. 5.9a). Accordingly, that relatively minor variation of <0.75%RSD identified in the K_{lf} precision test imposes large inaccuracies on the difference measurement between χ_{lf} and χ_{hf} (i.e. χ_{fd}). Prompted by that finding, and by the observation (Dr. Ian Foster, pers. comm.) that χ_{fd} determination is unreliable in low-concentration samples, estimates of error for the Harmignies χ_{fd} values have been calculated using a systematic error of ± 0.5%RSD. For small values of χ_{fd}, the error range is extremely large, confirming the Foster (2004) observation (Fig. 5.9b). In consequence, χ_{fd} appears to be an unreliable proxy for grain size in these samples.

An alternative granulometry parameter is found in the progressive randomisation of the individual magnetic moments in metastable SD magnetite grains near the SP threshold grain-size (Butler and Banerjee, 1975), known as viscous loss. It is, therefore, an indication of the presence of ultra-fine magnetite grains, which are likely to be pedogenic (Maher, 1992). Dearing *et al.* (1996) considers that it is more sensitive than χ_{fd}. In this

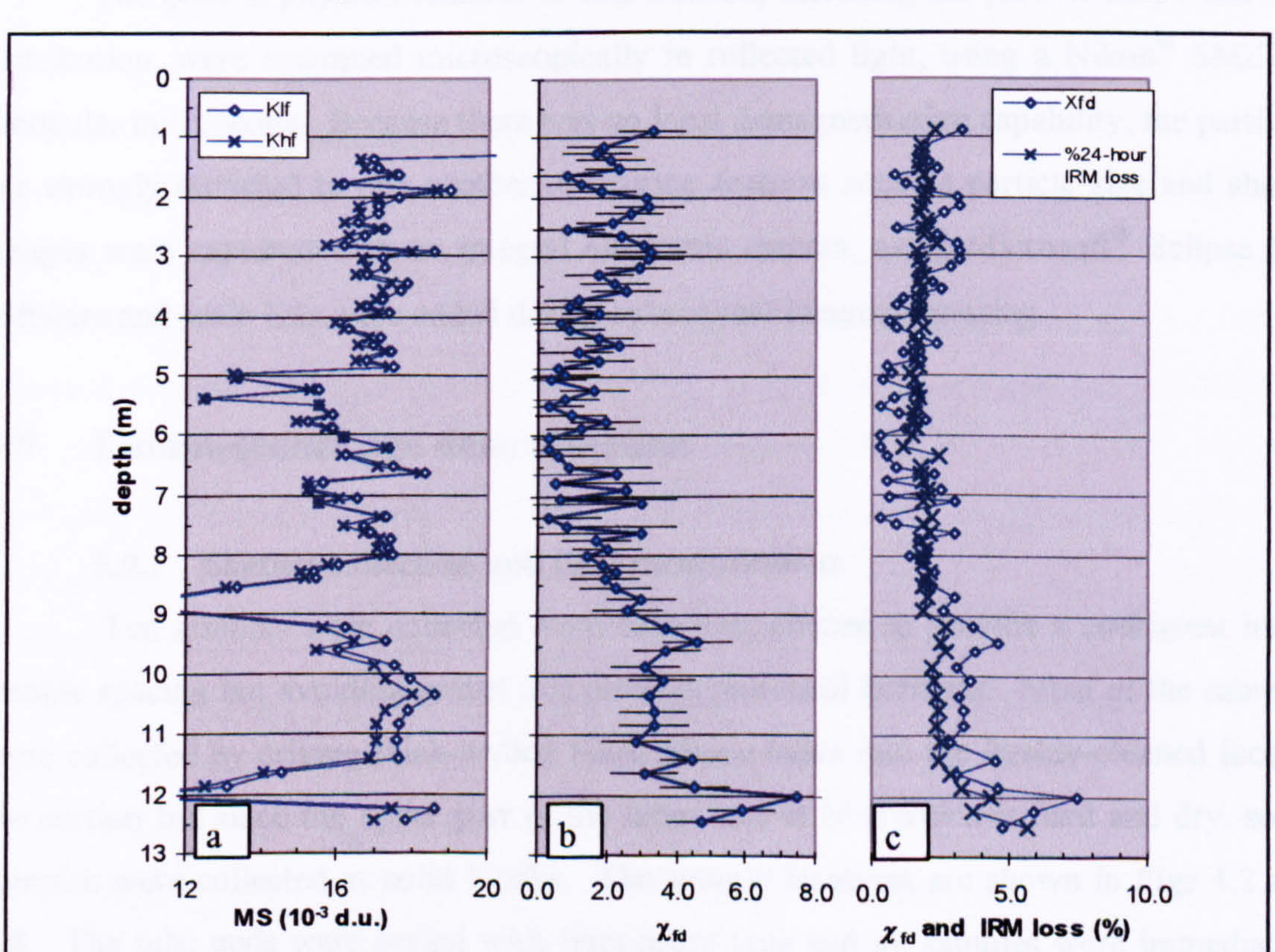

Fig. 5.9 Harmignies|: (a) selected range of the K_{lf} and K_{hf} data set, showing the limited difference between these parameters in most of the profile, (b) χ_{fd} with error bars representing a constant error of ±0.5%RSD on K_{lf} and K_{hf} values, and, (c) comparison of χ_{fd} and 24-hour IRM loss parameters.

study, viscous loss is defined as the IRM loss after 24 hours as a percentage of the initial IRM_{880mT} value. Fig. 5.9c demonstrates that it provides results generally comparable with χ_{fd}, but with greater apparent stability and it is used in this study.

5.8.6 Optical microscopy examination of the loess magnetic fraction

Initial enviromagnetic data analysis suggested that enviromagnetic properties were dominated by coarse-grain magnetite. It was decided to examine this fraction in isolation. A representative bulk sample from the aeolian part of each profile was dried and gently crushed to fine powder using a rubber pestle. A powerful hand magnet was used to separate the magnetic fraction from the loess matrix and this was used again to retain the magnetic fraction during washing with deionised water to remove as much as possible of the attendant silt. This provided two samples, each of approximately 0.05 g. It is now suspected, but unproved, that this technique selectively captured the coarse, strongly-magnetic fraction. The smallest particles visible in the images shown in Section 6.7.5 (e.g. Figs 6.51, 6.58) are approximately 10 μm (equivalent to PSD or MD magnetite); finer particles may have been cemented to silt particles or trapped in matrix, making them too heavy to lift. The technique's efficiency in extracting less-strongly-magnetic particles such as haematite is also suspect.

The general physical features of this fraction, including the particle shape and size distribution, were examined microscopically in reflected light, using a Nikon® SMZ800 binocular microscope. Because there was no local demagnetisation capability, the particles are strongly attracted to one another, obscuring features such as particle size and shape. Images were captured with an integral electronic camera, using Microsoft® Eclipse Net software and scale bars were added during subsequent image processing.

5.9 Luminescence age determination

5.9.1 Sample collection and field measurement

Ten samples were collected from each site, chosen to provide a consistent inter-sample spacing but avoiding gravel and obvious palaeosol horizons. Most of the samples were collected by driving thick-walled black plastic tubes into the freshly-cleaned face of the section but since the upper part of the loess face at Metternich is hard and dry, some samples were collected as solid blocks. The sample locations are shown in Figs 4.2 and 4.8. The tube ends were sealed with light-proof tape and all samples were immediately sealed in light-proof bags. At the same time, sub-samples were taken for moisture content determination.

In situ measurements of dose rate contributions (see Section 3.5.2) were made at Metternich using the EG&G microNomad portable NaI gamma spectrometer. *In situ* measurements were not obtained from Harmignies due to equipment failure. As a substitute, samples of sediment were taken from the cleaned face within a radius of 30 cm of each sampling point and subjected to Neutron Activation Analysis to quantify the dose rate contribution. For all samples, a homogenous radiation field is assumed.

5.9.2 Laboratory methodology

Samples were removed from their wrapping and processed in subdued red light. The solid blocks were shaved down to remove all the material that had been exposed to light. The light-exposed ends of the tubed samples were similarly shaved back and then the contents of the tube were removed.

The methodology followed Toms *et al.* (2004). Quartz grains in the 5-15 μm fraction, plus other mineral grains of varying density and size (including feldspars) were separated from the sample mass by acetone sedimentation. The carbonate content of this sub-sample was removed with 10% HCl; feldspars, other mineral grains and amorphous silica were removed by digestion in 35% H_2SiF_6 for two weeks (Berger *et al.*, 1980; Jackson *et al.*, 1976). After further treatment with 10% HCl to remove acid-soluble fluorides, grains degraded to <5 μm were removed by a further acetone sedimentation process, leaving a small sub-sample of processed grains in the size range 5-15 μm. Six aliquots (*ca.* 1.5 mg per sample) were mounted on aluminium discs.

Measurement was carried out using an automated TL-DA-5 Risø set. Blue light-emitting diodes, filtered by a 3 mm Schott GG420 (Bøtter-Jensen *et al.*, 1999) were used as the stimulating light source. The wavelength was 470Δ80 nm at a power of 15 $mWcm^{-2}$. Infra-red stimulation, provided by IR diodes, was used to indicate the presence of contaminating feldspars (Hütt *et al.*, 1988): none were detected, which shows that feldspars were successfully removed by the H_2SiF_6 acid digest treatment Photon emissions from each aliquot were filtered by three 2.5 mm HOYA U-340 and detected by a blue-green sensitive photomultiplier (EMI 9235QA) fitted with a bialkali photocathode. Natural luminescence signals were calibrated using regenerative-doses administered by a $^{90}Sr/^{90}Y$ beta source, itself calibrated for 5-15 μm quartz against the 'Hotspot 800' ^{60}Co gamma source at the National Physical Laboratory, UK.

Equivalent dose (D_e) estimates were made using a modified version of the single-aliquot regenerative dose (SAR) protocol (Murray and Wintle, 2000). Up to six different regenerative doses were given to define a linear portion of the dose response curve from each aliquot. The D_e value and associated error for each aliquot was then obtained by

interpolation from laboratory dose response and fitted using linear regression (Green and Margerison, 1978). A 260°C preheat was employed for 10 s prior to the measurement of the natural and regenerated luminescence. A 5 Gy test dose, made with a 180°C, 10 s preheat, was used to monitor the OSL response and correct for the change in sensitivity throughout the measurement of natural and regenerated luminescence. Optical stimulation of each aliquot occurred at 160°C to reduce the effects of phototransferred thermoluminescence. The weighted mean D_e value (central age model; Galbraith *et al.*, 1999) for each sample was calculated from the 6 aliquot results.

Dose rate calculations, based on the methodology described by Aitken (1985), incorporated dose rate conversion factors outlined by Adamiec and Aitken (1998) and the absorption coefficient for water content (Zimmerman, 1971), attaching a 25% relative uncertainty in an attempt to accommodate the effects of potential variations in past moisture content. The lower luminescence efficiency of alpha radiation was accommodated by incorporating an a-value for each sample of 0.051 ± 0.002 (Toms, pers. comm.). Cosmic dose rate estimations followed the Prescott and Hutton (1994) method. Luminescence ages were obtained by dividing the D_e value by the total dose rate value. The error in luminescence age estimates is quoted at 1σ confidence and is premised on the propagation of both systematic and experimental (1σ) errors associated with those parameters that lead to the calculation of D_e and dose rates (Toms, 2004). The dose rates, equivalent dose and optical age estimates are shown in Table 6.5.

Chapter 6. Results

This chapter addresses three of this study's objectives:

(a) for each site, production of detailed descriptions of major, minor and rare earth element concentrations,

(b) for each site, production of detailed descriptions of standard sedimentological parameters (grain size, organic carbon content, $CaCO_3$ content) and mineral magnetic properties, and,

(c) the application of new luminescence dating methodologies to enhance the rigour of the established chronology at each site, thus increasing confidence in correlations between loess-palaeosol sites and to other records of climate change.

6.2 Harmignies: geochemical analysis

6.1.1 Major element analysis - the carbonate-related elements Ca and Mg

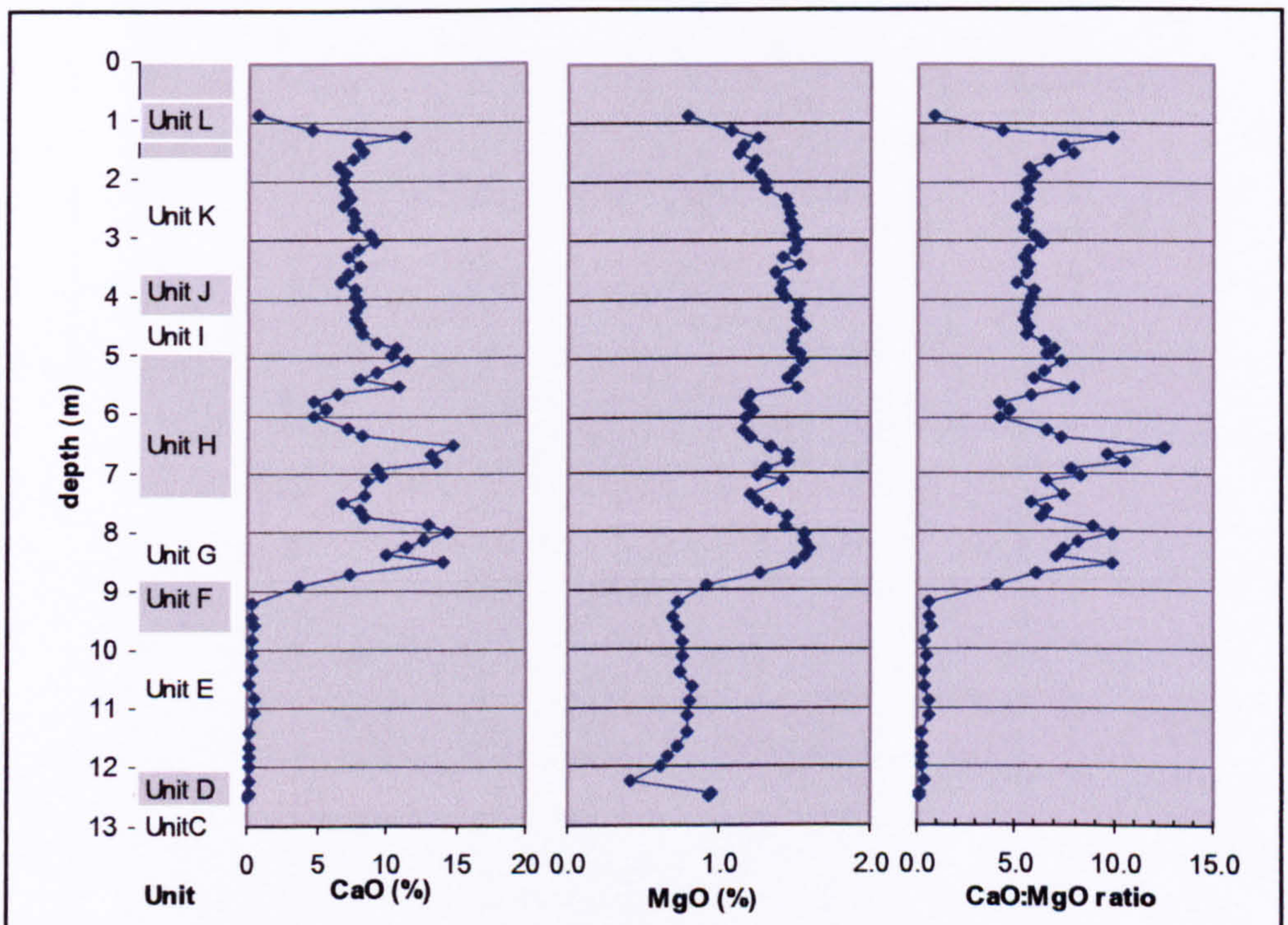

Figure 6.1 Harmignies: CaO and MgO concentrations, and CaO:MgO ratio.

Most of the major element variation at Harmignies is associated with the carbonate content (present in these ignited samples mainly as CaO). CaO has a profile mean of 6.8%, varying between 0.2-14.7% (Fig. 6.1). The very low CaO values in Unit D, E and lower Unit F are consistent with pedogenic decalcification from those palaeosols. The rapid increase in concentration in upper Unit F and Unit G is followed by a series of CaO peaks *c.* 8.5, 8.0, 6.5, 5.5, 5.0 and 1.3 m depth and troughs *c.* 7.5 and 5.7 m.

The MgO mean concentration is 1.4% (range 0.4-1.6%) (Fig. 6.1). Although, like CaO, the lowest values occur below mid-Unit F, consistent with pedogenic decalcification, MgO concentrations in those palaeosols are approximately half of the loess values, suggesting that Mg is also carried in non-carbonate, weathering-resistant minerals. MgO concentrations rise to a relatively constant level in Unit G. The MgO profile does not show the same degree of variation as CaO and the CaO:MgO ratio (Fig. 6.1) shows that during periods of carbonate increase, CaO increases by a larger proportion than MgO. During periods of little change (e.g. upper Unit H, Unit I, J and most of K) the ratio is invariant. This suggests that the CaO peaks are caused by the local reprecipitation of (Mg-poor) calcite. There are two episodes of MgO depletion, *c.* 7.5 and 6 m depth, coincident with CaO depletion, and there is slight depletion *c.* 1.5-1.4 m. Values then rise slightly at 1.2 m before diminishing rapidly in the base of the overlying post-glacial soil.

6.1.2 Major element analysis - the non-carbonate major elements: Si, Ti, Al, Fe, Mn, Na, K and P

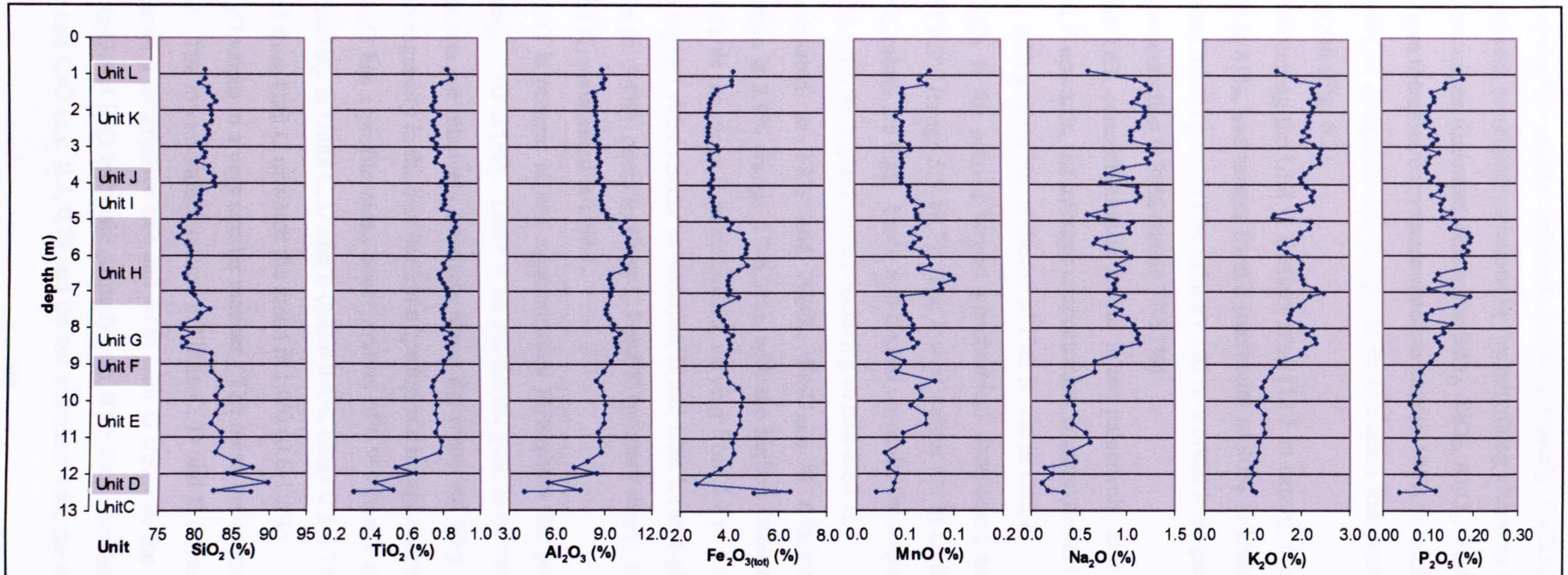

Figure 6.2. Harmignies: SiO_2, TiO_2, Al_2O_3, $Fe_2O_{3(tot)}$, MnO, Na_2O and K_2O concentrations (corrected to sum to 100%, independent of CaO).

Because of the 'constant sum' problem (that compositions total 100%), the high and independently-variable carbonate content (mainly $CaCO_3$) in these samples may impose apparent correlated variations in the remaining elements (Rollinson, 1993). The % composition values discussed below for SiO_2, TiO_2, Al_2O_3, $Fe_2O_{3(tot)}$, MnO, MgO, Na_2O and K_2O have therefore been recalculated to sum to 100% in each sample in order to allow their patterns of compositional change to be examined independently of variation in that $CaCO_3$ content (Fig. 6.2).

Discounting the Unit C Tertiary sand (12.5 m depth), the average SiO_2 content for the profile is 81%, and ranges from a maximum of 90% in Unit D (Eemian palaeosol) to 77%. From Unit F upwards (the primary and re-worked loess part of the profile), the SiO_2 average concentration is 80% (range 77-83%).

The TiO_2 concentration is lowest in the palaeosols, at 0.3-0.6% (Units D and E). From Unit F upwards, the average concentration is approximately constant at 0.8% (range 0.7-0.9%), with a slight rise at the top of Unit K and in Unit L.

Al_2O_3 is the second largest geochemical component and contributes an overall average of 9.2% (range 5.5-10.7). The lowest values are in Units C, D and lower Unit E, where SiO_2 values are high. From mid-Unit E upwards, the average content is 9.4% (range 8.5-10.7%), with the highest values occurring in mid-Unit H.

Compared to TiO_2 and Al_2O_3, $Fe_2O_{3(tot)}$ is relatively variable. The mean concentration is 3.9% (range 2.7-6.5%), with the highest concentration in Unit D. From Unit F upwards the range is more limited, varying from 3.2 to 4.8% about a mean of 3.8%. Here, the highest values occur in mid-Unit H and Unit L (post-glacial soil), and consistent low values (*c.* 3.4%) occur in Units I, J and K (primary loess). It shows a slight rise at the top of Unit K, maintained in Unit L.

MnO is present at low concentration throughout the profile, with an average of 0.06% (range 0.03-0.1%). There is no systematic pattern of variation: above mid-Unit H concentrations are relatively invariant about the mean but they vary below that, possibly due to heterogeneity in the distribution of pedogenic manganese nodules.

Na_2O has a profile mean concentration of 0.9% (range 0.1-1.6%), with the lowest values occurring in Units C, D and E (mean 0.4%, range 0.1-0.7%). Concentrations rise in Unit F and from Unit G upwards the mean is 1.0% (0.6-1.6%).

K_2O varies in a very similar manner. The mean concentration value is 1.9% (range 0.9-2.5%). The lowest values occur in Units C, D and E (mean 1.1%, range 0.9-1.4%), Unit F shows a progressive rise and from Unit G upwards the mean is 2.1% (range 1.4-2.5%). Na_2O and K_2O correlate strongly (c.c. 0.9); they correlate less strongly with MgO (c.c. 0.7) and CaO (c.c. 0.7, 0.8) and do not correlate with the remaining major elements.

This isolates Na, K, Ca, Mg (and Sr, see Section 6.1.3) as a group of co-varying elements. This is due to their common relatively high solubilities under weathering conditions (see Section 3.4): weathering behaviour is addressed in Section 7.4.

P_2O_5 is present at very low levels, below 0.2%. Variation in its distribution does not correlate with any stratigraphic features, except a slight increase at the base of Unit L, the post-glacial soil.

6.1.3 Minor element analysis

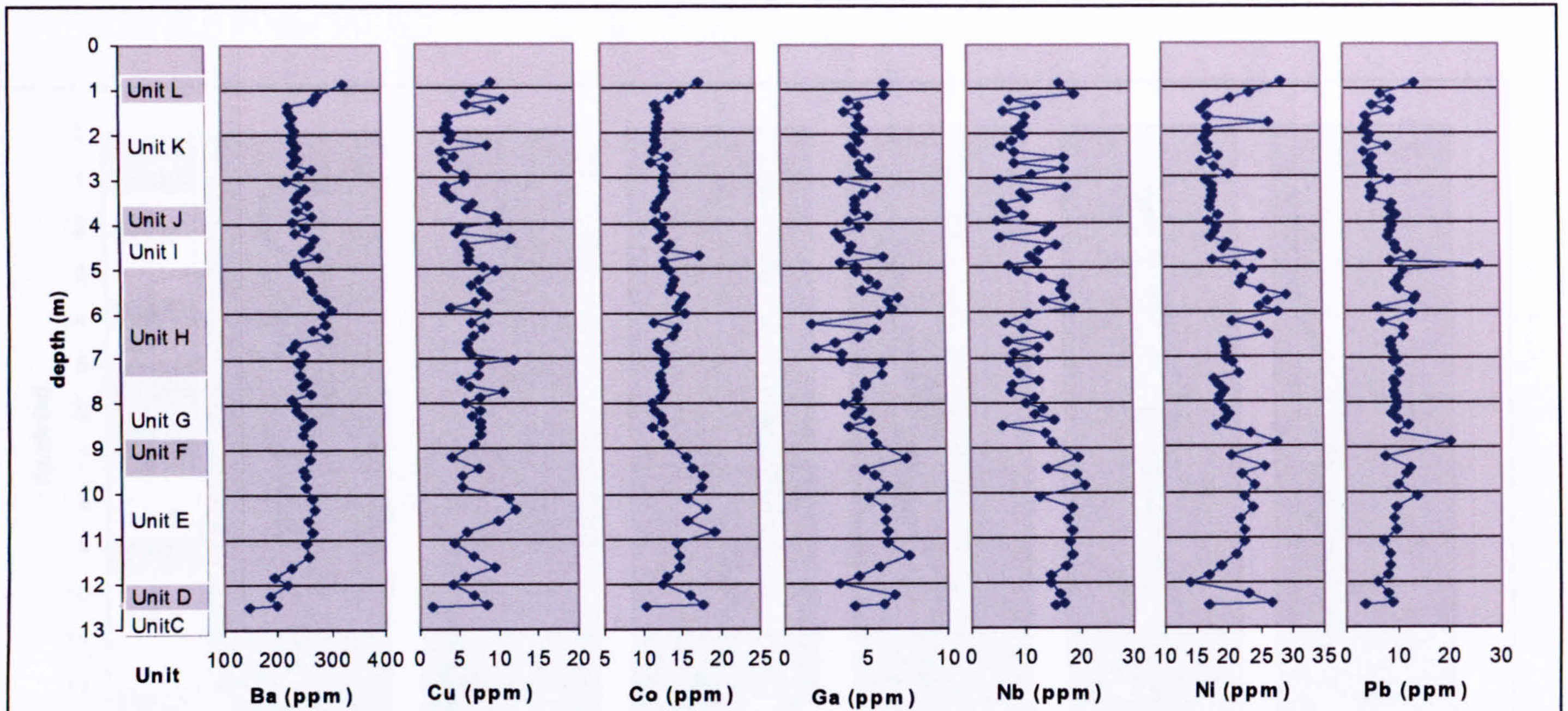

Fig 6.3a: Harmignies: minor element concentrations.

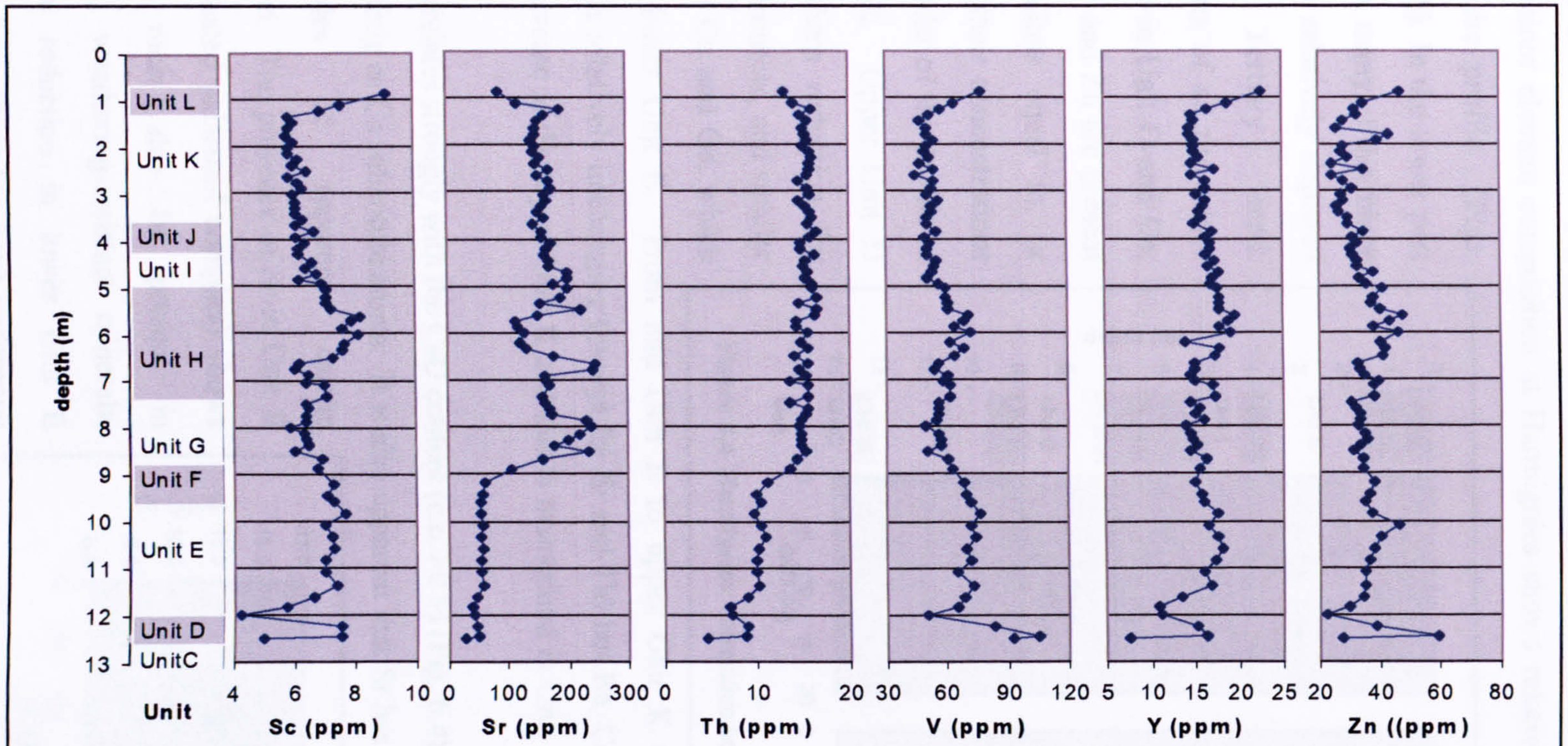

Figure 6.3b. Harmignies: minor element concentrations.

The minor elements analysed in this study are defined in Section 3.2.1. Minor element samples were taken from the original samples, which have high and variable carbonate contents. In consequence, results have been recalculated to 'carbonate-free' values as was done with the major elements, using the using the carbonate content determined by gasometric analysis (see Section 6.5).

The minor element composition at Harmignies shows relatively small variation against the site profile (Figs. 6.3a and 6.3b). In the lower part of the profile, many of the minor elements are relatively depleted in the Tertiary sand. Concentrations of all the minor elements rise in Unit D and Co, Ni, Sc, V, Y and Zn are present at concentrations equal to, or higher than, their concentrations in the remainder of the profile to upper Unit K. Upper Unit D exhibits a sharp reduction for those same elements, and smaller reductions in Cu and Ga, which extend into lower Unit E. From mid Unit E to upper Unit K the minor element composition is relatively unchanging (except for Sr and Th) but Ba, Co, Nb, Ni, Sc, V, Y and Zn all increase at the top of Unit K and this is maintained in Unit L – the post-glacial soil.

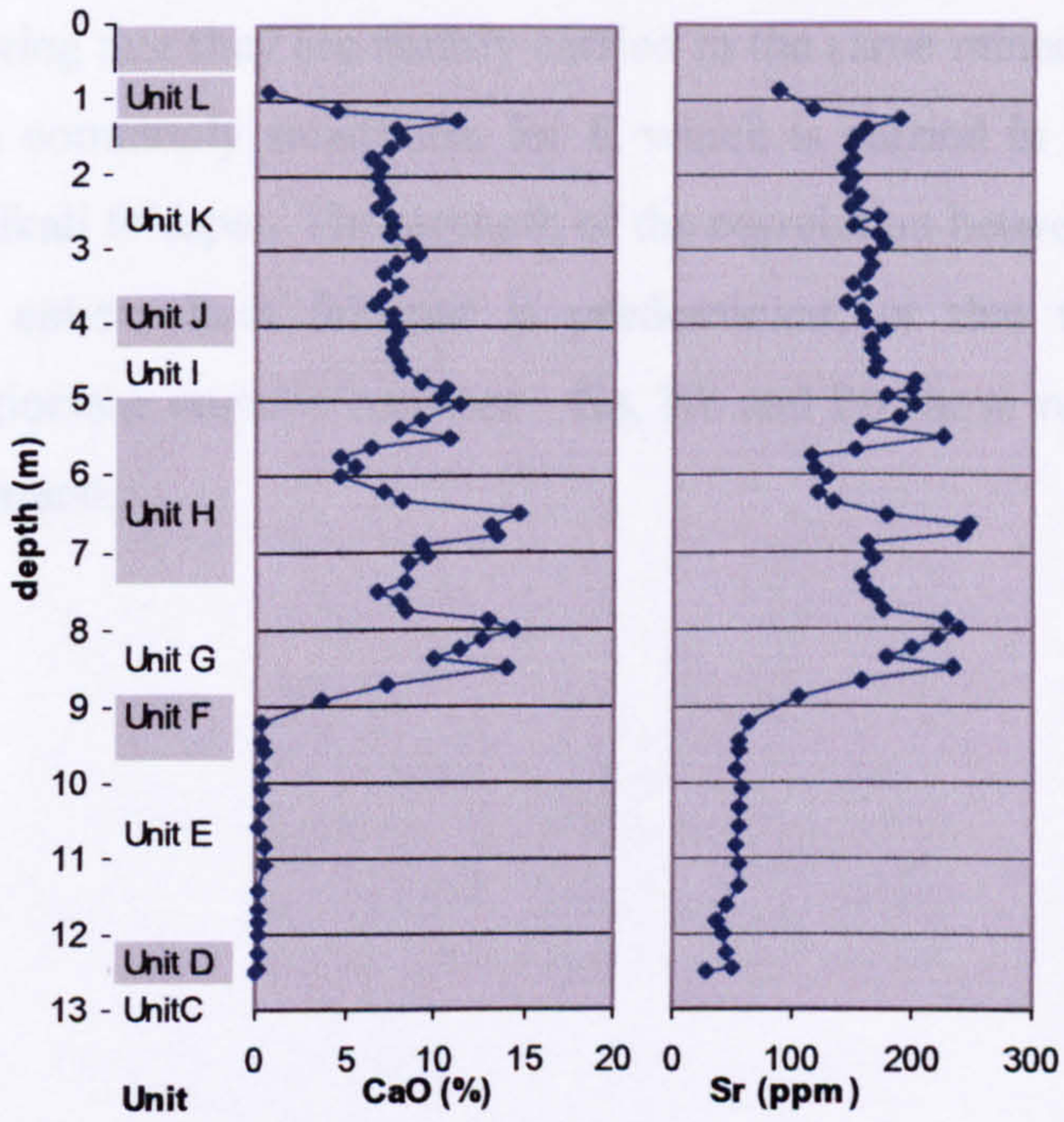

Figure 6.4 Harmignies: correlation between CaO and Sr.

Sr correlates strongly with the CaO content (c.c. >0.9) (Fig. 6.4), confirming that Sr is present mainly as Ca substitute atoms. It is also apparent that Sr has accompanied Ca in the episodes of apparent calcite reprecipitation. The presence of Sr in Unit E (the decarbonated palaeosol complex) shows that some must also be present in (unidentified) weathering-resistant minerals, although the reduction in lower Unit E suggests that here, those too have undergone weathering attack.

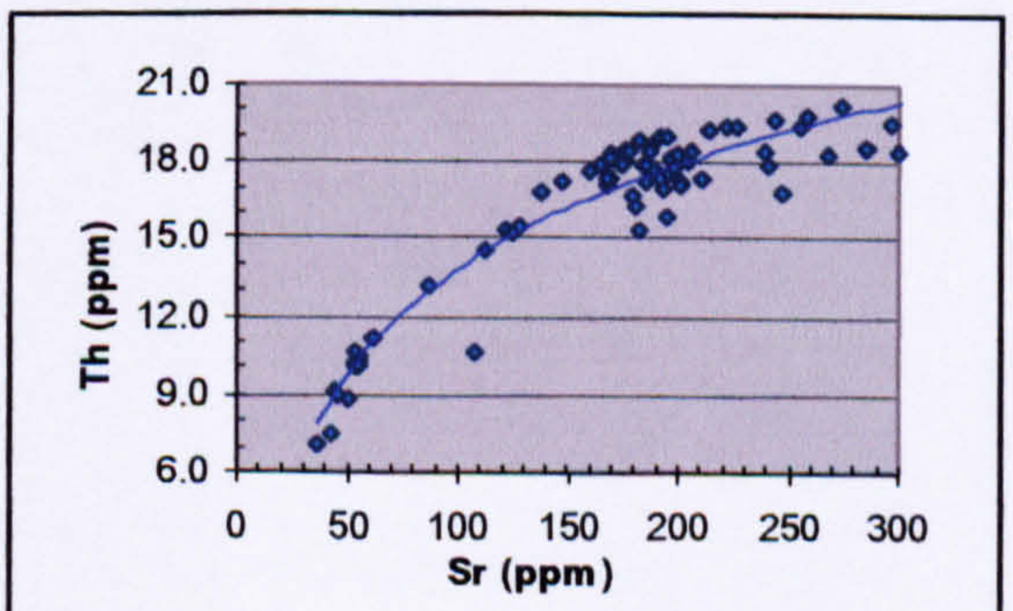

Figure 6.5. Harmignies: correlation between Sr and Th.

For reasons that are unknown, Sr correlates strongly with Th, with the best fit given by a logarithmic trendline[1] ($R^2 = 0.92$) (Fig. 6.5). Like Sr, Th is present in the palaeosol complex and in the overlying loess but unlike Sr, Th is carried by minerals such as monazite, quartz, biotite and orthoclase (anon., 2005).

Zn, Co, Ni, Cu, Sc, Y and V inter-correlate (c.c. 0.8-0.65), suggesting that they are carried in a linked group of minerals. Ni and V also correlate with $Fe_2O_{3(tot)}$ (c.c. 0.6, 0.7), possibly indicative of iron minerals such as magnetite (Gross, 1998). Ba correlates strongly with Al_2O_3 (c.c. 0.8), suggesting that they are mainly carried in the same mineral. Al is carried mainly in feldspars, Ba commonly substitutes for K which is carried in K-feldspar, so this mineral is probably alkali feldspar. The strength of the correlation between Ba and Al_2O_3 might indicate that either alkali feldspar is predominant, or that the proportion of alkali feldspar and plagioclase remains constant. Ga, Nb and Pb show very weak or no correlations with other elements.

[1] For logarithmic trendlines, Microsoft Excel calculates the least squares fit for a line represented by the equation $y = c\ln x + b$, where b and c are constants and ln is the natural logarithmic function. For linear trendlines, the equation is $y = mx + b$, where m is the slope and b is the intercept.

6.1.4 REE analysis

As with the major and trace elements, REE results have been corrected for the high and variable carbonate content using CaO values derived from ICP-OES major-element analysis and normalised against standard chondrite values (Taylor and McLennan, 1985), (Figs 6.6 and 6.7) except where stated.

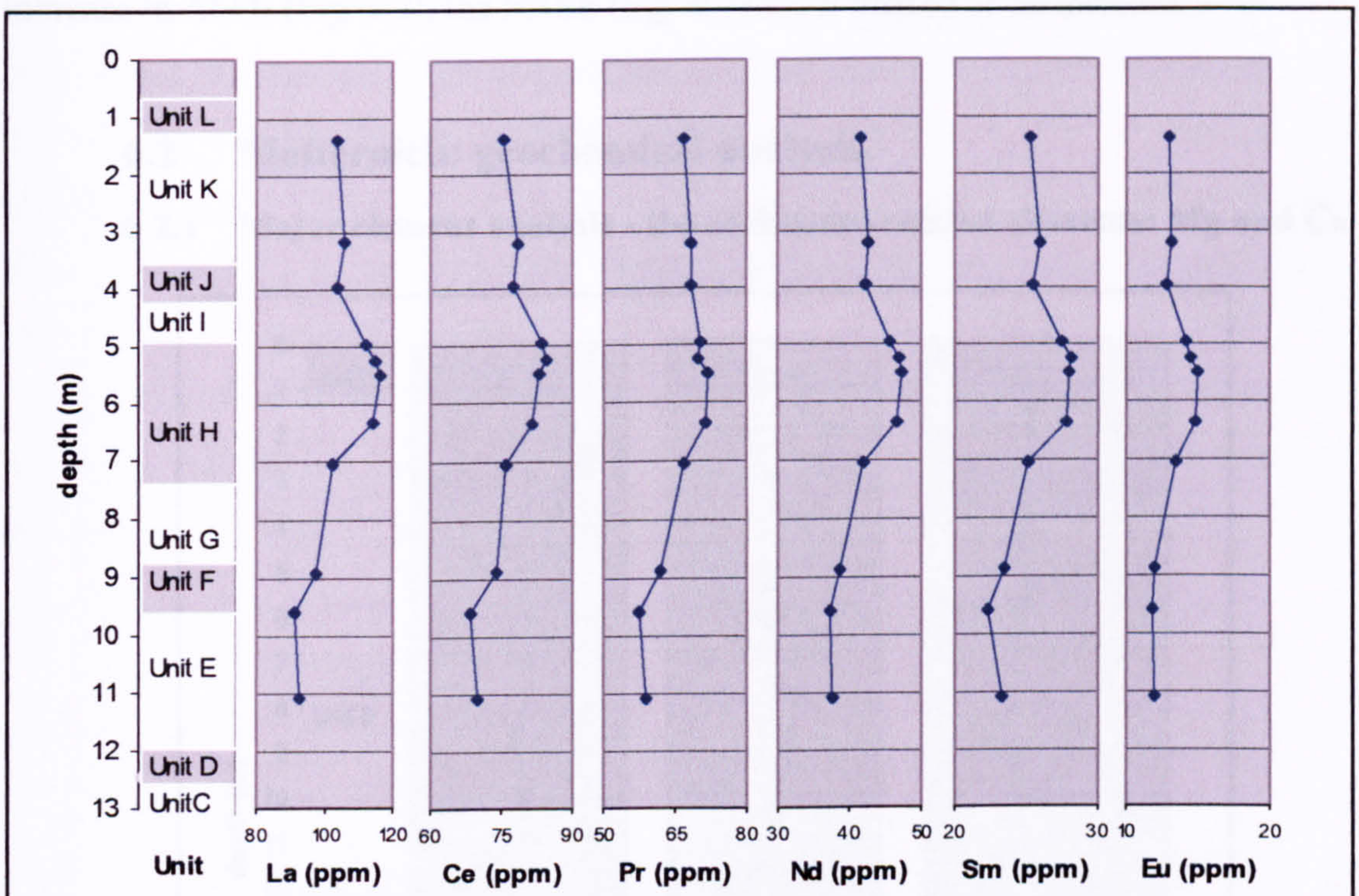

Figure 6.6. Harmignies: light rare-earth element concentrations.

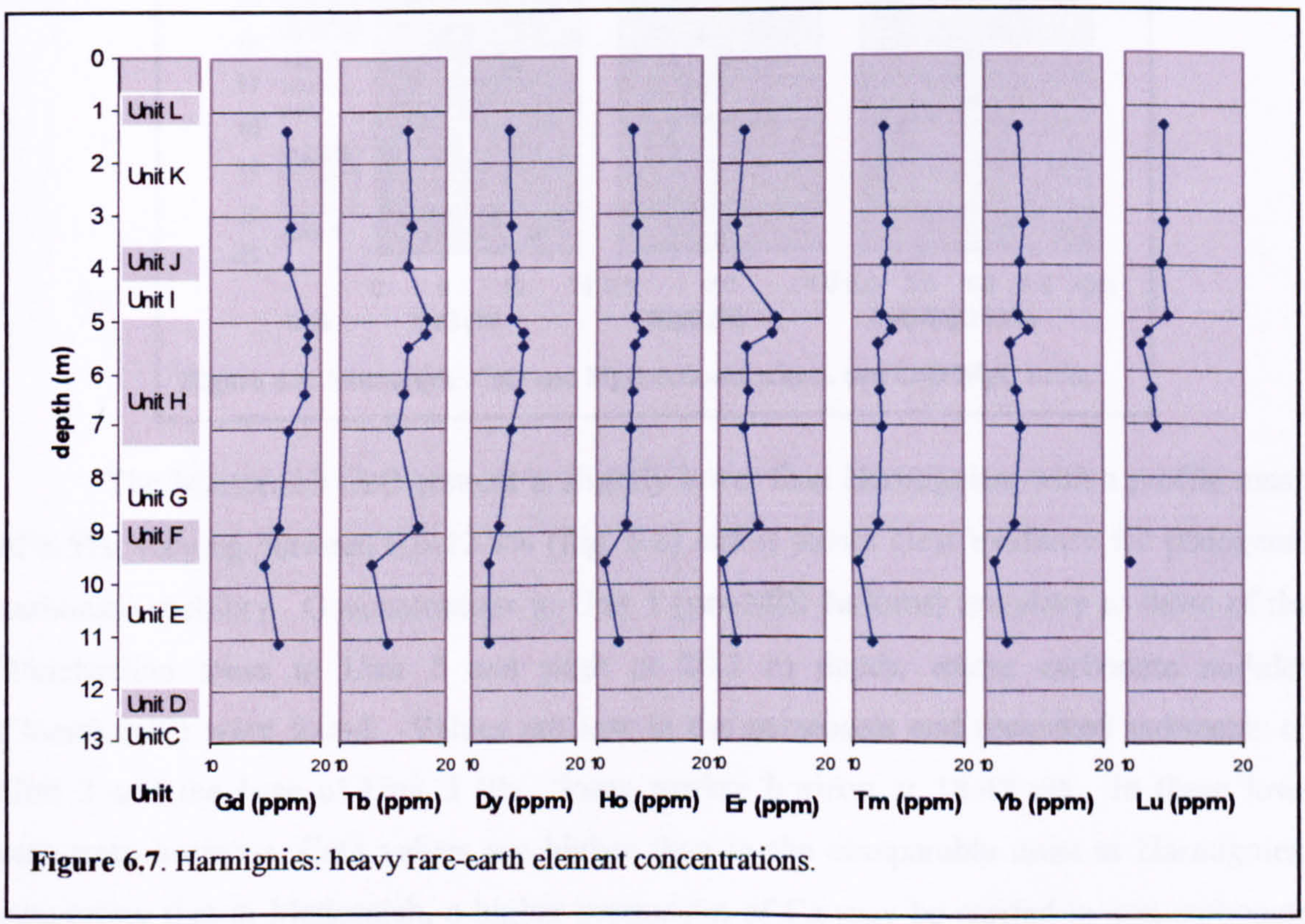

Figure 6.7. Harmignies: heavy rare-earth element concentrations.

The REE concentration at Harmignies is relatively low in Unit E and lower Unit F (early Weichselian palaeosols) and increases at the top of Unit F, coincident with the start of aeolian deposition. The LREE (Fig. 6.6) show a large increase in Unit H between at least 6.5-5.0 m and then return to their previous concentrations, correlating with the increase in Al_2O_3 (Fig. 6.2); the HREE (Fig. 6.7) show limited or no increase.

6.2 Metternich: geochemical analysis.

6.2.1 Major element analysis - the carbonate-related elements: Mg and Ca

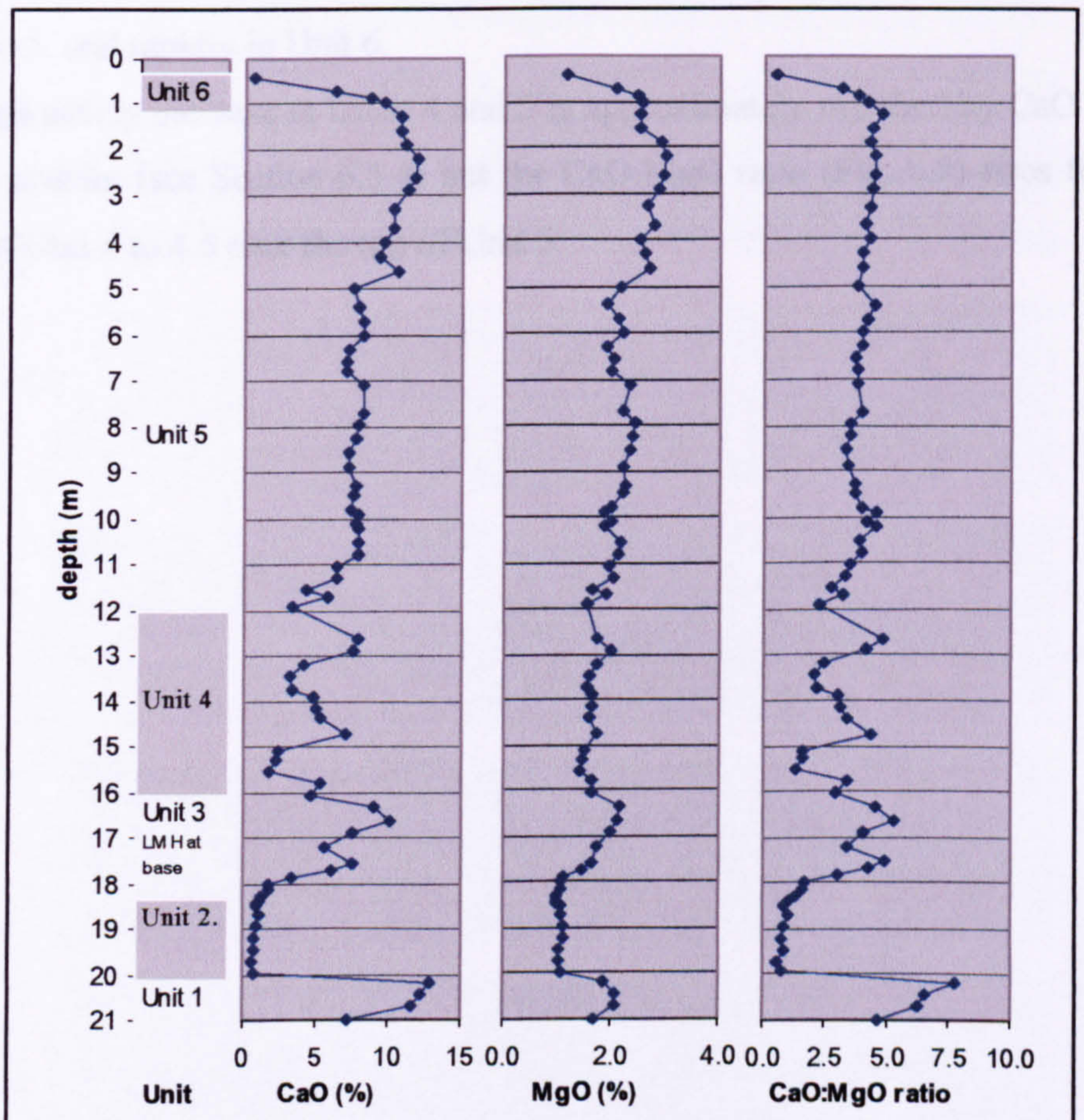

Figure 6.8. Metternich: CaO and MgO concentrations, and CaO:MgO ratio.

The Metternich CaO content is slightly lower than Harmignies, with a profile mean of 6.5%, varying between 0.6-12.8% (Fig. 6.8) and it shows clear evidence for pedogenic carbonate mobility. Concentrations in Unit 1 (pre-MIS 5a loess) are close to those of the Weichselian loess in Unit 5 and peak at 20.2 m depth, where carbonate nodules ('loesskindl') were found. Values are low in the palaeosols and reworked sediments of Unit 2 and the base of Unit 3 (the 'loess marker horizon at 18.45 m). In these low-carbonate horizons, CaO values are higher than in the comparable units at Harmignies, suggesting that at Metternich, a higher proportion of Ca may be carried in non-carbonate

minerals. Immediately above the 'loess marker horizon', the CaO content starts to rise and varies markedly throughout the remainder of Unit 3, Unit 4 and lower Unit 5. In Unit 5, above 11 m, values become less variable and show only a progressive increase to upper Unit 5 when values start to fall slowly at c. 2 m depth and rapidly above 1 m depth, in Unit 6 (post-glacial soil).

The mean MgO concentration is 1.8% (1.0-2.8%) (Fig. 6.8), approximately 50% higher than Harmignies. MgO concentrations follow the same overall trend as CaO but do not co-vary with the 'spikey' pattern of CaO concentration. MgO concentrations are relatively high in Unit 1, low in Unit 2, rising in Unit 3 and they increase progressively from 1.6% to 2.5% throughout Units 4 and 5. Values drop slightly above 2 m depth, at the top of Unit 5, and rapidly in Unit 6.

That steady increase in Units 4 and 5 is approximately matched by CaO and by the carbonate content (see Section 6.5.4) but the CaO:MgO ratio (Fig. 6.8) rises from c. 3 at the base of Unit 4 to 4.5 near the top of Unit 5.

6.2.2 Major element analysis - the non-carbonate major elements: Si, Ti, Al, Fe, Mn, Na, K and P.

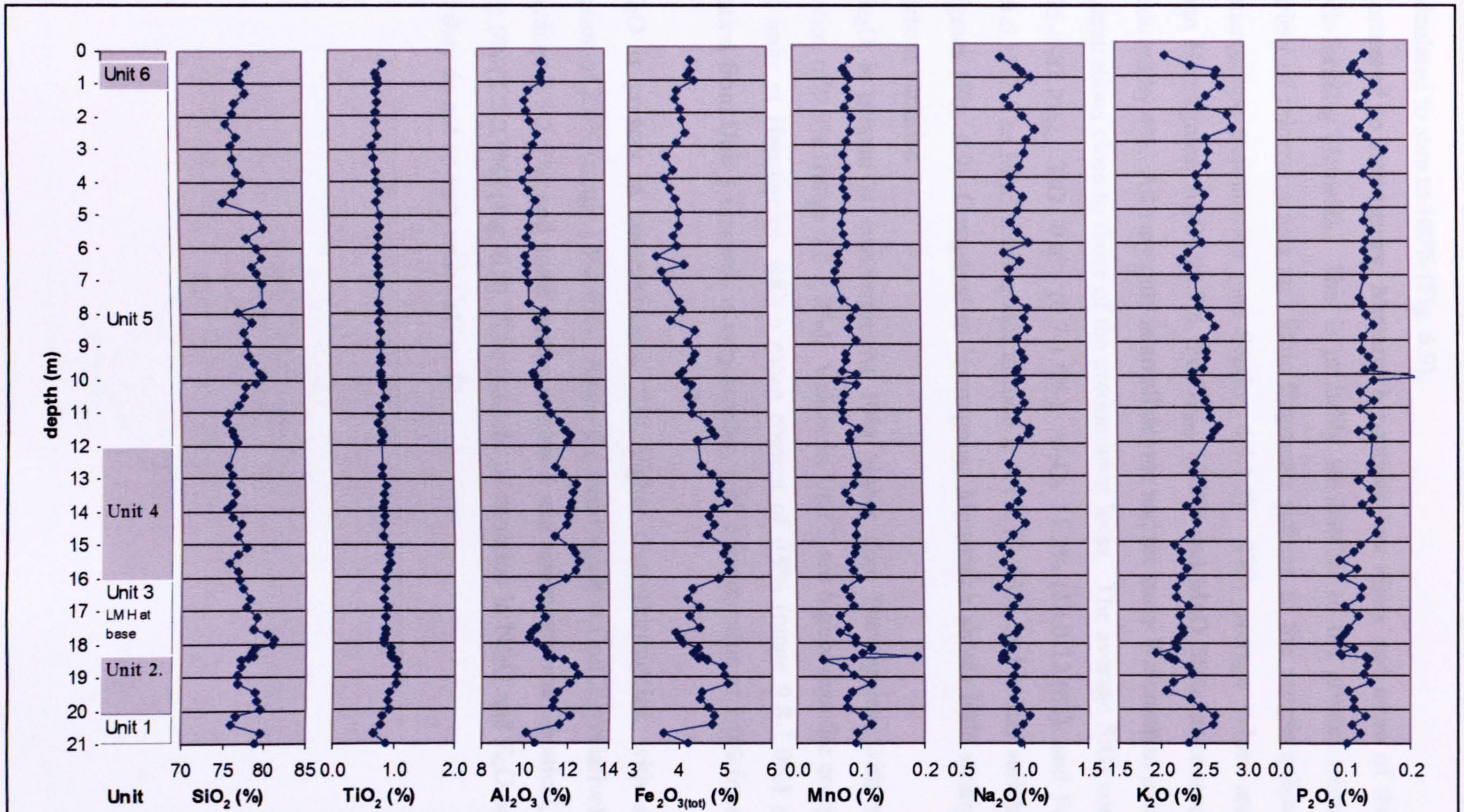

Figure 6.9. Metternich: SiO_2, TiO_2, Al_2O_3, $Fe_2O_{3(tot)}$, MnO, Na_2O and K_2O concentrations (corrected to sum to 100%, to be independent of CaO).

Because these samples have a high and variable carbonate content, the composition values discussed below for SiO_2, TiO_2, Al_2O_3, $Fe_2O_{3(tot)}$, MnO, MgO, Na_2O and K_2O have been recalculated to sum to 100% (Fig. 6.9).

Compared to Harmignies, Metternich contains less silica and more of the other major rock-forming elements. This is probably attributable to the greater amount and larger variety of mineral grains and lithic fragments present in the sample subjected to optical microscope examination (see Section 6.4.1.2). TiO_2 average values are 8.7% higher than Harmignies, Al_2O_3 22.9%, $Fe_2O_{3(tot)}$ 12.2% and MnO 56%; in consequence, SiO_2 is reduced by 4%. All vary only in small degree and the early Weichselian palaeosols have concentrations close to those of the predominant loess. The average SiO_2 content is 77.7% (75-3-81.2%), TiO_2 0.8% (0.7-1.0%), Al_2O_3 11.2% (10.0-12.6%), and $Fe_2O_{3(tot)}$ 4.4% (3.6-5.1%). The MnO mean concentration is 0.1% (0-.2%), and is less variable than at Harmignies (Fig. 6.9). Compared to Harmignies, Metternich shows little stratigraphic major-element variation

Na_2O is present at concentrations 10% higher than Harmignies, with a mean concentration of 0.9% (range 0.8-1.2%). Values in Unit 2 are higher than the comparable palaeosol units at Harmignies, with a mean content of 0.9% (range 0.8-1.0%) and the concentration from Unit 3 upwards is very similar, with a mean value of 1.0% (range 0.8-1.2%).

K_2O is present in concentrations 30% higher than Harmignies, with a mean concentration of 2.4% (range 1.9-2.9%). Again the mean value in Unit 2 is relatively high, at 2.3% (range 2.3-2.5%) and again values in Unit 3 and above are near identical, with a mean of 2.5% (2.2-2.9%) (Fig. 6.9). The patterns of variation in Na_2O and K_2O correlate at 0.8 but they do not co-vary with CaO or Sr.

6.2.3 Minor element analysis.

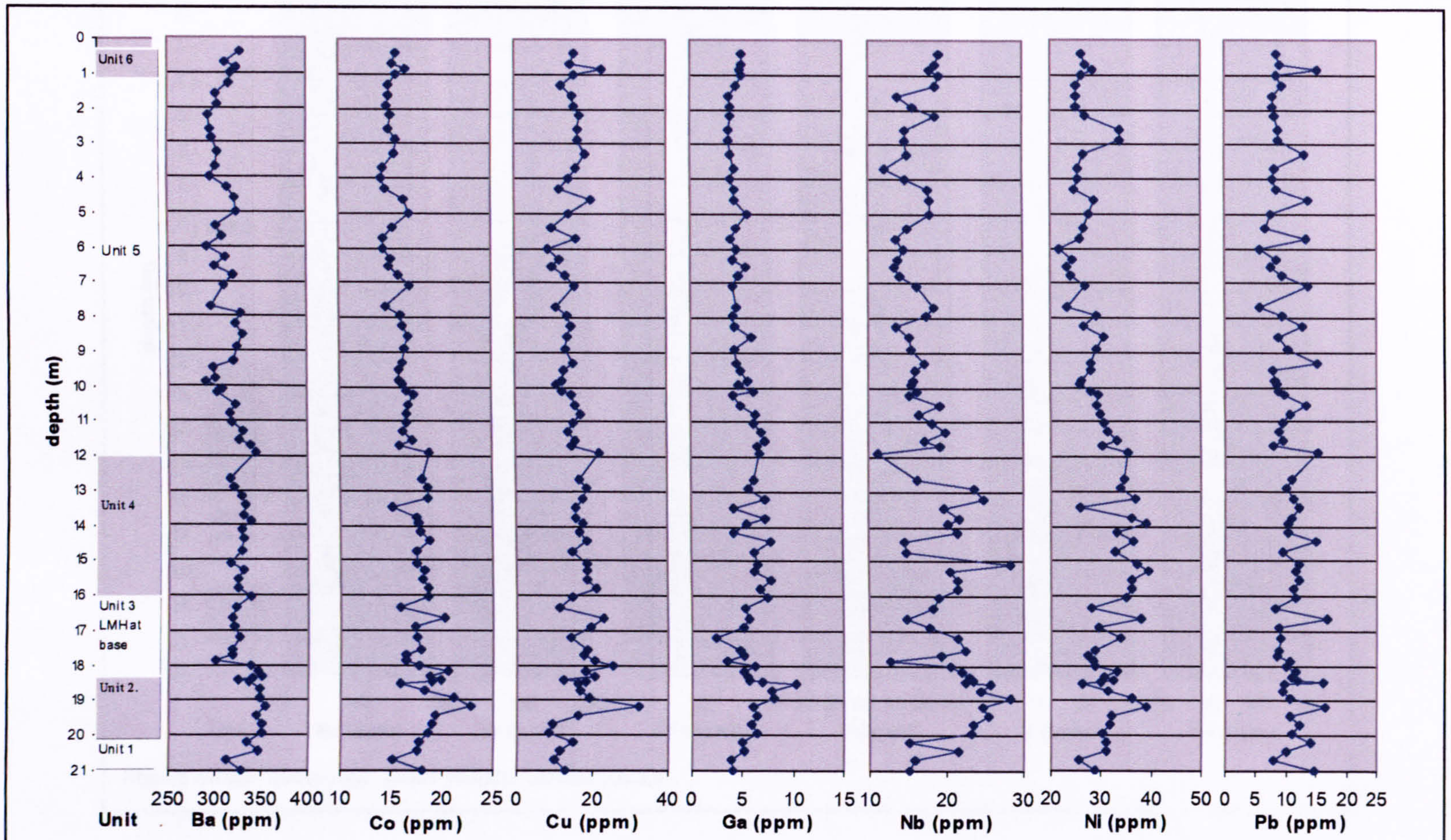

Figure 6.10a. Metternich: minor element concentrations.

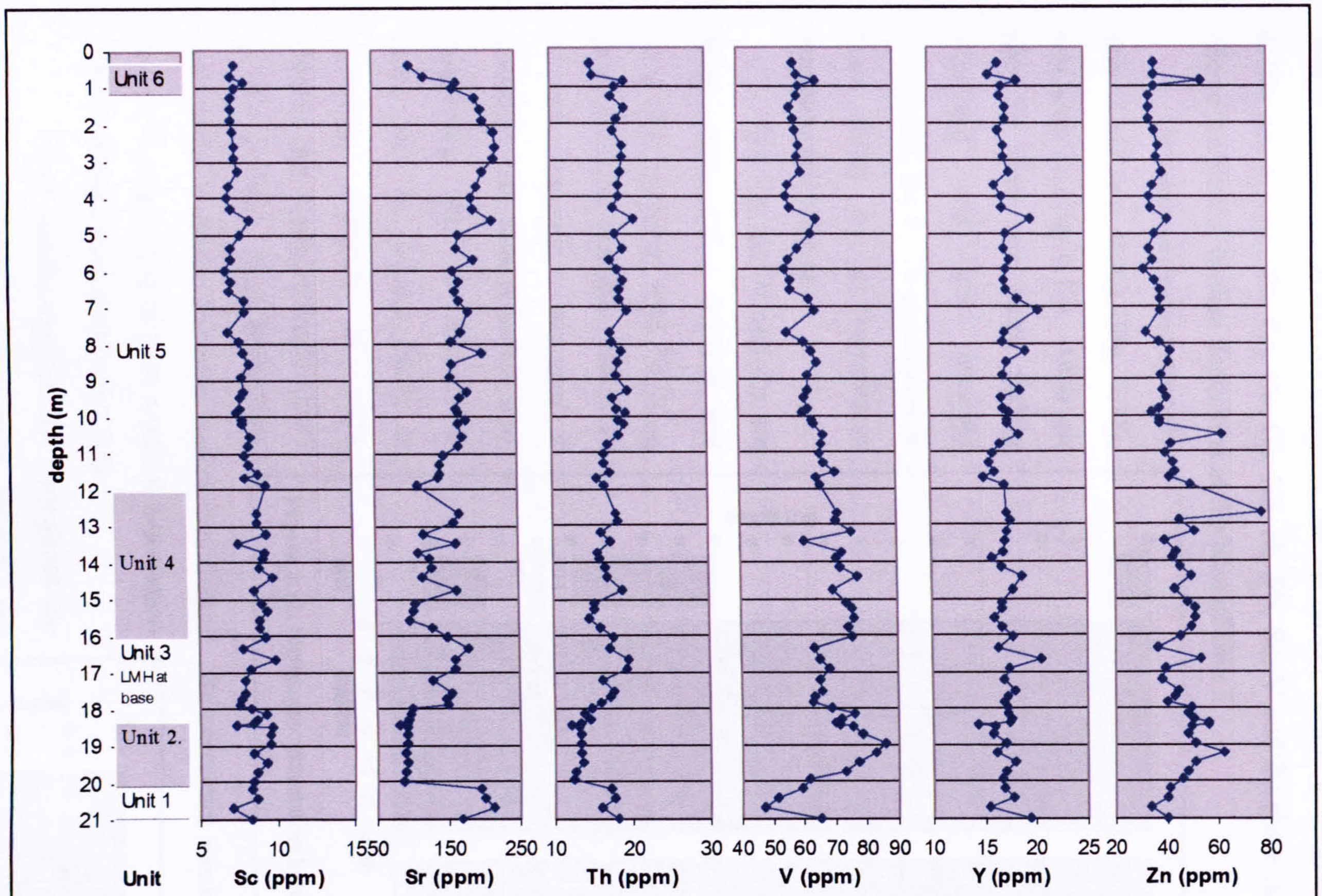

Figure 6.10b. Metternich: minor element concentrations.

Like the major element concentrations, the minor element concentrations at Metternich are substantially higher than at Harmignies, presumably for the same reasons. For the full profile, the mean minor element concentration is 27% higher but this is not equally distributed: Ga, Sr and Y are present at concentrations less than 10% higher while Nb and Ni are present at concentrations more than 40% higher. Like Harmignies, the minor element composition throughout the Metternich profile is relatively invariant (Figs. 6.10a and 6.10b). Ba, Co, Cu, Ga, Nb, Ni, Pb, Sc, V and Zn show no significant trend above the start of aeolian deposition at the base of Unit 3.

Sr again co-varies strongly with CaO (c.c. 0.95) (Fig. 6.11), and with Th (Fig. 6.12). Although the Th data are more tightly clustered and less strongly correlated, the Sr:Th correlation is best fitted by a logarithmic trendline ($R^2 = 0.64$).

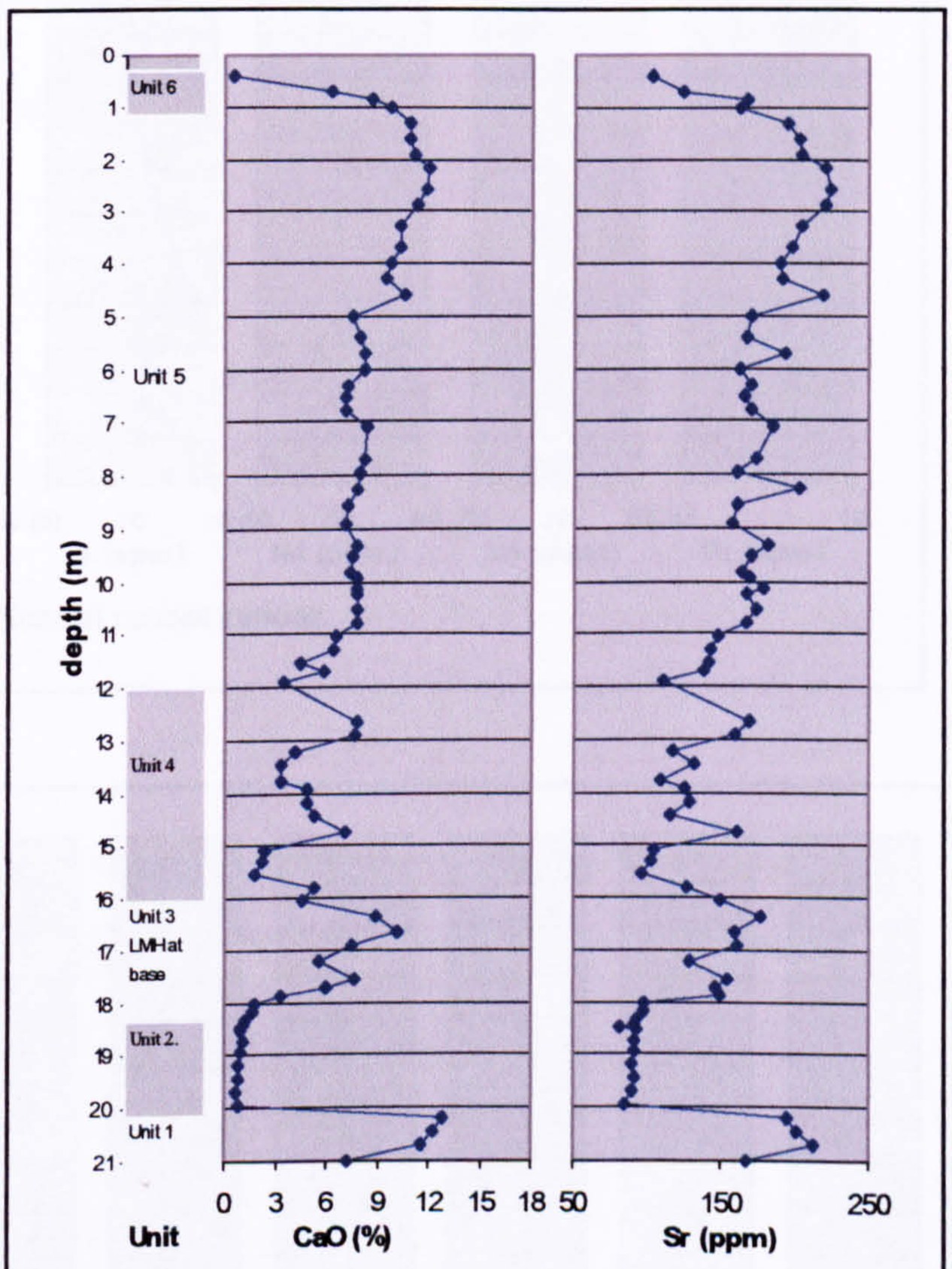

Figure 6.11. Metternich: correlation between CaO and Sr.

Ni, Co, Sc, V and Ga are inter-correlated (c.c. 0.7-0.9), and they also correlate with $Fe_2O_{3(tot)}$ (c.c. 0.7-0.8), possibly indicative of iron minerals. Nb and V correlate with TiO_2 (c.c. 0.7, 0.8), suggesting that at Metternich, these may be present partly as accessory elements in rutile, titanite and other minerals (Zack et al., 2004). This Nb/V/TiO_2 association is absent from the Harmignies dataset. Ba correlates moderately with Al_2O_3 (c.c. 0.7), suggesting at least a partial association with K-feldspar (see Section 6.1.2.3).

These results suggest that throughout the Metternich profile's formational period, the population of particles carrying the minor elements had a relatively constant composition.

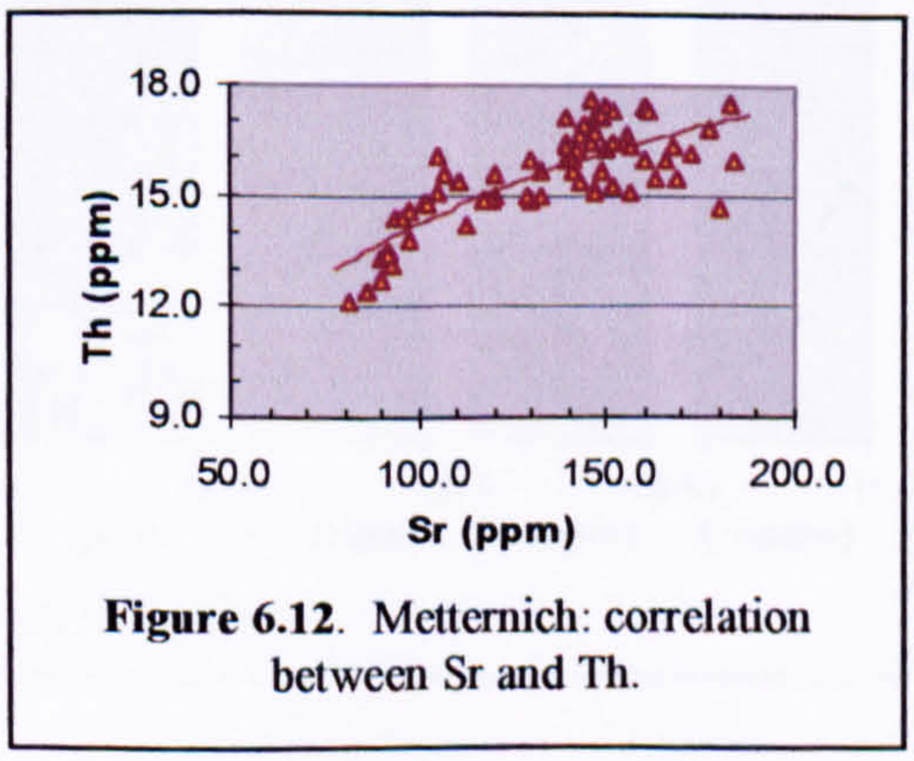

Figure 6.12. Metternich: correlation between Sr and Th.

6.2.4. REE analysis

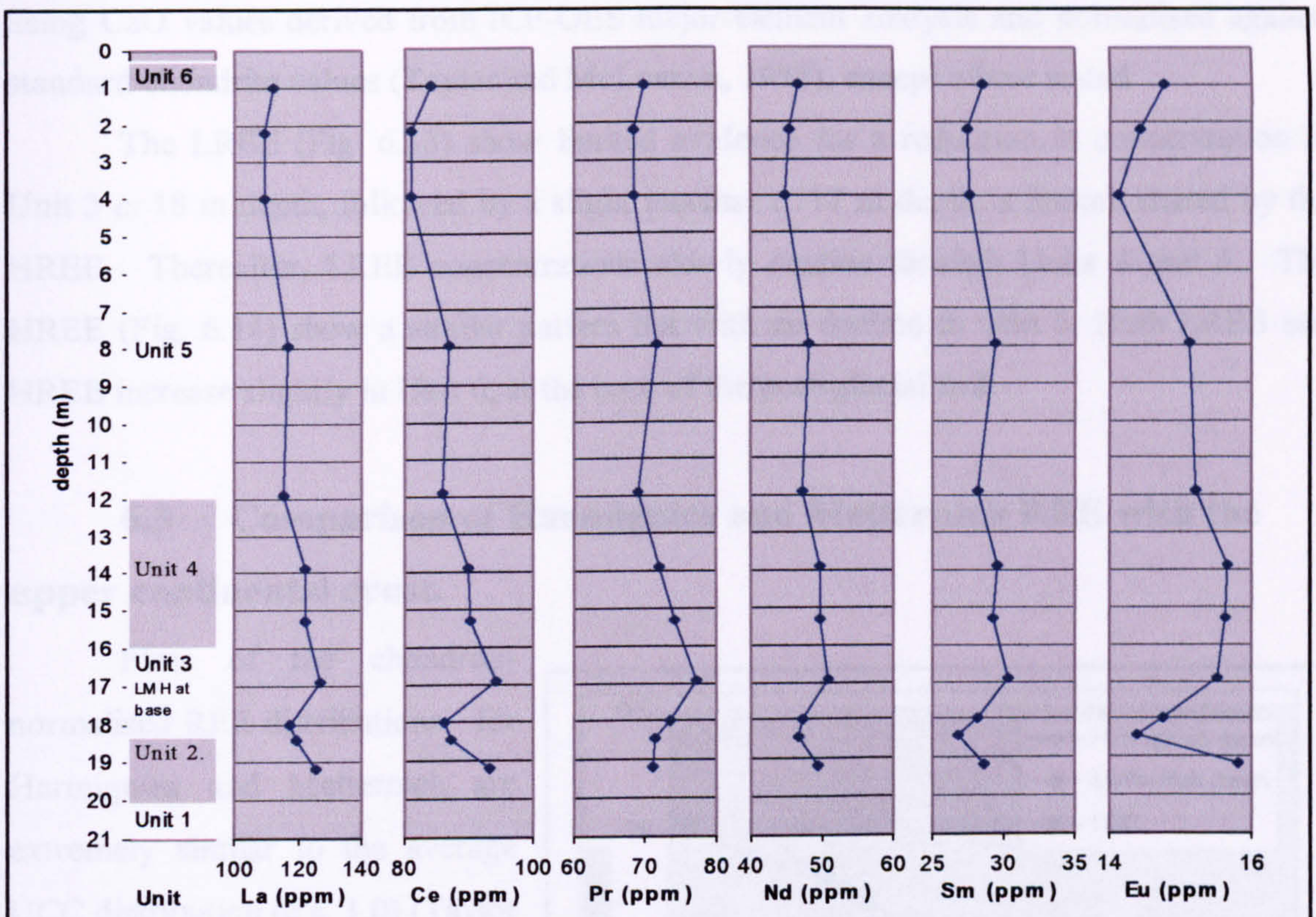

Figure 6.13. Metternich: light rare-earth element concentrations.

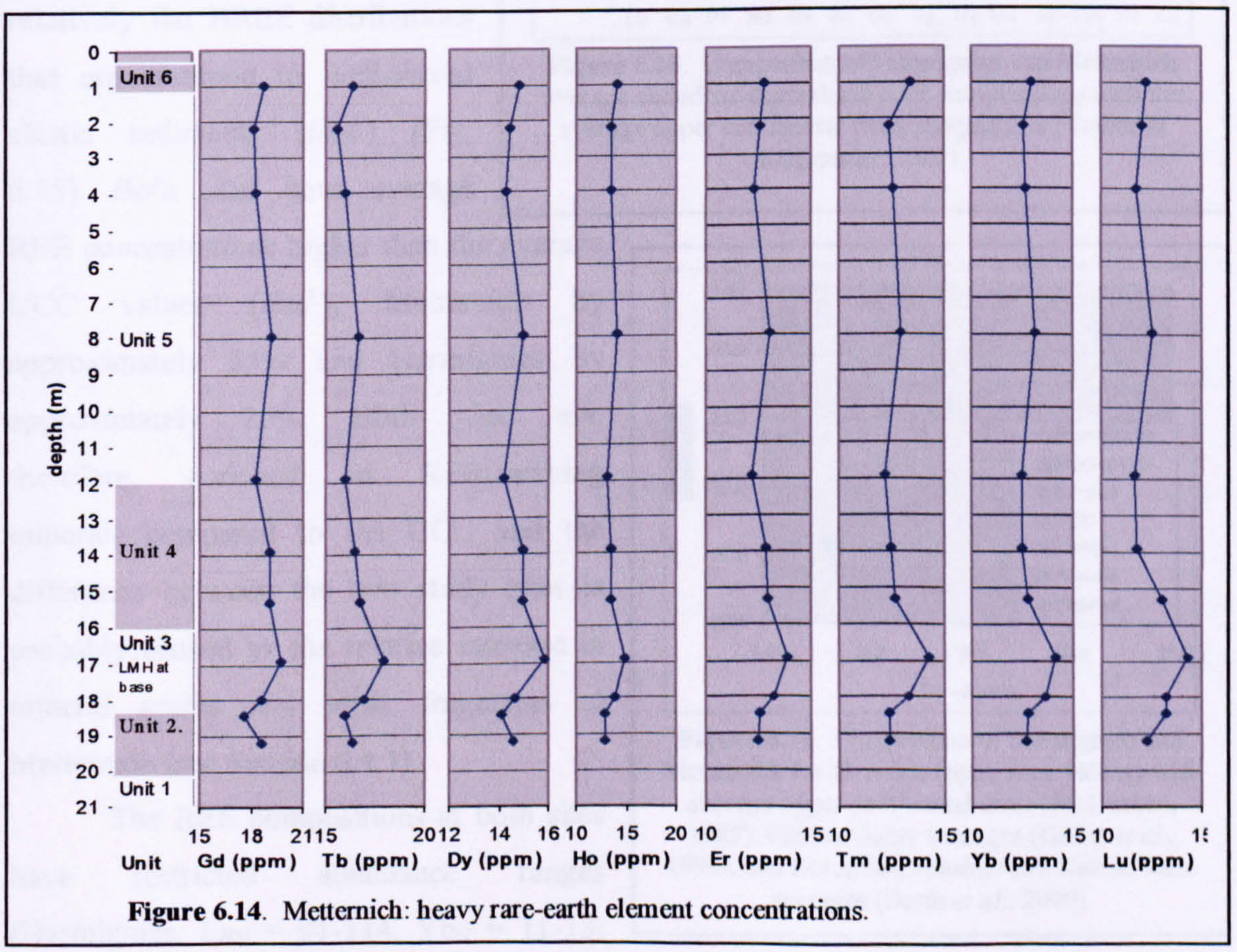

Figure 6.14. Metternich: heavy rare-earth element concentrations.

Results have been corrected for the high and variable carbonate content using CaO values derived from ICP-OES major-element analysis and normalised against standard chondrite values (Taylor and McLennan, 1985), except where stated.

The LREE (Fig. 6.13) show limited evidence for a reduction in concentration in Unit 3 *c.* 18 m depth, followed by a slight increase *c.* 17 m depth; a feature shared by the HREE. Thereafter, LREE concentrations slowly decline through Units 4 and 5. The HREE (Fig. 6.14) show a similar pattern but with no decline in Unit 5. Both LREE and HREE increase slightly in Unit 6, at the base of the post-glacial soil.

6.3 Comparison of Harmignies and Metternich REE with the upper continental crust.

Plots of the chondrite-normalised REE distributions for Harmignies and Metternich are extremely similar to the average UCC distribution (c.c. 1.0) (Taylor and McLennan, 1985), replicating the LREE enrichment and relatively flat HREE distributions that are common to well-mixed clastic sediments (*ibid.*) (Fig. 6.15). Both sites have average REE concentrations higher than the average UCC values (*ibid.*), Metternich by approximately 35% and Harmignies by approximately 25%. Both sites are, therefore, enriched in REE-carrying minerals compared to the UCC and the difference between the two study sites is probably caused by the relative increase in mineral grains and lithic fragments at Metternich (see Section 6.4.1).

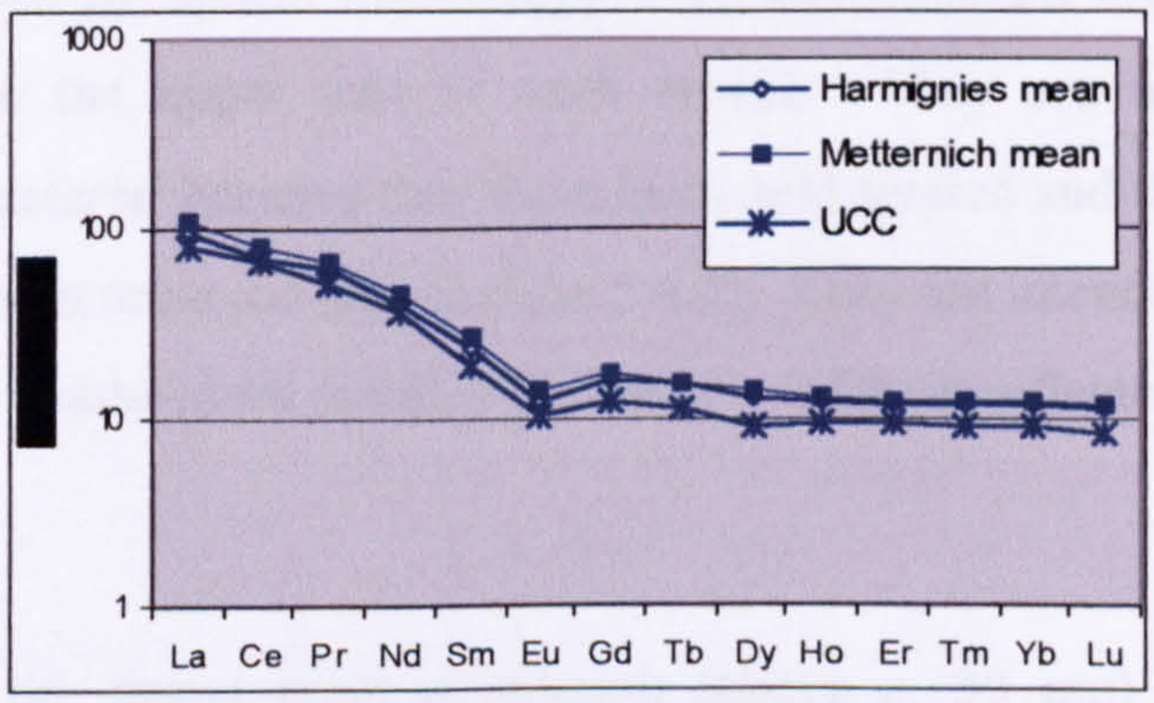

Figure 6.15. Comparison of Harmignies and Metternich average chondrite-normalised REE compositions with the average upper continental crust composition (Taylor & McLennan, 1985).

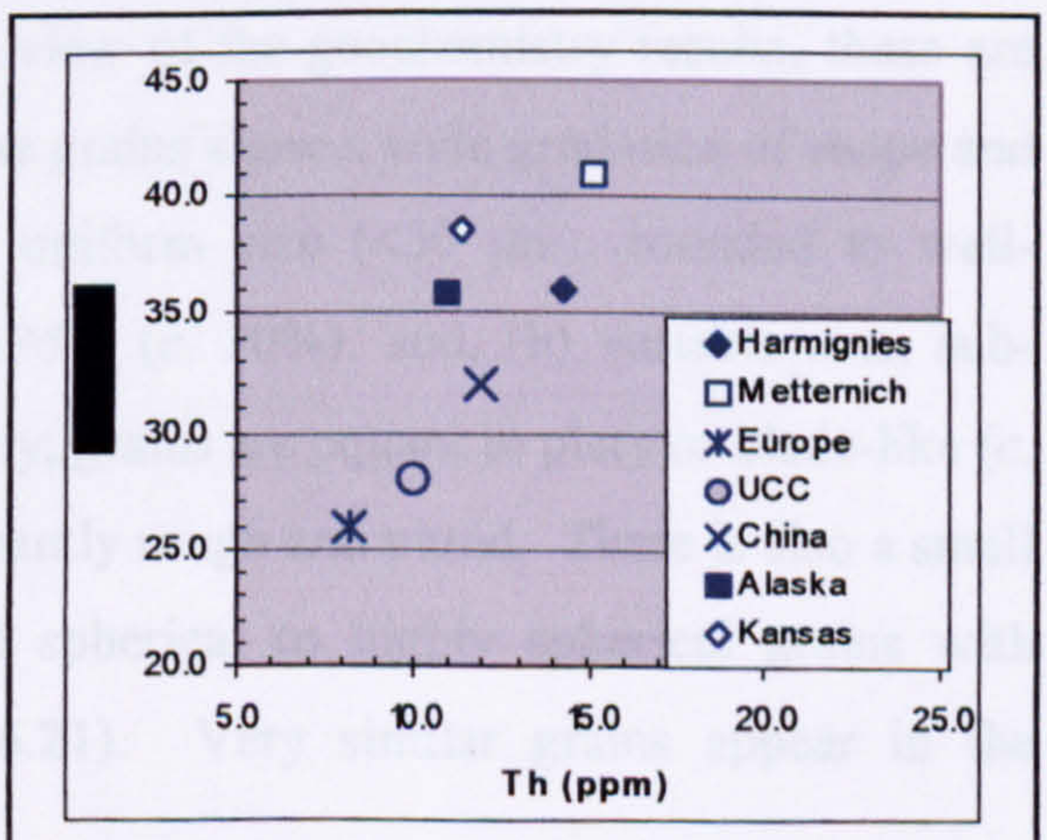

Figure 6.16. Comparison of Harmignies and Metternich La:Th ratios (ppm, rock values) with average upper continental crust (McLennan, 1989), Chinese loess averages (Gallet *et al.*, 1996), and European, Alaskan and Kansas loess averages (Barth *et al.*, 2000).

The REE compositions at both sites have restricted abundance ranges (Harmignies: La_N = 91-114, Yb_N = 11-13; Metternich: La_N = 109-127, Yb_N = 12.5-14 (ppm)). They show the same negative Eu

anomaly[1] characteristically observed in loess (Gallet *et al.*, 1996) with Eu/Eu* ratios[2] of 0.63 (Harmignies) and 0.65 (Metternich), which fall within the 'European loess province' range of 0.53-0.67 (Gallet *et al.*, 1998).

The La/Th ratio (Th from minor element analysis) has average values of 2.6 (Harmignies) and 2.8 (Metternich). This correlates closely with the upper continental crust value of 2.8 identified by McLennan (1989), and with similar values determined by Gallet *et al.* (1996) in Chinese loess and by Barth *et al.* (2000) for European, Alaskan and Kansas loess (Fig. 6.16).

6.4 Particle shape and size analysis

6.4.1 Description of particle shape

The samples that were examined by optical microscopy were amalgamated from several 'primary loess' samples from the upper part of each profile. They are not representative of the original sample material because they have been acid-treated and the finer fractions (below *c.* 30 μm) have been removed (see Section 5.4.2). They are intended only to show those aspects of the loess coarse-grain population that are visible in reflected-light optical microscopy.

6.4.1.1 Harmignies

Within the prepared sample, the coarse-grain population (above *c.* 30 μm) is relatively homogeneous (Figs. 6.17-6.20). Lithic fragments are absent; most of the particles present appear to be single-mineral grains. Opaque grains are relatively frequent, together with a wide range of other mineral grains. The large majority of grains are clear or pale opaque, some with iron staining. In view of the geochemistry results, these are likely to be mainly feldspars and quartz. These grains show a wide gradation of shape and texture but can be generally classed as (a) uniform size (<50 μm), rounded to well-rounded, with medium sphericity (Powers, 1953) (*c.* 30%), and, (b) variable size, sub-angular to very angular with very low sphericity; grains are equant to platy or blade-like (*c.* 70%). Surface textures appear to be predominantly rough and pitted. There is also a small population (1%) of large, well-rounded and spherical to highly spherical grains with smooth or polished surface textures (Fig. 6.21). Very similar grains appear in the Metternich sample, and are discussed there.

---

[1] This anomaly occurs when plagioclase in involved in fractional crystallisation.
[2] Calculated as the geometric mean ($Eu/Eu^* = Eu_N / \sqrt{[(Sm_N).(Gd_N)]}$; Taylor and Mclennan, 1985).

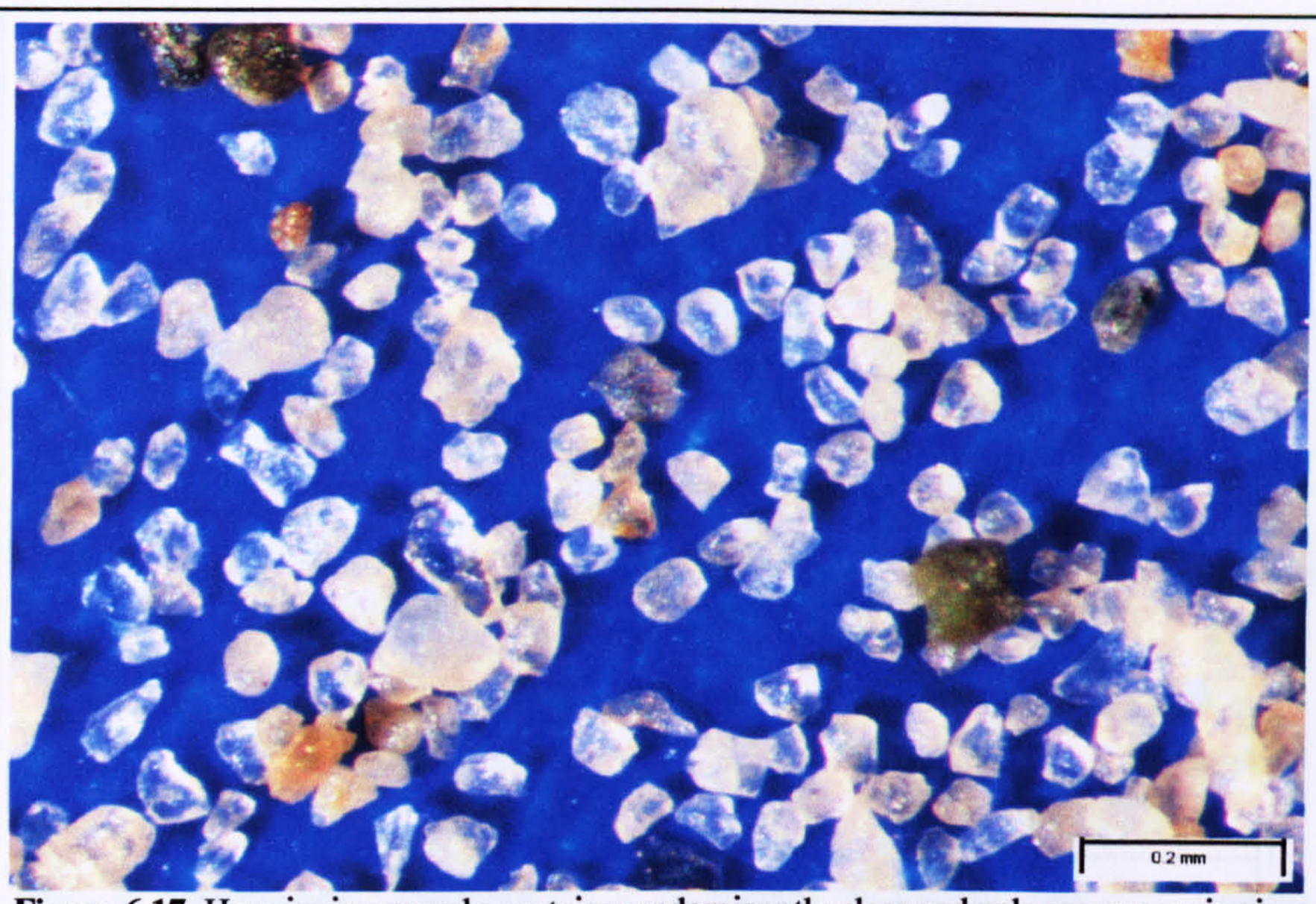

Figure 6.17. Harmignies: sample contains predominantly clear and pale opaque grains in a variety of shapes, with a small minority of other grains.

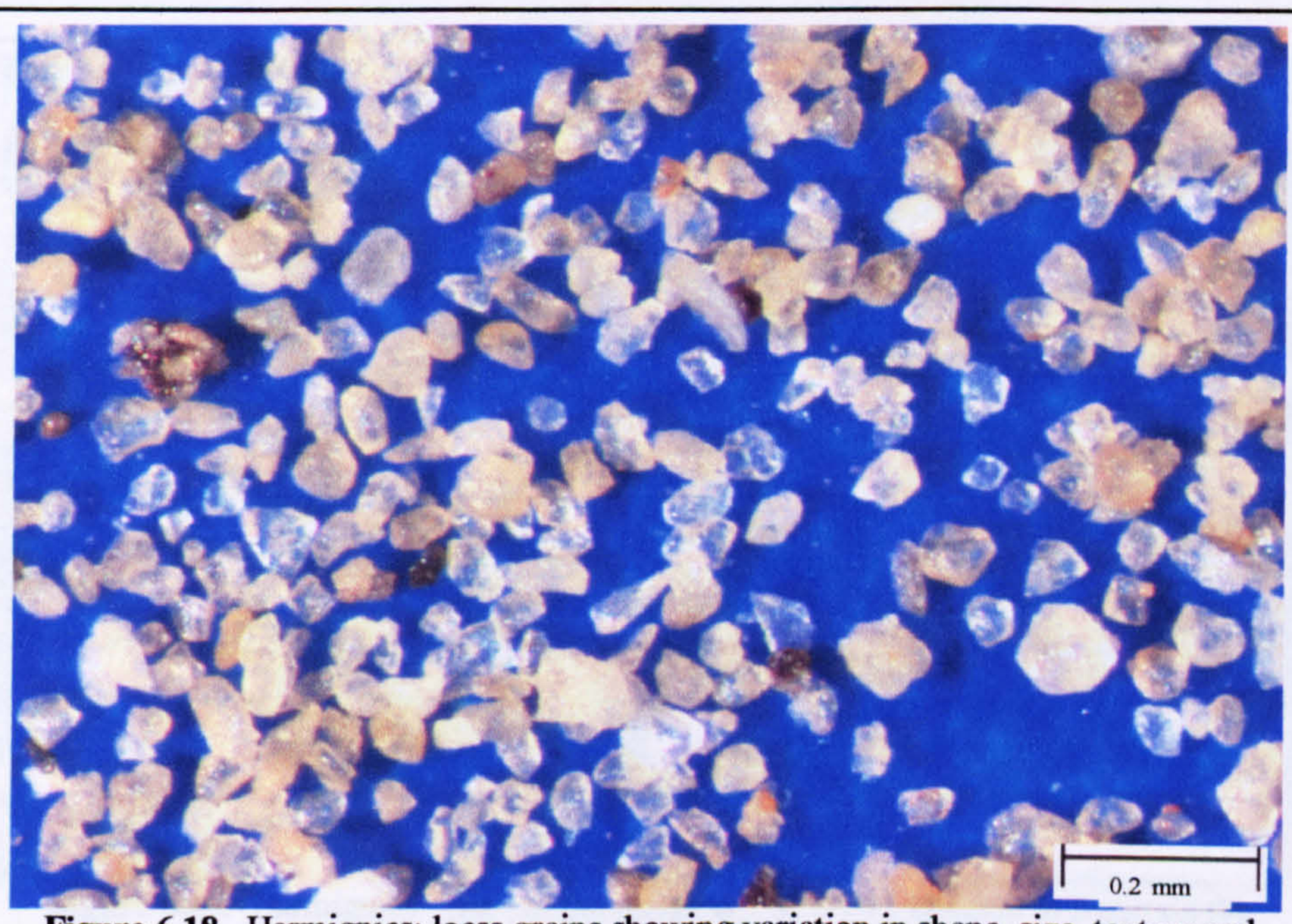

Figure 6.18. Harmignies: loess grains showing variation in shape, size, texture and mineralogy. Iron staining is apparent on some grains.

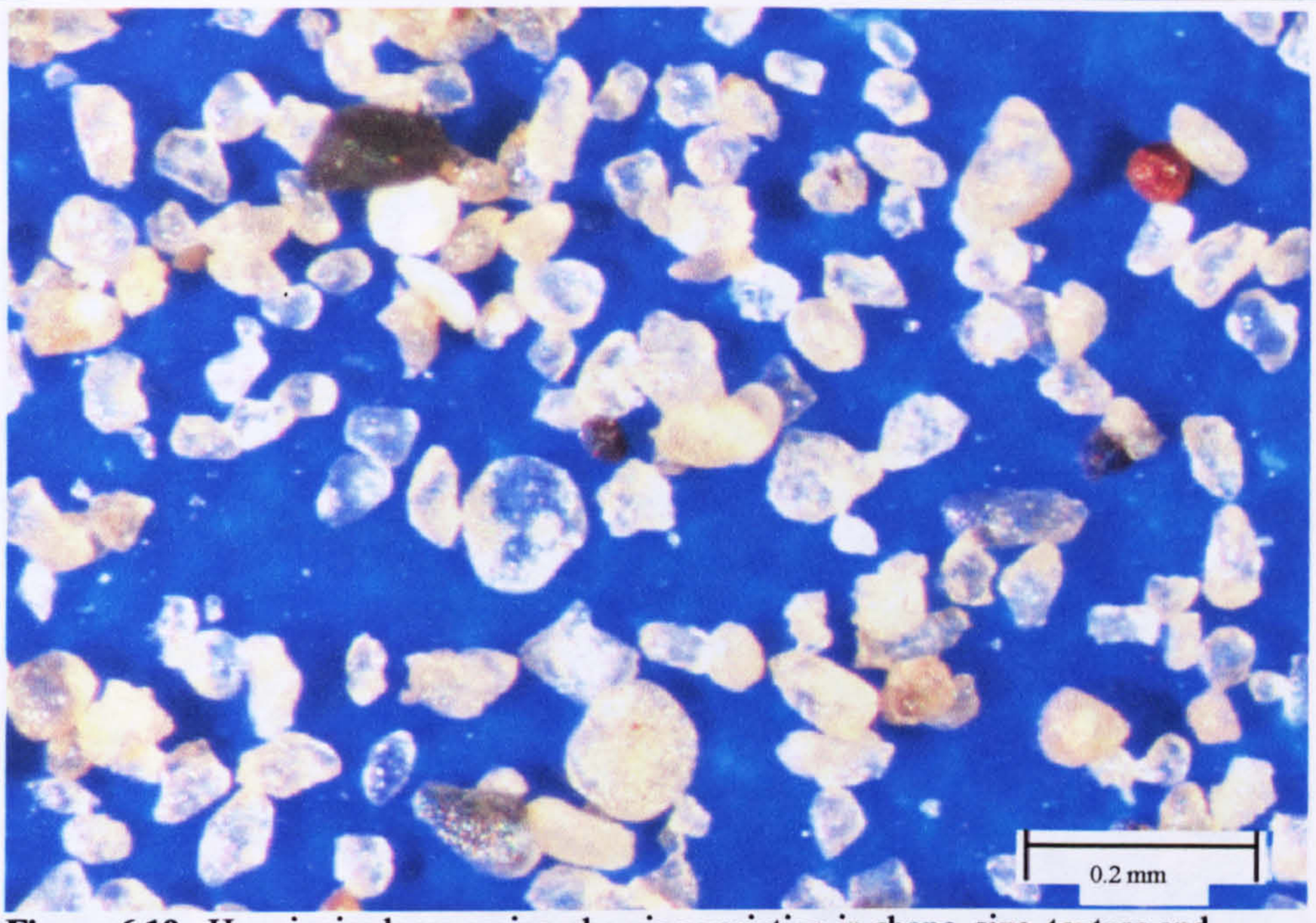

Figure 6.19. Harmignies loess grains, showing variation in shape, size, texture and mineralogy.

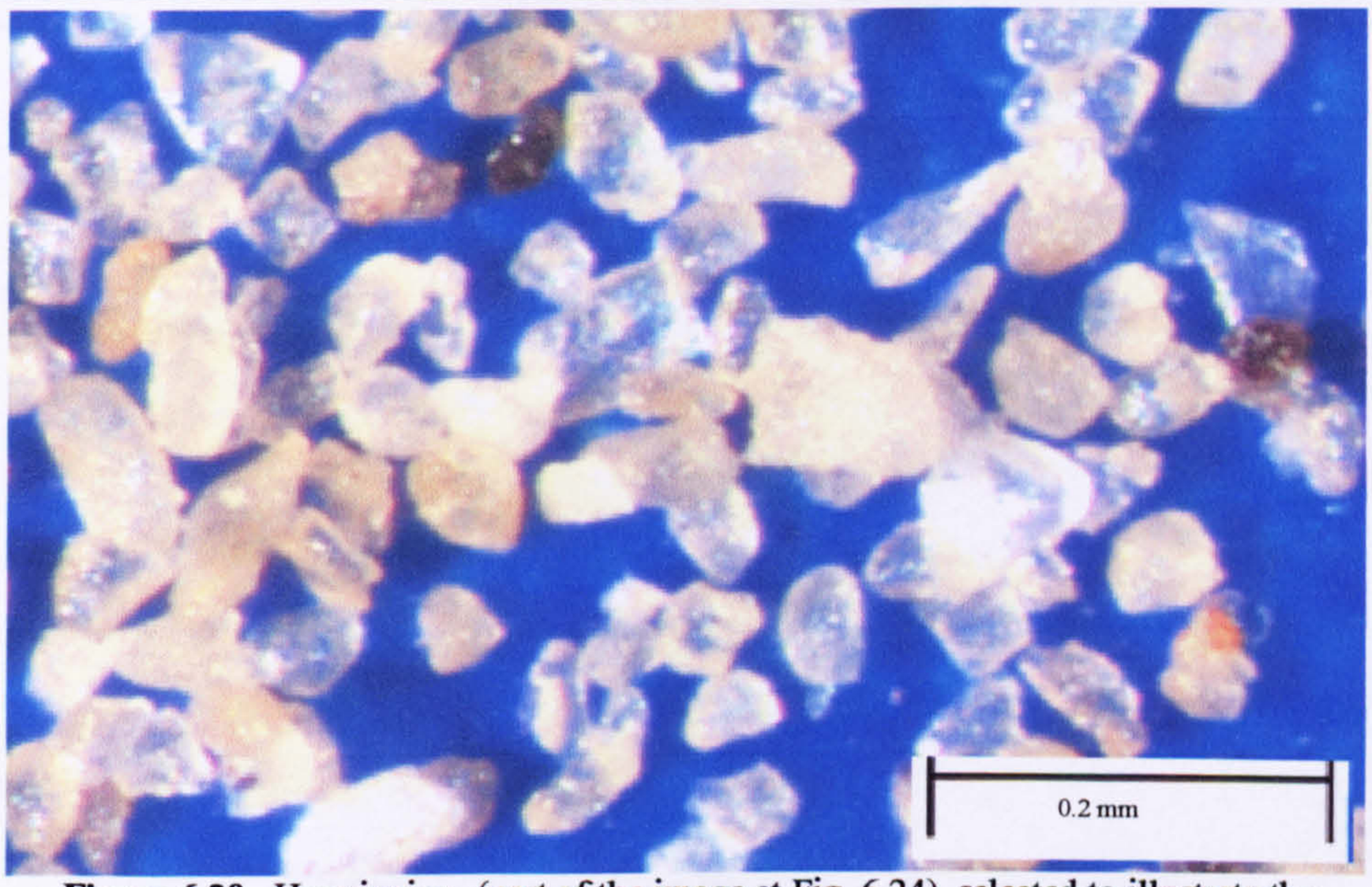

Figure 6.20. Harmignies: (part of the image at Fig. 6.24), selected to illustrate the extreme range of grain shapes present in this sample.

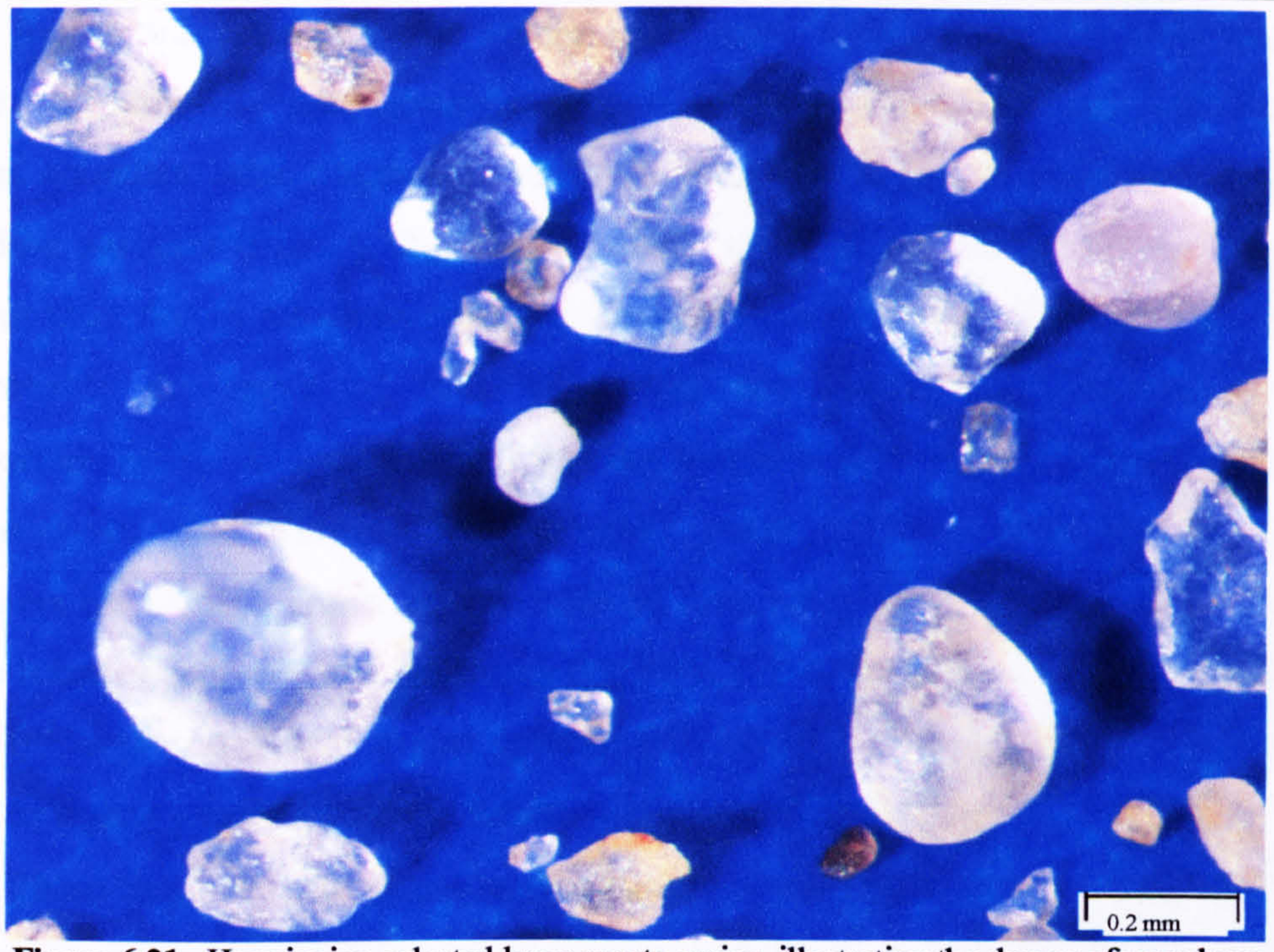

Figure 6.21. Harmignies, selected large quartz grains, illustrating the degree of roundness and smooth surface texture of some loess grains.

6.4.1.2 Metternich

In contrast, the prepared Metternich sample, again comprising only the coarse fraction, is extremely heterogeneous in grain shape, size, mineralogy and texture. It contains abundant lithic fragments and biotite mica flakes, and transparent to translucent crystalline particles (Figs. 6.22-6.23). Some of the lithic fragments are very broad (>2 mm) but thin, due to schistose cleavage. These fragments and irregular crystalline grains are probably the result of frost weathering and glacial comminution, acting on metamorphic rock. At least some of this has probably been carried down-stream by the Moselle from the Variscan metamorphic rocks visible from the site. The transparent/translucent grains are variable in size, angular to sub-angular, with rough surface textures and very low sphericity (Powers, 1953). There is also a small population (<1%) of large transparent grains (presumably quartz), rounded to well-rounded with frosted or highly polished surface textures and high sphericity (Figs. 6.24-6.25).

These large, rounded grains cannot have been produced by glacio-fluvial processes; this feature results from prolonged and multi-cyclic episodes of transport and abrasion, especially aeolian (Siever, 1988). Desert grains frequently have frosted surfaces (apparent in Fig. 6.24), caused by inter-grain collisions and grain surface modification by micro-scale dissolution and reprecipitation (Mizutanu and Suwa, 1966). However, this texture is removed by silica dissolution during subsequent fluvial transport, producing grains with very smooth surfaces (Siever, 1988) (apparent in Figs. 6.24 and 6.25). Since frosted grains arrived at Metternich with their surface texture still present, the episode of fluvial transport that delivered them to the general Metternich area cannot have had significant effect, in which case the polished grain surfaces must also be original features. It is concluded that these are relict grains with complex histories, weathered from desert sandstone. One likely source is the Lower Triassic Buntsandstein, which is exposed west and south of Metternich as continental red beds (Mader, 1982), within the Moselle catchment. It contains abundant aeolian sand deposits which include 'very well rounded, very coarse grains with frosted surfaces', identified as a desert 'creep population'. It also contains sub-rounded to sub-angular grains and fluvial deposits (*ibid.*).

Similar large, smooth and highly polished grains, but composed of magnetite, are visible in images of the Metternich magnetic fraction (Figs. 6.60, 6.61). These too are suspected to be Buntsandstein grains. These large quartz and magnetite grains were probably delivered to the Metternich area by Moselle flood events and then transported up-slope to the site primarily by creep. However, since this site was affected by surface flow (see Section 6.4.5), it is possible that some were also present in river terrace deposits higher on the valley side, and were washed down-slope.

The similar large, round and smooth quartz grains observed in the Harmignies sample may have delivered to the North Sea as Rhine sediment and then transported inland by creep and saltation after sea levels fell.

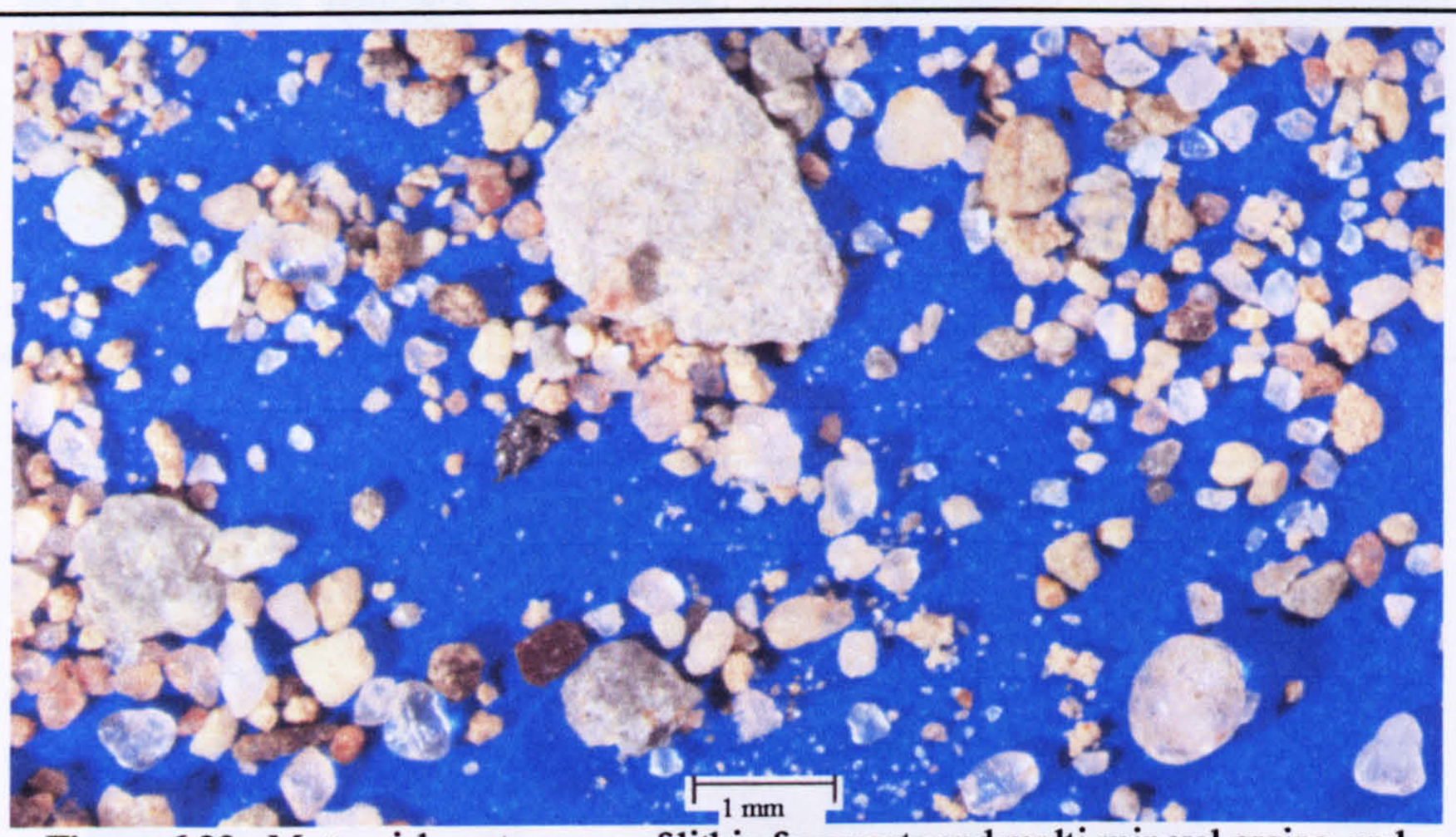

Figure 6.22. Metternich: note range of lithic fragments and multi-mineral grains, and contrasts in shape and texture.

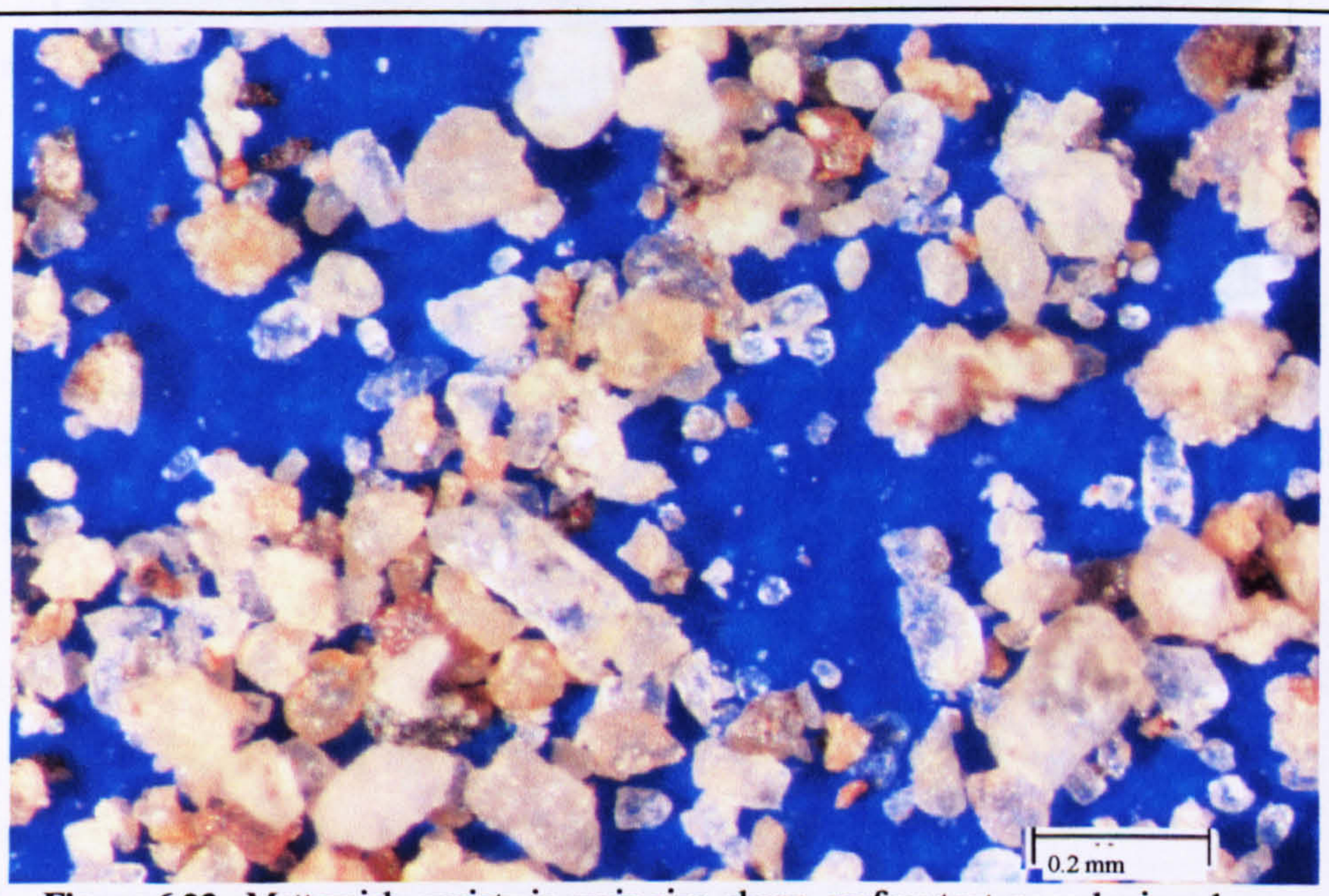

Figure 6.23. Metternich: variety in grain size, shape, surface texture and mineralogy.

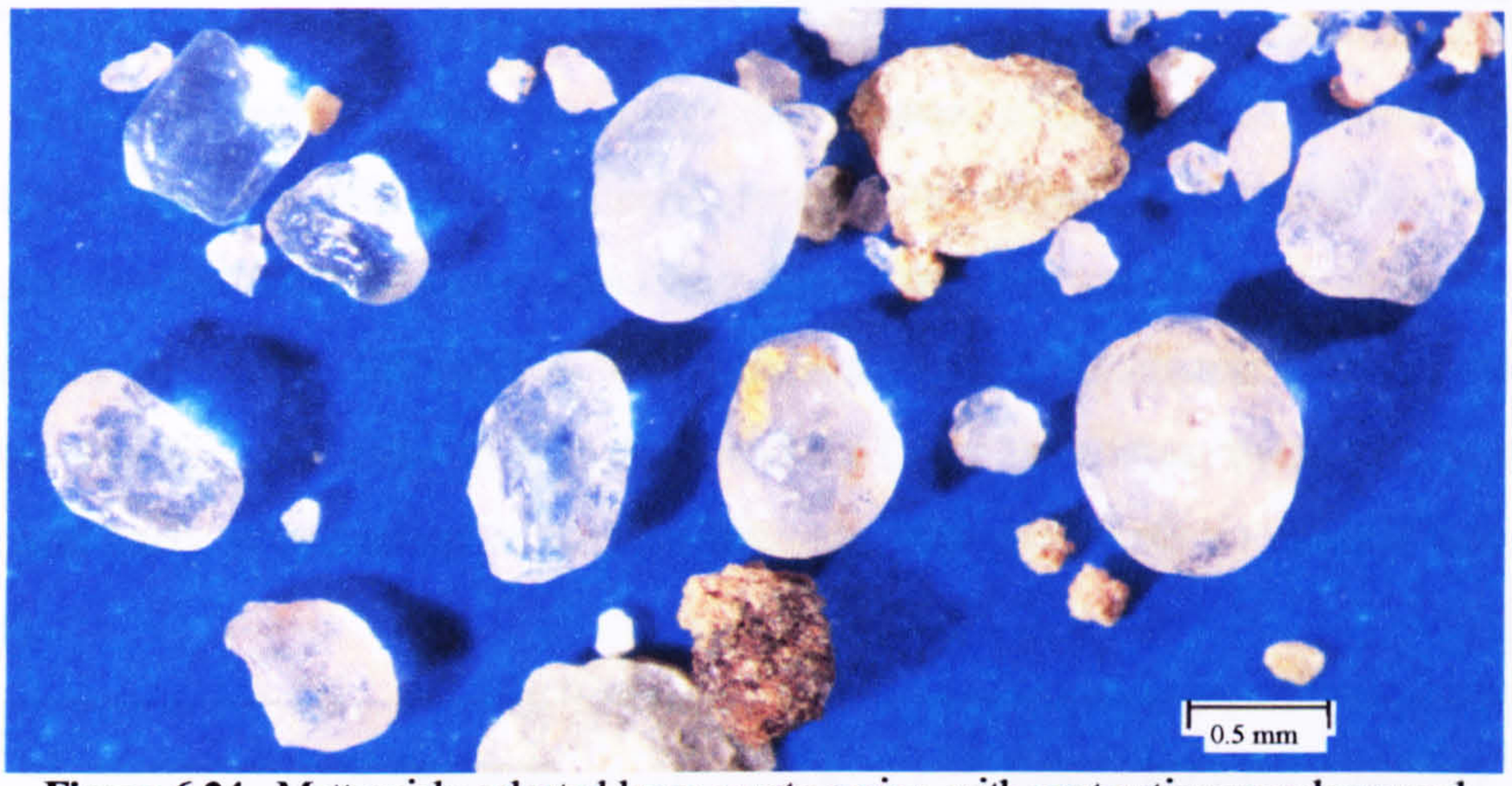

Figure 6.24. Metternich: selected large quartz grains, with contrasting roundness and surface textures (scale bar is 0.5 mm).

Figure 6.25. Metternich: contrasting surface textures in two highly-polished quartz grains, possibly indicating different erosional histories.

6.4.2 Grain size indices - critique

The sensitivity of grain size indices as wind strength proxies depends on the inter-sample variability present within the chosen size classes; indices which compare relatively invariant size fractions will fail to reflect accurately the actual wind strength variation. In the datasets for the two study sites, the variability of the total set of results in each Malvern size category between 1-100 μm has been assessed through associated %RSD values. The results are shown graphically in Figs 6.26 and 6.27 (for both sites, these graphs omit the Eemian and early Weichselian palaeosols because these are likely to contain non-aeolian particles).

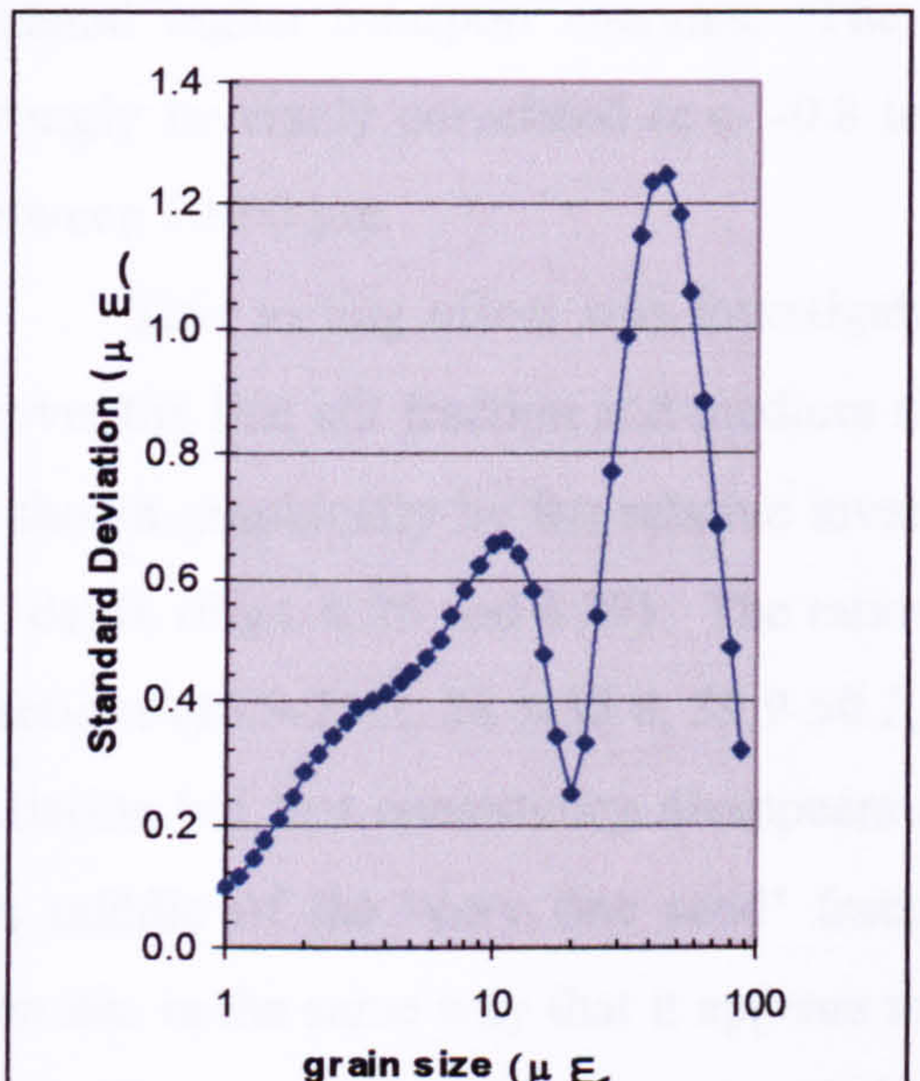

Figure 6.26. Harmignies: variability in each size category (expressed as the Standard Deviation).

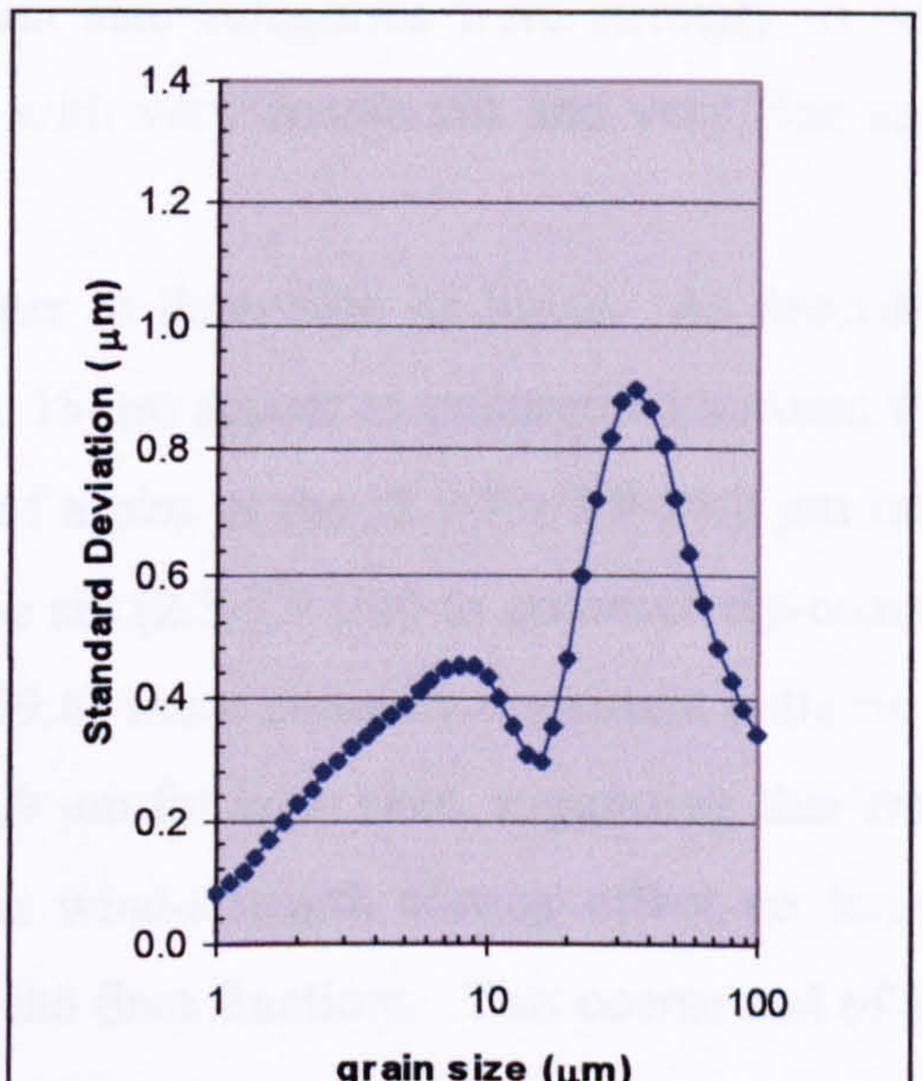

Figure 6.27. Metternich: variability in each size category (expressed as the Standard Deviation).

It is apparent that within this sample sub-set and size range, Harmignies shows more grain size variation than Metternich. For both sites, the variability plots are bimodal, with the variability concentrated in two main size classes – 5-20 and 20-100 μm. The pattern of variability shown in the two diagrams demonstrates that the grain size distribution is composed of at least two components, each with its own set of variability. The two obvious components are a medium silt fraction with a mode of approximately 9-10 μm and a dominant very coarse silt fraction with a mode of approximately 35-40 μm. The shoulder present below 5 μm may suggest that there is also a silt/clay component with a mode of approximately 2.5 μm. This would accord with McTainsh *et al.* (1997), who identified a mode of about 2.6 μm for long-term suspension dust and modes of 25–73 μm for rapidly-deposited sediment.

Correlation between the individual size categories in the grain size datasets was used to investigate size relationships (excluding the extreme tails which contain significant uncertainties, see Section 5.5.5). As would be expected, adjacent size fractions were very closely correlated (c.c. >0.9). Strong correlation (c.c. 0.9) was also observed between the fine/very fine silt size categories (2-7.8 μm) and the medium silt size categories (7.8-15.9 μm). This suggests that there is no significant wind-strength sorting effect within this fraction. Weaker correlation (c.c. 0.8-0.7) was present between the 2-7.8 μm size categories and coarse silt size fractions up to 20 μm. This accords with Pye (1995): particles smaller than 10 μm can easily be maintained in suspension while larger grains demand higher transport energies. The 2-20 μm size categories were strongly to very strongly inversely correlated (c.c. -0.8 to -0.9) with very coarse silt and very fine sand between 50-90 μm.

This sorting effect was investigated further to determine its limits. As described above, the fine silt fraction and medium silt to *c.* 15 μm appear to undergo no sorting; this is shown graphically by the relative invariance of a plot of the '2.5-7.1/7.9-14.2 μm ratio *vs.* depth (Figs. 6.28 and 6.29). The ratios of fine silt (2.5-7.9 μm) to successively-coarser fractions (15.9-25.2, 28.3-35.6, 39.9-50.2, 56.6-79.6) show mutually-consistent patterns of variation but that consistency disappears at >89.9 μm for both sites, suggesting that from the middle of the 'very fine sand' fraction, the wind-strength sorting effect no longer operates in the same way that it appears to do in the finer fractions. This coarse end of the grain size spectrum is, therefore, unsuitable for use in grain size indices.

It is apparent that the grain size indices examined here are all measuring essentially the same ratio - 'fine and medium silt' *vs.* 'coarse and very coarse silt'. These two fractions equate, approximately, to the Tsoar and Pye (1987) division of loess into long-term and short-term suspension components.

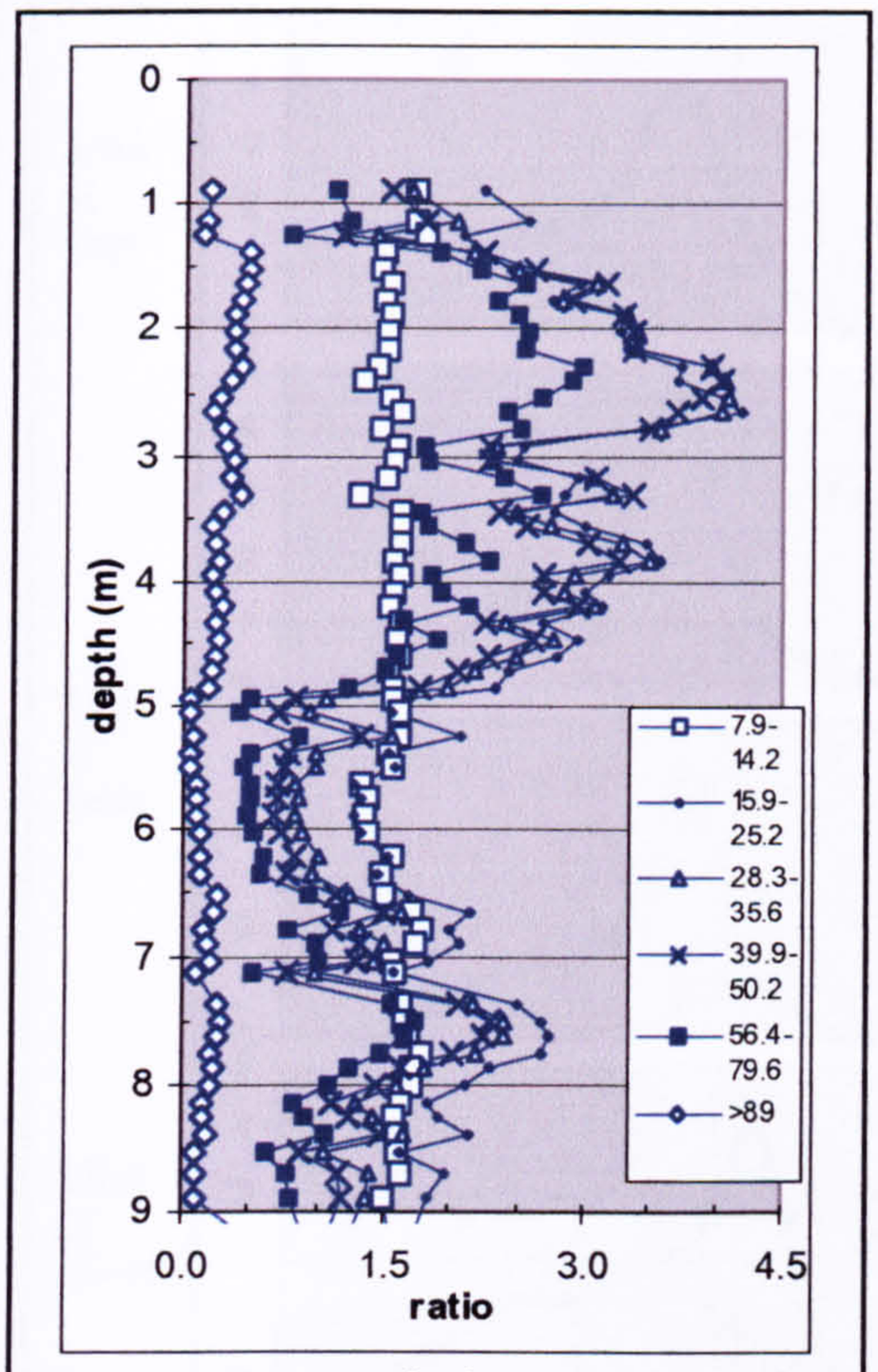

Figure 6.28. Harmignies: the ratios of fine silt (2.5-7.9 μm) to progressively-coarser fractions.

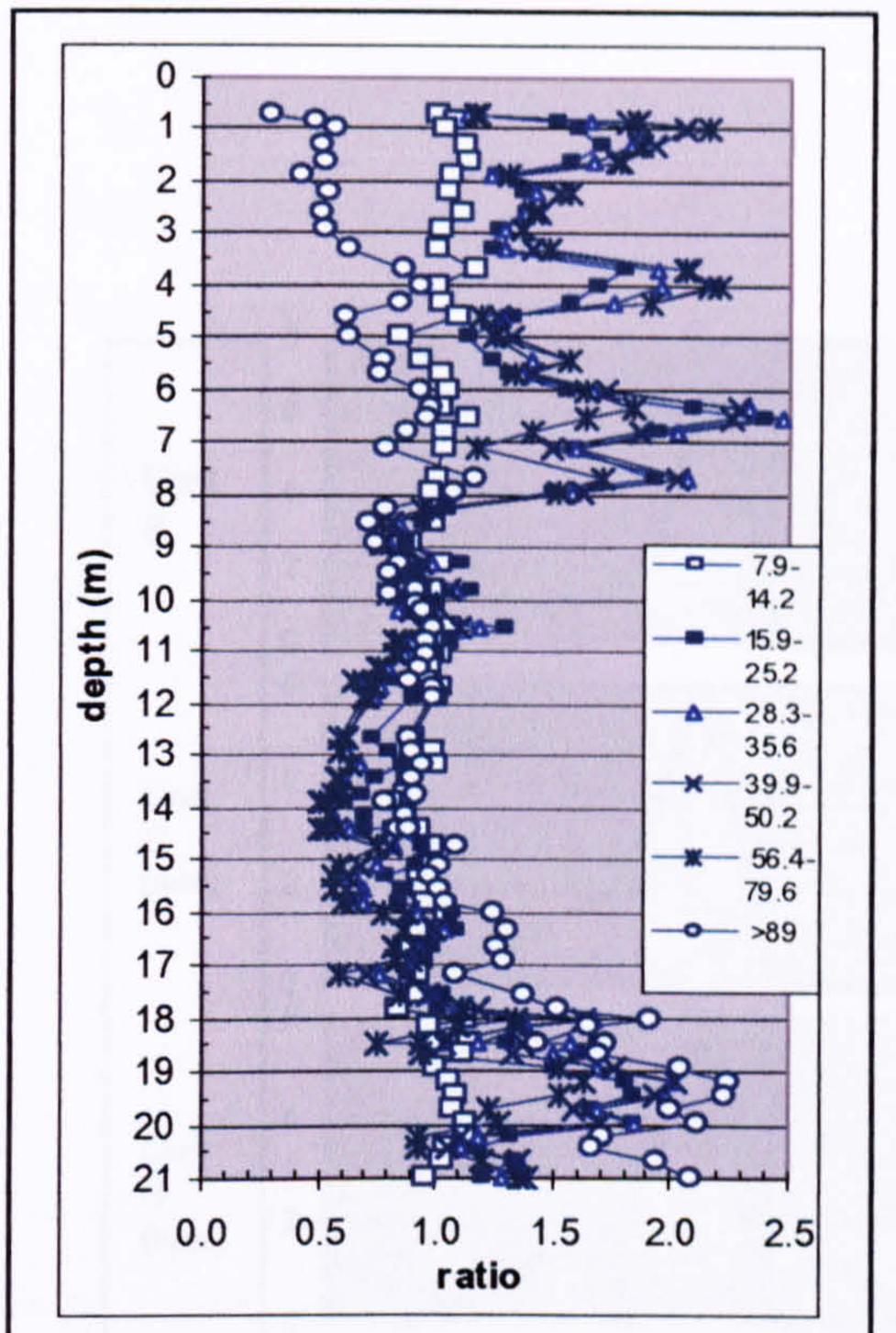

Figure 6.29. Metternich: the ratios of fine silt (2.5-7.9 μm) to progressively-coarser fractions.

6.4.3 Grain size analysis

6.4.3.1 Harmignies

The clay/silt/sand content of the Harmignies profile (as defined by GRADISTAT) is shown in Fig. 6.30. The clay content is relatively constant throughout, below 10% for all samples. The silt and sand profiles exhibit significant, and inverse variation. This variation is shown graphically in Fig. 6.31 and is described below.

Unit C (Tertiary sand)

This has a strongly bimodal distribution with a tightly defined major mode *c.* 130 μm (fine sand) and a poorly-defined minor mode at 5.5 μm (fine silt). Sand composes 67% of the

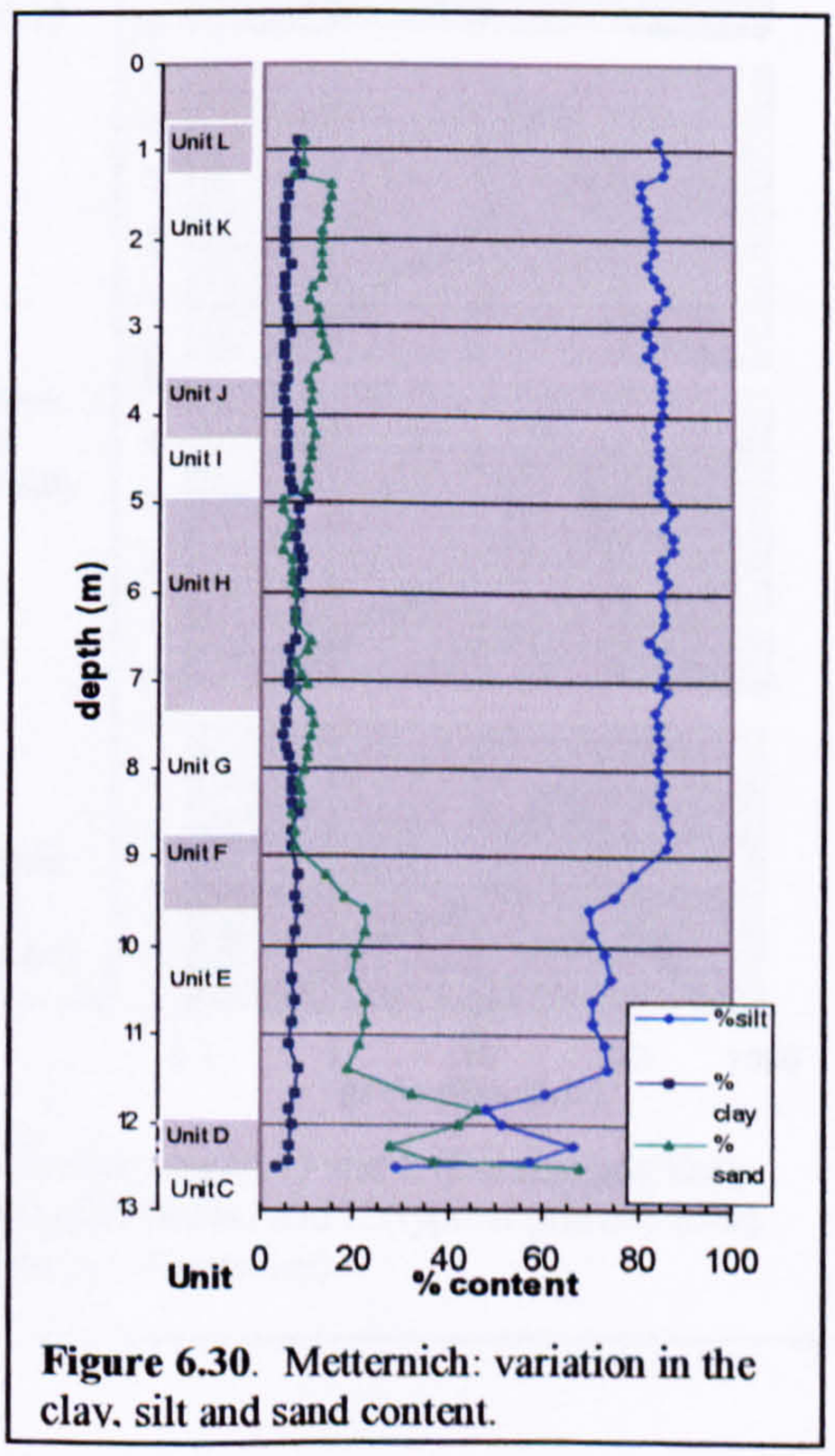

Figure 6.30. Metternich: variation in the clay, silt and sand content.

total sample, with most of the remainder being silt.

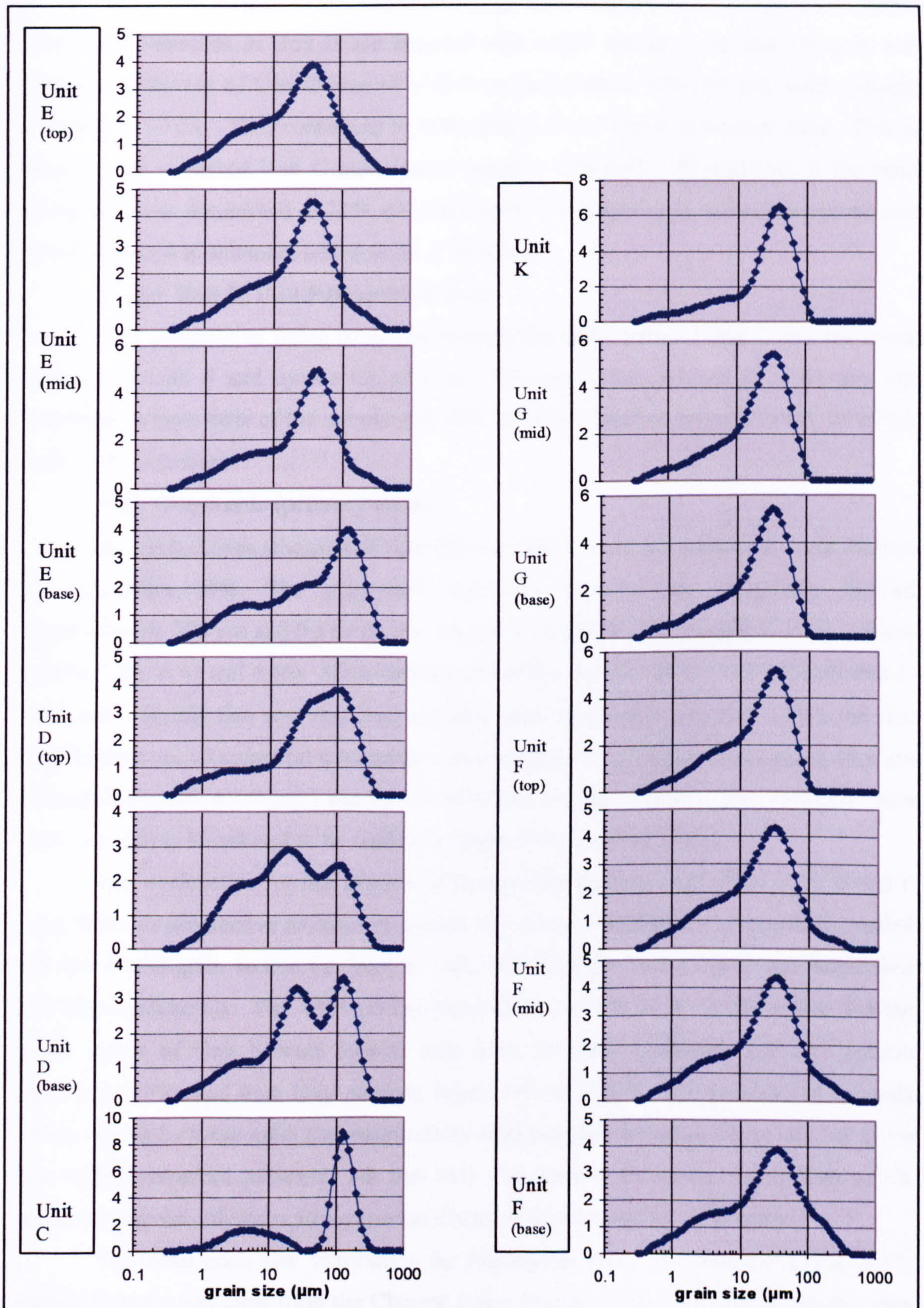

Figure 6.31. Harmignies: grain size distributions for Unit C (Tertiary sand), D and E (Eemian and Early Weichselian palaeosols), F (transition to loess deposition), part of G (loess) and K (typical primary loess, added for comparison). (Y-axis is % volume content in Malvern size categories).

Units D, E and F (palaeosol complex)

The lower samples in this sequence change from bimodal to unimodal distributions. The lowest samples in Unit D are bimodal with major modes *c.* 25 and 140 μm, and samples at the top of Unit D/base of Unit E are unimodal c 120-140 μm, with a strong shoulder *c.* 30 μm. They contain up to 45% sand, 2.5% of which is medium sand. This is likely to be reworked Unit C sand (major mode *c.* 130 μm). By mid-Unit E the sand component has diminished to 22%, of which 1.8% is medium sand, silt has increased and the distribution is unimodal with a mode *c.* 50-40 μm.

Upper Unit E, Unit F (transition zone)

This progressive fining continues through the upper parts of Unit E and the lower samples in Unit F and by the top of Unit F the mode has reduced to *c.* 34 μm; silt comprises almost 80% of the sample and sand has diminished to less than 14%, of which only 0.9% is medium.

Unit G upwards (primary loess)

By depth 8.90m (the start of Unit Fb) the sand content has reduced to only 7% and silt comprises 86%. The grain size spectrum extends only marginally beyond approximately 100 μm and the mode is c. 36 μm. This typifies the remainder of the vertical profile (Figs. 6.45 and 6.46). Most samples above this contain between 80-85% silt and 5-10% sand (mainly fine and very fine: medium sand contributes less than 0.5%), the size distributions are all unimodal with modal values distributed tightly around a mean 39.9 μm (Standard Deviation 3.9 μm) and the distributions are fine-skewed. This sequence from Unit G upwards is assessed to be aeolian in origin (Frechen *et al.* 2001).

One explanation for this process of change between sand and silt in Units E and F may be that a progressive increase in aeolian silt delivery blanketed and eventually sealed off the coarse-grain source (at least in part, probably the Unit C sand and associated reworked sediments). Van Vliet (1975) (reprised in Frechen *et al.*, 2001) argues that the upper layers of Unit E were formed only from reworked sediments and that aeolian deposition, reworked from local sources, began only in Unit F. The progressive upwards fining shown by these grain size distributions suggests that the upper layers of Unit E are not simply reworked sediments but that they also contain increasing proportions of silt grains which can only have arrived on the Cuesta D'Harmignies by wind action.

The mean grain size distribution for Harmignies loess (in Units G-K) (Fig. 6.32) differs from typical loess from the Chinese Loess Plateau (Sun *et al.*, 2002). Harmignies loess contains less fine and very fine silt (the 'long-term suspension' component) and more medium and coarse silt (the 'short-term suspension' component): it more closely resembles the size distribution for 'locally-derived loess' deposited close to the Yellow River (*ibid.*).

Changes in the average wind strength in the primarily-aeolian part of the profile, above c. 9 m depth can be examined by grain size indices (see Fig. 6.33). These suggest that wind strengths rose through Unit F and reached a maximum *c.* 7.5 m depth, in upper Unit G. A reduction at 7.11 m, at the base of Unit H, was followed by a marked reduction which reached a minimum *c.* 5.5 m depth, in mid-Unit H. A further minimum occurred *c.* 5 m, coincident with the tundra gley at the top of Unit H and thereafter wind strengths increased irregularly, reaching a profile maximum in Unit K, followed by a progressive reduction to a minimum in the tundra gley at the top of Unit K. A slight increase is indicated at the base of the Holocene soil but this may be contaminated by fine, illuvated particles.

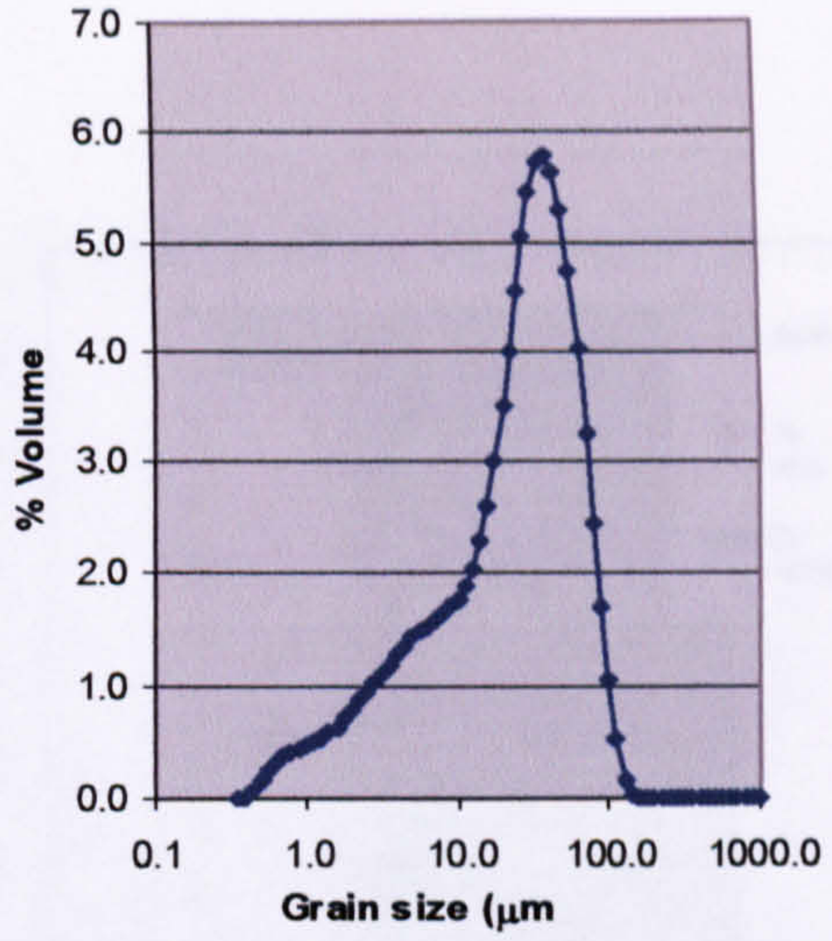

Figure 6.32. Harmignies: mean grain size distribution for Units G-K (loess).

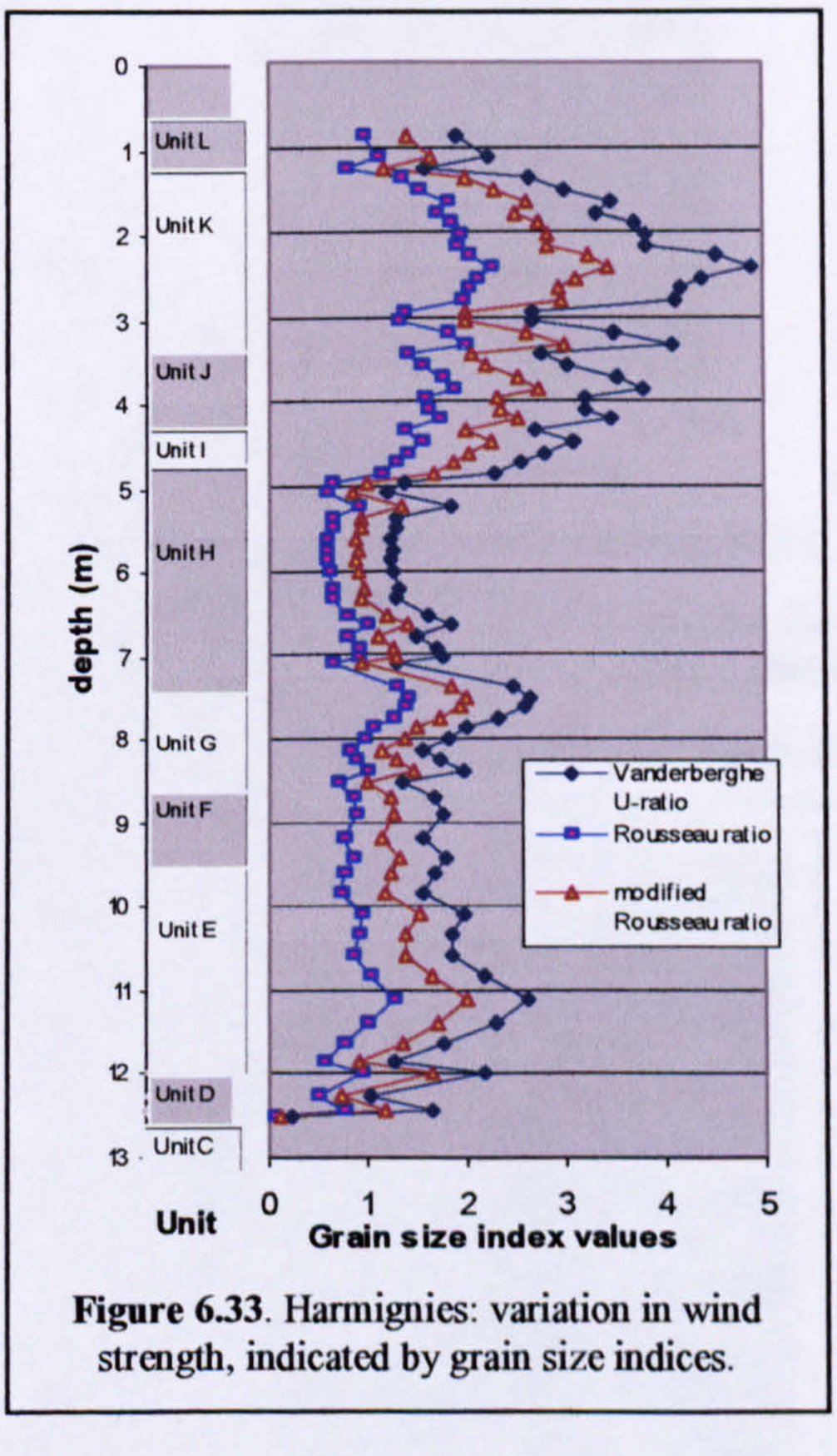

Figure 6.33. Harmignies: variation in wind strength, indicated by grain size indices.

6.4.3.2 Metternich

The grain size range is less variable than Harmignies. Like Harmignies, the clay content is relatively constant throughout, below 10% for all samples; most of the variance is present in the silt and sand fractions (Fig. 6.34). Silt is predominant, varying between *c.* 77-84%, with sand inversely varying between *c.* 8-16%. Metternich contains a slightly wider range of grain sizes, with more silt <10 μm and more sand >100 μm. The Standard Deviation values for the Metternich grain size dataset are more limited than Harmignies (Figs. 6.26, 6.27), demonstrating that Metternich has, overall, less grain size variability than Harmignies (Fig. 6.36). The sorting, skewness and kurtosis values provided by GRADISTAT are similar for both sites.

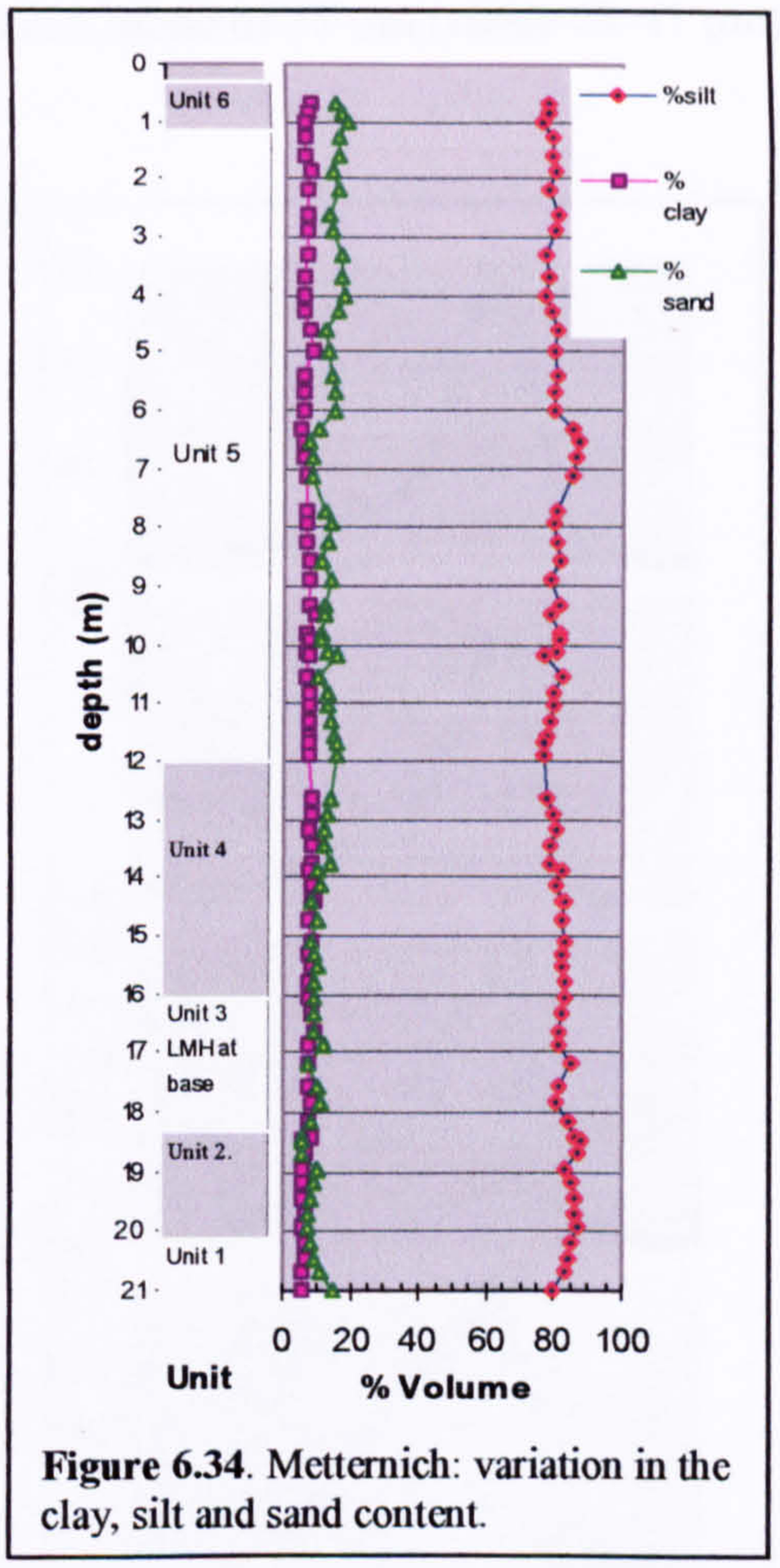

Figure 6.34. Metternich: variation in the clay, silt and sand content.

The average size distribution for Units 3, 4 and 5 (predominantly loess and reworked loess) is close to that of the primary loess units at Harmignies (Fig. 6.35) and it shares those differences from typical Chinese loess (Sun *et al.*, 2002). The increased proportion of medium and coarse silt (the 'short-term suspension' component) is probably attributable to the proximity of the site to its probable source areas.

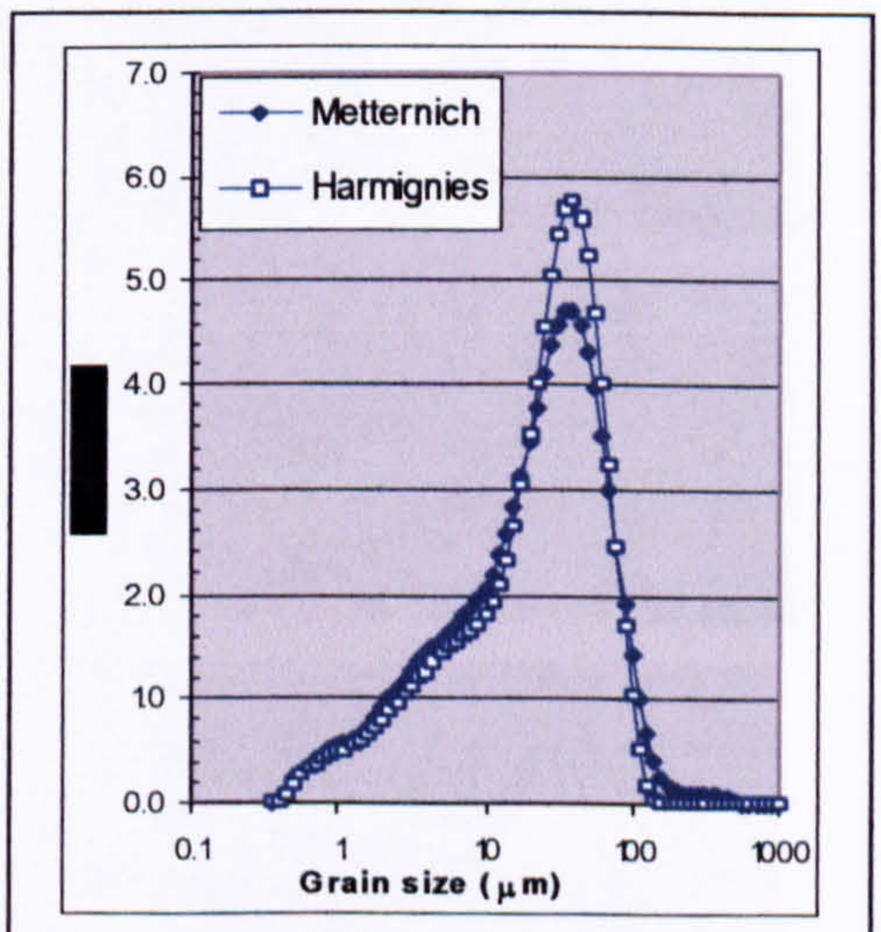

Figure 6.35. Harmignies and Metternich: comparison of mean loess grain size distributions.

All the samples are unimodal with a profile mean mode of 35 μm (range 28-41 μm) (Fig. 6.36).

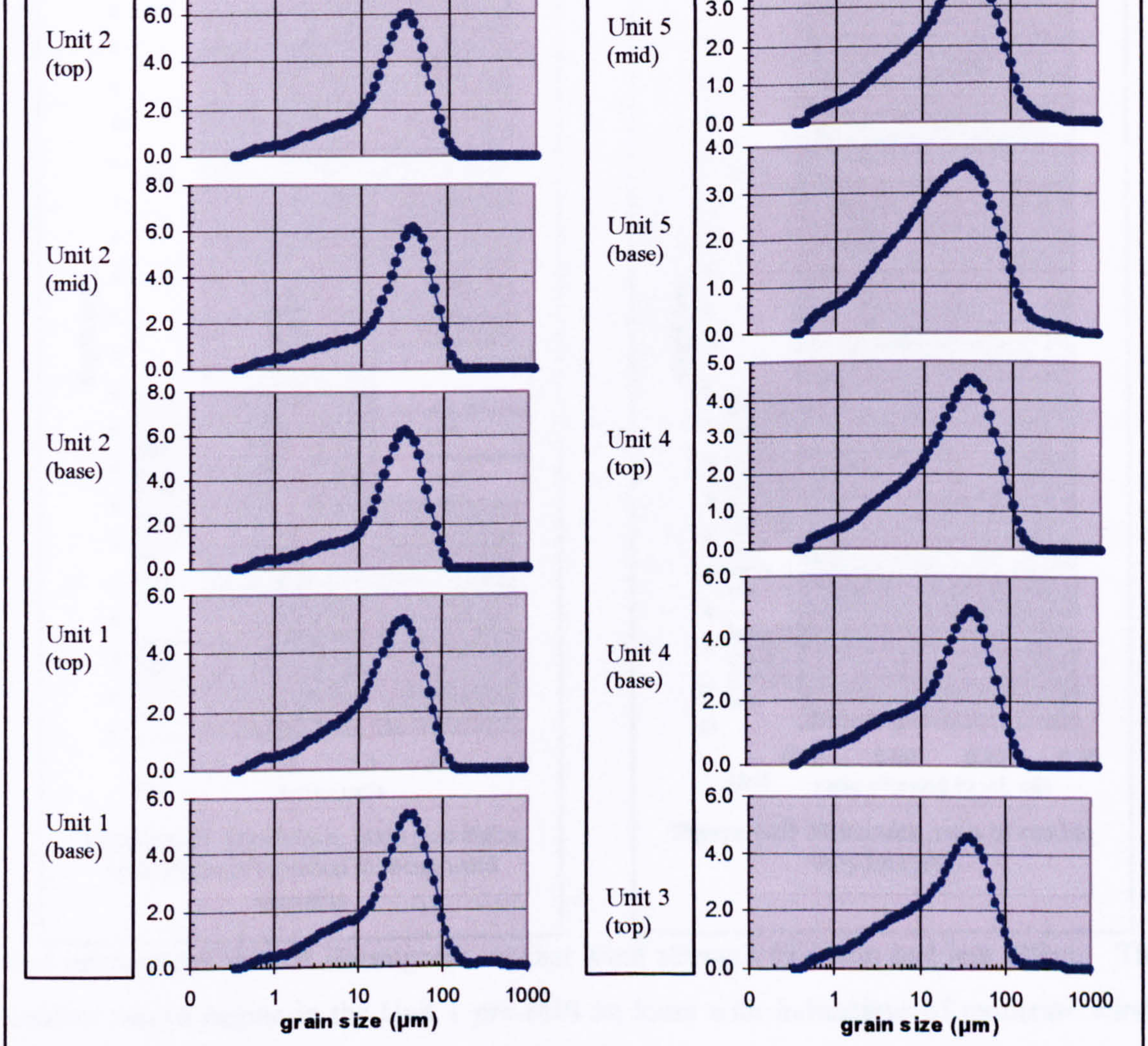

Figure 6.36. Metternich: grain size distributions for Unit 1 (pre-MIS 5a loess), Unit 2 (early Weichselian palaeosols), Units 3-5 (reworked sediment and loess) and Unit 6 (base of post-glacial soil) (Y-axis is % volume content in Malvern size categories).

Unit 1 (pre-MIS 5a loess), Unit 2 (early Weichselian palaeosol complex) and Units 3, 4 and 5 (Weichselian loess) have mean modes of 35, 34 and 35 μm respectively. The largest inter-sample variation here is not between loess and palaeosol units but between different loess samples, and is mainly caused by the changing proportions of silt <10 μm and sand >100 μm. This predominant homogeneity in grain size distributions suggests that the Unit 2 early Weichselian palaeosols were developed entirely from the Unit 1 pre-MIS-5a loess and that pedogenesis has not significantly altered that original grain-size distribution. The upper Unit 3 loess, together with Units 4 and 5 has grain size distributions resembling Unit 1.

The indicated wind strengths at Metternich, shown by grain size indices (see Section 6.4.2) (Fig. 6.37), suggest either that variation in the average wind strength was

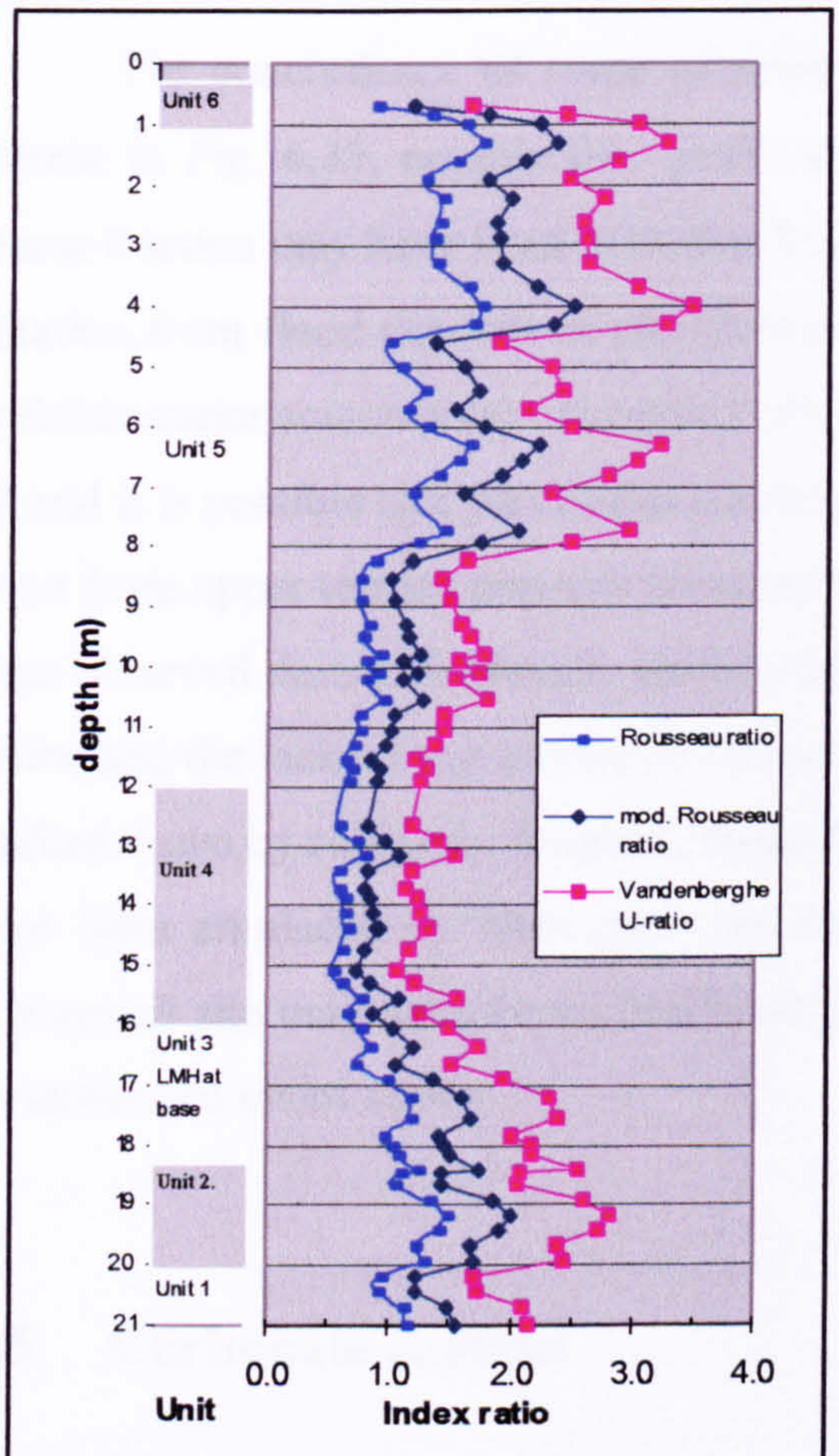

Figure 6.37 Metternich: grain size index indications of variation in mean wind strengths.

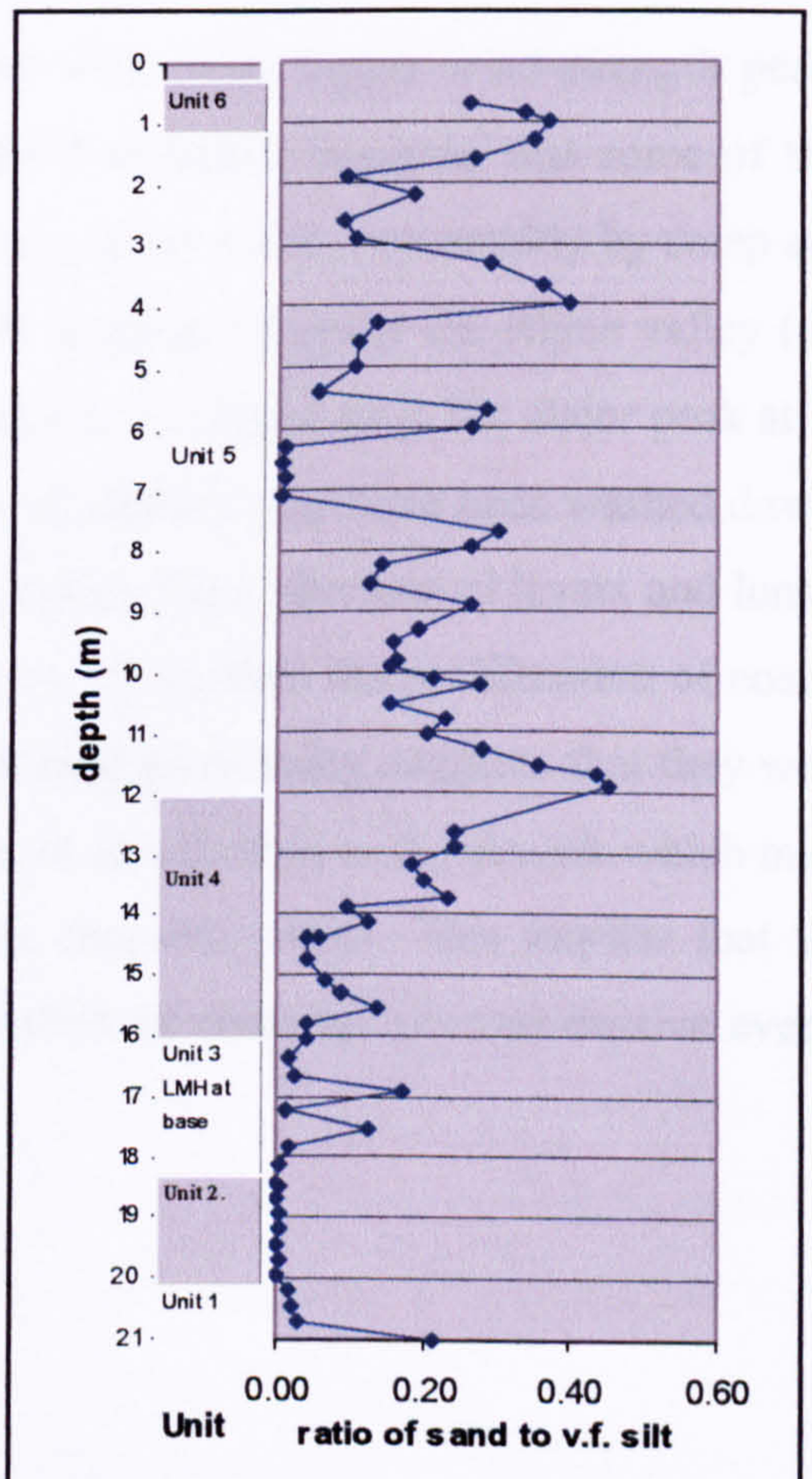

Figure 6.38 Metternich: ratio of sand to very fine silt.

less pronounced than at Harmignies, or that wind strength variation had less effect. The aeolian record begins in the Unit 1 pre-MIS-5a loess with indications of moderate winds (relative to the rest of the profile). Values in Unit 2 appear to show high wind strengths at some time prior to pedogenesis but this part of the record is unreliable due to that pedogenic episode. The start of Weichselian aeolian deposition occurs with the 'loess marker horizon' at the base of Unit 3, which is followed by an indicated reduction in wind

strength and then an increase to a broad peak in mid-Unit 3, followed by a period of apparently-decreasing wind strength to mid-Unit 4, at 14 m. At this point indicated wind strengths start a slow, fluctuating rise with maxima in mid- and upper Unit 5 at *c.* 7.7, 6.3, 4.0 and 1.5m depth. In Unit 6 wind strengths appear to decrease rapidly, at the base of the post-glacial soil.

6.4.3.3 Metternich: indications of non-aeolian content

The grain size data show up to 5.2% of fine, medium and coarse sand intermixed with the loessic silt. This coarse population is also apparent in the optical microscopy images (Figs. 6.22-6.25). The loess units at Harmignies, in contrast, contain very little material coarser than very fine sand. The ratio of this coarse Metternich sand fraction to the very fine silt fraction is shown at Fig. 6.38.

The concordance of some of these peaks with those higher-wind-strength peaks present in Fig. 6.37, notably the peaks at 1 and 4 m depth) suggests that some of this coarse fraction may have been delivered by vigorous wind action, presumably by creep and saltation from flood deposits of the Moselle (200 m down-slope) or the Rhine valley (the probable major source area). However, other peaks do not match (e.g. the major peak at 12 m) and it is possible that part of this coarse grain population may have been washed down-slope from upper terrace deposits (evidence for surface flow, plus gravel layers and lenses were observed during fieldwork, see Section 4.2.2). If so, then the proliferation of coarse grains and the lack of any visible stratification in their positioning suggests that they were washed down by relatively frequent, minor flows, in comparison to the gravels which must have been emplaced by more powerful but less frequent events. This implies that the Metternich site may have been significantly modified by contemporaneous erosive events on minor and major scales.

6.5 Carbonate content

As described in Sections 5.5 and 5.6, the carbonate content was determined by both gasometric and sequential loss-on-ignition methods. This section presents the results of both methods.

6.5.1 Evidence for the presence of a mix of carbonates

In the gasometric tests, the acid-alkali reaction proceeded rapidly and concluded quickly with calcium carbonate powder and bedrock chalk samples. However, with loess samples from both sites, the rapid initial reaction decreased to a very slow conclusion, with

strings of fine bubbles originating at a few, scattered points in the flask. This was especially obvious with samples from Metternich and is attributed to the presence of dolomite, in which the magnesium component reacts more slowly than the calcium component (Busenberg and Plummer, 1989). This is consistent with the geochemical results discussed in Section 6.1.3 and with:

(a) Juvigné and Moors (1995): Belgian loess contained predominantly calcium carbonate, with a small proportion of dolomite (values unknown),

(b) Pye (1983): silt-sized detrital calcite and dolomite grains were present at 3:1 ratio in loess in the upper Rhine valley in Germany, and,

(c) Hahn (1969): calcite and dolomite were present in 2:1 ratio in Swiss Rhine sediments.

This dual-rate reaction is, therefore, a reflection of that mixed carbonate composition.

6.5.2 Harmignies: carbonate content analysis

The Harmignies gasometric and LOI carbonate correlate strongly (c.c. 0.96). The pattern of variation in the carbonate content correlates strongly (c.c. 0.99) with variation in the CaO content (see Section 6.1.1), demonstrating that carbonates are the primary carrier of Ca.

In the Eemian and early Weichselian palaeosols of Units D, E and lower F, the carbonate content is extremely low (Fig. 39). In mid-Unit F (coincident with the start of primary loess deposition), it commences a rapid rise and by lower Unit G, at 8.52 m, it reaches a brief peak of approximately 25%. The profile then shows two steep reductions, the first between approximately 8-7 m which extends through the upper part of Unit G into H. A second reduction occurs in Unit H between 6.5-5.5 m. A transient peak occurs at 4.95 m, immediately below the well-defined tundra gley at the top of Unit H. Carbonate values then fall in Units I, J and lower K, with another brief peak at c. 3 m. Values then fall again to 1.5 m (upper Unit K) with an average carbonate content of approximately 15% until depth 1.25m, when there is a further brief peak followed by a rapid reduction to extremely low levels in the overlying Holocene soil.

The Unit G-Unit K loess appears to show a slow drop in carbonate content from *c.* 20% to 15%, though this is difficult to interpret in such a variable carbonate profile.

Chalk granules are present between Unit F and upper Unit K, blown onto the ridge from its exposed face (van Vliet, 1975). Analysis of sieved sub-samples shows that granules >0.5 mm constitute up to 15% of the total carbonate content for each sample,

contributing between 1 and 1.5 % to the total value. There is no correlation between the 'granule carbonate content' and grain size variation (using the Vandenberghe U-ratio) and so variation in the amount of granular chalk is not a wind-strength proxy.

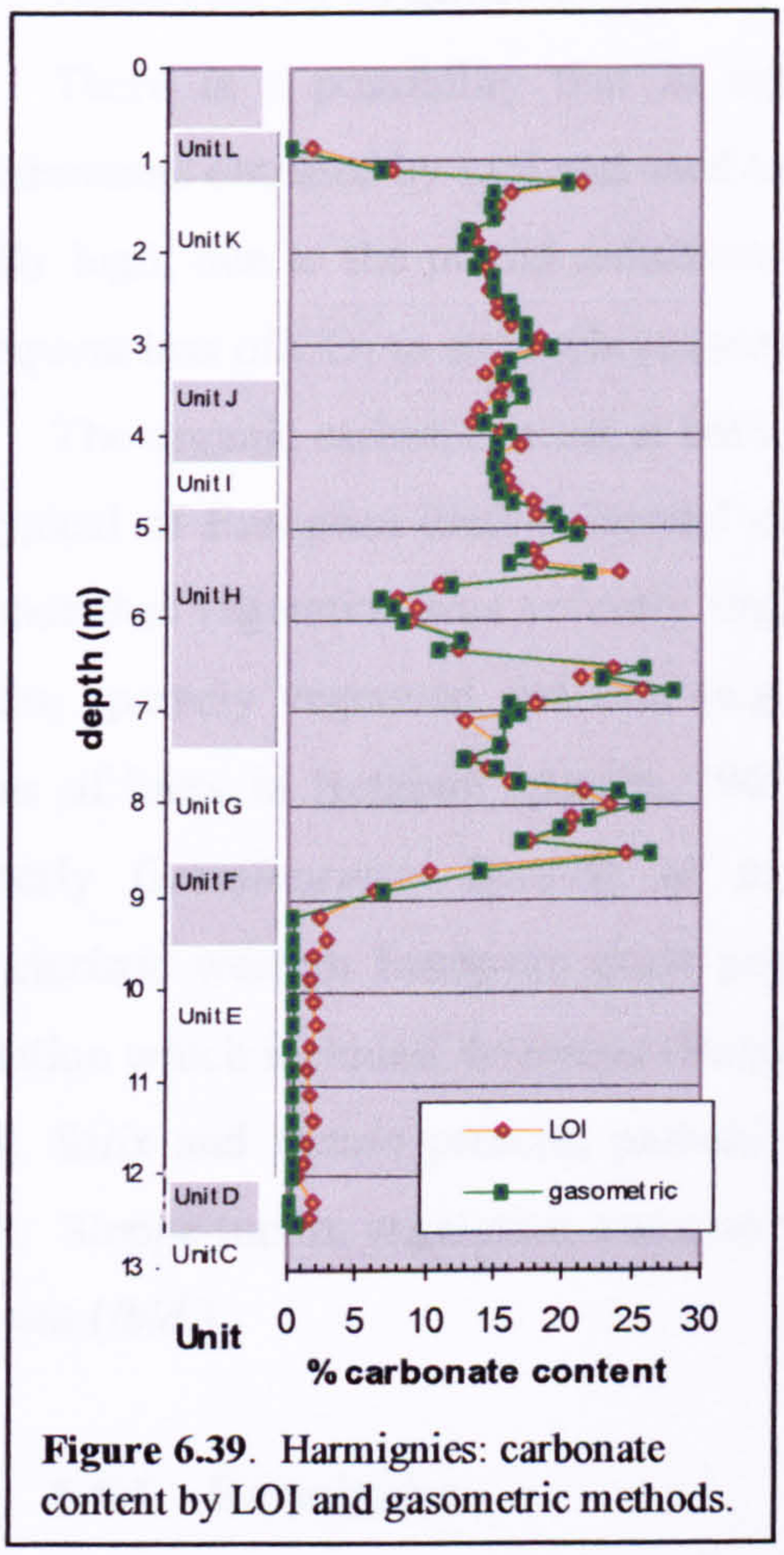

Figure 6.39. Harmignies: carbonate content by LOI and gasometric methods.

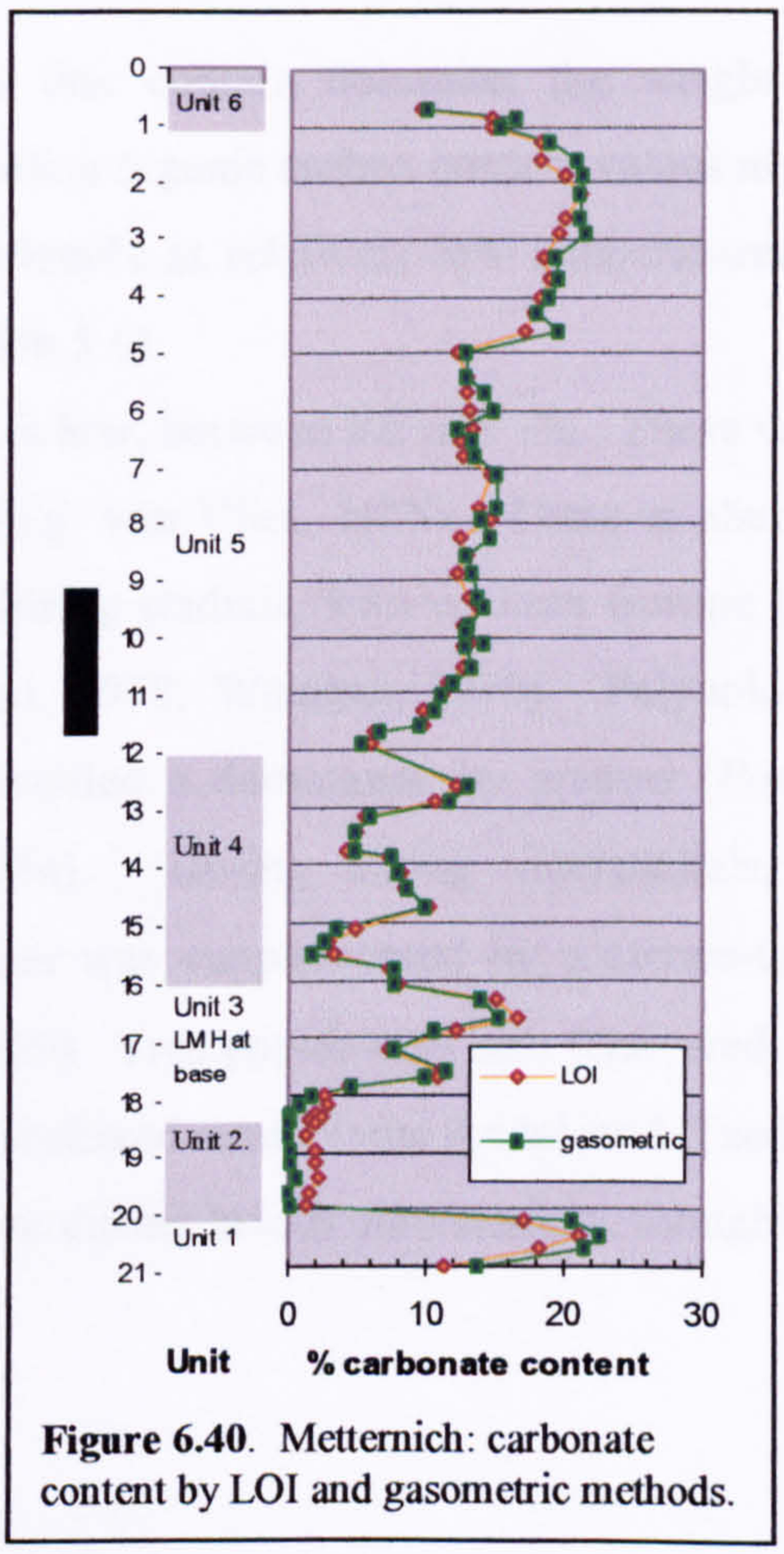

Figure 6.40. Metternich: carbonate content by LOI and gasometric methods.

6.5.3 Metternich: carbonate content analysis

Like Harmignies, the Metternich gasometric and LOI results show the same profile (Fig. 6.40). The average carbonate content at Metternich is lower, mainly between 10-20%, but it increases slowly up-profile to reach the highest values at the top of the sequence, due to the increase in the amounts of calcite and dolomite (see Section 6.1.3). At 21-20 m depth, in Unit 1, carbonate values are very high but field examination revealed the presence of pedogenic carbonate nodules at the top of the unit, so at least part of these high values is caused by reprecipitated carbonate, weathered from the low-carbonate Unit 2 palaeosol. The loess marker horizon at the base of Unit 3 shows no increased carbonate content but values begin to rise immediately above that horizon, as reworked sediments become progressively more loessic. Carbonate values reach a peak in Unit 3 *c.* 17-16 m, in primary loess, and then describe three sharp oscillations, with troughs between *c.* 16-15 m, 14-13 m and 12-11.5 m. Thereafter the carbonate content becomes much less variable and rises slowly to a maximum of approximately 21% at depths of 3-1.5 m. These high values

are likely to include carbonate enhancement from the decalcified Unit 6 post-glacial soil but this feature is not as well-defined as it is at Harmignies.

6.6 Analysis of organic content

There is a possibility that in samples that contain dolomite, the weight loss measurements obtained by LOI and used to calculate organic carbon content values may be slightly high, due to the partial reduction of dolomite at relatively low temperatures and consequent loss of CO_2 to atmosphere (see Section 5.6).

The organic carbon content at both sites is low, between 0.2 and 1%. These values are typical of European loess-palaeosol units (e.g. van Vliet, 1975). There is abundant evidence that vegetation was severely limited during stadials, with western Europe being treeless, sparsely vegetated and arid (e.g. West, 1978; Weniger, 1990). Palynological studies of loess in Belgium (Bastin, 1969) identified a dominance by grasses (*Poacea*) (formerly *Graminaceae*: Bennett *et al.*, 1994). During strong interstadials, this characteristic western European grass population was supplemented by a steppe-tundra vegetation which included *Artemisia* (Bastin, 1969). Tree populations also recovered, with *Pinus, Salix* and *Betula* present, probably in sheltered areas (van Andel and Tzedakis, 1996). Steppe-tundra vegetation was also present during briefer interstadials, though trees were not (*ibid.*).

6.6.1 Harmignies

The lowermost part of this profile (Fig. 6.41) shows a strong peak associated with the Unit D 'terra fusca' soil but the overlying complex of early Weichselian soils in Unit E do not appear as significant organic carbon peaks, though values as a whole are higher than the primary loess in Units I, J and K. The peak at 8.14 m equates to a tundra gley; 7.11 m to a 'humic horizon' and the pronounced peak at 5.75 m to the 'Les Vaux' soil. Thereafter, organic carbon values drop to very low levels through Units I, J and K, climbing again at the top of the profile in a tundra gley soil at the top of Unit K and in Unit L (post-glacial soil).

6.6.2 Metternich

The organic carbon content at this site (Fig. 6.42) can be divided into three sequences. Unit 1 (pre-MIS 5a loess) has low organic carbon content but Unit 2 (early Weichselian palaeosols) contains up to 1%, close to values in the Unit 6 post-glacial soil. The 'marker loess horizon' at the base of Unit 3 shows a brief reduction and the recycled sediment in the lower part of Unit 3 contains substantial, but diminishing organic content,

as the sediment becomes increasingly loessic. Upper Unit 3, plus Units 4 and 5 (Weichselian loess) present a series of diminishing saw-tooth oscillations, marking a slow reduction in organic content. Significant minima occur c. 17.6, 16.65, 14.75 and 13.75 m,

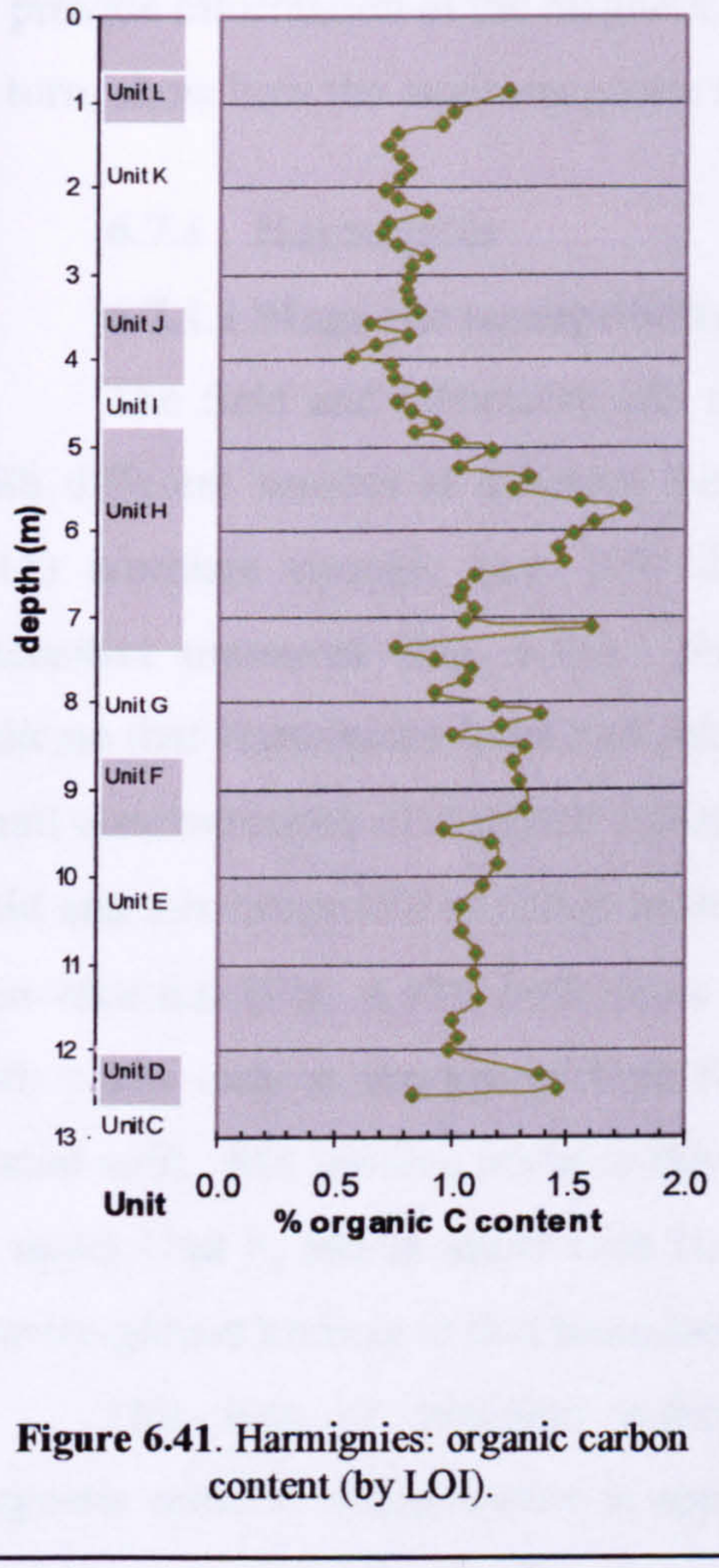

Figure 6.41. Harmignies: organic carbon content (by LOI).

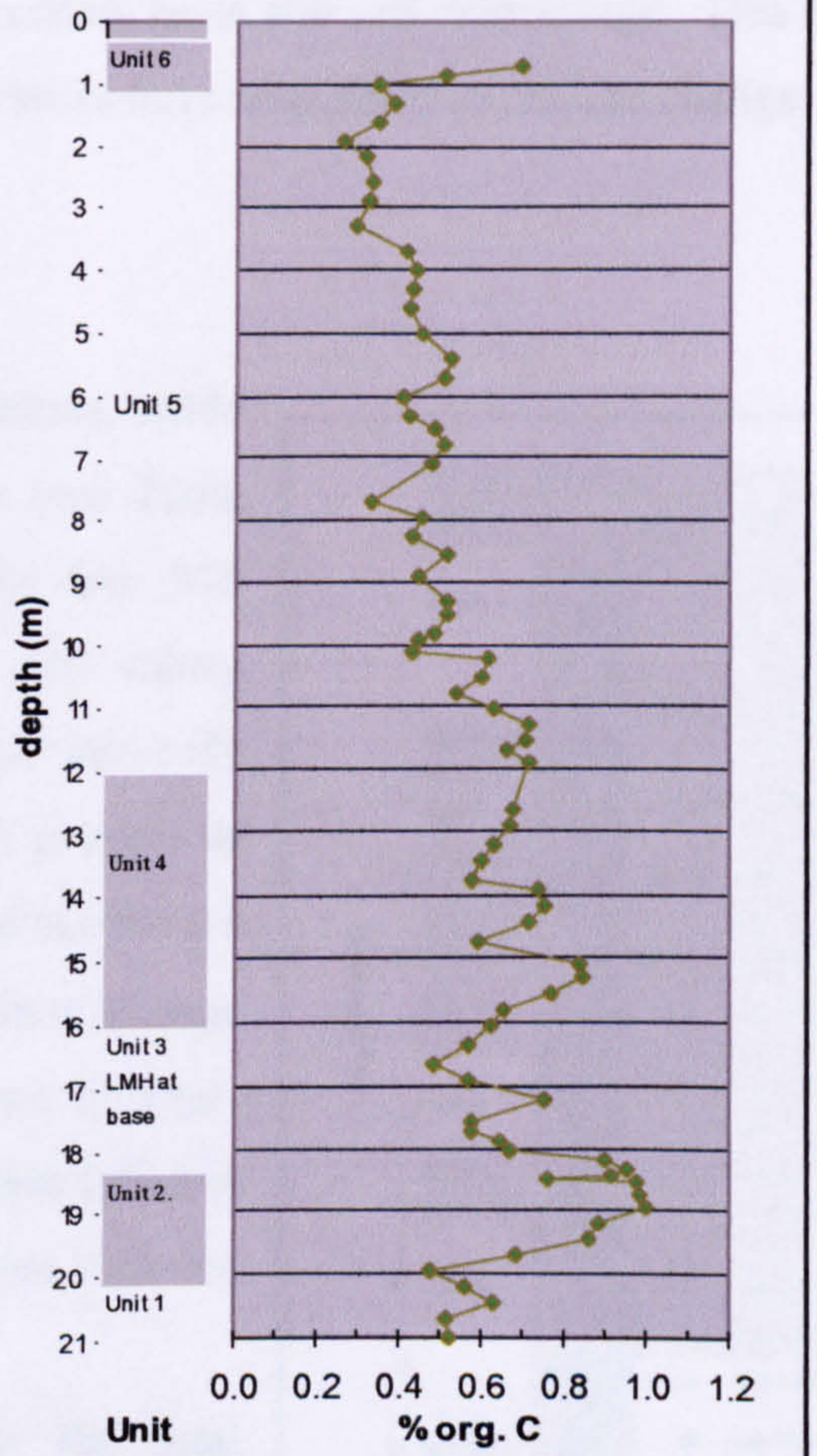

Figure 6.42. Metternich: organic carbon content (by LOI).

with maxima c. 17.2, 15.3 and 11.9-11.3 m depth. This sequence finishes with an absolute minimum occurring c. 2 m depth. Values rise slightly at the top of Unit 5 and rapidly in Unit 6 (post-glacial soil).

6.7 Analysis of enviromagnetic characteristics

As described in Section 5.8.2, mass-specific results have been corrected to carbonate-free values. The results of the magnetic tests (see Section 5.7) can be interpreted to provide information of the magnetic concentration, grain size and mineralogy. This can, in turn, show how the enviromagnetic characteristics have responded to climate change.

6.7.1 Harmignies

6.7.1.1 Magnetic susceptibility

The field and laboratory MS measurements, made with different sensors at different frequencies (see Table 5.11) correlate strongly (c.c. 0.9) despite the low MS intensities measured (Fig. 6.43). Such low MS values indicate that Harmignies loess and palaeosols contain only small concentrations of magnetic minerals. The patterns of field and laboratory MS variation in the vertical profile are near-identical (Fig. 6.43); both show only minor change with peaks only at the top of Unit K and Unit L (post-glacial soil). MS minima occur at the top of Unit D/lower E, upper Unit F, and in upper Unit H, coincident with the heavily-gleyed horizon at that boundary.

This lack of variation indicates that the total magnetic mineral concentration is approximately constant throughout most of the profile; the only major change is the evidence for magnetic enhancement (relative to the parent loess) in the overlying Holocene soil.

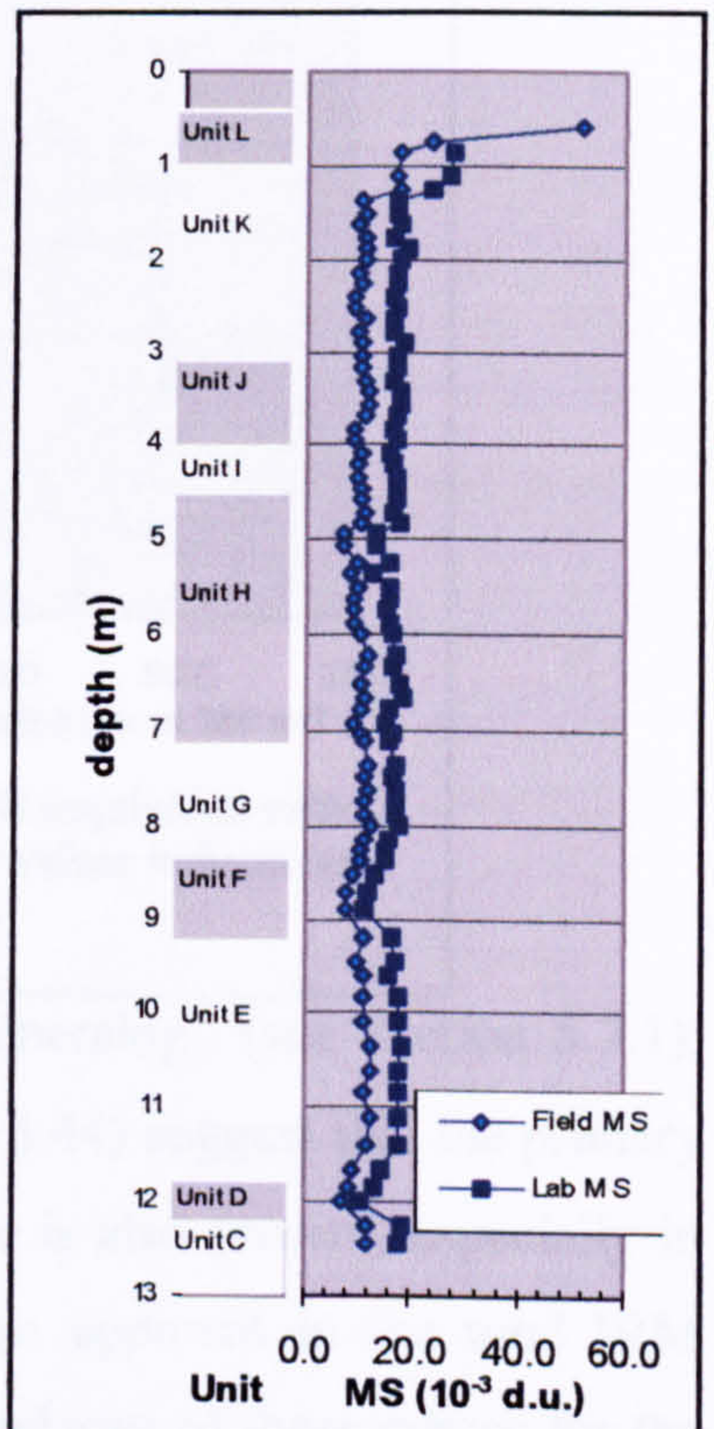

Figure 6.43. Harmignies: variation in magnetic susceptibility.

6.7.1.2 S-ratio and %IRM acquisition

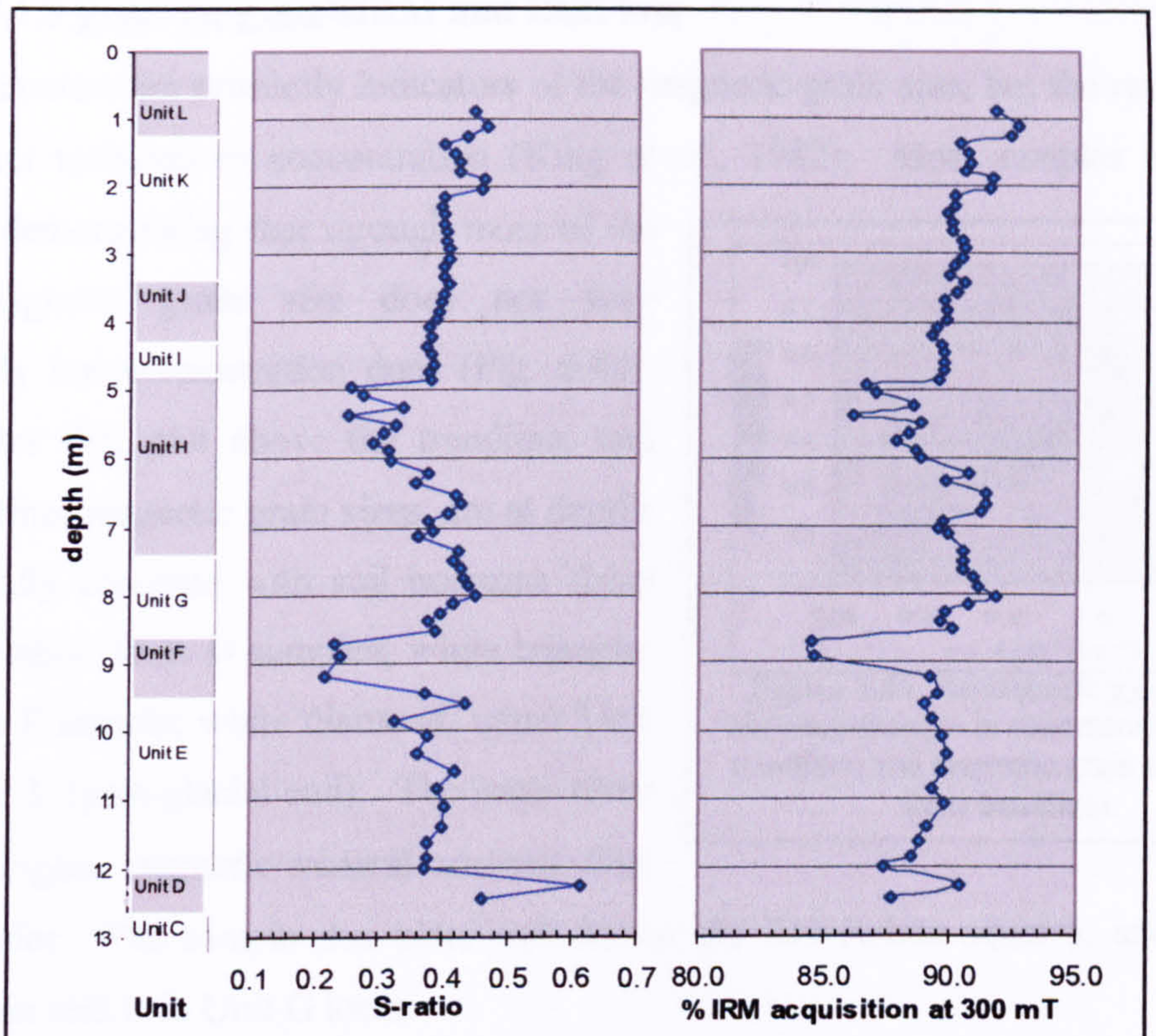

Fig 6.44. Harmignies: S-ratio values close to 1 and IRM acquisition values close to 100% indicate dominance by magnetite, lower values indicate an increasing contribution by haematite.

These parameters are indicators of the magnetic mineralogy (see Section 5.7.1). The profile plots of the S-ratio and % IRM acquisition (Fig. 6.44) suggest that the primary magnetic mineral is magnetite/maghemite, though haematite is also present, especially in Unit F and upper Unit H. This mixed mineralogy is also apparent in the total IRM acquisition plots. Fig. 6.45 shows the upper and lower boundaries of these curves for the total Harmignies dataset (the intervening curves have been omitted for clarity). The upper curve is from Unit D and shows the typical low-coercivity (magnetite) response to increasing field strength (c.f. Fig. 3.3). The fact that it does not reach saturation by approximately 300 mT is attributable to a small high-coercivity (haematite) content, contributing approximately 9% to IRM acquisition. The lower curve is from Unit F and shows that this sample must contain a larger high-coercivity component which does not approach saturation even at 880 mT. It contributes approximately 15% to IRM acquisition.

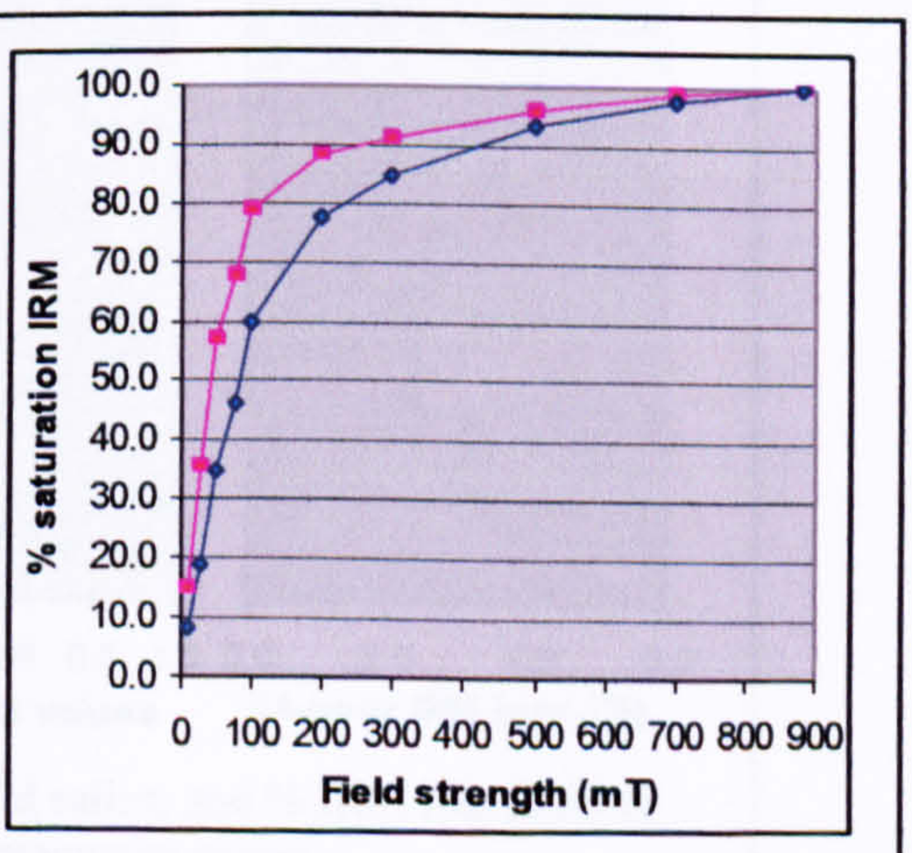

Figure 6.45. Harmignies: upper and lower boundaries of the total IRM acquisition envelope.

6.7.1.3 χ_{ARM}/χ_{lf}, χ_{ARM}/SIRM and IRM loss

These parameters are primarily indicators of the magnetic grain size, but the ratio χ_{ARM}/χ_{lf} also reflects variation in concentration (King *et al.*, 1982). Most samples are closely clustered, demonstrating that through most of the profile magnetic grain size does not vary significantly but concentration does (Fig. 6.46). The samples that plot above the trendline, and thus have finer magnetic grain sizes, are at depths that generally correlate with soil horizons (blue triangle symbol: Unit D samples; white triangle: upper Unit F sample; white diamond; upper Unit K and Unit L (post-glacial soil). The latter three also have higher magnetic mineral contents than the remainder. The sample that plots well below the line (white square), and thus has coarser grain size is in Unit G loess.

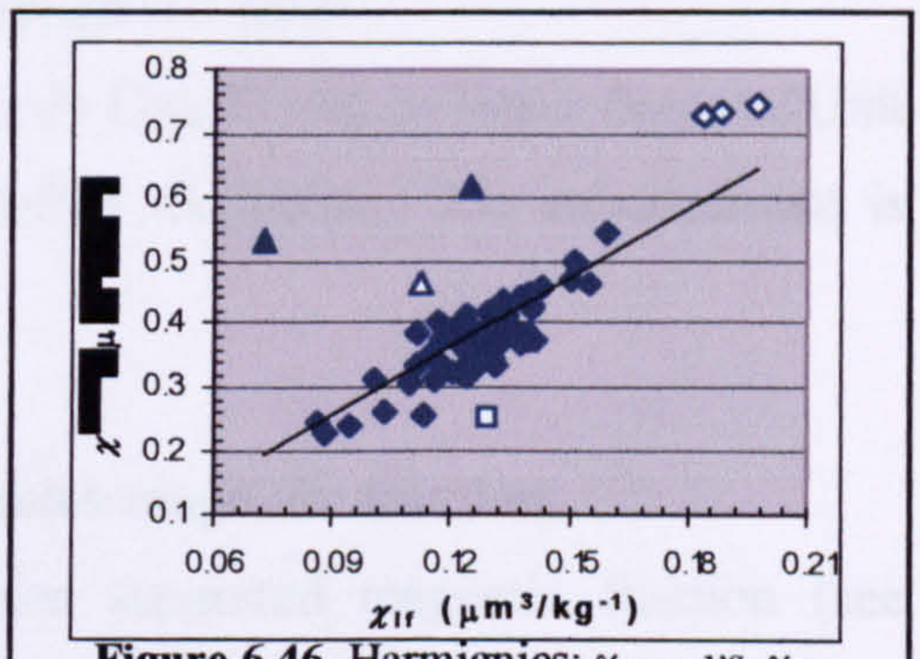

Figure 6.46. Harmignies: χ_{ARM} *vs.* χ_{lf}, showing changes in concentration (along trendline) and magnetic grain size (away from trendline).

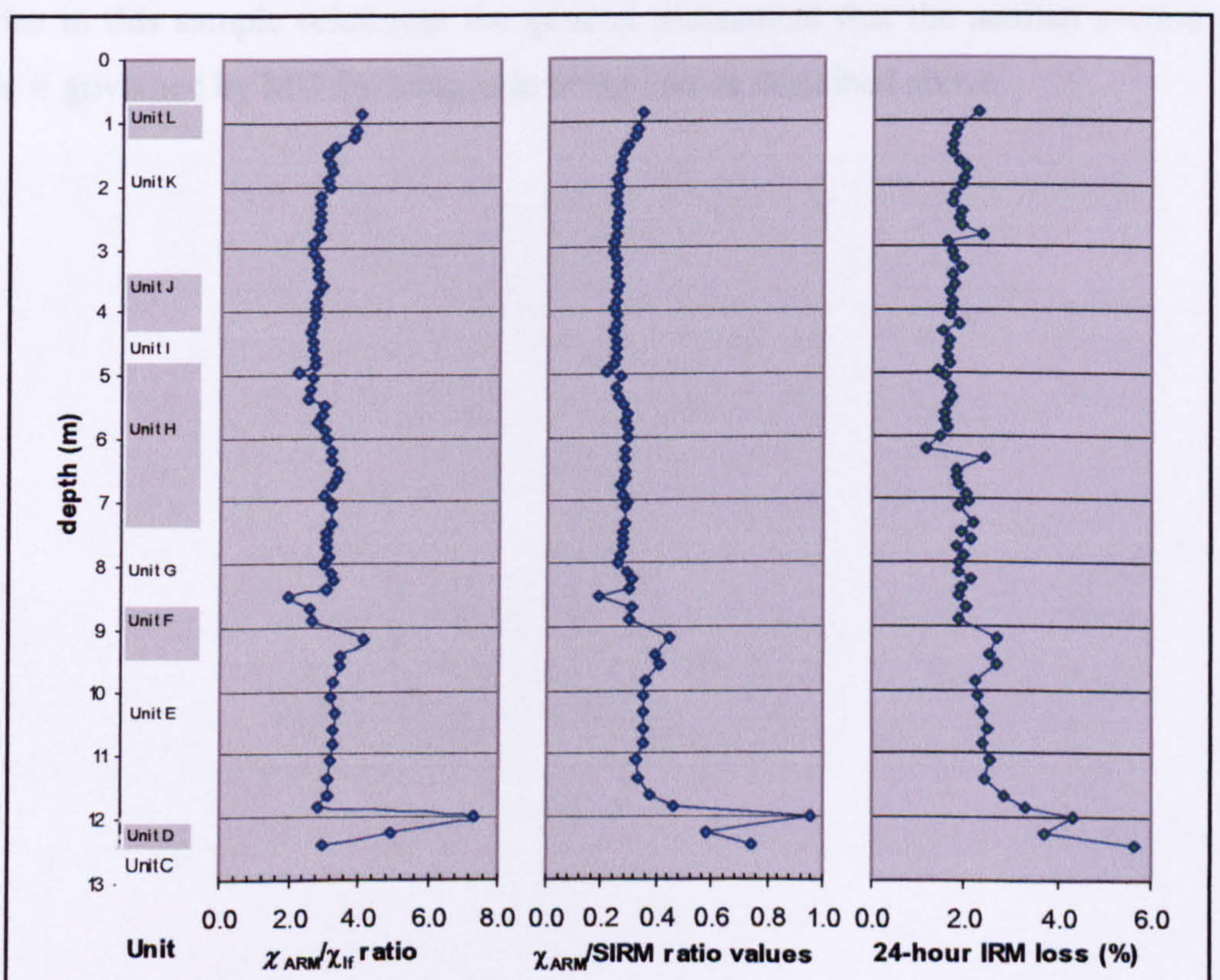

Figure 6.47. Harmignies: χ_{ARM}/χ_{lf} and χ_{ARM}/SIRM ratios, and % IRM loss indicate relative abundance of ultra-fine magnetite grains.

Plots of χ_{ARM}/χ_{lf} and χ_{ARM}/SIRM *vs.* depth (Fig. 6.47) show the relative abundance of ultra-fine magnetite grains (Sugiura, 1979; Zhou *et al.*, 1990), and the pattern of IRM viscous loss identifies populations of metastable grains close to the SP/SD boundary. All

three graphs show broadly the same set of features: Unit D (Eemian palaeosol) shows strong enhancement at 12 m depth; values in Unit E (early Weichselian palaeosols) are lower and stable but possible minor enhancement occurs in mid-Unit F. Values then drop again and are flat throughout Units H, I, J and mid-K (Weichselian loess). They rise slightly in upper Unit K and rise again in Unit L (post-glacial soil).

This evidence suggests that at Harmignies, only Unit D and, to lesser degrees, Unit E and Unit L contain increased amounts of ultra-fine magnetite. No enhancement is apparent in the loess of Units G-K.

6.7.1.4 Optical examination of the Harmignies magnetic fraction

Microscopic examination of the Harmignies separated magnetic fraction (see Section 5.5.1) shows that it is composed of strongly-magnetic, irregular, black crystals with well-defined crystal faces and a pronounced metallic lustre; this is probably magnetite (Figs.6.48-6.51). Most of these particles are silt-sized or smaller (<50 μm) and variable in shape: most are angular to sub-angular, a small proportion are rounded. Within the limitations described in Section 5.7.5, the apparent predominance of coarse magnetite particles in this sample reinforces the general assessment that the aeolian section of the profile is governed by MD ferrimagnetic behaviour as described above.

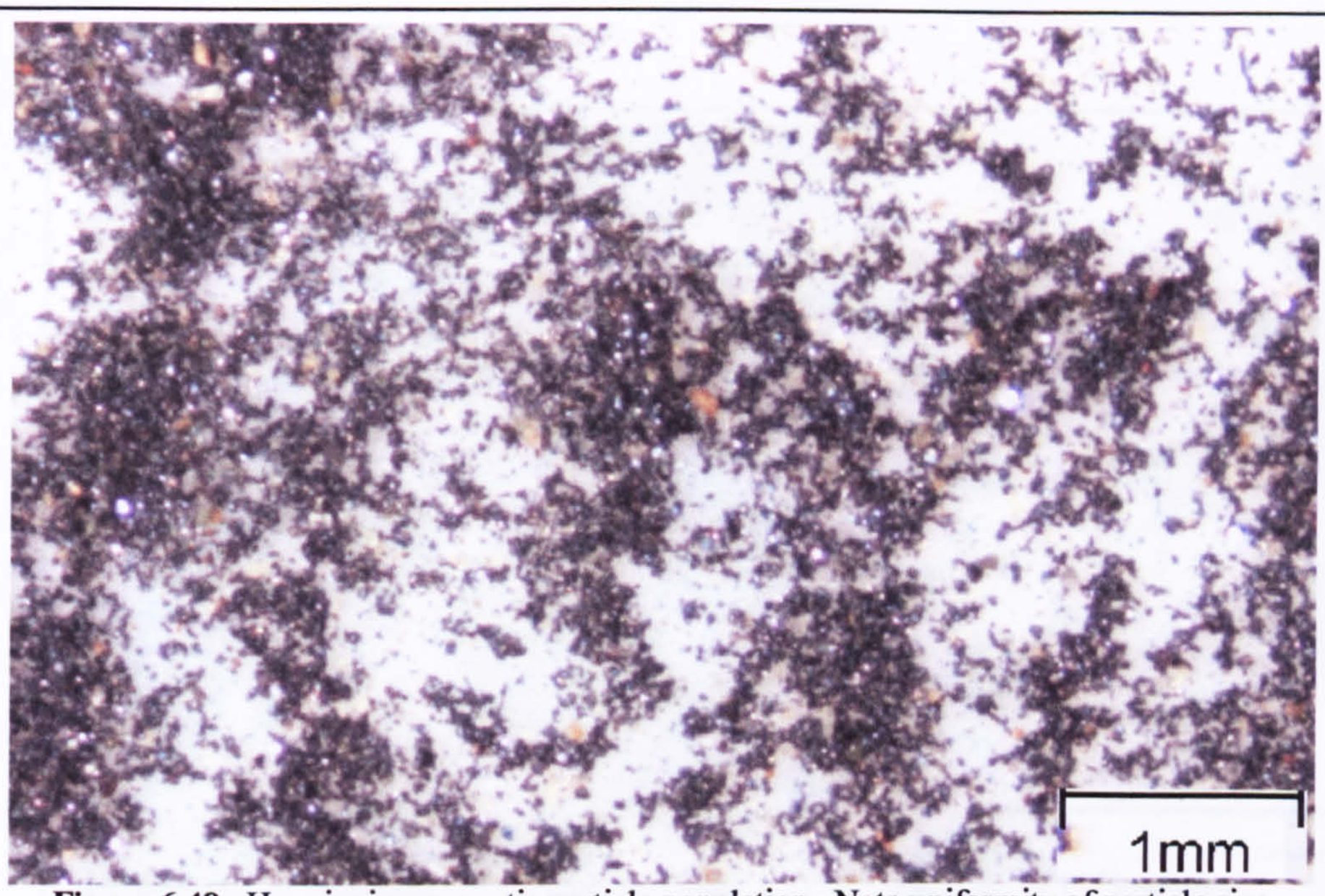

Figure 6.48. Harmignies magnetic particle population. Note uniformity of particle size.

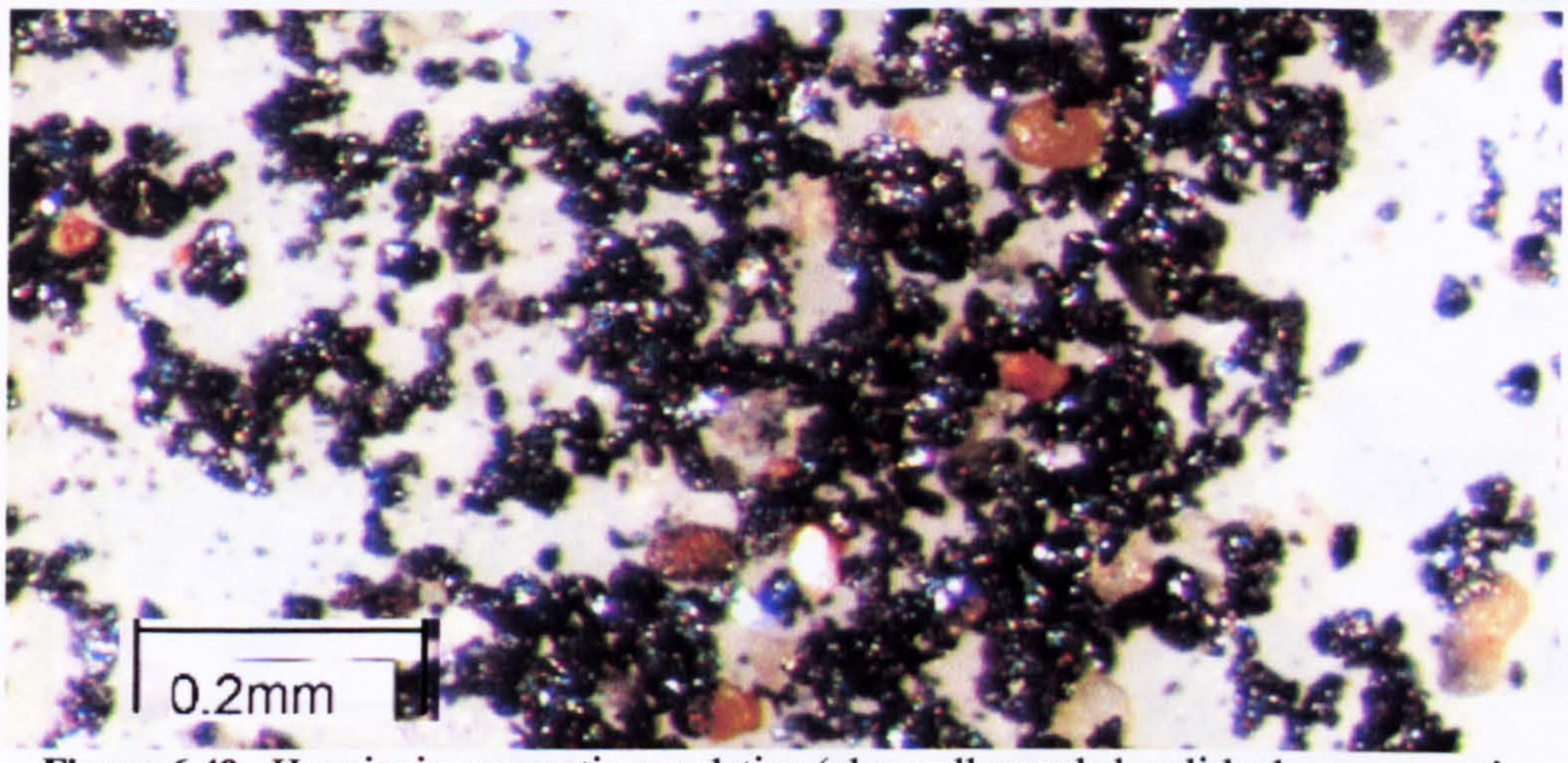

Figure 6.49. Harmignies magnetic population (plus well-rounded, polished non-magnetic mineral grains).

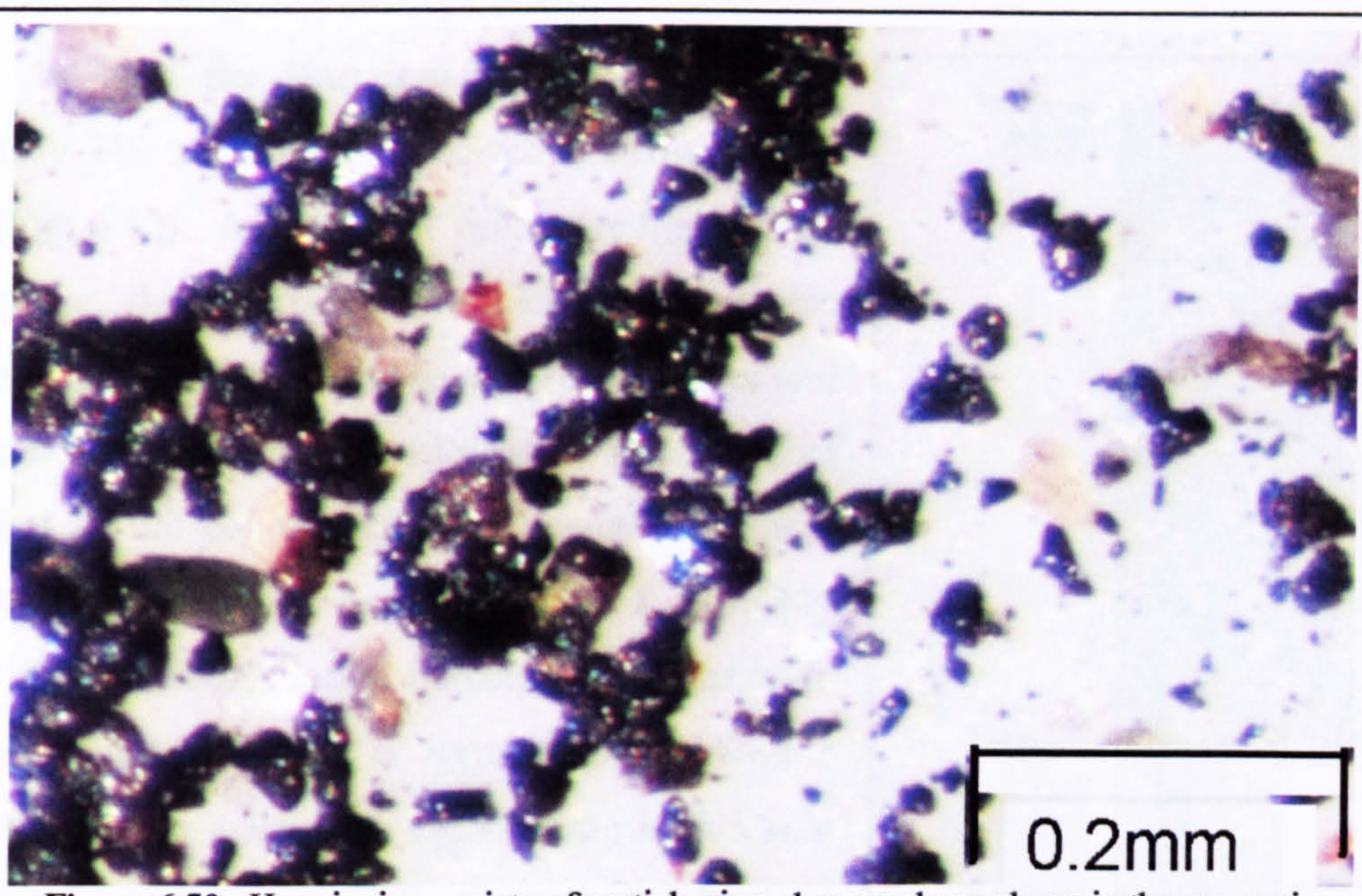

Figure 6.50. Harmignies: variety of particle size, shape and roundness in the magnetic population.

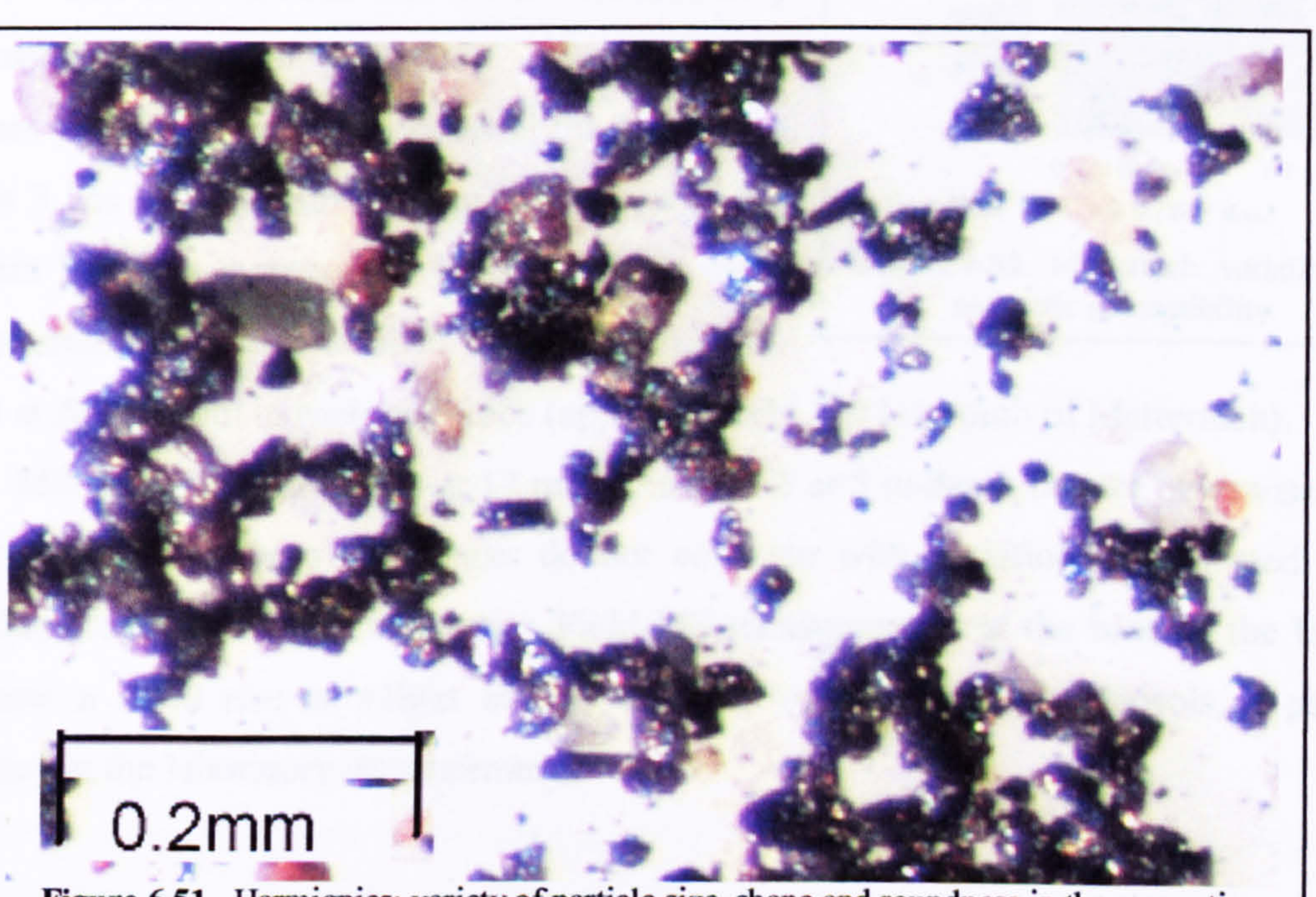

Figure 6.51. Harmignies: variety of particle size, shape and roundness in the magnetic population.

6.7.3 Metternich

6.7.2.1 Magnetic susceptibility.

As with the Harmignies results, field and laboratory MS measurements correlate strongly (c.c. 0.96) (Fig. 6.52). Average MS values are higher than Harmignies, showing that Metternich loess contains more magnetic mineral particles than Harmignies and the range is greater. The profile shows a progressive reduction in the concentration of magnetic mineral particles between Unit 3 and upper Unit 5, probably due to the increasing influx of calcite and dolomite particles. A major peak is apparent in the Unit 2 early Weichselian palaeosol, representing high levels of magnetic enhancement. The loess marker horizon at the base of Unit 3 shows a major reduction in MS values, which demonstrates that it contains relatively few magnetic mineral particles. The reworked sediment above the marker horizon in the lower part of Unit 3 has high but diminishing MS values as the sediment becomes increasingly loessic. This pattern closely resembles that described by Rousseau *et al.* (1998) at Achenheim in eastern France (approximately 110 km south of Metternich).

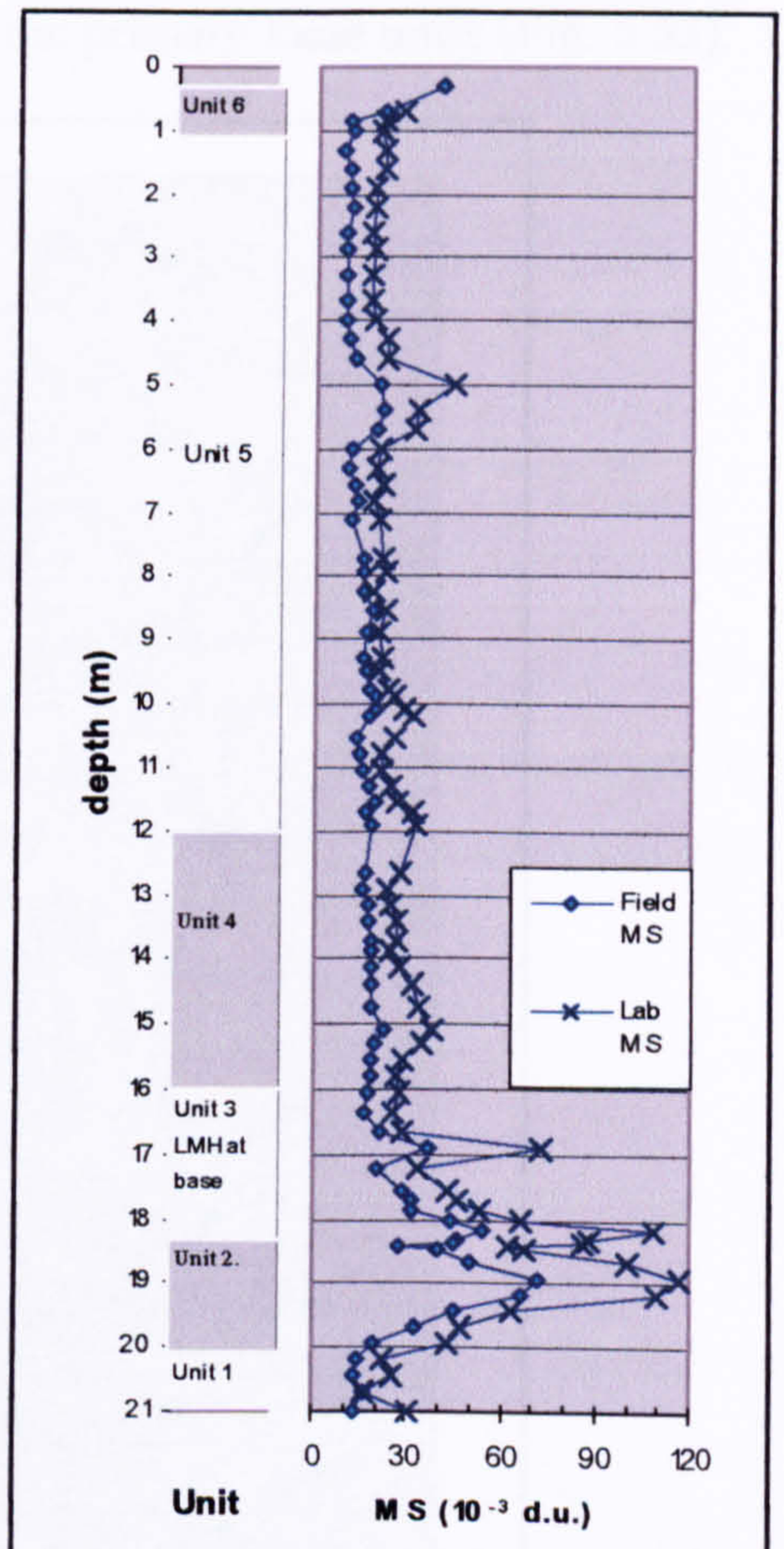

Figure 6.52. Metternich: variation in magnetic susceptibility.

MS values rise in Unit 3 at 17 m and in Unit 5 at 5 m depth but are otherwise very flat until Unit 6. These two peaks do not correlate with variation in indicated wind strengths, grain size or geochemistry. Field MS measurements at the base of the Unit 6 soil show a rapid rise to values similar to those of the Unit 2 palaeosols, a pattern replicated in the laboratory measurements.

6.7.2.2 S-ratio and % IRM acquisition.

The S-ratio and % IRM acquisition values (Fig. 6.53) are similar to Harmignies, and suggest that the magnetic mineralogy is similar, with dominant magnetite (and/or maghemite), plus a haematite component, especially in the primary loess units (Fig. 6.53).

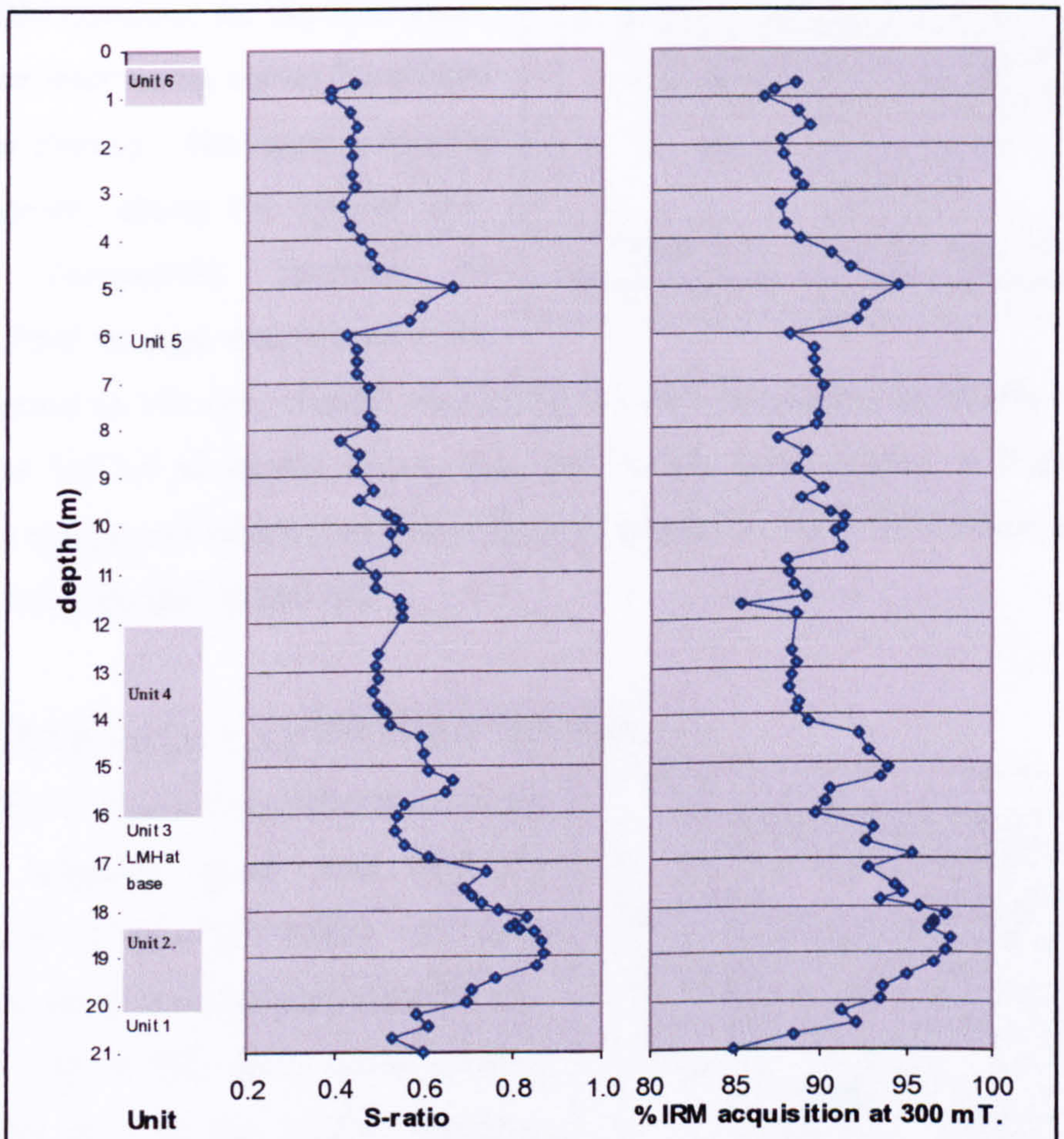

Figure 6.53. Metternich: S-ratio values close to 1 and IRM acquisition values close to 100% indicate dominance by magnetite, lower values indicate an increasing contribution by haematite.

Unit 1 (pre-MIS 5a loess) has relatively low values, close to those of the Weichselian loess but Unit 2 has very high values, indicating strong enhancement during the early Weichselian. The loess marker horizon at the base of Unit 3 has values similar to those of the adjacent sample levels, showing that its magnetic content is mainly magnetite. The diminishing values above that horizon are probably attributable to the dilution of recycled sediment as loess deposition increases. The indicated magnetite content diminishes slowly in Units 4 and 5 but increases strongly in Unit 5 at *c*. 5 m depth (*c.f.* MS values). Magnetite then continues to diminish until Unit 6, when there is a minor increase at the base of the post-glacial soil.

This mixed magnetite and haematite content is also apparent in the total IRM acquisition plots. Fig. 6.54 shows the upper and lower boundaries of the total IRM envelope for the Metternich data set (the intervening curves have been omitted for clarity). The upper curve (at 18.95 m depth) shows the typical low-coercivity (magnetite) response to increasing field strength and is only 2.7% from saturation at 300 mT, closely resembling the pure magnetite curve (Fig. 3.3). The lower curve (at 1.0 m depth) shows that this sample must contain a high-coercivity (haematite) component which contributes approximately 13.5% to IRM acquisition at 300 mT and it is unsaturated at 880 mT.

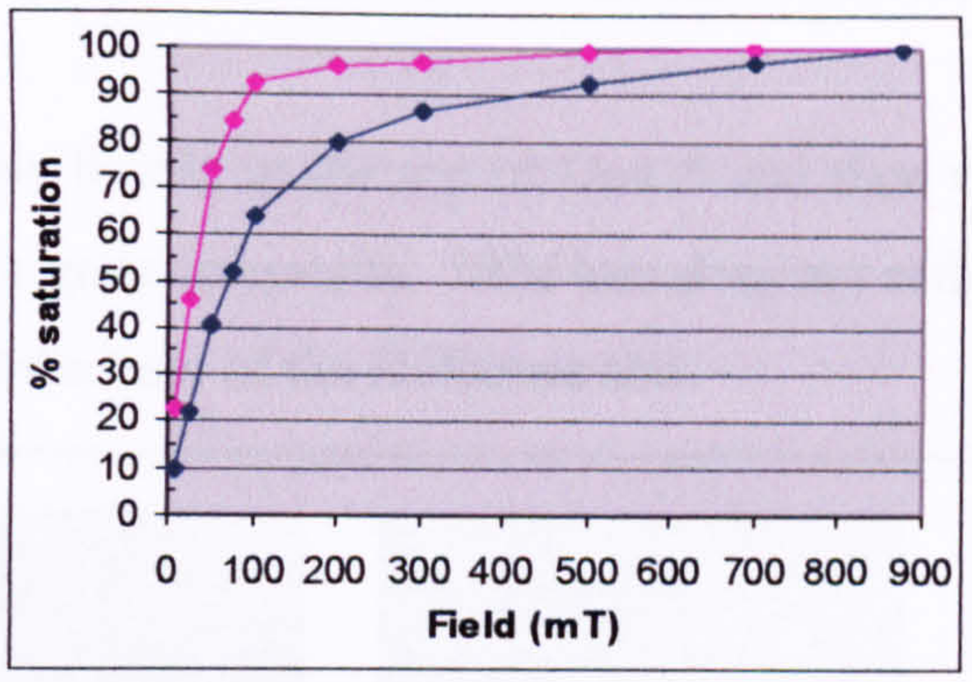

Figure 6.54. Metternich: upper and lower boundaries of the total IRM acquisition envelope.

6.7.2.3 χ_{ARM}/χ_{lf}, χ_{ARM}/SIRM and IRM loss.

The ratio χ_{ARM} *vs.* χ_{lf} reflects variation in both magnetic grain size and in concentration (King *et al*, 1982). As with Harmignies, most samples plot close to the trend line (Fig. 6.55), again demonstrating that through most of the profile magnetic grain size does not vary significantly but concentration does. The samples that are marked with crosses plot above the line and thus have finer magnetic grain sizes, and are present at relatively high concentrations. These are in the early Weichselian palaeosols.

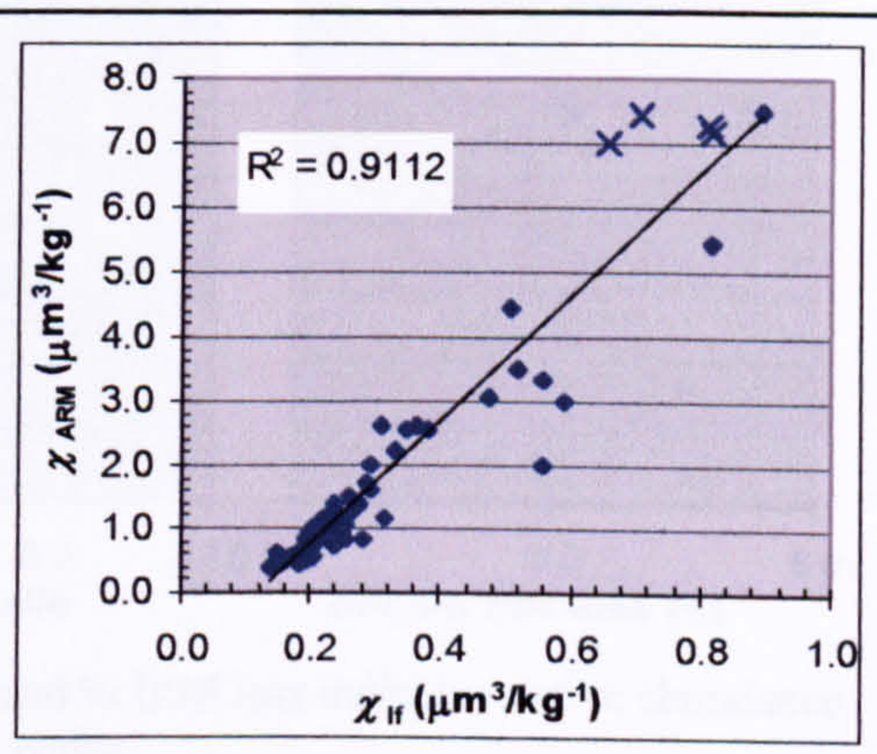

Figure 6.55. Metternich: χ_{ARM} *vs.* χ_{lf}, showing changes in concentration (along trend line) and magnetic grain size (away from trend line).

Plots of χ_{ARM}/χ_{lf}, χ_{ARM}/SIRM and 24-hour IRM loss *vs.* depth (Fig. 6.56) show the changing relative abundance of ultra-fine magnetite grains, compared to coarser grains through the profile. All three graphs show the same general pattern as has been described above, of low values in the Unit 1 loess, higher values in the Unit 2 palaeosols and lower Unit 3 sediments, and predominantly low values in Units 4 and 5. These latter two units appear to be dominated by MD magnetite. These plots particularly emphasize the lack of ultra-fine grains in the loess marker horizon at the base of Unit 3. This suggests that it is

not derived from the underlying palaeosol complex, which contains an abundance of these grains.

χ_{ARM}/χ_{lf} and χ_{ARM}/SIRM ratios increase briefly at the top of Unit 5 and then rise again in the Unit 6 soil, indicating a rise in fine-grain magnetite. IRM loss does not reflect the 1.3 m peak but gives a stronger response at the base of the Holocene soil.

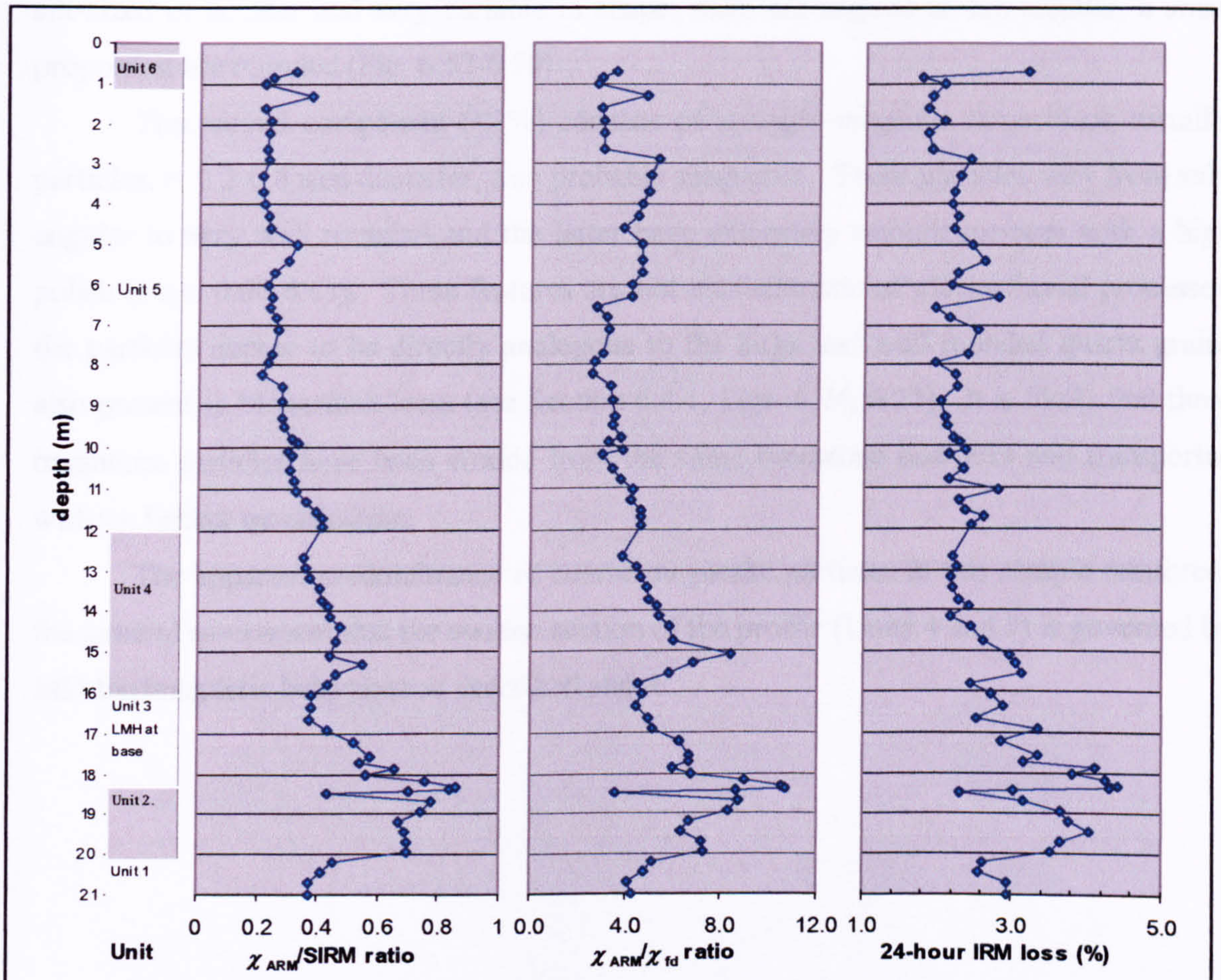

Figure 6.56. Metternich: χ_{ARM}/χ_{lf} and χ_{ARM}/SIRM ratios, and % IRM loss indicate relative abundance of ultra-fine magnetite grains.

6.7.2.4 Optical examination of the Metternich magnetic fraction

Microscopic examination of the Metternich separated magnetic fraction reveals that it contains two components. The first closely resembles the Harmignies magnetic fraction and consists of strongly-magnetic, irregular, black crystals with well-defined crystal faces and a pronounced metallic lustre. This is probably magnetite. Most of these particles are silt-sized or smaller and very variable in shape: most are angular to sub-angular, a small proportion are rounded (Fig. 6.57-6.59).

The second component (<1%) consists of strongly-magnetic large black metallic particles, *c.* 0.2-0.8 mm diameter, also probably magnetite. These particles vary from sub-angular to very well rounded and the latter have extremely smooth surfaces with a high polish (Figs. 6.60-6.61). These features are not characteristic of glacio-fluvial processes, the particles appear to be directly analogous to the large and well-rounded quartz grains also present in Metternich loess (see Section 6.4.1, Figs. 6.24, 6.25). It is likely that these magnetite particles have been eroded from the same sandstone bedrocks and transported without further modification.

The apparent predominance of coarse magnetite particles in this sample reinforces the general assessment that the aeolian section of the profile (Units 4 and 5) is governed by MD ferrimagnetic behaviour as described above.

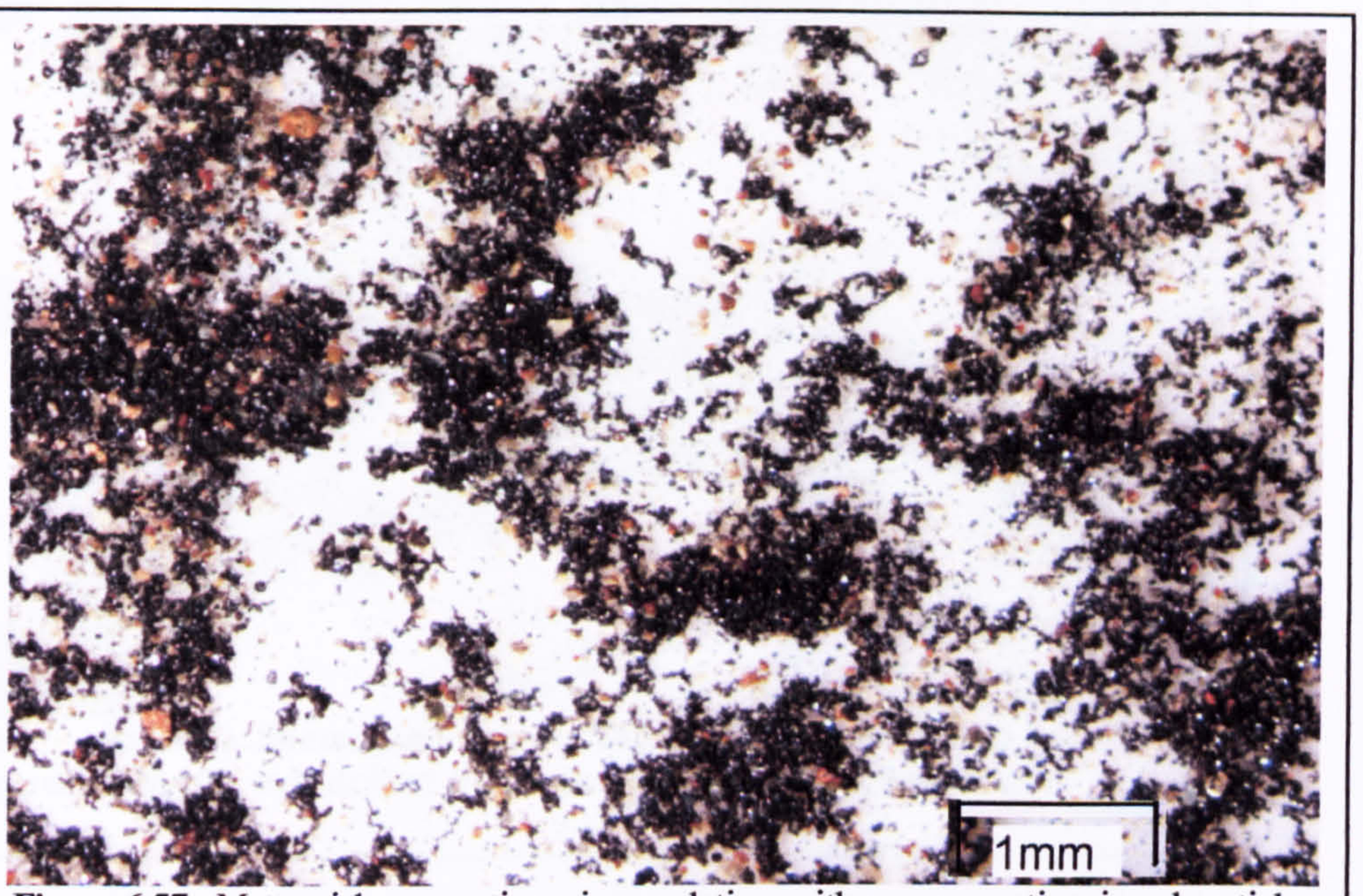

Figure 6.57. Metternich: magnetic grain population, with non-magnetic mineral particles also present.

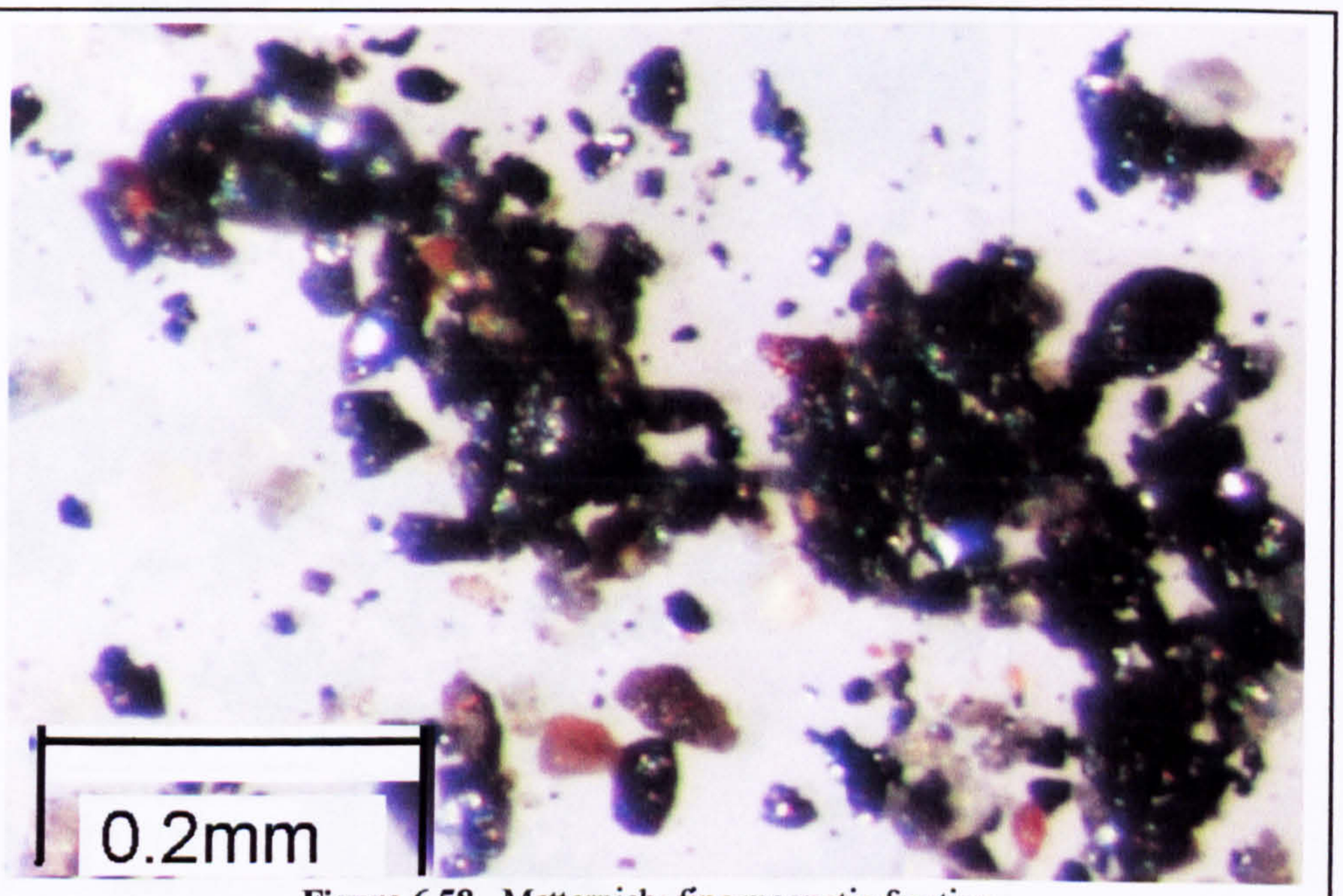

Figure 6.58. Metternich: fine magnetic fraction.

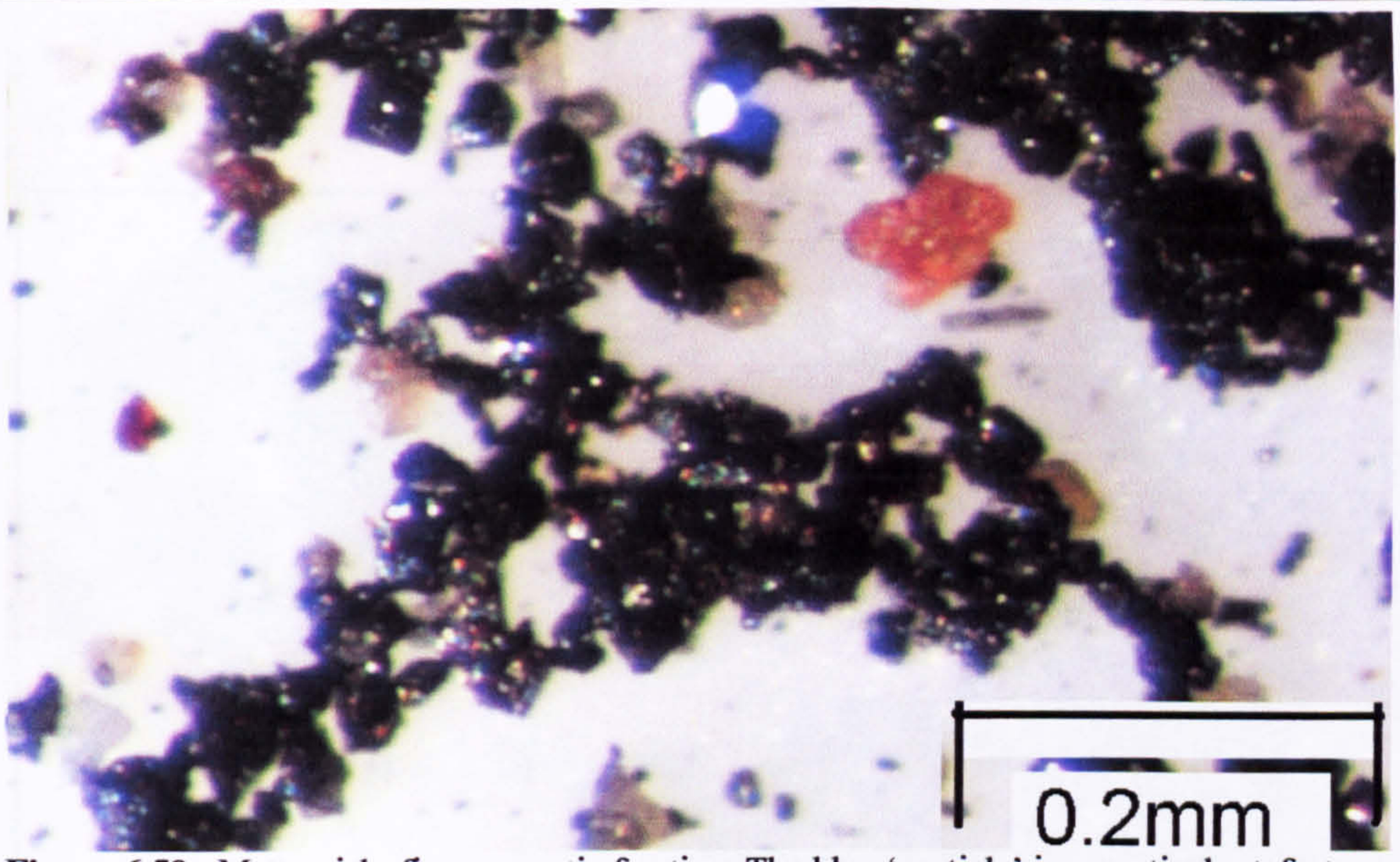

Figure 6.59. Metternich: fine magnetic fraction. The blue 'particle' is an optical artefact caused by reflection off a well-defined crystal face; the red crystal is unidentified.

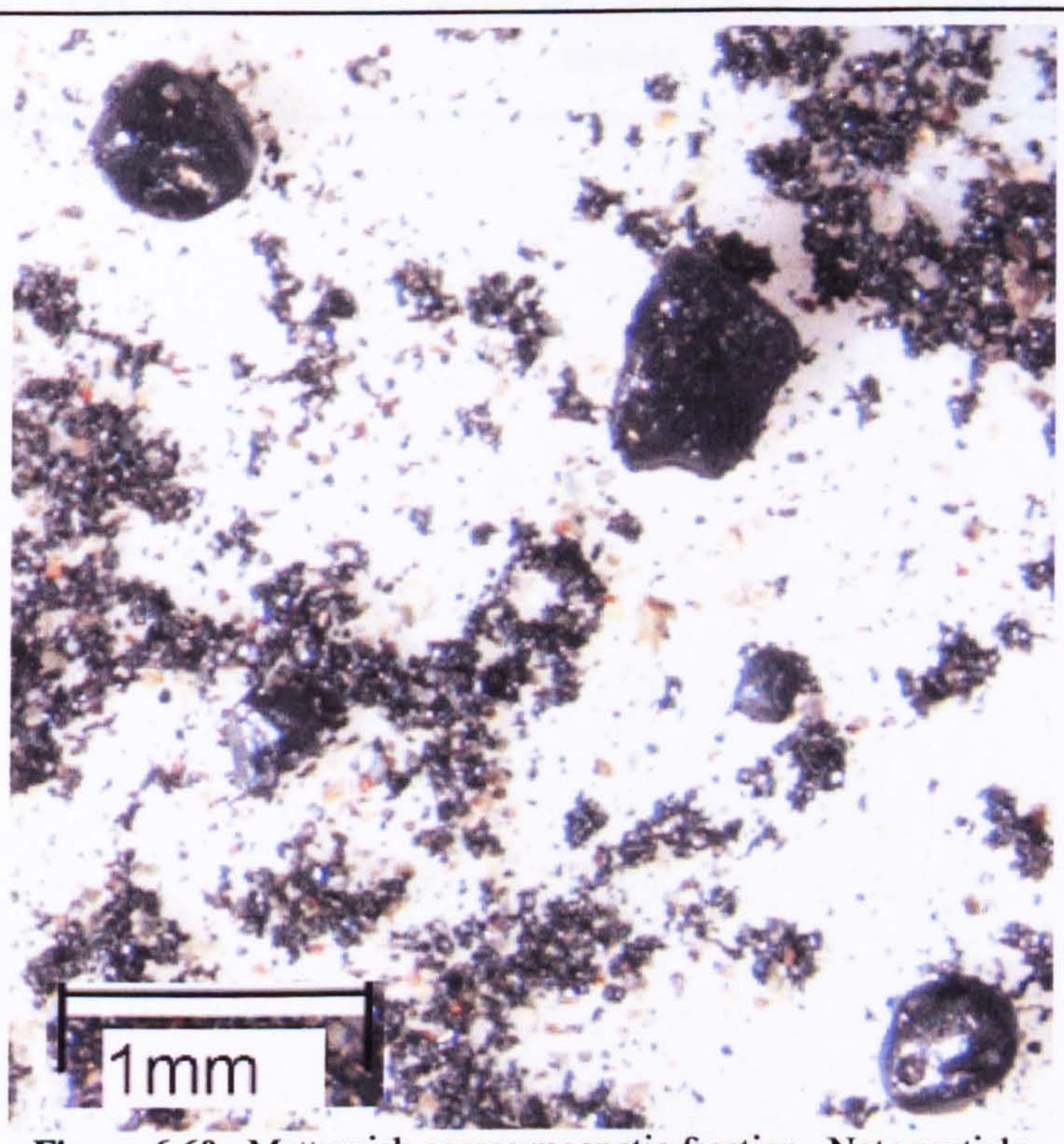

Figure 6.60. Metternich coarse magnetic fraction. Note particle size, roundness and surface polish.

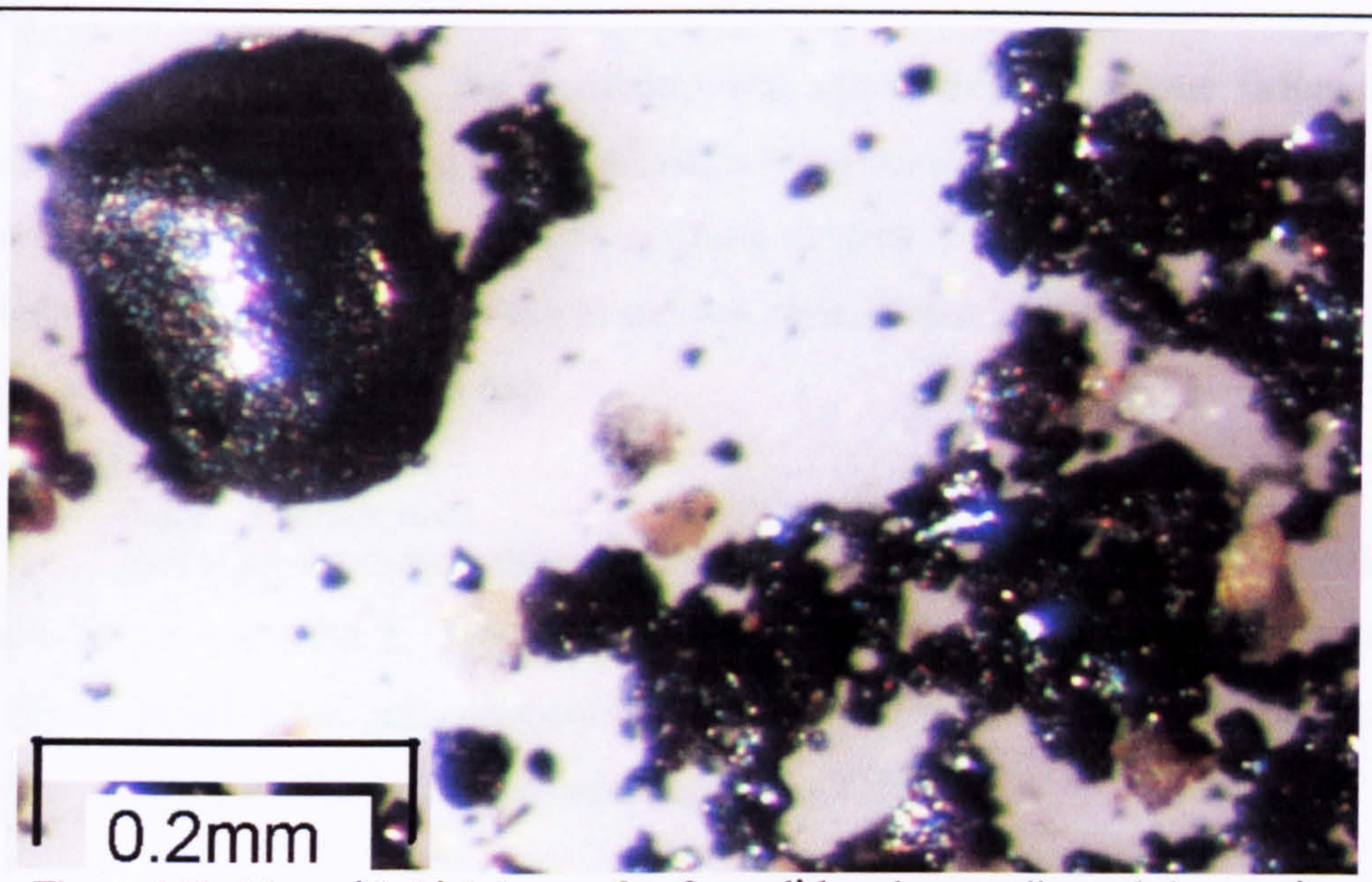

Figure 6.61. Metternich: high degree of surface polish on large, well-rounded magnetite particle.

6.8 Analysis of luminescence chronology

The full luminescence dataset, containing NaI γ-spectrometry (in situ) and Neutron Activation Analysis results, dosimetry, D_e (Gy) and age (ka) data for Harmignies and Metternich is shown in Table 6.6.

In Section 3.4.2, the possibility was raised that anomalous fading by feldspars might have produced age under-estimates in previous studies and so this study used a methodology that eliminated feldspars (see Section 5.8.2). The new age determinations from both sites do not show any systematic divergence from those previous TL and IRSL age estimates (Figs. 6.62, 6.63).

6.8.1 Harmignies.

Ten samples were collected and processed according to the protocols defined in Section 5.8.1 and 5.8.2. These covered the profile in approximately 1 m increments from Unit E (in the lower palaeosol complex) to the top of Unit K, just below the base of the post-glacial soil. The results are summarised in Table 6.1.

Table 6.1. Summary of Harmignies luminescence dating results.

Depth	Unit	Luminescence age (ka)
1.25	K	22.1 ± 1.3
2.28	K	22.2 ± 1.2
3.18	K	22.0 ± 1.5
4.08	I	27.4 ± 1.7
4.73	I	26.2 ± 1.9
5.75	H	44.1 ± 3.9
6.65	H	65.2 ± 4.0
7.67	G	65.5 ± 4.0
		67.0 ± 4.3
8.90	F	68.9 ± 5.0
10.10	E	80.6 ± 4.9

These dates are mutually consistent and (within 1σ error) contain no age reversals. In Frechen *et al.* (2001), Harmignies fine silt (4-11 μm) polymineral samples were analysed using TL and IRSL multiple-aliquot additive and regenerative-dose protocols (see Section 3.4.2). In that study, sample locations were referenced against an idealised profile, not measured depths, and their luminescence age estimates were placed in an 'idealised chronological interpretation'; this makes it difficult to correlate this study's results accurately with those findings. The 'mean luminescence ages' quoted in Frechen *et al.* (2001) are an average of the 2, 3 or 4 results for each sample, regardless of the apparent

anomalies present in some individual results. The results that are assessed to be stratigraphically close to this study's sample locations are listed in Table 6.2). The methodology used to estimate the quoted errors for the mean ages cannot be deduced from the published data; it is not the geometric mean of the errors attached to the individual age estimates.

Table 6.2. Harmignies: TL and IRSL age estimates from Frechen *et al.* (2001).

This study	Unit	IRSL (regen.) (ka)	IRSL (add.) (ka)	TL (regen.) (ka)	TL (add.) (ka)	Mean age (k)
1.25	K	22.0 ± 3.3	-	26.7 ± 2.8	25.5 ± 2.3	(not included, value is 24.7)
		16.9 ± 2.3	-	19.8 ± 2.0	20.4 ± 1.8	19.0 ± 1.5
2.28	K	21.5 ± 3.3	-	25.1 ± 2.5	26.0 ± 2.1	24.2 ± 1.9
3.18	K	19.8 ± 3.0	24.5 ± 2.8	26.6 ± 2.6	26.5 ± 2.3	24.4 ± 2.8
		21.8 ± 3.8	-	27.0 ± 3.3	24.2 ± 2.2	22.2 ± 2.6
4.08,	I	20.3 ± 2.6	-	23.9 ± 2.3	23.7 ± 2.1	(not included, value is 22.6)
4.73		21.7 ± 2.9	-	21.5 ± 2.5	21.2 ± 2.2	21.5 ± 0.5
5.75	H	53.4 ± 8.2	57.1 ± 15.8	55.4 ± 6.3	53.2 ± 5.2	(not included, value is 54.8)
6.65	G	-	68.4 ± 9.9	-	65.1 ± 5.7	66.8 ± 1.7
		56.5 ± 7.3	67.7 ± 7.7	61.2 ± 6.4	59.9 ± 5.8	61.3 ± 4.7
8.9	F	-	96.4 ± 14.0	-	61.7 ± 5.4	79.1 ± 4.1
10.1	E	71.7 ± 10.2	85.2 ± 16.8	80.2 ± 8.2	83.9 ± 7.6	89.3 ± 2.5 (*sic.* correct mean is 80.3)

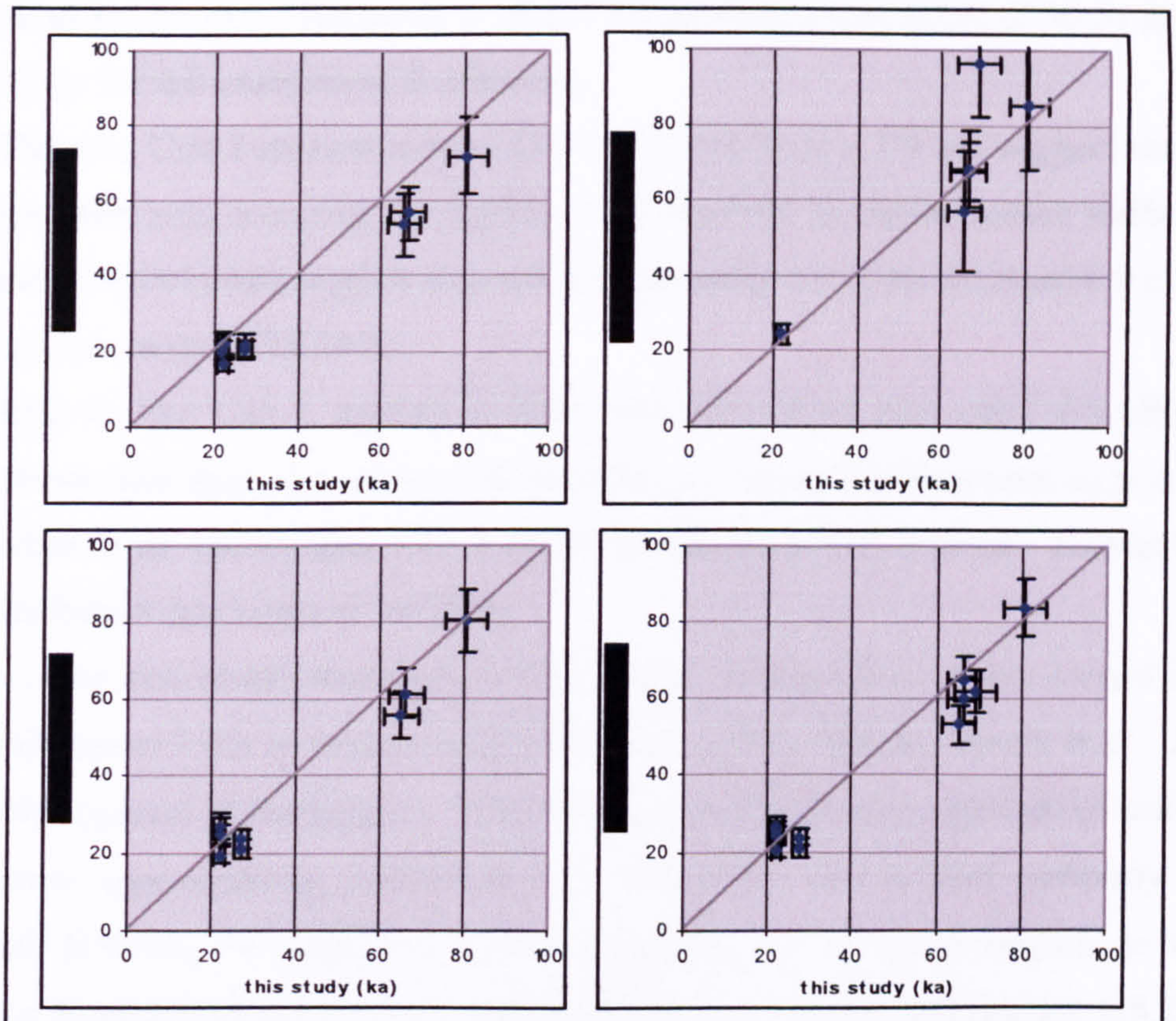

Figure 6.62. Harmignies: comparison of this study's luminescence age estimates with the Frechen *et al.* (2001) results quoted in Table 6.2.

In general, the new results provided by this study correspond with those earlier results. The lowermost sample, dated to 80.6 ± 4.9 ka is from the 'Sol de Malplaquet' in Unit E. Haesaerts *et al.* (1999) identify this palaeosol as having been formed during the 'St Germain II interval', which occurred *c.* 85-75 ka (*ibid.*).

Mid-Unit F is linked by changing grain size distribution patterns (see Section 6.4.3) to the start of primary loess deposition. The luminescence date for this unit indicates that this occurred at 68.9 ± 5.0 ka. This corresponds closely to the date of 67.2 ± 3.4 ka obtained on the Metternich 'loess marker horizon', which is assessed to mark the start of aeolian deposition there and by implication, elsewhere in central Europe (see Section 6.8.2).

There is a significant mismatch between the new results for the lower Unit H sample (65.2 ± 4.0 ka) and the mean value of 54.8 ka for the nearest horizon, listed in (Frechen *et al.*, 2001) (although that value was not included in the final chronological summary). This apparent discrepancy may be attributable to the inaccuracy of the D_e and/or does rate values. However, given the uncertainty in stratigraphic association between the chronological controls, attempts to reconcile differences forced by luminescence dating is futile.

The mid-Unit H sample at 5.75 m, dated to 44.1 ± 3.9 ka, corresponds to the 'Les Vaux' palaeosol horizon. Haesaerts *et al.* (1999) attribute a date range of 50-34 ka but the methodology for this assessment is unknown.

The two Unit I measurements (27.4 ± 1.7 and 26.2 ± 1.9 ka) suggest that at this time, deposition was occurring too rapidly to be resolved by luminescence methods. The Frechen *et al.* (2001) data suggest a age of approximately 21-22 ka; Haesaerts *et al.* (1999) attribute a date range of 26-24 ka.

Unit K, like Unit I, appears to have been formed by very rapid deposition. As shown above, this study has generated mutually-consistent luminescence ages *c.* 22 ka. The Frechen *et al.* (2001) data have a wider spread, from 19 to 24 ka. Haesaerts *et al.* (1999) attribute a date range of 24-23 ka.

These new results may explain why a major stratigraphic marker present in many western European loess sequences (e.g. Gullentops, 1954, Van den Haute *et al.*, 1998) is not overtly apparent at Harmignies. This marker was formed by an episode of solifluction and erosion approximately coincident with the LGM and known variously as the Nagelbeek Horizon, the Nagelbeek-Kesselt complex, the 'niveau à langues de Kesselt' [trans: the Kesselt tongued horizon] and the Eben Discordance (see Section 6.8.2). Van Vliet-Lanoë (1992) identified it as a significant and widespread stratigraphic marker and suggested an age of 23 ka. Van den Haute *et al.* (1998) determined a luminescence age of 21.8 ± 2.6 ka (TL, fine-grain polymineral technique); this corresponds with a radio-carbon date of 22.3 ± 0.4 ka on organic debris (Gullentops, 1981).

Haesaerts *et al.* (1999) locates the Nagelbeek Horizon in the cryoturbated horizon at the top of Unit K and attributes an age *c.* 23 ka, but does not qualify or explain this conclusion. The Frechen *et al.* (2001) paper contains internal contradictions about its age and stratigraphic position. Van Vliet-Lanoë's input to Frechen *et al.* (2001) (based on Haesaerts *et al.*, 1981; van Vliet-Lanoë, 1989, 1992) is that it is represented by a warming episode in Unit J. However, Frechen *et al.* (2001) also suggested that it is present at the top of Unit H and that it occurred *c.* 26 ka. Either of those stratigraphic positions implies that some Harmignies loess was deposited after the peak of the LGM – either Unit K alone, or Units I, J and K together. Part of this problem may be caused by professional disagreements, illustrated by Haesaerts' assertion that some of van Vliet-Lanoë's research has 'far-fetched interpretations' (Haesaerts *et al.*, 1999). The problem of the location of the Nagelbeek Horizon at Harmignies also has an enviromagnetic dimension and is considered further in Section 7.2.4.

6.8.2 Metternich

Ten samples were collected and processed in parallel with the Harmignies samples according to the protocols defined in Section 5.8.1 and 5.8.2. These covered the profile in approximately 1.6 m increments from the loess marker horizon at the base of Unit 3 to the top of Unit 5, just below the base of the post-glacial soil. The results are broadly consistent with the samples' relative stratigraphic positions and are summarised in Table 6.3.

Table 6.3. Summary of Metternich luminescence dating results.

Depth	Unit	Luminescence age (ka)
1.00	5	11.1 ± 1.5
2.60	5	12.2 ± 0.7
4.30	5	14.3 ± 0.7
6.00	5	21.9 ± 1.4
7.70	5	21.1± 1.1
9.80	5	18.2 ± 1.8
12.65	4	27.1 ± 1.4
15.20	4	41.9 ± 2.0
17.85	3	61.1 ± 5.3
18.45	3 (Loess Marker Horizon).	67.2 ± 3.4

The Metternich 'marker loess horizon' is dated here to 67.2 ± 3.4 ka. A similar marker horizon has been identified at Achenheim (in eastern France, south of Metternich) and in eastern Europe (Rousseau *et al.*, 1998), and the Metternich marker is considered to be its equivalent (Boenigk and Frechen, 2001). TL dating (regenerative-dose and additive-dose, fine-grain polymineral) of sediments associated with the Achenheim horizon established a minimum age of 64.9 ± 6.9 ka (Rousseau *et al.*, 1998).

The age of 61.1 ± 5.3 ka for the 17.85 m horizon was obtained on sediment which may have included reworked grains. Since these may have undergone incomplete bleaching during reworking; this age may be an overestimate. The age estimate for the sample taken at 9.8 m depth is statistically consistent with those for 7.7 and 6.0 m at 2σ error.

As with Harmignies, these results can be compared to some of the results quoted in Frechen *et al.* (1995), which used polymineral/TL/IRSL methodologies. Sample locations were identified on three overlapping profiles, each of which was measured separately from different and poorly-defined start points (*ibid.*). This, plus the absence of unambiguous

key horizons in the upper half of the Metternich profile, makes it difficult to correlate these new findings accurately with that earlier information. The results that most closely equate to the sample levels used in this study are shown in Table 6.4. Unlike Frechen *et al.* (2001), Frechen *et al.* (1995) presented the four sets of results without averaging them.

Table 6.4. Metternich: luminescence dating results (from Frechen *et al.*, 1995), using multiple-aliquot additive-dose and regenerative-dose protocols.

This study	Nearest equivalent	TL (regen) (ka)	TL (add) (ka)	IRSL (regen) (ka)	IRSL (add) (ka)
1.00	Met35	16.7± 3.4	12.8 ±4.5	14.5 ±2.5	14.1 ±2.5
2.60	Met33	13.5 ±3.4	14.3 ±4.4	16.3 ±2.1	17.0 ±3.1
4.30	Met30	25.5 ±6.8	22.4 ±5.4	17.7 ±3.0	19.4 ±3.5
6.00	Met25	26.8 ±4.6	23.5 ±4.1	18.0 ±2.0	17.5 ±2.2
„	Met24	28.5 ±5.1	30.2 ±6.0	17.2 ±2.8	20.0 ±4.8
7.70	Met 23	21.3 ±2.9	18.3 ±2.7	16.1 ±1.9	16.8 ±3.3
„	Met22	22.9 ±4.2	20.1 ±3.6	19.1 ±3.1	19.1 ±3.9
9.80	Met21	26.3 ±4.1	23.0 ±2.8	-	17.2 ±1.8
12.65	Met19	29.4 ±4.2	27.9 ±3.0	23.1 ±2.5	23.3 ±5.1
„	Met18	35.3 ±4.5	31.7 ±3.1	29.7 ±3.1	30.4 ±3.5
15.20	Met16	33.0 ±4.1	26.0 ±2.6	27.6 ±3.5	23.6 ±3.6
„	Met 17	31.5 ±4.9	33.6 ±5.1	31.5 ±4.9	33.5 ±5.6
17.85	Met 13	56.5 ±6.9	66.6 ±7.2	75.3 ±8.4	55.0 ±12.4
„	Met12	55.4 ±4.7	59.4 ±4.9	44.6 ±4.2	44.2 ±7.9
18.45	Met11	95.5 ±11.0	85.2 ±7.3	62.6 ±22.8	107.1 ±14.6
„	Met10	40.2 ±3.5	51.9 ±4.3	39.5 ±3.4	46.8 ±13.5
„	Met9	63.2 ±9.0	77.8 ±6.7	-	61.0 ±26.5

sediments is close to those of the underlying soils but levels fall rapidly. A minor organic carbon peak at 17 m correlates with reduced carbonate content, as does the Unit 4 peak *c.* 15.6-15.1 m but the minor peaks that occur above that level are not matched by episodes of carbonate depletion. Thereafter organic carbon values diminish steadily to a minimum near the top of Unit 5, *c.* 12-11 ka. A rapid rise occurs at the base of Unit 6, correlating with indicated wind strength reduction and strong carbonate depletion.

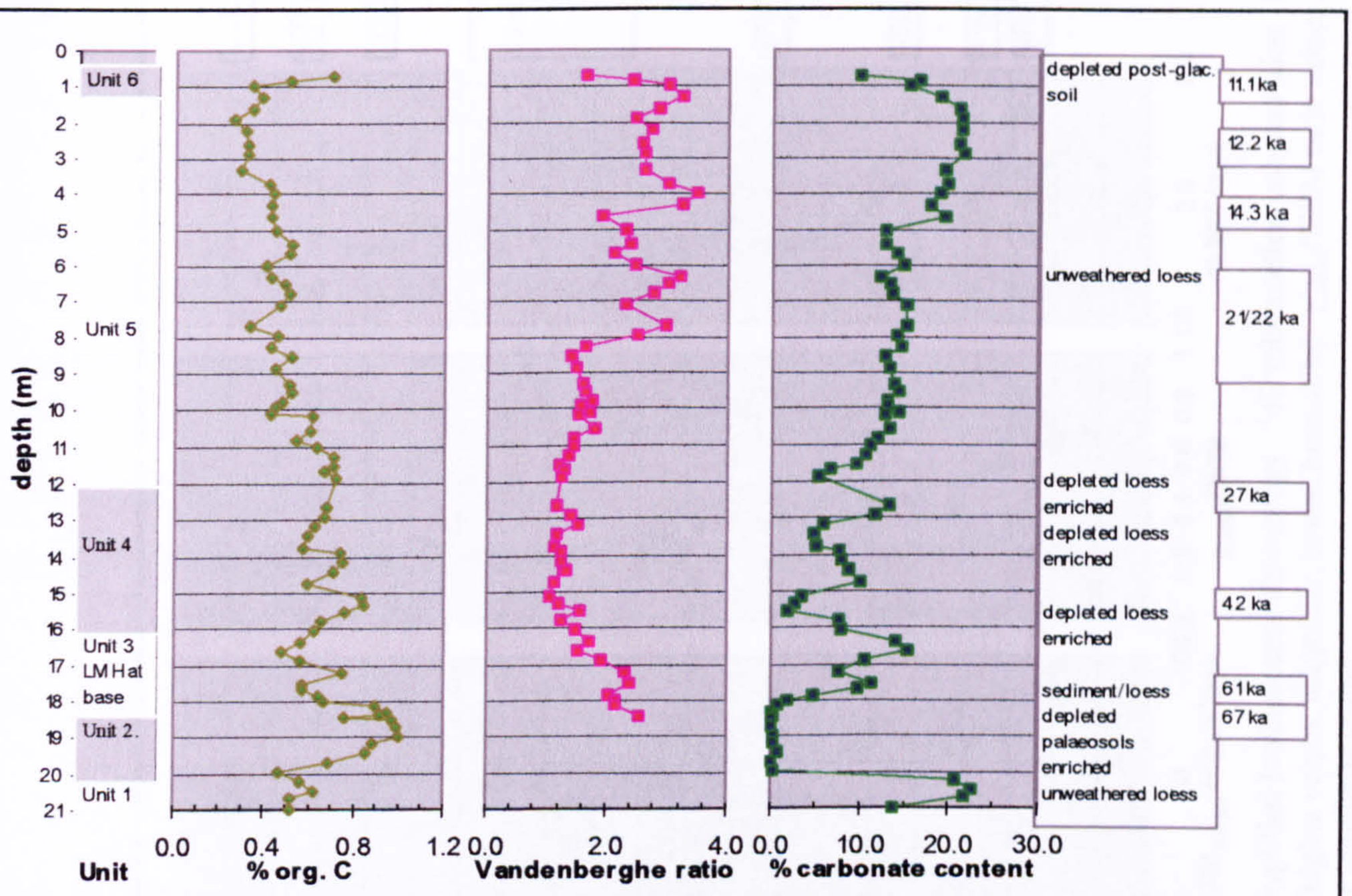

Figure 7.9 Metternich: comparison of organic carbon content with the Vandenberghe grain size index and the carbonate content (gasometric), with a stratigraphic interpretation of the main features and a simplified luminescence chronology.

only by surface flow, eroding pre-existing loess and depositing gravels. This has significant implications for other periods of climatic amelioration that may also have resulted in erosion rather than pedogenesis, especially as loess built up to greater thicknesses, increasing the steepness of the slope down to the Moselle.

6.8.3 Precision of luminescence chronology

The luminescence age determinations produced in this study have levels of precision higher than those achieved in previous studies (Table 6.5). The luminescence ages determined for the start of aeolian deposition at both sites are statistically concordant at 1σ levels, and are concordant with the age determined by Rousseau *et al.* (1998) for this same event at Achenheim. The age determinations for the silicate depletion event *c.* 44 ka are also concordant, as are five of the six ages *c.* 22 ka (all six are concordant at 2σ levels). This luminescence chronology appears to be precise and stratigraphically consistent.

Table 6.5 Comparison of precision of luminescence age determinations as % 1σ error. Harmignies comparison data from Frechen *et al.*, 2001; Metternich comparison data from Frechen *et al.*, 1995.

	This study	IRSL regenerative-dose	IRSL additive-dose	TL regenerative-dose	TL additive-dose
Harmignies	6.2%	14.5 %	16.5 %	10.6	9.1%
Metternich	6.5%	13.4%	19.6%	15.6%	15.4%

Table 6.6 Dose rate, equivalent dose (D_e) and optical ages obtained for samples from Harmignies and Metternich

Site/depth	Laboratory Code	Grain size (μm)	Moisture content	NaI γ-spectrometry (in situ)			Total γ dose rate (Gy.ka^{-1})	Neutron Activation Analysis			Total α dose rate (Gy.ka^{-1})	Total β dose rate (Gy ka^{-1})	Cosmic Dose Rate (Gy.ka^{-1})	Total Dose Rate (Gy.ka^{-1})	D_e (Gy)	Age (ka)
				K (%)	Th (ppm)	U (ppm)		K (%)	Th (ppm)	U						
Harm 1.25	GL03038	5-15	0.17 ± 0.04	-	-	-	0 93 ± 0.07	1.49 ± 0.07	10 90 ± 0 55	2.36 ± 0.12	0 45 ± 0 04	1.44 ± 0.12	0.17 ± 0.02	2.99 ± 0.14	65 9 ± 2.4	22.1 ± 1.3
Harm 2.28	GL03037	5-15	0.13 ± 0 03	-	-	-	1 04 ± 0.06	1 38 ± 0.07	11.70 ± 0.59	2.92 ± 0.15	0 55 ± 0 04	1.54 ± 0.10	0.14 ± 0.01	3.28 ± 0.13	72.7 ± 2.6	22.2 ± 1.2
Harm 3 18	GL03036	5-15	0.14 ± 0.03	-	-	-	0 99 ± 0.06	1 44 ± 0.07	10.30 ± 0.52	2 91 ± 0.15	0.51 ± 0.04	1.52 ± 0.10	0.13 ± 0.01	3.15 ± 0.13	69.3 ± 3.7	22.0 ± 1.5
Harm 4 08	GL03035	5-15	0.17 ± 0 04	-	-	-	0.94 ± 0.07	1.35 ± 0.07	11.00 ± 0.55	2.62 ± 0.13	0.48 ± 0.04	1.39 ± 0.11	0.11 ± 0.01	2.91 ± 0.14	79.9 ± 3 3	27.4 ± 1.7
Harm 4.73	GL03034	5-15	0.18 ± 0.05	-	-	-	0.93 ± 0 07	1.34 ± 0.07	11.00 ± 0.55	2.81 ± 0.14	0.48 ± 0.04	1.37 ± 0.12	0.10 ± 0.01	2.88 ± 0.14	75.4 ± 3.9	26 2 ± 1.9
Harm 5.75	GL03033	5-15	0.17 ± 0.04	-	-	-	0 90 ± 0.07	1.36 ± 0.07	11.10 ± 0.56	2.29 ± 0.11	0.45 ± 0.04	1.35 ± 0.11	0.09 ± 0.01	2.78 ± 0.17	122.8 ± 9.0	44.1 ± 3.9
Harm 6.65	GL03032	5-15	0.16 ± 0.04	-	-	-	0 81 ± 0 06	1.38 ± 0.07	9 55 ± 0.48	1.70 ± 0.09	0.37 ± 0.03	1.28 ± 0.10	0.08 ± 0 01	2 53 ± 0.12	165.1 ± 6.7	65 2 ± 4.0
Harm 7.67	GL03031	5-15	0.16 ± 0.04	-	-	-	0 87 ± 0 06	1.33 ± 0 07	9 91 ± 0.50	2.42 ± 0.12	0 44 ± 0 04	1.34 ± 0.10	0.07 ± 0 01	2 71 ± 0.13	177.6 ± 7.0	65.5 ± 4.0
Harm 8,9	GL03030	5-15	0.20 ± 0.05	-	-	-	0.78 ± 0.07	1.28 ± 0 06	9 68 ± 0.48	2.08 ± 0.10	0.38 ± 0.04	1.19 ± 0.11	0.06 ± 0 01	2 41 ± 0.13	166 2 ± 7.7	68.9 ± 5.0
Harm 10.1	GL03029	5-15	0.17 ± 0 04	-	-	-	0 99 ± 0.07	1.40 ± 0.07	11 50 ± 0 58	2.85 ± 0.14	0 51 ± 0.05	1.46 ± 0.11	0.05 ± 0.00	3 01 ± 0.14	242.6 ± 9.5	80.6 ± 4.9
Mett 1.00	GL03048	5-15	0.10 ± 0 03	1.54 ± 0.03	9.33 ± 0 23	4 03 ± 0.15	1.27 ± 0.02	-	-	-	0.70 ± 0 04	2.02 ± 0.09	0.18 ± 0.02	4.17 ± 0.11	48 1 ± 6.3	11.1 ± 1.5
Mett 2.60	GL03047	5-15	0.02 ± 0 00	1.44 ± 0.03	9.32 ± 0.23	3 98 ± 0.15	1.24 ± 0.02	-	-	-	0.71 ± 0.02	1.96 ± 0 03	0.14 ± 0 01	4 05 ± 0.05	49 5 ± 2.7	12.2 ± 0.7
Mett 4.30	GL03046	5-15	0.02 ± 0 01	1.47 ± 0.03	9 71 ± 0.24	4 30 ± 0.15	1.31 ± 0.02	-	-	-	0.76 ± 0.02	2 04 ± 0.04	0.11 ± 0 01	4.21 ± 0.05	60.3 ± 2.9	14 3 ± 0.7
Mett 6.00	GL03045	5-15	0.11 ± 0.03	1.39 ± 0.03	10.50 ± 0.25	4 20 ± 0.15	1.31 ± 0.02	-	-	-	0.75 ± 0.05	1.96 ± 0.10	0.08 ± 0.01	4.11 ± 0.11	90 2 ± 5.4	21.9 ± 1.4
Mett 7.70	GL03044	5-15	0.13 ± 0.03	1 45 ± 0.03	9.75 ± 0.24	4.28 ± 0.15	1.30 ± 0.02	-	-	-	0.73 ± 0 05	2.00 ± 0.11	0 07 ± 0.01	4.10 ± 0.12	86 6 ± 3 5	21.1 ± 1.1
Mett 9 80	GL03043	5-15	0.14 ± 0.04	1.26 ± 0.03	9 92 ± 0.24	4.31 ± 0.15	1.27 ± 0.02	-	-	-	0.74 ± 0 06	1 86 ± 0.12	0.05 ± 0.00	3.92 ± 0.13	71.3 ± 6 5	18 2 ± 1.8
Met 12 65	GL03042	5-15	0.15 ± 0.04	1.17 ± 0.03	8 65 ± 0.22	3.58 ± 0.14	1.10 ± 0.02	-	-	-	0 62 ± 0.05	1.65 ± 0.11	0.04 ± 0.00	3 41 ± 0.12	92.3 ± 3.2	27.1 ± 1.4
Mett 15.20	GL03041	5-15	0.07 ± 0.02	1.35 ± 0.03	9 86 ± 0.24	3.79 ± 0.15	1.23 ± 0 02	-	-	-	0.70 ± 0.03	1.86 ± 0.06	0.03 ± 0 00	3.82 ± 0.07	160.2 ± 7.0	41 9 ± 2.0
Mett 17.85	GL03040	5-15	0.10 ± 0.03	1.29 ± 0 03	9.20 ± 0.23	3.15 ± 0.14	1.11 ± 0.02	-	-	-	0.60 ± 0.04	1.70 ± 0 08	0.03 ± 0.00	3.44 ± 0.09	209.9 ± 17.3	61.1 ± 5.3
Mett 18.45	GL03039	5-15	0.16 ± 0.04	1.27 ± 0.03	10.36 ± 0.25	3.30 ± 0.14	1.18 ± 0.02	-	-	-	0 64 ± 0 05	1.73 ± 0.12	0.02 ± 0.00	3 57 ± 0.13	239 8 ± 8.5	67.2 ± 3.4

ALL MISSING PAGE BLANK

IN

ORIGINAL

Chapter 7. Interpretation and synthesis of results

This chapter examines the hypotheses set out in Section 1.4:

a) that heterogeneity in geochemical, sedimentological and enviromagnetic parameters in the vertical profile at both sites has been imposed on originally-homogeneous compositions,

b) that patterns of heterogeneity correlate, and,

c) that these correlated patterns represent the sites' response to climate change.

7.1 Evidence for homogeneity

The extent to which loess-palaeosol sequences are homo- or heterogeneous is controlled by the many different processes that have operated on those sequences. Some of these processes were operative before the depositional event, such as the formation (or exposure) of the source sediment at one or more locations and its delivery to the site by one or more transport mechanisms. Some operated during deposition, such as enrichment with locally-derived lithic fragments and surface reworking. Other processes came into operation after the particles had been deposited, including the conversion of the dust deposit into loess by, for example, the formation of inter-grain cementation bonds (Pécsi, 1990; Cilek, 2001, see Section 2.1.2), together with episodes of cryoturbation, erosion, pedogenesis, geochemical weathering and carbonate reprecipitation. In consequence, not even 'primary loess' has the same composition, texture or structure that it had when first deposited. This chapter seeks to understand how those different processes have interacted to create the loess-palaeosol sequences now apparent at the study sites by comparing aspects that resist change with those that respond to change.

Among the major rock-forming elements, Al, Ti and Si are relatively immobile under moderate weathering conditions, as are the REE, and so can reflect the homogeneity or heterogeneity of the original sediment independent of subsequent weathering-induced change. Aspects of the site's sedimentology and mineralogy, including grain size distributions, enviromagnetic characteristics, organic carbon content and carbonate content, can also help to illuminate the degree of original homogeneity.

Heterogeneity can be examined once the degree of original homogeneity has been determined. Stratigraphic variation in concentrations of the mobile elements - the alkali metals and alkaline earth metals – may be caused by changes in provenance or by *in-situ* weathering processes. If the relatively immobile elements (Al, Ti, Si and the REE) indicate that the sediment is generally homogeneous, then stratigraphic variation in the mobile elements can be considered to be a significant indicator of post-depositional,

weathering-induced change. Investigation of geochemical heterogeneity can again be supported by sedimentological and mineralogical characteristics.

7.2 Harmignies and heterogeneity/homogeneity

7.2.1 Geochemistry

The major, minor and REE geochemistry data for Harmignies identify two conflicting trends. The first reflects the geochemical homogeneity of the sediments delivered to the site and is demonstrated by the consistent concentrations of the relatively immobile elements Si, Ti, Al and the REE.

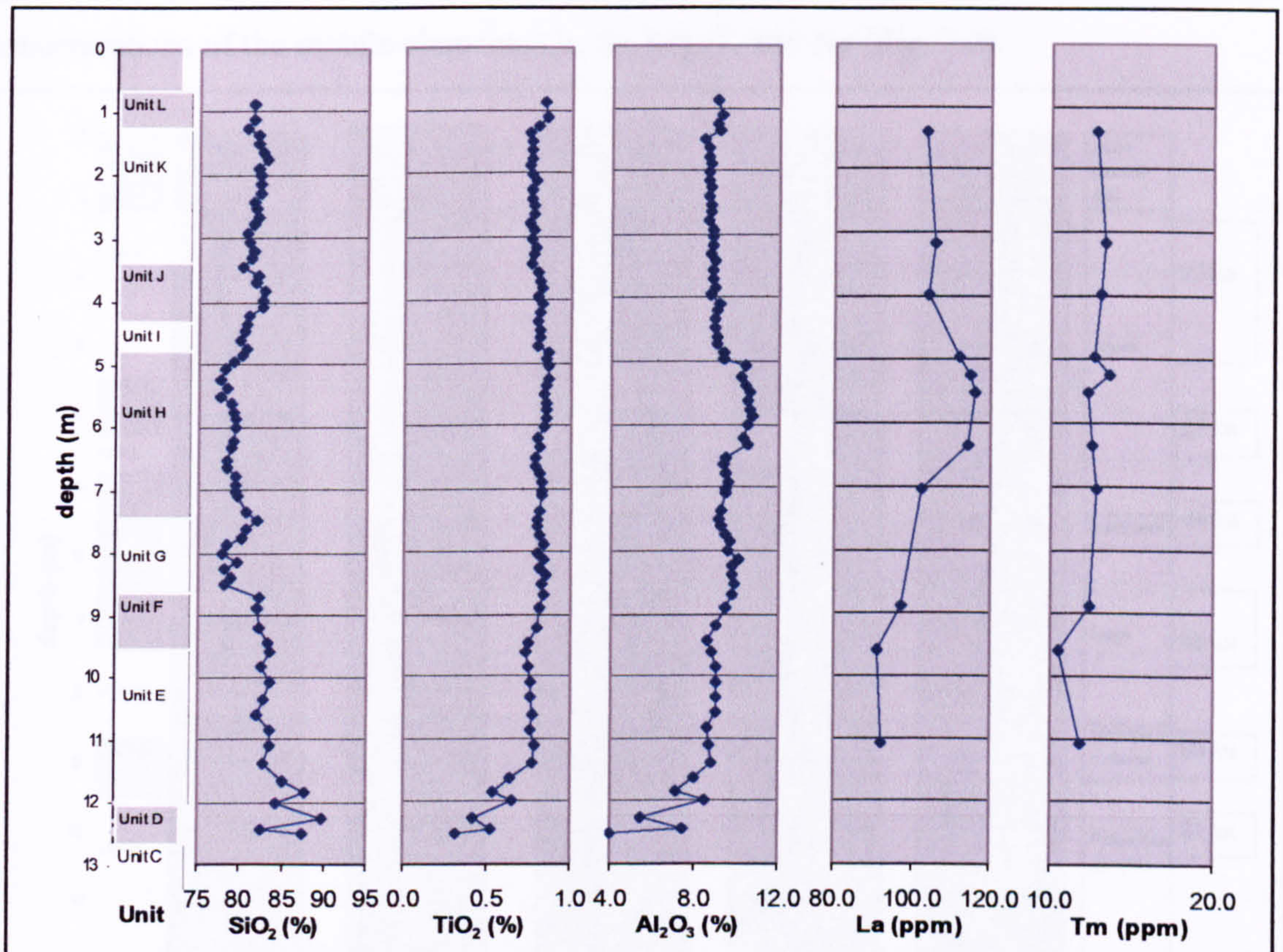

Figure 7.1. Harmignies: concentration values for major oxides SiO_2, TiO_2, Al_2O_3, LREE La and HREE Tm (chondrite-normalised).

The three main stratigraphic divisions at Harmignies (Unit C - Tertiary sand, Units D, E and lower Unit F - palaeosols and transition zone, and upper Unit F to Unit K - loess) are not reflected by the data on immobile elements (Fig. 7.1). These show that only Unit D and lower Unit E have geochemical compositions that differ markedly from the remainder of the profile, with more silica and smaller amounts of the other rock-forming elements. From mid-Unit E to upper Unit K, SiO_2, TiO_2 and Al_2O_3 concentrations are relatively unchanging, except *c*. 6-5 m depth, where Al_2O_3 and La increase and SiO_2 decreases. Grain size indices show that indicated wind strengths were low at this level (Fig. 6.33), possibly reducing the influx of coarse particles. Since many of these are likely to be sand grains,

this would reduce the quartz dilution effect. The REE are present at reduced levels in the Unit E palaeosol and the LREE are slightly enriched in Unit H but are otherwise relatively invariant.

The strong consistency present from mid-Unit F upwards suggests that deflation from the source area (the exposed North Sea bed) did not systematically sample sedimentary units with significantly-different compositions; the deflation area must be formed from well-mixed sediments which, from the REE evidence, are representative of the average upper crust.

The second trend reflects the heterogeneity imposed by pedogenesis and other episodes of post-depositional weathering, now represented by extensive variation in the concentrations of the mobile elements Ca, Sr, Mg, K and Na (Fig. 7.2).

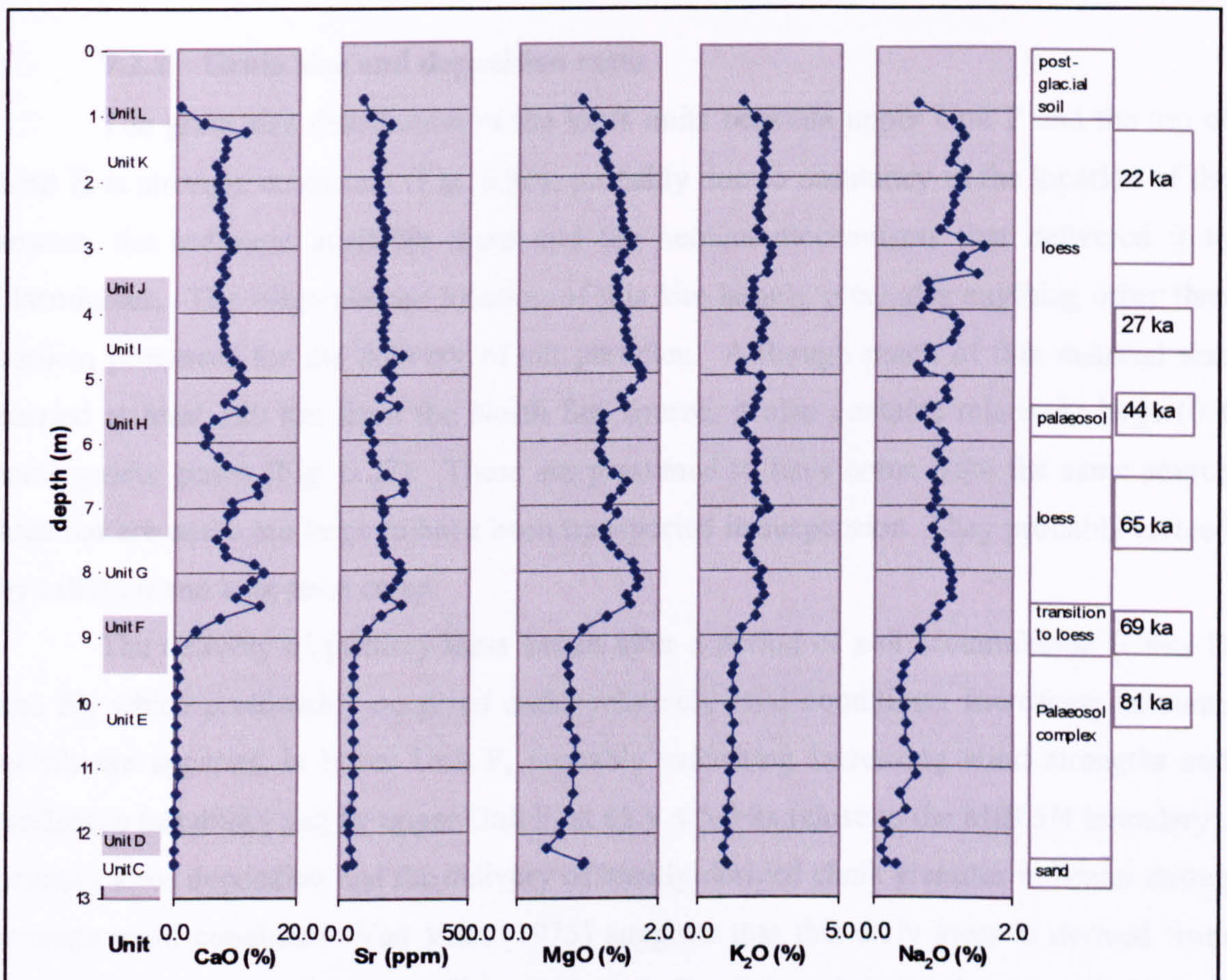

Figure 7.2 Harmignies: weathering-induced variation in the concentrations of Sr, CaO, MgO, K_2O and Na_2O, with stratigraphic interpretation and a simplified luminescence chronology.

These show varying degrees of weathering response, depending on the minerals they are carried in. CaO is presented here as a proxy for the carbonate content, which is dominated by calcite and calcitic limestone. These are easily weathered, especially when converted to silt-sized particles, and Sr follows Ca (c.c. 1.0) as substitute atoms. The remaining carbonate mineral, dolomite, is less readily weathered than calcite/calcitic

limestone and in horizons marked by carbonate depletion, MgO concentrations diminish less than CaO. In horizons marked by carbonate peaks, MgO values rise less than CaO, suggesting that the increase is due to the reprecipitation of Mg-poor calcite and not to a brief increase in the total proportion of carbonate particles. Not all of the main CaO enrichment peaks can convincingly be equated to episodes of depletion from overlying layers which may suggest that some evidence for depletion is missing, possibly by the erosion of palaeosurface layers during late stages of pedogenesis.

K_2O and Na_2O together follow similar trends (c.c. 0.7, 0.8 with CaO, c.c. 0.9 with each other) but do so at much smaller levels of change, suggesting that the minerals they are carried in are more resistant to weathering (probably micas and feldspars, see Section 3.4.1). Their specific response to weathering is examined in Section 7.4.

7.2.2 Grain size and deposition rates

The grain size distribution in the loess units between upper Unit F and the top of Unit K is strongly consistent (Fig. 6.30), probably due to constancy in the location of the source, the sediment available there and the aeolian mechanisms that delivered it to Harmignies. The ridge-plateau location of this site largely precludes anything other than aeolian processes for the delivery of silt particles. Although much of this material was carried at least 120 km from the North Sea source, it also contains relatively large (0.4 mm) quartz grains (Fig. 6.27). These are presumed to have come from the same source area but are much too large to have been transported in suspension. They probably arrived by saltation and long-term creep.

The delivery of primary loess began after a period of soil accumulation (Units D and E), which presumably occurred under relatively mild conditions. Increasing amounts of silt are apparent in lower Unit F, probably indicating increasing wind strengths and landscape instability and by upper Unit F, at 68.9 ± 5.0 ka (close to the MIS 5/4 boundary), primary loess deposition and the delivery of locally-derived chalk granules indicates strong average wind conditions. Van Vliet (1975) suggests that this early loess is derived from local sediment and that 'long-distance loess' deposition did not begin until Unit I. However, in this study's results, there is no apparent geochemical or granulometric difference between loess below and above Unit I. The North Sea source area would have been available even at the very start of loess deposition at Harmignies: according to van Andel and Tzedakis (1996), sea levels had been falling since 75 ka and by 65 ka were *c.* 75 m lower than present level.

The luminescence chronology allows this study to examine the relationship between indicated wind strengths and calculated deposition rates (Fig. 7.3). The

assumption has been made that where loess has been deposited in a period too short to be resolved by successive luminescence ages, that period is 1 ka. Using the Vandenberghe ratio, it is possible to generalise that at Harmignies, low ratio values (below approximately 1.5) correspond with low or very low deposition rates and that high values (above 3) correspond with high deposition rates of 0.5 to >1 m/ka.

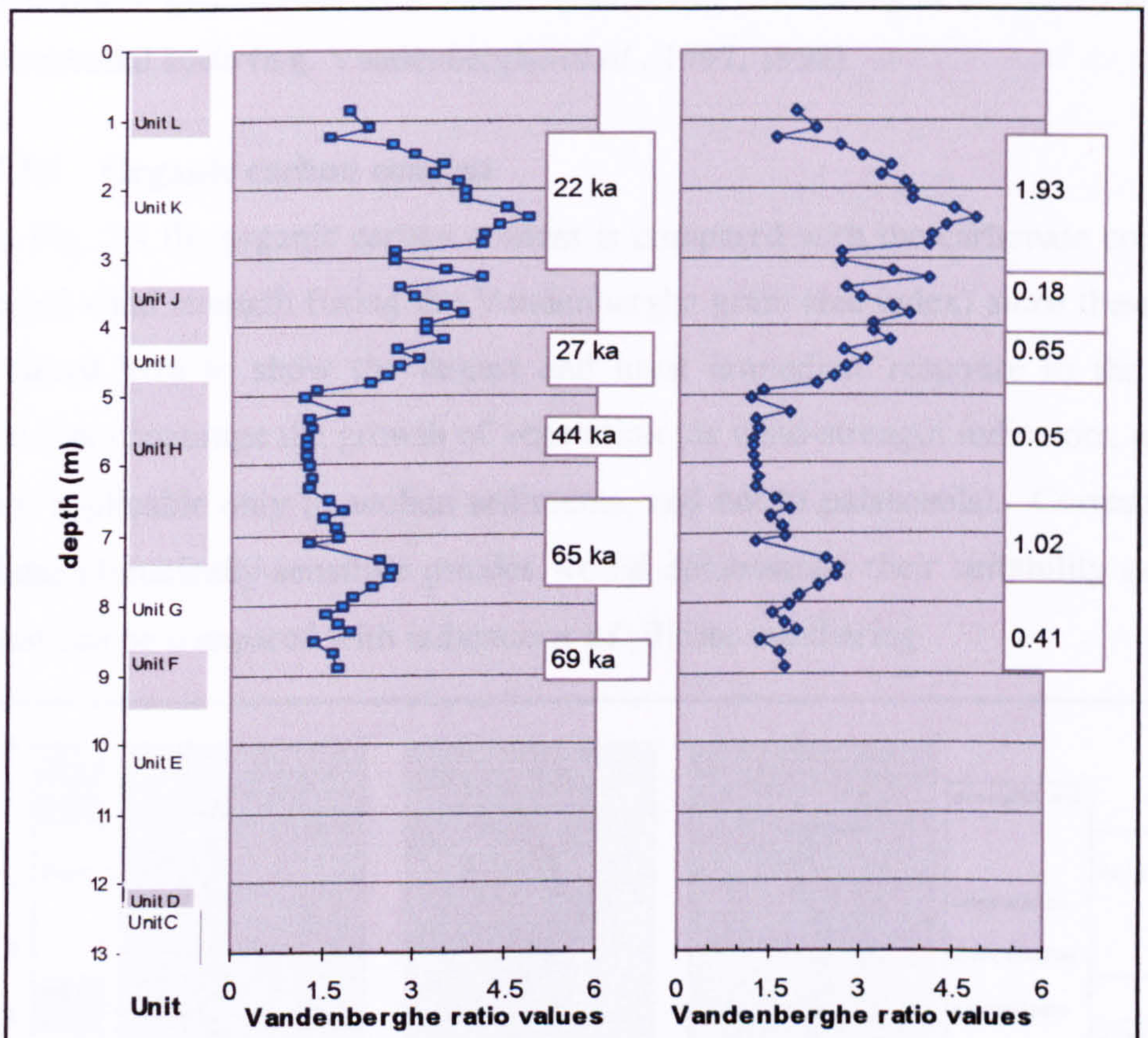

Figure 7.3 Harmignies: relative wind strength variation (using the Vandenberghe grain size index) compared to a simplified luminescence chronology, and loess deposition rates (in m/ka), calculated on thicknesses between luminescence-dated horizons, compared to relative wind strength variation.

Between the start of primary loess deposition *c.* 69 ka (8.9 m depth) and *c.* 65 ka, loess accumulated at *c.* 0.4 m/ka under conditions of increasing wind strength. This reached a maximum at approximately 65 ka (7.5 m depth), with an accumulation rate of *c.* 1 m/ka, and then reduced. Between 65 ka and 27 ka, wind strengths were consistently low and only small amounts of loess were deposited, *c.* 0.05 m/ka. Wind strength began to increase some time prior to 27 ka and continued to rise in a saw-tooth pattern. By approximately 27 ka deposition rates had risen to *c.* 0.65 m/ka, and continued to rise to a maximum of *c.* 1.9 m/ka around 22 ka, matched by an absolute wind strength maximum at 2.4 m depth. In upper Unit K, above that peak but still within the 22 ka date range, indicated wind strengths drop rapidly but at this point the profile enters the base of Unit L (post-glacial soil).

This correspondence between the indicated mean wind strength and the rate of loess accumulation demonstrates the validity of grain size indices as palaeowind proxies and shows that the deposition rate is directly related to the mean wind strength. The general conclusion, that loess is deposited most rapidly during periods of high mean wind strength, accords with the multitude of grain size analyses which have examined variation on the glacial/interglacial scale (e.g. Shackleton *et al.*, 1995, Ding *et al.*, 1996) and on the stadial/interstadial scale (e.g. Vandenberghe *et al.*, 1997, 1998).

7.2.3 Organic carbon content

In Fig. 7.4 the organic carbon content is compared with the carbonate content and the indicated wind strength (using the Vandenberghe grain size index) since these proxies are considered here to show the largest and most immediate response to the climatic conditions that encourage the growth of vegetation (as wind-strength indicators, grain size indices are applicable only to aeolian sediments, and not to palaeosols). Correspondence among these climatically-sensitive proxies would demonstrate their suitability as climate proxies that can be compared with indications of silicate weathering

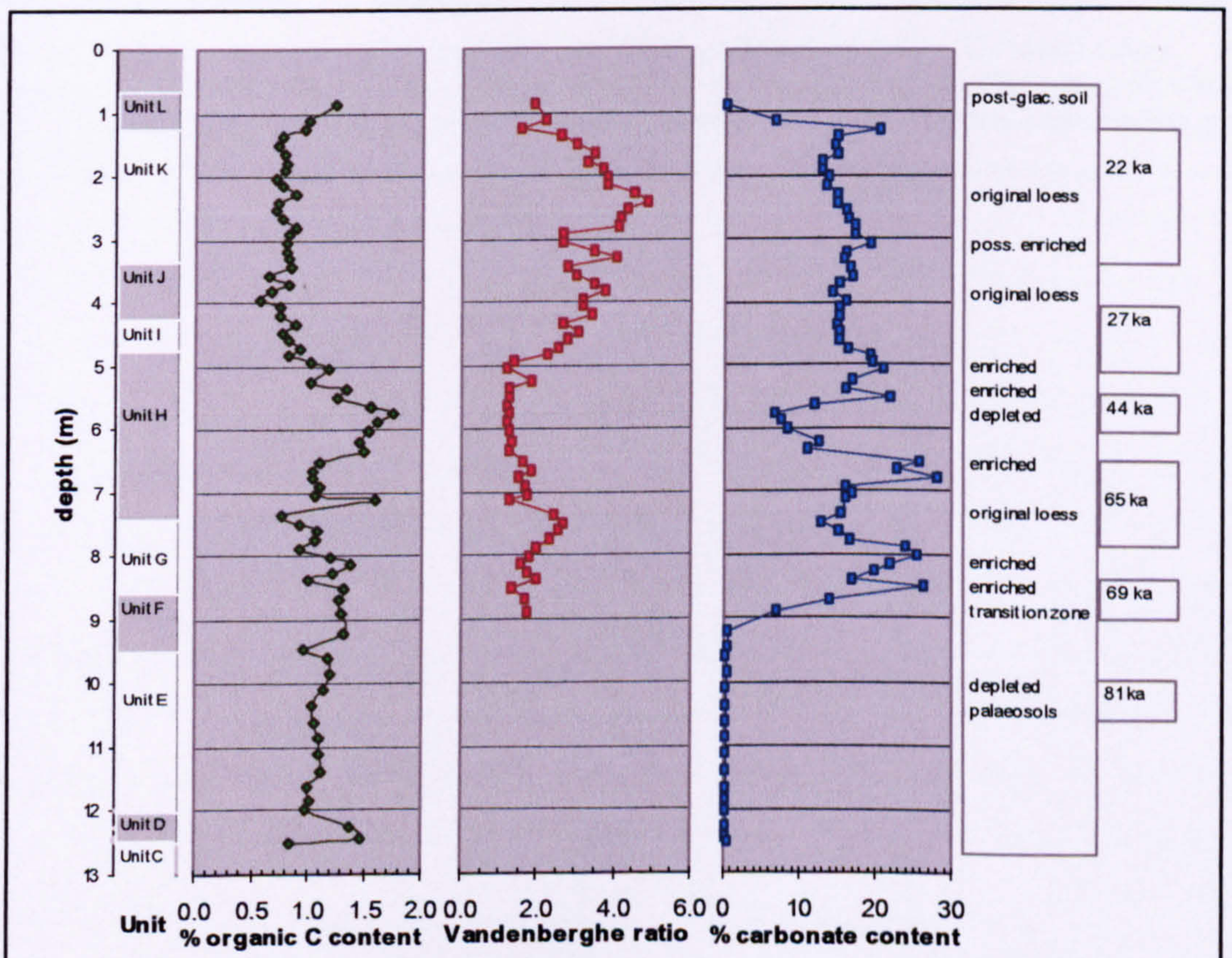

Figure 7.4 Harmignies: comparison of organic carbon content with the Vandenberghe grain size index and the carbonate content (gasometric), with an interpretation of the main carbonate features and a simplified luminescence chronology. (Grain size indexes are only valid in primary loess).

In the Unit D and E palaeosols, high to moderate organic carbon values correlate with low carbonate content (i.e. pedogenic depletion). The transition to loess deposition in

mid-Unit F is not matched by a reduction in the organic carbon content. The peak in Unit G approximately matches an episode of carbonate depletion and low indicated wind strengths but values then diminish in upper Unit G, accompanied by evidence for increased wind strength and no carbonate depletion. The peaks in lower and mid-Unit H both occur in conditions of low indicated wind strengths, the upper peak corresponds with strong carbonate depletion and represents the 'Les Vaux soil'.

In Units I, J and K low organic carbon values correlate with the rapid deposition of unweathered loess under strong wind conditions (Fig. 7.3) during the period 27-22 ka. Organic carbon values rise at the very top of Unit K and continue to rise in Unit L, correlating with a reduction in indicated wind strength and strong carbonate depletion.

7.2.4 Enviromagnetic characteristics

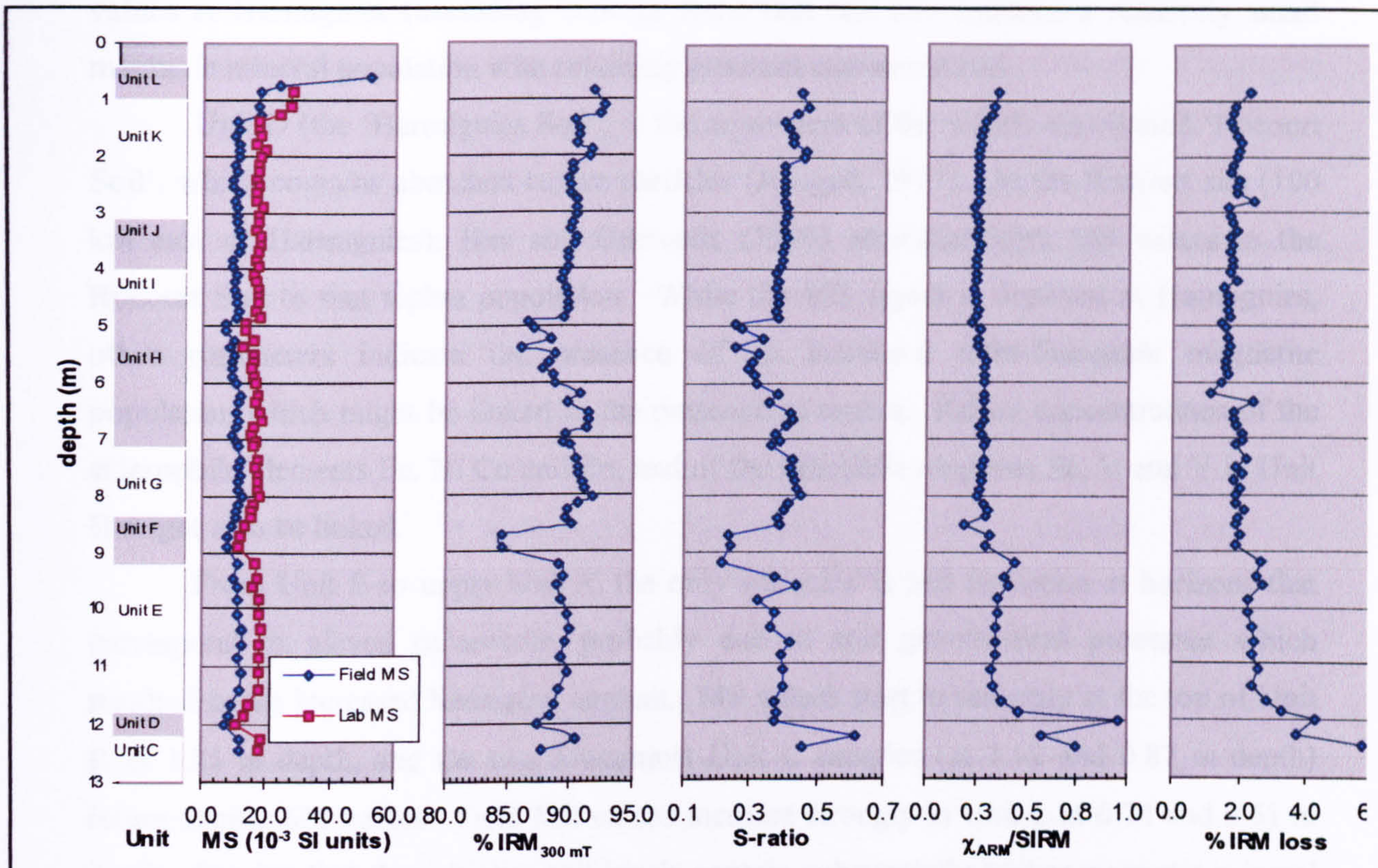

Figure 7.5. Harmignies: composite magnetic profile, with profile interpretation at left. MS values reflect concentration; % IRM acquisition and S-ratio indicate the magnetic mineralogy (higher values: magnetite, lower: haematite). χ_{ARM}/SIRM ratio values and 24-hour % IRM loss indicate the relative abundance of ultra-fine grains.

A composite magnetic profile is shown in Fig. 7.5. The consistently-low MS values at Harmignies (excluding Unit L) show that this site contains a relatively small magnetic mineral population with relatively constant concentrations.

Unit D (the 'Harmignies Soil') is the equivalent of the widely-distributed 'Rocourt Soil', which contains abundant tephra particles (Juvigné, 1977). At the Rocourt site (100 km east of Harmignies), Hus and Geeraerts (1999) attributed high MS values in the Rocourt Soil to that tephra population. While the MS signal is depleted at Harmignies, other parameters indicate the presence of an increased ultra-fine-grain magnetite population which might be linked to the presence of tephra. Raised concentrations of the siderophile elements Fe, Ni Co and Zn, and of the lithophile elements Sc, V and Y in Unit D might also be linked.

From Unit E to upper Unit K the only variation is MS depletion at horizons that correspond to gleyed palaeosols, probably due to soil geochemical processes which resulted in the increased haematite content. MS values start to rise only at the top of Unit K at 1.25 m depth, and the two lowermost Unit L samples (at 1.12 and 0.87 m depth) return similar MS values. Field MS values increase strongly in Unit L at 0.74 and 0.61 m depth, showing that these higher soil levels contain substantially higher magnetic mineral concentrations. It is not possible to examine the other enviromagnetic parameters since no samples were collected this high in the profile.

The most obvious conclusion is that pedogenic ultra-fine magnetite has been illuvated beyond the base of Unit L into Unit K, but this is not supported by the other enviromagnetic parameters. Although mineralogy indicators show an increase in magnetite, granulometry indicators give weak or no evidence for a change in grain size.

An alternative possibility is that this is another tephra horizon, which would be contemporary with loess deposition. Although it is not yet known whether any tephra is present at Harmignies, it has previously been identified at Metternich at a similar stratigraphic level (see Section 7.3.4). There, raised MS values and increased magnetite content at 5 m depth may be attributable to the Eltville tephra. Elsewhere in the Rhine area, this was deposited shortly before the 'Eben Discordance' episode of cryoturbation and erosion, which is approximately coeval with the peak of the LGM (Ikinger and Schirmer, 2002).

At Harmignies, in a pattern similar to that present in Unit D (which may also contain tephra), the siderophile elements Fe, Ni and Co, and the lithophile elements Ti, V, Nb, Y and Sc are all present at slightly raised levels at this possible tephra horizon in upper Unit K and this is maintained in Unit L. The former group may be present as iron or ferromagnesian minerals (Cullers, 1988), the latter as rutile, titanite and other minerals

(Zack *et al.*, 2004). The increased MS values in Unit L mid-soil levels would be attributable to post-glacial pedogenesis.

If the Eltville tephra is indeed present in upper Unit K, then the top of the loess profile is also approximately coeval with the peak of the LGM. This corresponds with the luminescence age determined in this study for the top of Unit K (22.1 ± 1.3 ka) and also with the apparent absence of the 'Nagelbeek Horizon' anywhere stratigraphically lower in the profile (the Nagelbeek Horizon is synonymous with the Eben Discordance). This conclusion accords with the statement by Haesaerts *et al.* (1999) that the Nagelbeek Horizon is present at the top of unit K. An alternative is that it lay stratigraphically higher and has been eroded or reworked as parent material for the post-glacial soil. And if so, then the Harmignies profile, as currently exposed, does not contain post-LGM loess.

The pedogenic MS enhancement in at least the mid-level parts of the post-glacial soil proves that this process can occur in Harmignies loess-derived soils under conditions of climatic amelioration. It is unclear why the Unit D palaeosol fails to return relatively high MS values when it does contain a higher ultra-fine-grain magnetite population. The lack of MS enhancement from Unit D to Unit K may be due to unfavourable conditions such as insufficient warming or excessive wetness.

Taken in its totality, the enviromagnetic evidence suggests that Harmignies is dominated by a relatively small population of magnetically coarse-grain ferrimagnetic particles, except in the lower palaeosol and upper soil horizons. This accords with the microscopy evidence for the presence of silt-sized magnetite particles and with the generally-low $Fe_2O_{3(tot)}$ concentration (3-4%).

This correlation of variation in environmental magnetic characteristics only to major climate change events (i.e. the current and possibly the last interglacial periods), and not to interstadials, suggests that for most of the Weichselian, local conditions did not support MS enhancement or other changes in magnetic mineralogy or grain size (see Section 3.3.5). In consequence, it is not possible to use variation in the Harmignies magnetic profile to identify interstadials.

7.3 Metternich and heterogeneity/homogeneity

7.3.1 Geochemistry

The geochemical data for Metternich identify the same two trends observed at Harmignies – homogeneity in the insoluble elements and heterogeneity in the soluble ones. The major element composition at Metternich varies very little throughout the profile; it shows no major relative changes that correlate with stratigraphic changes. Across the aeolian part of the profile, above 17 m, SiO_2, TiO_2 and Al_2O_3 vary only slightly, with %RSD values of 1.8, 5.1 and 6.8%, similar to those at Harmignies. This lack of variance is illustrated in Fig. 7.6.

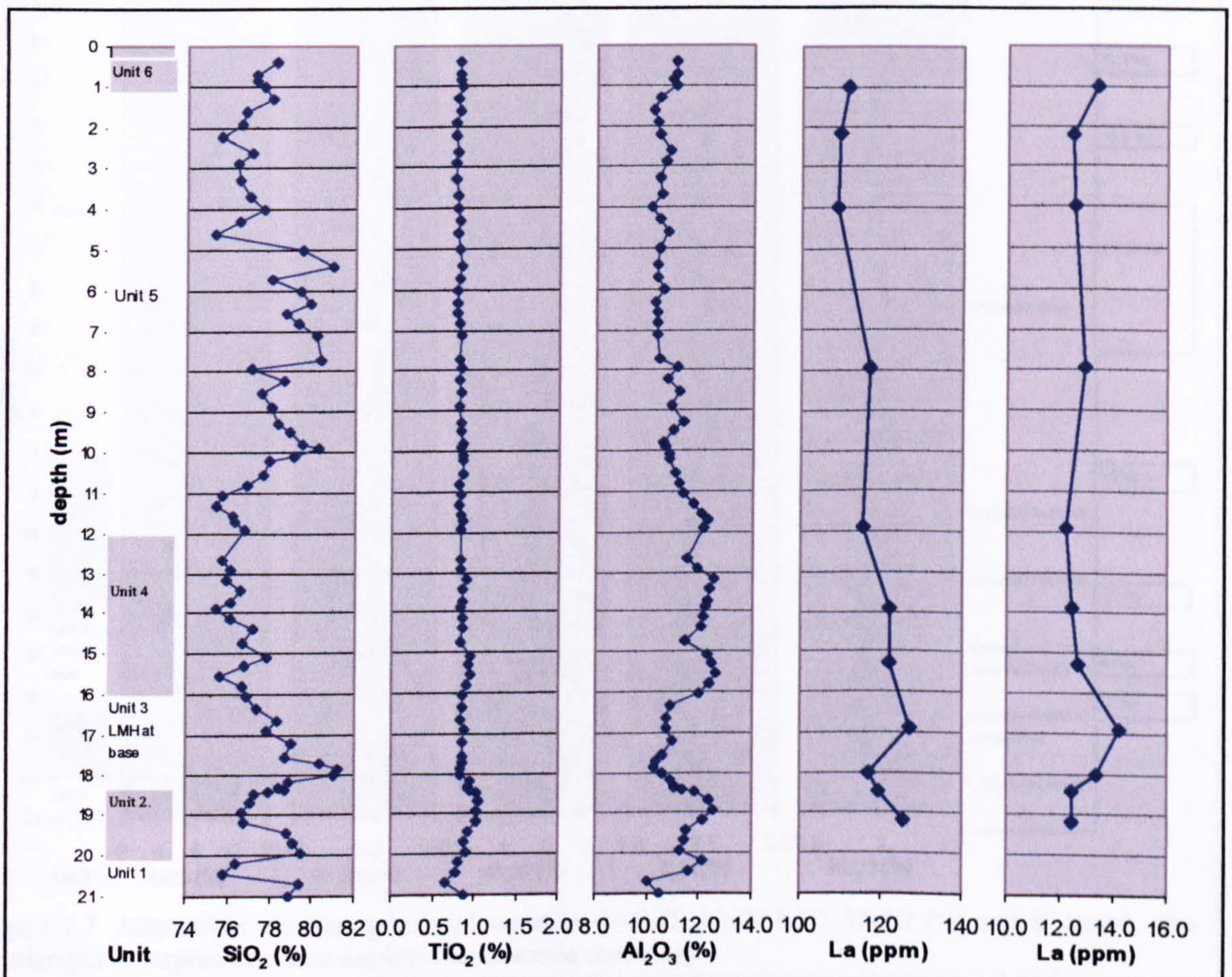

Figure 7.6 Metternich: concentration values for SiO_2, TiO_2, Al_2O_3 and LREE La and HREE Tm (chondrite-normalised).

The minor element population shares this same general trend and most show no systematic variation. The REE are less variable than at Harmignies. There is slight variation in Units 2 and 3 but in Unit 3 above 17 m, and in Units 4 and 5, values change very little (Figs. 7.6, 6.13, 6.14).

The only significant trend that can be identified as affecting the homogeneity of the aeolian particles delivered to Metternich is a change in the carbonate content (and Sr). While the proportions of both CaO and MgO gradually increased, the changing CaO:MgO

ratio (Fig. 6.8) suggests that the supply of Ca-carbonates increased faster than Mg-carbonates (i.e. dolomite). One explanation may be that under conditions of progressively more intense weathering and glacial comminution, calcitic limestone in the Rhine's Alpine catchment area was reduced to silt-sized particles more readily than the dolomite also present there.

The second trend has been imposed by pedogenesis and other episodes of post-depositional weathering, now shown by variation in the concentrations of the mobile elements Ca, Mg, K, Na and Sr (present as Ca substitute atoms) (Fig. 7.7).

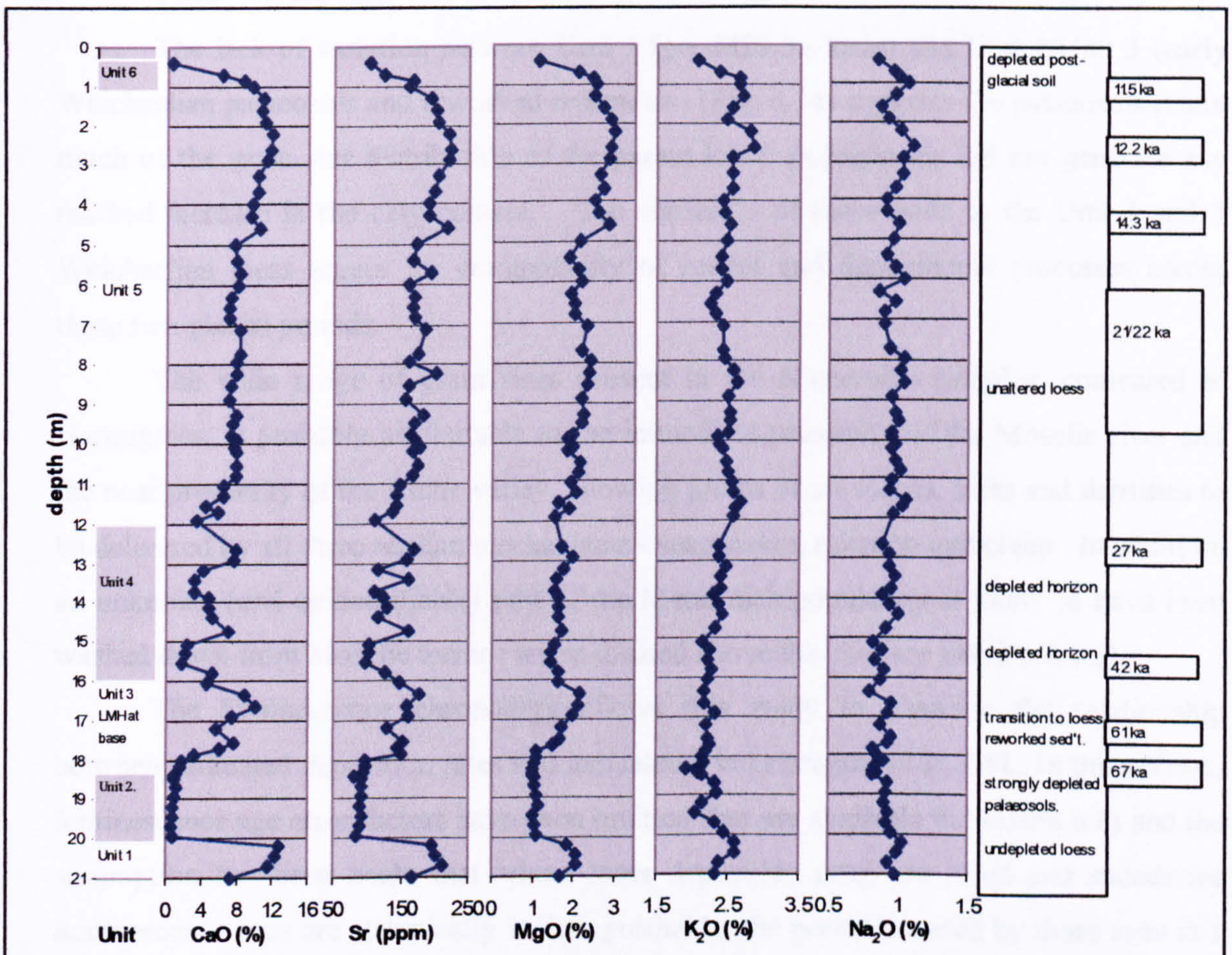

Figure 7.7 Metternich: weathering-induced variation in CaO, MgO, K2O, Na2O (%) and Sr (ppm), plus stratigraphic interpretation and a simplified luminescence chronology.

The rising carbonate content at Metternich (represented in Fig. 7.7 by CaO and MgO) makes it more difficult to interpret trends. The pre-MIS 5a loess of Unit 1 has a carbonate content similar to that of the Weichselian lateglacial loess and is overlain by a decalcified palaeosol. CaO values start to rise in Unit 3 and reach a series of peaks at 17.5, 16.5, 14.8 and 12.7 m. Thereafter, the profile values rise steadily until close to the base of the post-glacial soil, where concentrations of al the mobile elements fall.

The lack of variation in Unit 5 above 11.5 m is surprising since tundra gley soils have been identified in this section of the profile (methodology unknown; Boenigk *et al.* 1994; Boenigk *et al*, 1999; Boenigk and Frechen, 2001). It is possible that minor

carbonate depletion has been masked by later reprecipitation. Further, some palaeosurface layers (and possibly some deeper layers) may have been eroded by surface wash on this sloping site, aided by mass wasting and other agents.

K_2O and Na_2O correlate (c.c. 0.8) and together follow a similar trend to CaO (c.c. 0.7) but do so at smaller levels of change, suggesting that the minerals they are carried in are more resistant to weathering (probably micas and feldspars, see Section 3.4.1). Their specific response to weathering is examined in Section 7.4.

7.3.2 Grain size

The lack of variation between Unit 1 (pre-MIS 5a loess) and Unit 2/Unit 3 (early Weichselian palaeosols and reworked sediments) (Fig. 6.34) suggests the palaeosols retain much of the grain size distribution of the parent loess; pedogenesis did not generate any marked increase in the clay content. The similarity of those units to the Unit 4 and 5 Weichselian loess argues for commonality of source and depositional processes across these two glacial periods.

The wide range of grain sizes present in the Metternich samples, compared to Harmignies, is probably attributable to the immediate proximity of the Moselle river and the near proximity of the Rhine valley, allowing grains of all shapes, sizes and densities to be delivered by all three aeolian mechanisms - suspension, saltation and creep. In addition, an unknown (and unidentifiable) part of the Metternich population is likely to have been washed down from Moselle terrace levels located above the site (see Section 6.4.5).

The luminescence chronology allows this study to examine the relationship between estimated deposition rates and indicated wind strengths (Fig. 7.8). In this section, luminescence age error factors have been omitted (but are available in Section 6.8) and the assumption has been made that where loess deposition rates are rapid and successive luminescence ages are statistically indistinguishable, the period covered by those ages is 1 ka.

The results replicate the Harmignies findings: low and high indicated wind strengths correspond with low and high deposition rates respectively. Peak deposition rates are higher than Harmignies, probably due to Metternich's proximity to its source areas. Between the start of loess deposition at approximately 69 ka (lower Unit 3) and approximately 61 ka (mid-Unit 3), loess accumulated at 0.1 m/ka. The wind-strength peak apparent at Harmignies (Fig. 7.4) at approximately 65 ka is absent from Metternich. In Unit 4 wind strengths and deposition rates remained low. In upper Unit 4 and lower Unit 5, around 27 ka, indicated wind strengths rose, the loess deposition rate increased to approximately 0.5 m/ka and both continued to rise to a maximum deposition rate of 3.8

m/ka *c*. 21/22 ka in mid-Unit 5. This is coincident with the LGM *c*. 22-19 ka (Yokoyama *et al*., 2000). Wind strengths then fell in upper Unit 5 until *c*. 14 ka, accompanied by a reduction in the deposition rate. A brief rise occurred at that time, followed by a fall at approximately 12 ka and another rise around 11 ka, with a very high deposition rate of 1.6 m/ka. Indicated wind strengths then fell again as the profile entered the post-glacial soil (Unit 6).

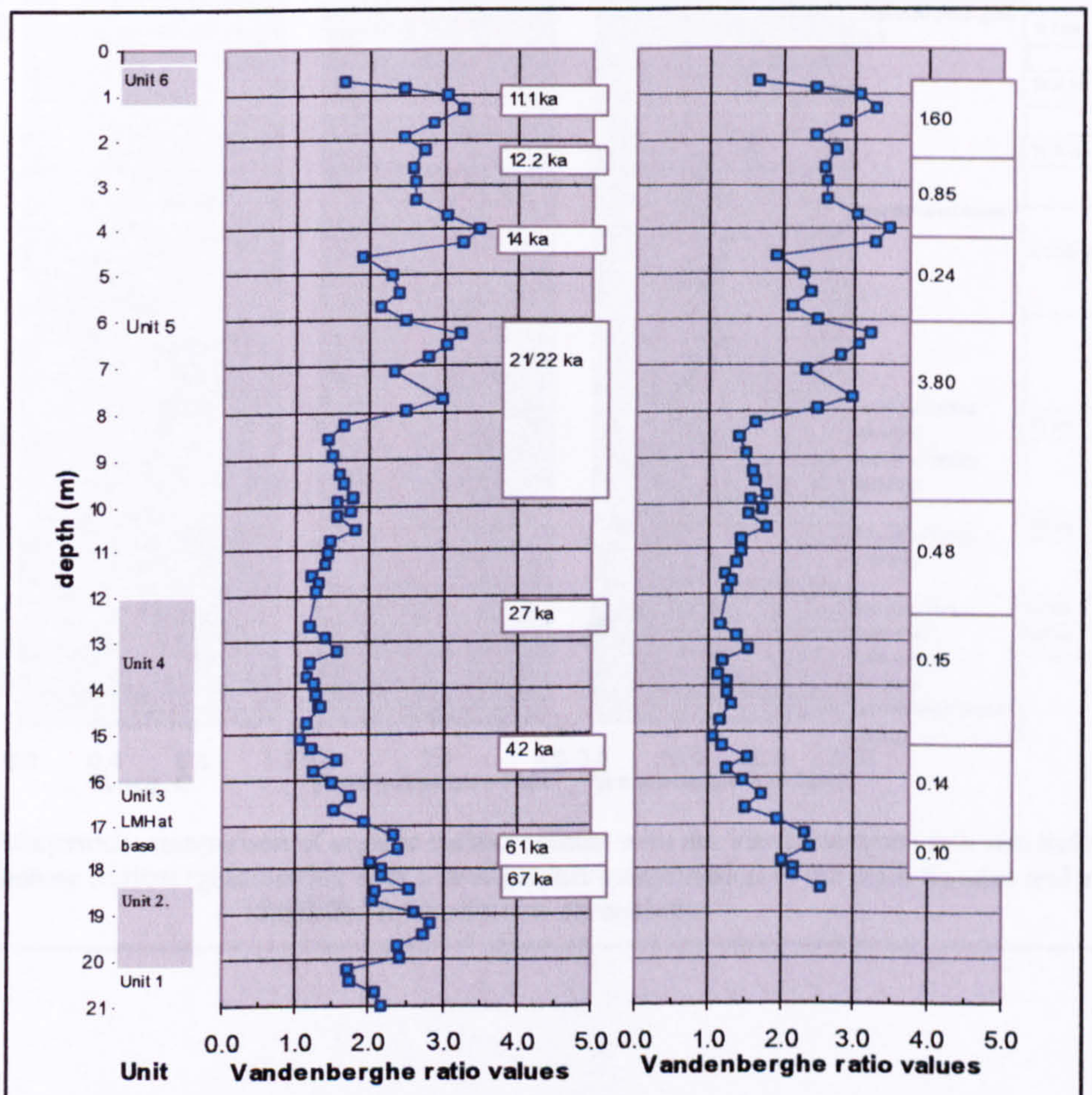

Figure 7.8. Metternich: relative wind strength variation (using the Vandenberghe grain size index) compared to a simplified luminescence chronology, and loess deposition rates (in m/ka), calculated on thicknesses between luminescence-dated horizons, compared to relative wind strength variation.

7.3.3 Organic carbon content

For the same reasons that were explained in Section 7.2.3, the organic carbon content at Metternich is compared with the carbonate content and the indicated wind strength (Fig. 7.9). This reveals a complex pattern of response to climate change. The Unit 1 loess contains low organic carbon levels, matching those of the Unit 4 and 5 Weichselian loess. The Unit 2 palaeosols contain much more, up to 1% and correlate with low carbonate levels. The loess marker horizon at the base of Unit 3 shows a sharp organic carbon reduction, reinforcing enviromagnetic indications that it is not derived locally from those palaeosols (see Section 6.7.8). The organic carbon content of the Unit 3 reworked

sediments is close to those of the underlying soils but levels fall rapidly. A minor organic carbon peak at 17 m correlates with reduced carbonate content, as does the Unit 4 peak *c.* 15.6-15.1 m but the minor peaks that occur above that level are not matched by episodes of carbonate depletion. Thereafter organic carbon values diminish steadily to a minimum near the top of Unit 5, *c.* 12-11 ka. A rapid rise occurs at the base of Unit 6, correlating with indicated wind strength reduction and strong carbonate depletion.

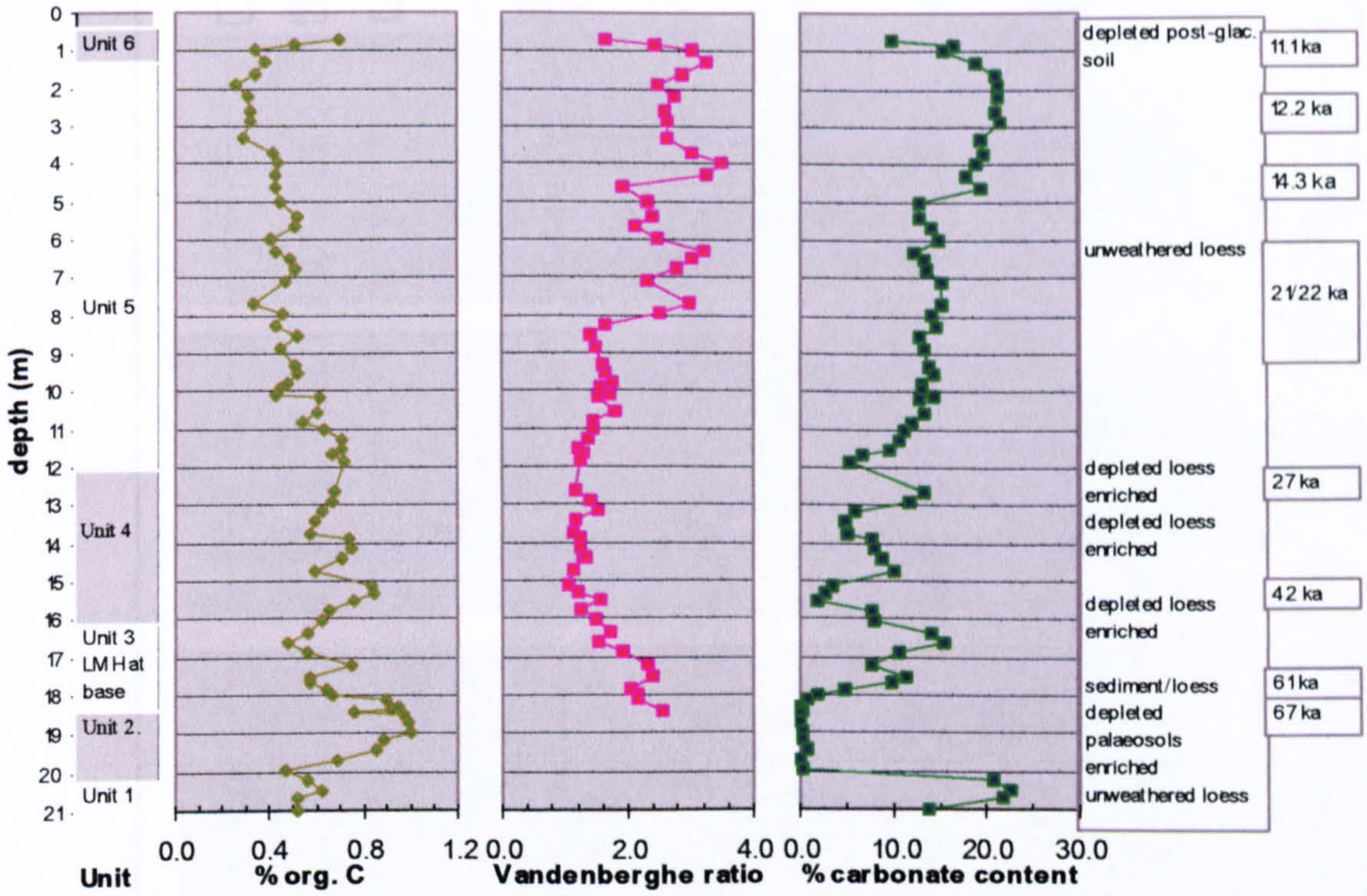

Figure 7.9 Metternich: comparison of organic carbon content with the Vandenberghe grain size index and the carbonate content (gasometric), with a stratigraphic interpretation of the main features and a simplified luminescence chronology.

7.3.4 Enviromagnetic characteristics

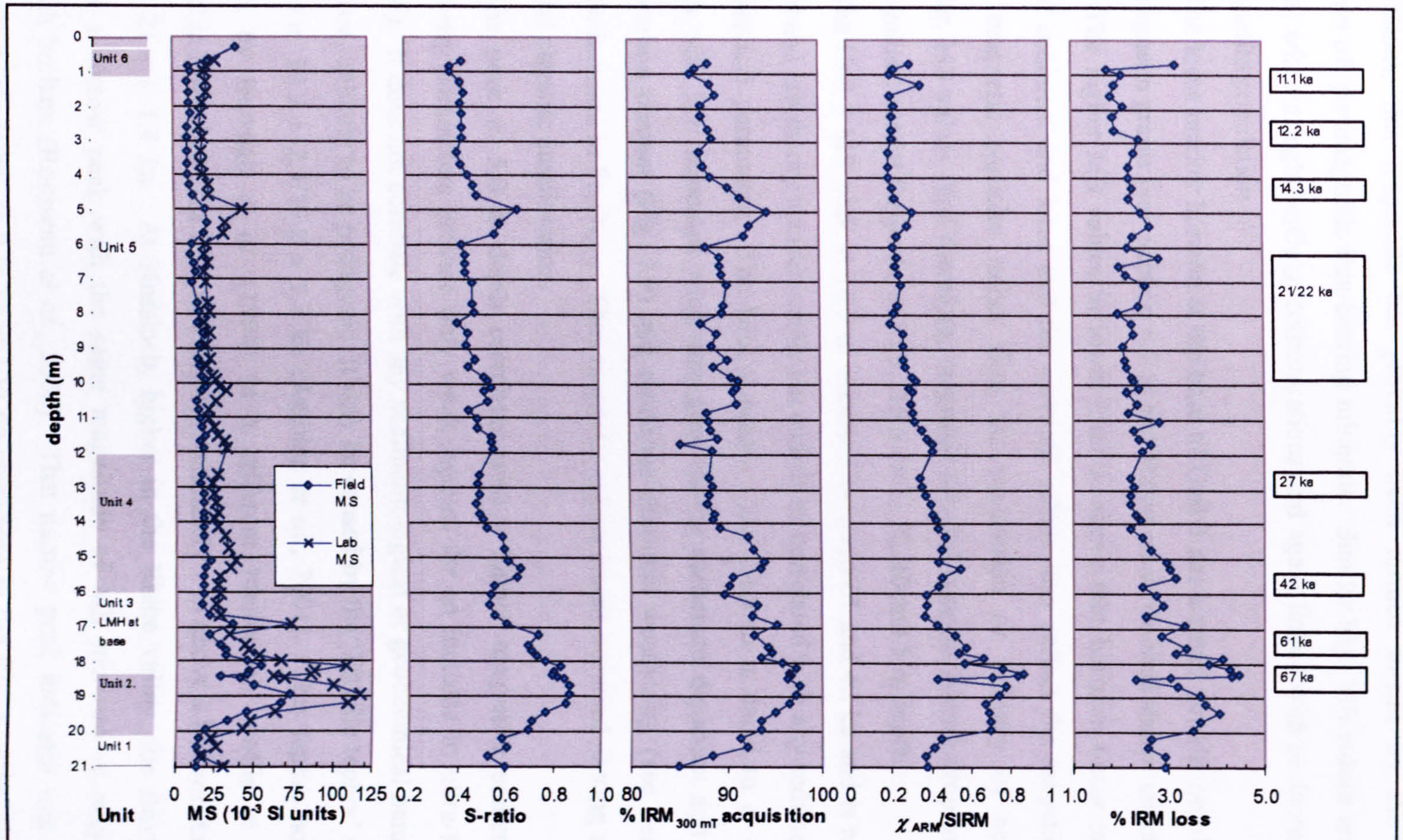

Figure 7.10. Metternich: composite magnetic profile, with a simplified luminescence chronology. MS values reflect concentration. S-ratio and % IRM acquisition indicate the magnetic mineralogy (higher values: magnetite, lower: haematite). χ_{ARM}/SIRM ratio values and 24-hour % IRM loss indicate the relative abundance of ultra-fine magnetite grains.

The MS profile at Metternich (Fig. 7.10) is more variable than Harmignies and reaches very high values in Unit 2. Granulometric and mineralogical enviromagnetic measurements indicate that this part of the profile contains elevated levels of ultra-fine magnetite. Since this part of the profile does not contain markedly increased $Fe_2O_{3(tot)}$ concentrations, this magnetite has probably been formed *in-situ* by the pedogenic conversion of paramagnetic iron-bearing minerals. Similar high MS values are observed in Unit 6, without high $Fe_2O_{3(tot)}$ concentrations and again linked with an increased ultra-fine magnetite population.

The loess marker horizon at the base of Unit 3 has a small population of relatively coarse magnetic grains (see Section 6.7.8) and shows as an isolated sharp reduction in MS values. The higher MS values in lower Unit 3, above that horizon, occur in a mix of reworked sediment and loess and the elevated values may reflect the recycling of pre-existing magnetic particles rather than the production or delivery of new grains. Thereafter, MS values (and therefore, magnetic mineral concentrations) drop to relatively constant values, except for peaks *c.* 16.9, 15.5-14.5, 12, 10 and 5 m depth.

The Unit 3 MS peak at 16.9 m occurred between 61 and 42 ka and is recorded in both field and laboratory measurements but cannot be correlated with any sedimentological or geochemical parameter. The Unit 4 peak *c.* 15.5-14.5 m is dated to *c.* 42 ka and correlates with low indicated wind strengths, strong carbonate depletion and increased organic carbon content (Fig. 7.9) and moderate chemical weathering (see Section 7.4); there is no increase in $Fe_2O_{3(tot)}$. Thus magnetic enhancement occurred during a period of interstadial climatic amelioration.

The peak *c.* 5.0 m depth correlates with a higher magnetite content but the granulometry parameters provide only weak support for an increase in ultra-fine grains (Fig. 7.10). It does not correlate with any sedimentological or geochemical parameter and is, therefore, unlikely to be pedogenic. It may be caused by the 'Eltville tephra' which was deposited *c.* 19.5 ± 2.3/19.2 ± 1.7 ka (Antoine *et al.*, 2001). This tephra horizon was identified by Boenigk *et al.* (1994) in a different Metternich profile at a similar stratigraphic level; here, the MS peak lies approximately 1 m above a horizon dated in this study to 21.9 ± 1.4 ka. At Nussloch, higher in the Rhine valley, the Eltville tephra produced a narrow peak with the same magnitude of MS increase as occurs at this Metternich horizon (Rousseau *et al.*, 2002). That narrow peak indicates that the tephra there forms a thin layer, as it is known to do elsewhere in the Rhine valley (Ikinger and Schirmer, 2002); however, at Metternich the raised MS values occur in a zone rather than a distinct horizon, which may indicate surface reworking.

A weak increase in fine-grain magnetite at 1.6-1.3 m depth correlates with a minor increase in organic carbon content and may represent magnetic enhancement during lateglacial climatic amelioration.

The geochemical and enviromagnetic evidence surrounding the raised MS values in the Unit 2 MIS 5a-5d soil and the Unit 6 post-glacial soil proves that Metternich undergoes MS enhancement during periods of strong climatic amelioration; similar evidence for the Unit 4 peak demonstrates magnetic enhancement during interstadial climatic amelioration. This accords with Terhorst *et al.* (2001), who identified magnetic enhancement in interstadial palaeosols in southern Germany. This study has now identified it in western Germany. In contrast, Hus and Geeraerts (1999) detected no interstadial enhancement in Belgian loess which accords with the Harmignies data.

7.4 Weathering

The results presented in Section 6 and the discussion in Sections 7.2 and 7.3 demonstrate that the aeolian sections of the Harmignies and Metternich profiles each display uniformity in the concentrations of the relatively immobile elements and variability in the concentrations of the relatively mobile alkali metals and alkaline earth metals. These profiles are, therefore, suitable for analysis by chemical weathering indices.

The Chemical Index of Alteration (CIA) (Nesbitt and Young, 1982) has been used to examine weathering in loess worldwide (Gallet *et al.*, 1998) and China (Honda and Shimuza, 1998; Chang *et al.*, 2000; Chen *et al.*, 2001). It is based on the chemical composition of aluminosilicate minerals (mainly biotite and feldspars) which decompose to produce aluminous clays and Ca, Na and K ions in solution (see Sections 3.2.2 and 3.2.3). The CIA formula is:

$$CIA = [Al_2O_3 / (Al_2O_3 + CaO^* + Na_2O + K_2O)] \times 100$$

calculated in molecular proportions (i.e. % concentration/molecular weight), where CaO* is the amount of CaO present in silicate minerals.

That CaO* requirement causes a significant problem in loess that contains carbonates. Although this study used ignited samples, each sample's measured CaO content is an accurate reflection of its original carbonate content, which swamps any Ca silicate fraction. As noted by Gallet *et al.* (1998) there is no simple way to correct that measurement for the carbonate fraction. This study has adopted the proposal by McLennan (1993) that 'approximate corrections can be made by assuming reasonable Ca/Na ratios in silicate material', making CaO* equivalent to Na_2O. Since Ca is more

prone to weathering than Na, this assumption is likely to produce CIA values that are 1-3 units lower than would be the case with the true values (*ibid.*). Values of about 45–55 indicate little or no weathering (the average upper continental crust has a CIA value of approximately 47); values of 100 indicate intense weathering with complete removal of the alkali and alkaline earth elements (Nesbitt and Young, 1989). Taylor and McLennan (1985) identified a CIA value for loess of 55-70.

7.4.1 CIA indications of weathering at Harmignies

The CIA values for Harmignies are compared with the organic carbon content, indicated wind speed and carbonate content in Fig. 7.11, since these are considered to be sensitive proxies, showing the largest and most immediate responses to the climatic conditions that encourage weathering. This will establish the sensitivity of the CIA.

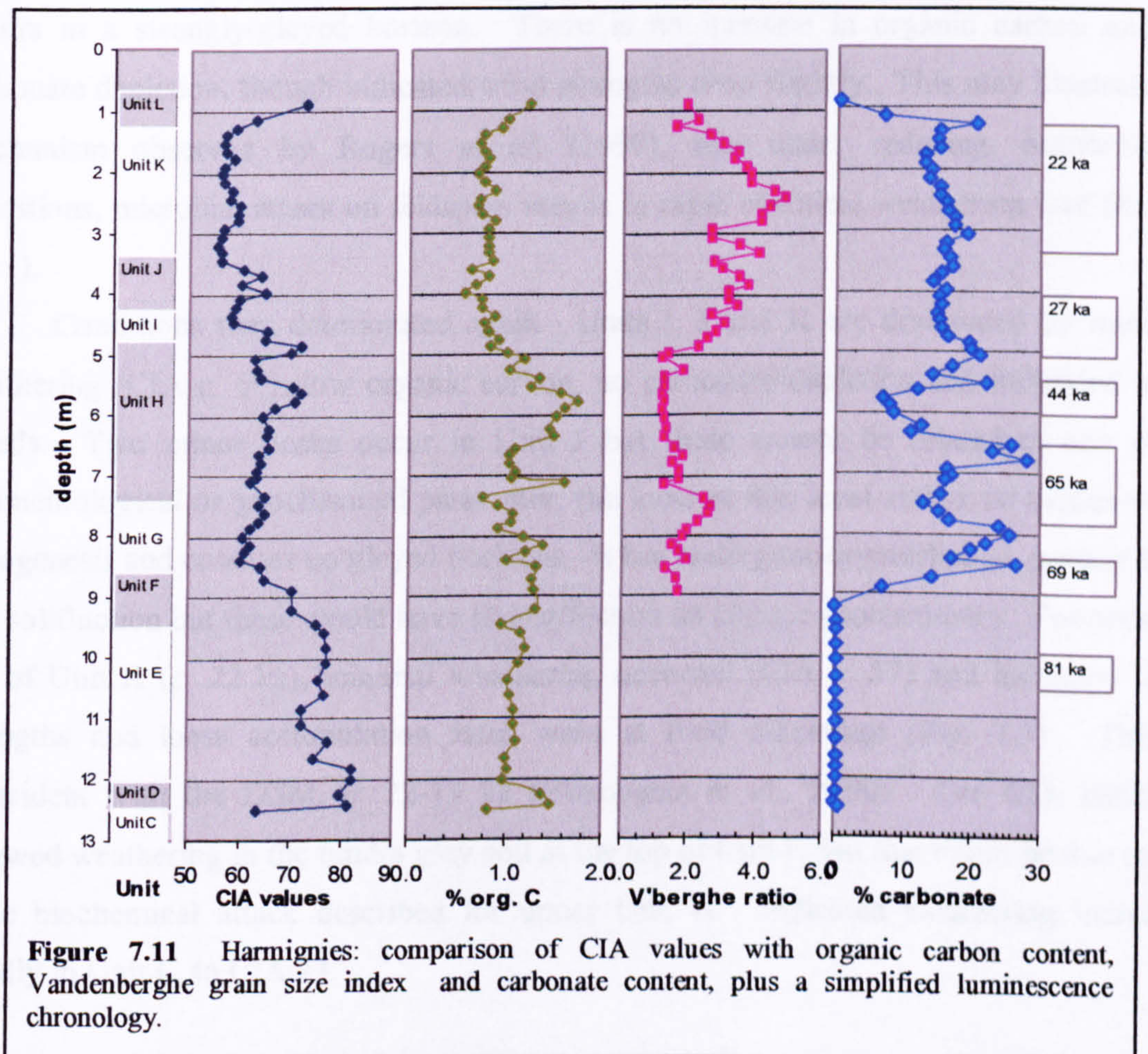

Figure 7.11 Harmignies: comparison of CIA values with organic carbon content, Vandenberghe grain size index and carbonate content, plus a simplified luminescence chronology.

CIA values at Harmignies vary from >80, indicating strong weathering to 56, indicating very little weathering and the set of values for the loess units fits within the 55-70 range identified by Taylor and McLennan (1985). There is a clear relationship between CIA and stratigraphy: Unit D and lower Unit E (Eemian and early Weichselian soils) have CIA values *c.* 80, with major loss of alkali metals and alkaline earth metals. Upper Unit E between 11.65-9.6 m, is less weathered (CIA values *c.* 75), suggesting that these early

Weichselian palaeosols were formed under cooler and less humid conditions than the previous ones. The changing grain size distribution, and the rising carbonate content suggest that the change from soil formation (albeit with some aeolian input) to the deposition of primary loess occurred in mid-Unit F, *c.* 69 ka. However, the CIA profile suggests that minimal weathering conditions were not established until lower Unit G, when CIA values dropped to *c.* 60. Weathering intensity increased slightly in Unit H, corresponding to the period of slow loess accumulation (see Section 7.2.2) and at approximately 6 m depth (*c.* 44 ka) increased significantly (CIA *c.* 70), accompanied by an increase in organic carbon, carbonate depletion and reduced indicated wind strengths (Fig. 7.11). Corresponding soil micro-features were identified by van Vliet (1975) who identified this as the 'Les Vaux' soil. A reduction in CIA values then indicates that decreased weathering occurred to the top of Unit H, where a weathering peak (CIA *c.* 70) occurs in a strongly-gleyed horizon. There is no increase in organic carbon and no carbonate depletion, though indicated wind strengths drop slightly. This may illustrate the mechanism observed by Rogers *et al.* (1998), that under reducing, nutrient-poor conditions, microbial attack on feldspars results in rapid chemical weathering (see Section 3.4.1).

Conditions then deteriorated again. Units I, J and K are dominated by minimal weathering (CIA *c.* 60), low organic carbon, no carbonate depletion and increased wind speeds. Two minor peaks occur in Unit J but these cannot be related to any other sedimentological or geochemical parameter; the loess at this level shows no evidence for pedogenesis and contains no gleyed horizons. It has undergone cryoturbation, surface flow and solifluction but these would have little effect on its silicate geochemistry. Towards the top of Unit K (*c.* 22 ka), minimal weathering occurred (CIA *c.* 57) and indicated wind strengths and loess accumulation rates were at their maximum (Fig. 7.3). This is coincident with the LGM, *c.* 22-19 ka (Yokoyama *et al.*, 2000). The CIA indicates renewed weathering in the tundra gley soil at the top of Unit K but this might be due to the same biochemical attack described for upper Unit H. Indicated weathering increases rapidly in Unit L, to CIA 73.

7.4.2 CIA indications of weathering at Metternich

The CIA values for Metternich are compared with the organic carbon content, indicated wind speed and carbonate content in Fig. 7.12. The general trend is that CIA values are slightly higher than Harmignies and vary less. The higher values are caused by significant differences between the average major element compositions for Metternich and Harmignies: Metternich contains 23% more Al and 29% more K than Harmignies, but

only 9% more Na. This may suggest that the source material here is more enriched in biotite and/or alkali feldspar than in plagioclase feldspar. Biotite is a likely candidate because of the proximity of the Eifel volcanic region which has undergone abundant potassic volcanism (see Section 4.1.2).

CIA values *c.* 64 show that the pre-MIS 5a loess in Unit 1 has undergone little weathering, similar to that undergone by the Unit 5 Weichselian loess. The early Weichselian palaeosols of Unit 2 undergone only slightly more (CIA *c.* 68) and weathering values diminish in lower Unit 3, as reworked (and weathered) sediments become increasingly loessic. Weathering minima occur in mid-Unit 3, *c.* 61 ka, which corresponds

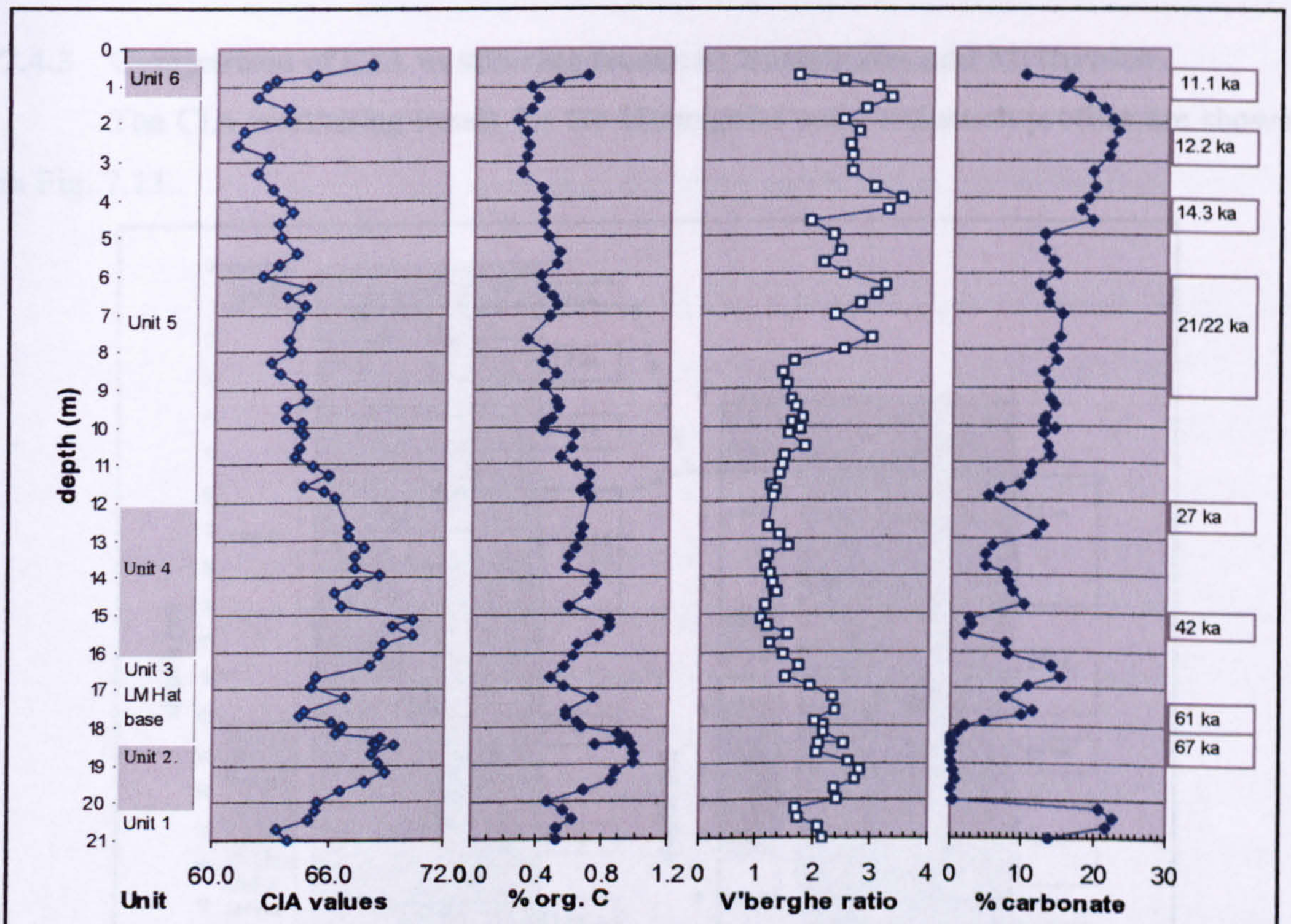

Figure 7.12 Metternich: comparison of CIA values with organic carbon content (%), Vandenberghe grain size index and carbonate content (%), plus a simplified luminescence chronology.

with Harmignies. Indicated weathering then rises to a maximum in Unit 4 *c.* 15.2 m, coincident with increased organic carbon content, low indicated wind strengths and strong carbonate depletion, and MS enhancement (Fig. 7.10). This represents weathering during a period of climatic amelioration at approximately 42 ka and again matches Harmignies. The brief peak in mid-Unit 4 at 13.9 m correlates with an organic carbon peak but no carbonate depletion is apparent. Thereafter CIA values drop steadily to a minimum of 61 in Unit 5 at 2.6 m, c. 12.2 ka.

A weathering peak is apparent in upper Unit 5 between 1.9-1.6 m (*c.* 12.2-11.1 ka), during a period of reduced wind strength (Fig. 7.15). It is not matched by carbonate depletion. However, the MgO:CaO ratio (see Section 6.1.2.1) provides some evidence that

the 1.6 m sample level has undergone calcite reprecipitation and good evidence that the 1.3 m sample level has been enriched, followed by depletion at 1.0 m in the Unit 6 post-glacial soil. This may be interpreted as carbonate mobility and calcite reprecipitation caused by post-glacial pedogenesis. A similar feature is present at Harmignies; there it resulted in raised carbonate levels. Here, it may have returned carbonate-depleted sediments to their previous values, thereby masking supporting evidence for the silicate weathering episode.

Unit 6 shows a pronounced increase in weathering intensity, to CIA values *c.* 68 (similar to Unit 2), accompanied by decreasing wind strengths, increased organic carbon and a rapid decrease in carbonate content.

7.4.3 Comparison of CIA weathering trends at Harmignies and Metternich

The CIA weathering trends for the Harmignies and Metternich profiles are shown in Fig. 7.13.

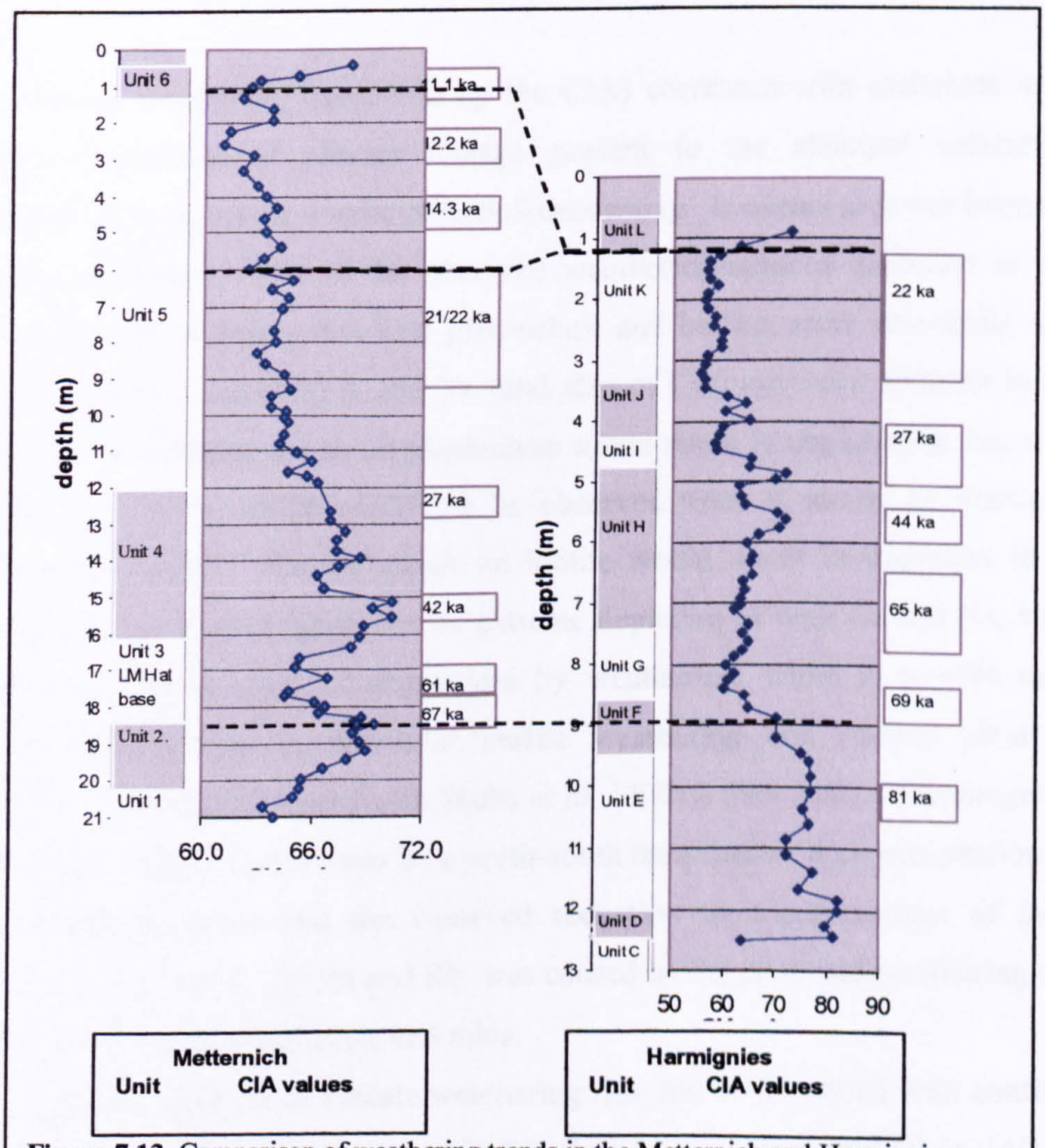

Figure 7.13 Comparison of weathering trends in the Metternich and Harmignies profiles, using luminescence chronologies and soil horizons as tie points.

The two sites had different accumulation rates at different times and the new luminescence chronology (a) provides age estimates for a coarse sampling strategy and (b)

does not resolve periods of rapid change. This makes detailed inter-site correlation unreliable. However, within the time period covered by both profiles (early Weichselian to LGM), the same general trends can be observed – moderate silicate weathering in the pre-69 ka palaeosols, reduced weathering after the start of aeolian deposition in Unit3/Unit F, increased weathering *c.* 42-44 ka and then steadily-diminished weathering to *c.* 22 ka.

7.5 Conclusions

Both sites have undergone post-depositional geochemical weathering which has induced heterogeneity in sediment that was initially near-homogenous. The dominant form of weathering at both study sites is carbonate dissolution, affecting the alkaline earth metals Ca and Mg. Calcitic limestone and reprecipitated calcite are easily weathered and both profiles show repeated episodes of carbonate depletion and calcite reprecipitation. Dolomite is less readily weathered, and the MgO profile is much flatter than the CaO profile.

Silicate weathering (measured by the CIA) correlates with carbonate weathering and with indications of climate change present in the standard sedimentological parameters. It is, therefore, a valid palaeoclimate proxy. It occurs at lower intensities than carbonate weathering; most of the observed weathering-induced depletion in the alkali metals K and Na probably involved plagioclase and biotite, since muscovite and alkali feldspar (the other carriers of K and Na (and also of Ca)) are more resistant to moderate weathering. Weathering attack on plagioclase would result in depletion in Na, which was observed, and in Ca, which could not be observed since it would be masked by the carbonate Ca content. Similar attack on biotite would result in depletion in K. The Eemian palaeosol at Harmignies shows extreme depletion of both Ca and Na, which may indicate near-total removal of plagioclase by weathering, while K is only moderately depleted, possibly due to near-total biotite weathering and limited alkali feldspar weathering. This would accord with Muhs *et al.* (2001), who analysed homogenous low-carbonate Mississippi valley loess in a north-south temperature and precipitation gradient. Their conclusions were that the observed reduction in concentrations of the mobile elements Ca, Mg, Na, K, Sr, Ba and Rb was caused by the chemical weathering of calcite, dolomite, hornblende, plagioclase and mica.

The only episodes of silicate weathering that can be identified with confidence are linked to well-developed Eemian or early Weichselian palaeosols, the GI 16/14/12/8 group of strong interstadials (Fig. 1.4) and the modern post-glacial soil. Weaker soils have been identified at both sites by previous researchers through features such as soil

micromorphology (e.g. van Vliet, 1975), but they have not undergone identifiable silicate weathering.

There are two possibilities, therefore, to explain the limited degree of silicate weathering described above. One is that interstadials other than the GI 16/14/12/8 group were simply too cold and too brief to support silicate weathering. The alternative possibility is based in loess geochemistry. In carbonate-rich sediments, meteoric water present at the surface will dissolve a small fraction of the carbonate with the result that the weathering solutes are alkaline, with high values of Ca^{2+}/H^{+}. Nesbitt and Young (1984) calculate that under these conditions, feldspar and mica are stable and will not undergo chemical weathering. If this process is in operation in loess, then those minerals will not begin to weather until a major reduction in the carbonate content allows neutral or acidic water to percolate through the sediment. However, Williams *et al.* (2003) found that under modern field conditions, the presence of carbonate minerals in experimental soils did not inhibit feldspar dissolution. This suggests that the first possibility is more likely, and thus silicate weathering occurs under conditions of significant and prolonged climatic amelioration.

Chapter 8. Comparison with global climate records, discussion and conclusions.

'knowing more and more about loess and loess' (pers comm.. F.M. Chambers, 2005)

This chapter examines the suitability of the study sites and addresses the hypotheses set out in Section 1.4:

d) that the responses to climate change observed at the two study sites can be correlated with the known patterns and chronology of Weichselian climate change in the western Europe/North Atlantic region, and,
e) that geochemical variation in loess-palaeosol sequences can be used as a chemostratigraphic tool in northwest Europe.

8.1 The utility of the sites selected for this study

Before drawing final conclusions about the observed climatic responses at the study sites, described in Sections 6 and 7, it is necessary to re-examine those sites. Both have been studied by previous workers and at the start of this study were considered to present near-continuous coverage of the period between the Eemian/early Weichselian and at least the lateglacial period, within the limitations discussed in Section 3.5 (e.g. the loess record is episodic and prone to erosion and reworking).

Concern was also expressed in Section 3.5 that luminescence ages developed for palaeosol horizons could only provide a chronology of deposition, not of pedogenic modification. Comparison of the new luminescence chronology with the climatic proxies analysed here proves that within that method's accuracy limits, that difference is not significant.

The evidence produced in this study highlights other limitations at both sites. The luminescence chronology, plus data on indicated wind strengths and deposition rates (see Section 7.2.2 and 7.3.2) strongly emphasise the episodic nature of deposition at both sites: at Harmignies, peak rates of 1.0 to 1.9 m/ka lasted for only 1 ka, while rates of 0.05 m/ka may have persisted for 40 ka. At Metternich, peak rates reached 3.8 m/ka while rates less than .02m/ka lasted for at least 30 ka. The difference between the two sites' deposition rates is very probably a function of distance from source – more than 150 km for Harmignies, less than 5 km for Metternich. The general correspondence between the grain size distributions and the climatic events recorded by organic carbon content and

weathering shows that in general, the episodes of climate change that caused weathering were approximately synchronous with deposition.

Both sites show evidence for erosion and reworking. The plateau location of Harmignies did not prevent the formation of deep gullies during at least one episode of increased precipitation, and sediment horizons have been distorted and, in places, obliterated by cryoturbation. However, most of the site appears not to have undergone major reworking.

The Metternich site is located against a steep valley slope with a ridge behind it and there are multiple examples of modification by surface flow, including erosion horizons and gravel lenses, washed down-slope from locations higher on the ridge. In addition, Metternich lacks a major cryoturbation/erosion horizon present at many other loess sites in that area and a characteristic tephra layer linked with that horizon may have been reworked into a broad zone. This suggests that despite its apparent continuity, the loess record at Metternich is not fully representative of the loess stratigraphy found elsewhere in the Rhine valley and it does not present an accurate and comprehensive record of climate change in this area. With hindsight, it is apparent that a flat site might have undergone less erosion and contamination, and could have provided more comprehensive results.

During initial reconnaissance, the profusion of ice segregation features at Harmignies and the lack of such features at Metternich led to speculation that these two sites could contrast a predominantly 'Atlantic maritime' climate with one showing more continentality (see Section 1.4). It is now suspected that their absence at Metternich is more attributable to topography than to climatic difference.

8.2 Correlation of weathering response with the other parameters measured in this study

The aeolian sections of the profile at both sites (Harmignies: mid Unit F to Unit K; Metternich: Units 3, 4 and 5) have been formed from loessic particles that have homogeneous, though differing, compositions. The minor variations that have been identified, such as the progressive rise in carbonate content at Metternich, can be identified and have been accounted for. This homogeneity appears to extend downwards; the early Weichselian palaeosol complexes are similar to the overlying loess, particularly at Metternich. This may be due to the typical 'very well mixed' nature of loessic sediment at each site.

Against that background of homogeneity, both sites show heterogeneity in the 'standard' sedimentological parameters (grain size, carbonate content, organic carbon content) and in enviromagnetic characteristics. These have patterns of variance that

correlate strongly and consistently, and which match previously-identified patterns of local response to climate change. Heterogeneity in geochemical parameters, identified by carbonate mobility and silicate weathering (measured by the CIA), correlate with these patterns of variation. As a proxy for climatic amelioration, the CIA provides indications of weathering at the study sites that are equal to, or better than the organic carbon record in both magnitude of response and apparent sensitivity to the prevailing palaeoconditions (Figs. 7.11, 7.12). Further, the silicate minerals that it addresses do not suffer from reprecipitation. It is, therefore, a permanent record that is unlikely to be overwritten by subsequent events.

Sections 8.3 and 8.4 compare this local response with the wider record, using the GRIP ice core as an arbitrary but consistent standard for climate change studies (see Section 1.2.2).

8.3 Correlations between Harmignies and the GRIP record.

8.3.1 GRIP correlation with the geochemical record

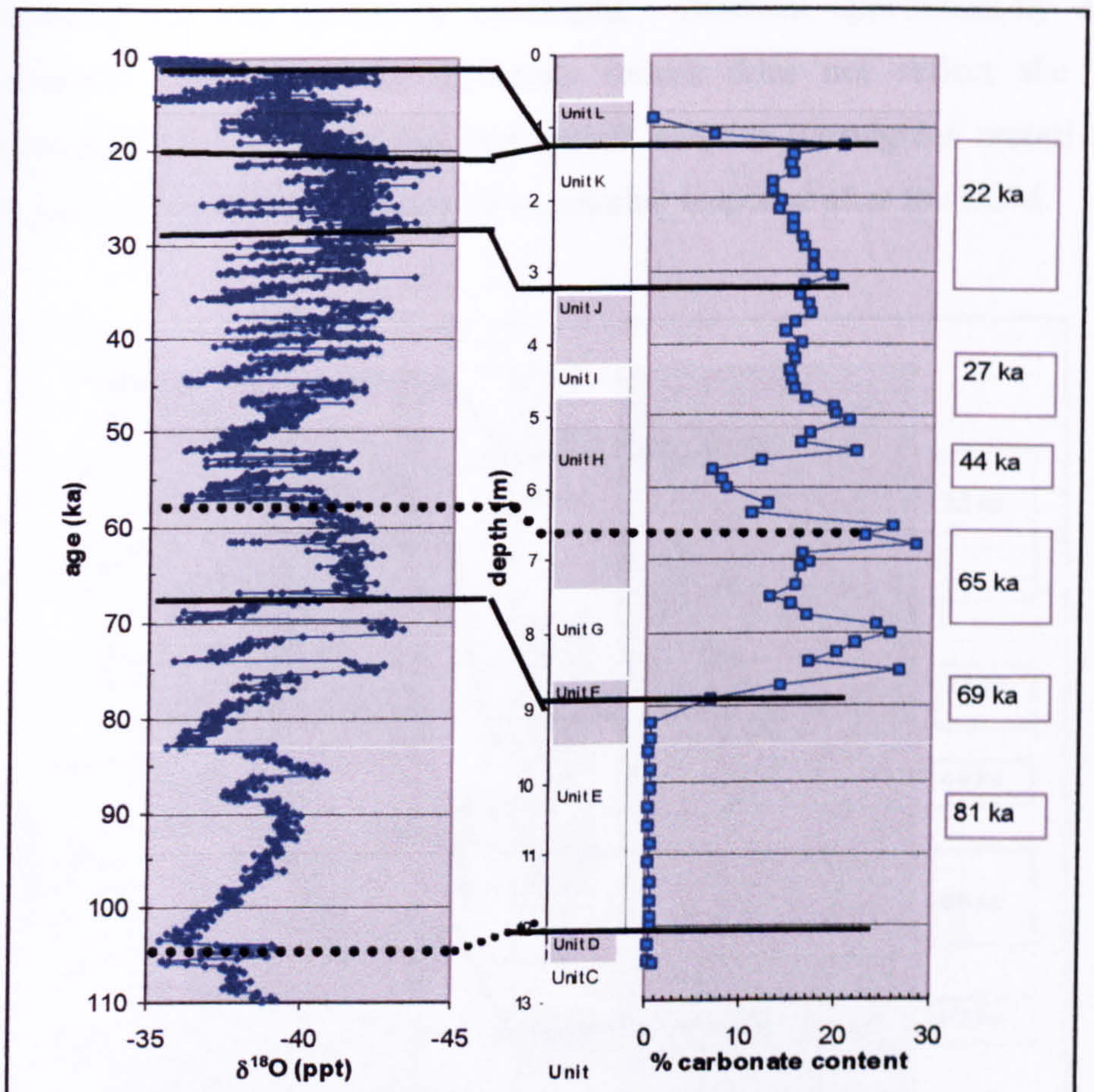

Figure 8.1. Harmignies: comparison of carbonate content with $\delta^{18}O$ climate signal in GRIP core (Dansgaard *et al.*, 1993), with a simplified luminescence chronology and temporal correlations (dotted lines are tentative correlations). Correlations in this and subsequent figures are based on the luminescence chronology and variation in the GRIP profile.

Comparison of the Harmignies carbonate content record with the $\delta^{18}O$ climate signal in the GRIP core[1] (Dansgaard *et al.*, 1993) (Fig. 8x) confirms the findings in Sections 6 and 7: the carbonate content responds only to major climatic change. It is diminished effectively to zero during the early Weichselian period of soil formation and only increases when aeolian deposition delivers a fresh supply of carbonate particles at approximately 69 ka.

During the general period 60-30 ka, the GRIP record shows multiple strong interstadials (GI 16, 14, 12 and 8, shown in Fig. 1.4; occurring c. 57, 52, 44 and 36 ka respectively (Dansgaard *et al.*, 1993). Each of these is likely to have caused carbonate weathering, accompanied by down-profile carbonate reprecipitation. However, because

[1] Data provided by the National Snow and Ice Data Center, University of Colorado at Boulder, and the WDC-A for Paleoclimatology, National Geophysical Data Center, Boulder, Colorado.

loess accumulation rates were low, the record is of low resolution. Using the luminescence age estimate of 44.1 ±3.9 ka, obtained at 5.75 m depth, it is possible tentatively to equate the carbonate depletion troughs *c.* 6.3, 5.7-6.0 and 5.4 m depths to GI 16/14, 12 and 8 respectively but this cannot be confirmed. Between approximately 30-22 ka loess accumulated rapidly but the carbonate record does not reflect the rapid climatic fluctuations that occurred during that period, and the Harmignies record finishes at that point, precluding any examination of weathering response after the LGM.

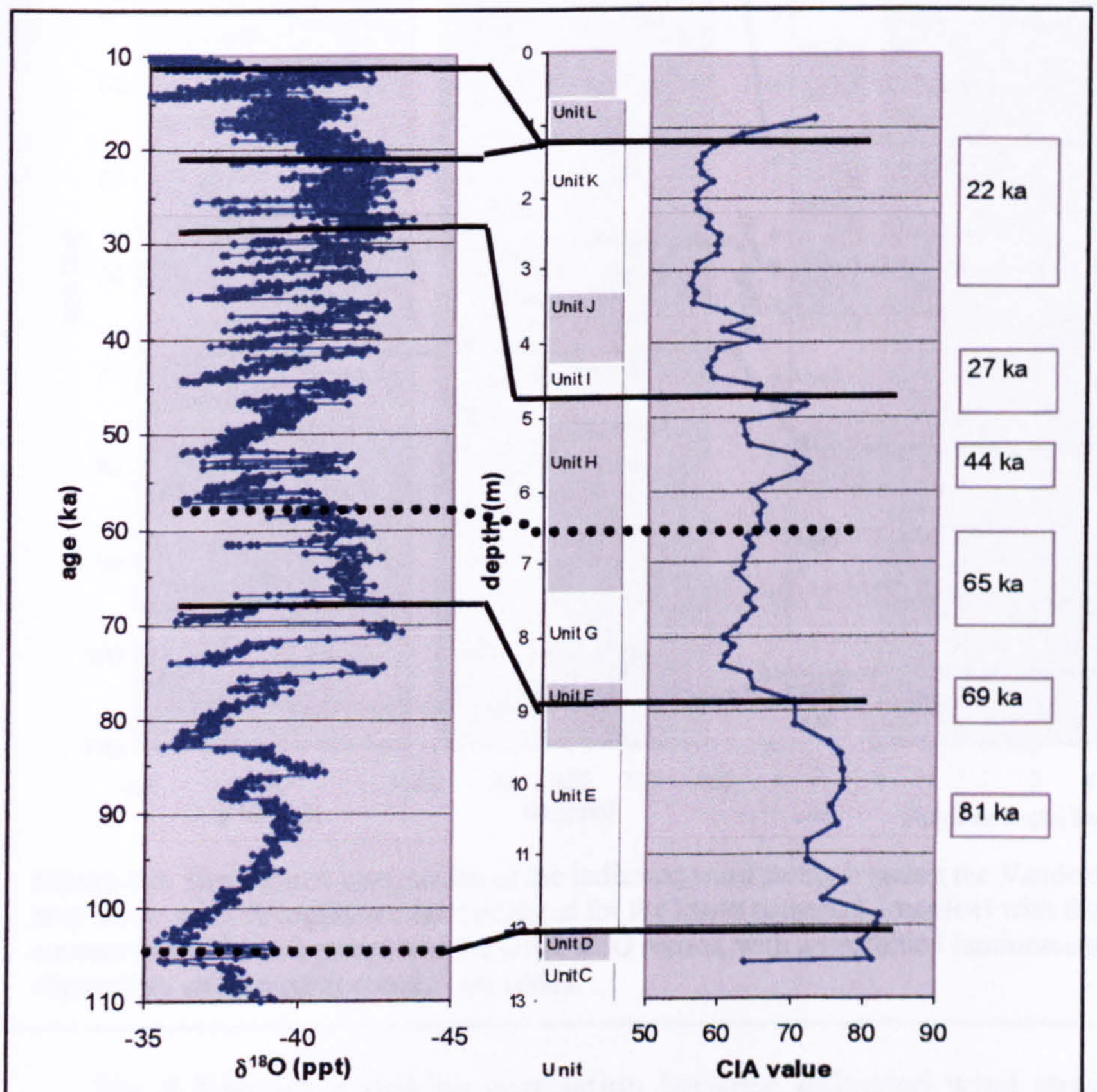

Figure 8.2. Harmignies: comparison of the degree of silicate weathering (using the Chemical Index of Alteration) with the GRIP $\delta^{18}O$ record, with a simplified luminescence chronology and temporal correlations added.

As discussed in Section 7.4 and 7.5, silicate weathering occurred with lower intensity than carbonate weathering. Comparison of the weathering index values with the GRIP climate signal expressed in the $\delta^{18}O$ record (Dansgaard *et al.*, 1993) (Fig. 8.2) shows that silicate weathering only occurred during episodes of intense weathering – either interglacial conditions or during the GI 16-8 group of strong interstadials. The luminescence age estimate of 44.1 ±3.9 ka, obtained at 5.75 m depth and within this peak may indicate that it was formed during GI 12; no CIA weathering peaks correspond to the

carbonate weathering peaks at 6.3 and 5.4 m depths that might equate to GI 16/14 and GI 8.

8.3.1 GRIP correlation with the wind strength record

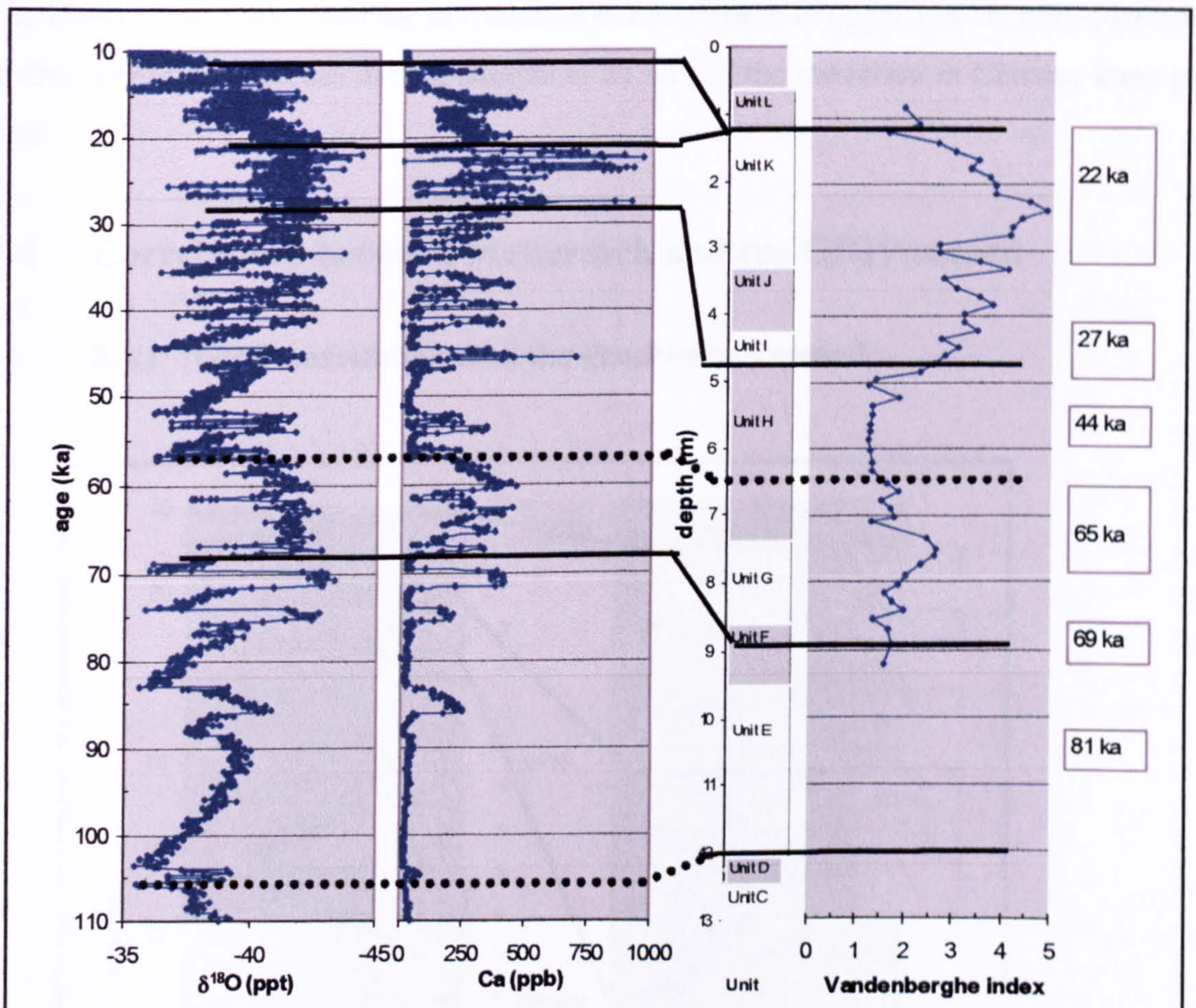

Figure 8.3. Harmignies: comparison of the indicated wind strength (using the Vandenberghe grain size index; wind strengths are not calculated for the lower palaeosol complex) with the GRIP dust content (using Ca as a proxy) and the GRIP $\delta^{18}O$ record, with a simplified luminescence chronology and temporal correlations added.

Fig. 8.3 shows a striking correlation between indicated wind strengths, the GRIP climate signal expressed in the $\delta^{18}O$ record (Dansgaard *et al.*, 1993) and the GRIP Ca content[1] (a proxy for total dust content (Fuhrer *et al.*, 1993)). This chart emphasises that much of the profile was deposited very rapidly. The start of loess deposition in Unit F and the peak in indicated wind strength c. 65 ka in Units G/H corresponds to GRIP evidence for raised atmospheric dust content and major ice sheets. It is followed by a period of low indicated wind speeds and low rates of loess accumulation which correspond with GRIP indications of climatic amelioration and reduced dust content between approximately 60-30 ka. Indicated wind strengths start to rise in Unit I *c.* 27 ka and reach a maximum in

[1] Data provided by the National Snow and Ice Data Center, University of Colorado at Boulder, and the WDC-A for Paleoclimatology, National Geophysical Data Center, Boulder, Colorado.

Unit K *c.* 22 ka, with corresponding rapid loess accumulation; the GRIP record shows maximum ice sheet development and maximum atmospheric dustiness occurring *c.* 24-22 ka. The mean diameter of Chinese loess particles reaches a 'coarseness peak' at 21.3 ka, followed by a rapid reduction in size, reflecting that same wind strength pattern (Xiao *et al.*, 1999). The rapid decrease in indicated wind strength in upper Unit K may correspond to the very rapid decrease in dust content *c.* 22 ka and the reduction in Chinese loess grain size.

8.4 Correlations between Metternich and the GRIP record

8.4.1 GRIP correlation with the geochemical record

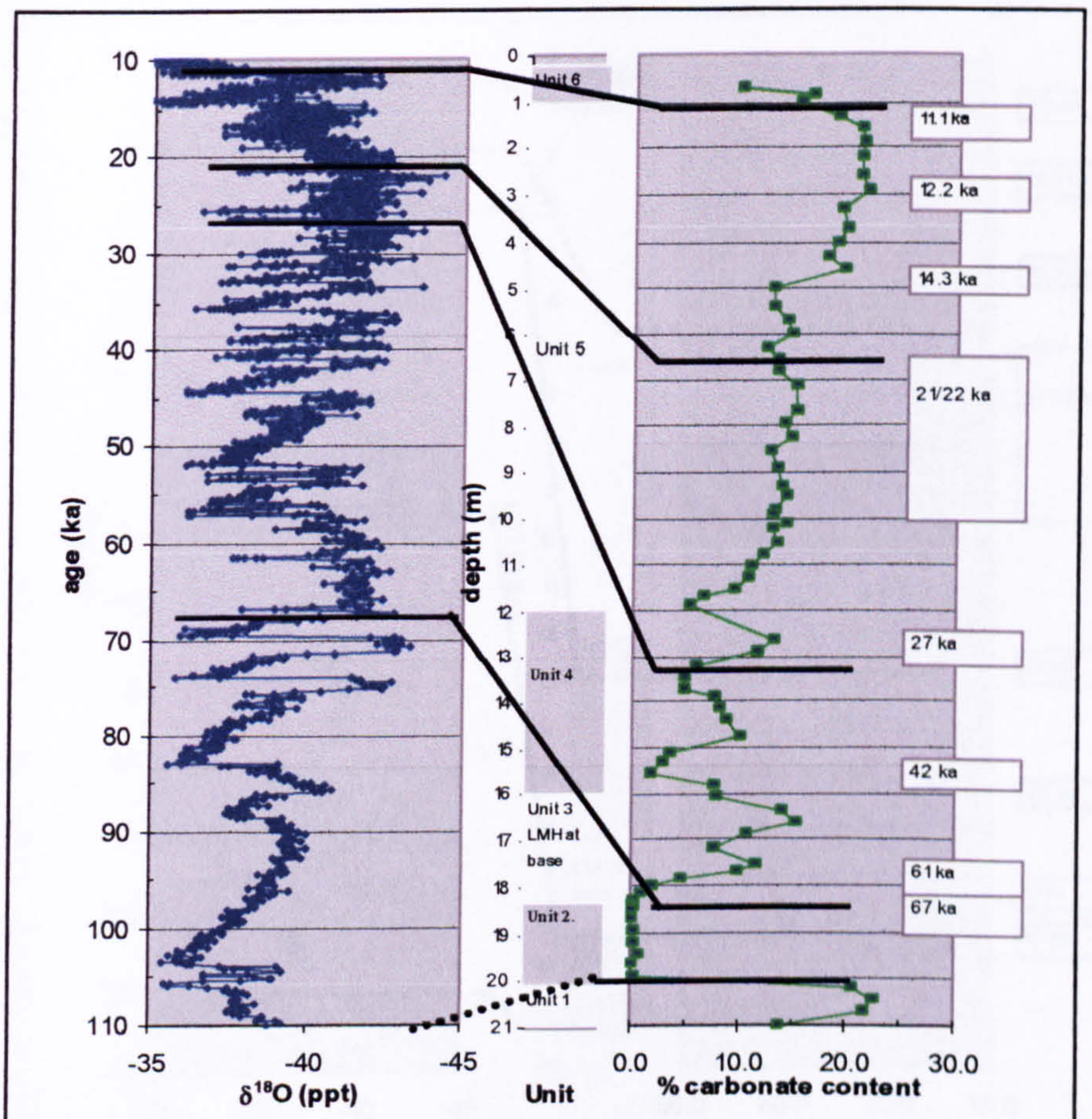

Figure 8.4. Metternich: comparison of carbonate content with $\delta^{18}O$ climate signal in GRIP core (with a simplified luminescence chronology and temporal correlations).

Fig. 8.4 compares the Metternich carbonate content record with the $\delta^{18}O$ climate signal in the GRIP core. The results are broadly similar to Harmignies: the carbonate content was diminished effectively to zero during the Eemian and early Weichselian period of soil formation (Unit 2) and only increased when aeolian deposition delivered a fresh

supply of carbonate particles at approximately 67 ka (Unit 3). Although Metternich has higher accumulation rates than Harmignies, the depositional record of the period between approximately 60-30 ka is still low resolution. Using the luminescence age of 41.9 ±2.0, obtained at 15.2 m depth, it is possible tentatively to equate the carbonate depletion episodes at 17.2, 15.5-15.1 and 13.8-13.5 m with GI 16/14 (*c* 57/52 ka), GI 12 (*c*. 44 ka) and GI 8 (*c*. 36 ka) (ages from Dansgaard *et al.*, 1993).

In upper Unit 4 and Unit 5, between approximately 30-22 ka, loess deposition is rapid but the carbonate record does not reflect the rapid climatic fluctuations that occurred during that period, nor does it appear to respond to the more pronounced climatic variation that followed the LGM. Carbonate weathering is apparent only near the top of Unit 5, in the late glacial period; stronger weathering occurred in the Unit 6 post-glacial soil.

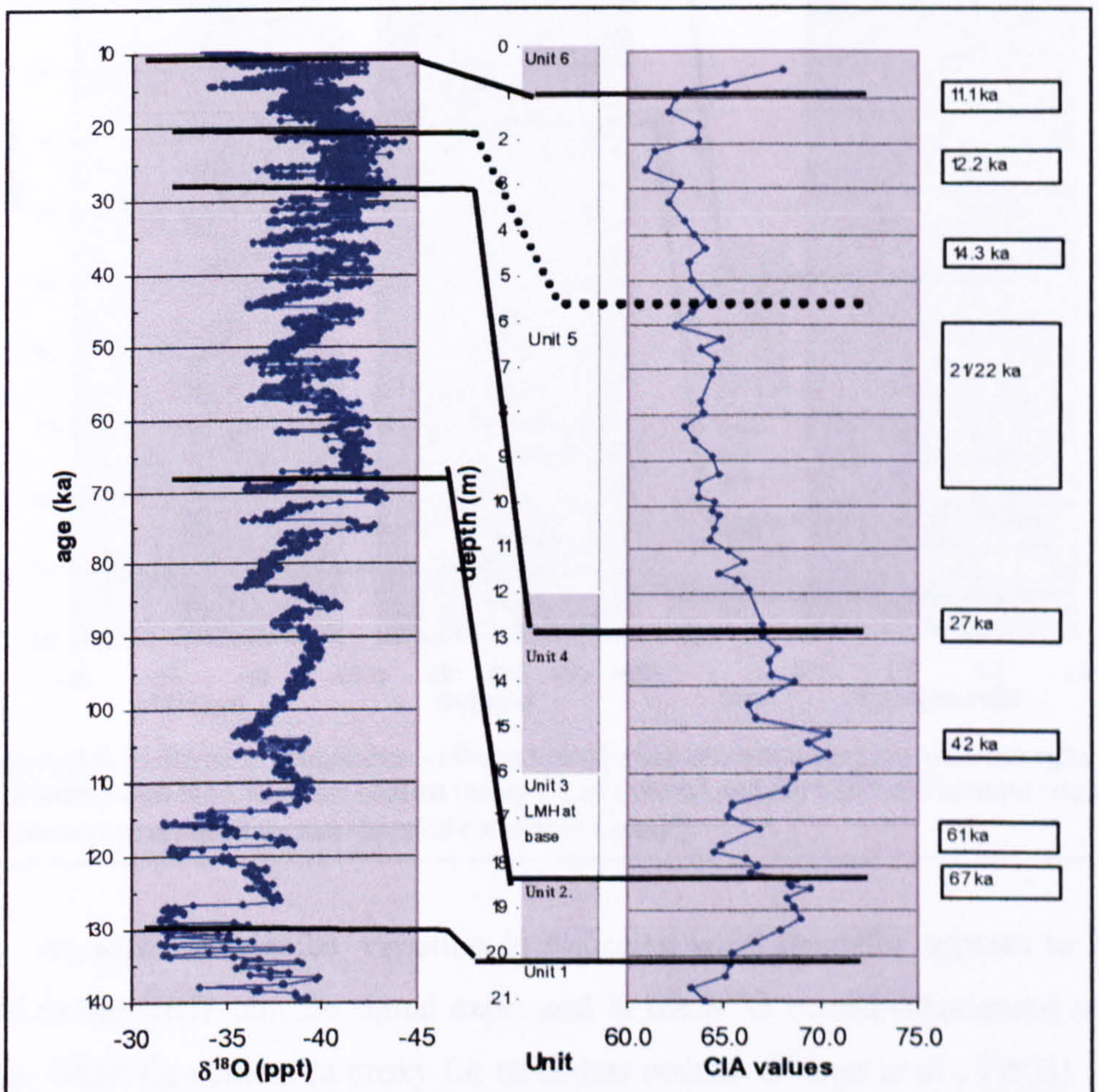

Figure 8.5. Metternich: comparison of the degree of silicate weathering (using the Chemical Index of Alteration) with the GRIP $\delta^{18}O$ record (simplified luminescence chronology and temporal correlations added).

Silicate weathering again occurred with lower intensity than carbonate weathering. Comparison of the weathering index values with the $\delta^{18}O$ record (Fig. 8.5) shows that silicate weathering only occurred during the early Weichselian (Unit 2), the GI 16/14/12/8

group of strong interstadials between approximately 57-36 ka (lower Unit 4), during the lateglacial warming *c.* 13 ka (upper Unit 5) and in the post-glacial soil (Unit 6). It is apparent that at both sites, both carbonate and silicate weathering can only be interpreted in terms of major climatic change.

8.4.2 GRIP correlation with the wind strength record

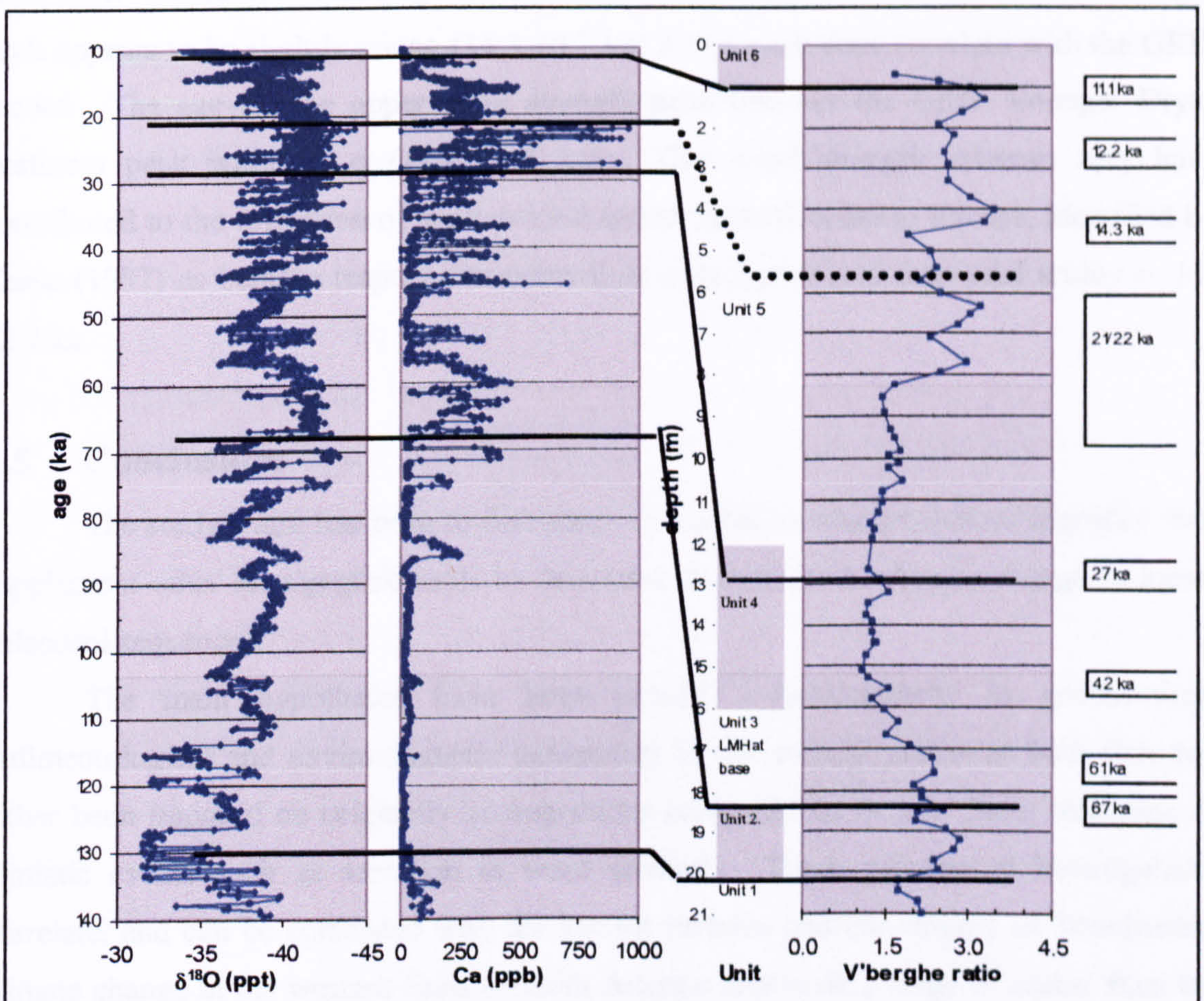

Figure 8.6. Metternich: comparison of the indicated wind strength (using the Vandenberghe grain size index) with the GRIP dust content (using Ca as a proxy) and the GRIP $\delta^{18}O$ record (simplified luminescence chronology and temporal correlations added).

As with Harmignies, variation in indicated wind strengths appears to be strongly related to the GRIP climate signal expressed in the $\delta^{18}O$ record (Dansgaard *et al.*, 1993) and the GRIP Ca content (a proxy for total dust content (Fuhrer *et al.*, 1993)). More than half the profile (upper Unit 4, Unit 5) was deposited in approximately 15 ka, before and after the LGM. The major wind strength peak present in the Harmignies record *c.* 65 ka is not apparent in Unit 3 at Metternich but the period of indicated weak winds between *c.* 60-30 ka (upper Unit 3 and Unit 4) again matches the period of strong interstadials and low dust content. Indicated mean wind strengths start to increase in Unit 5 *c.* 27 ka and reach

multiple peaks *c.* 21/22 ka, which correlate with the peak dustiness and ice-sheet indications in the GRIP core.

Two further increases in wind strength, *c.* 4 m and 1 m depth may correspond to two major late-stage GRIP dustiness peaks *c.* 17-15.5 and 12.6-12.0 ka. The older peak occurred during the late stages of the LGM, which terminated at 14.5 ka (Severinghaus and Brook, 1999); the younger peak occurred during the Younger Dryas (12.9-11.6 ka, Alley *et al.*, 1993). The luminescence age for a horizon close to the lower indicated wind strength peak appears to be slightly young (14.3 ±0.7 ka) if that peak does correlate with the GRIP record. The age for the upper wind strength peak matches the GRIP Younger Dryas dustiness peak within 1 σ (11.1 ±1.5 ka). This wind strength increase may have contributed to the formation of aeolian sand-sheets in north-western Europe, identified by Kasse (1997) as being a response to permafrost degradation and increased aridity *c.* 14-12.4 ka.

8.5 Conclusions

The study's aim has been to determine the extent to which chemostratigraphy can supplement other stratigraphic tools to determine the effects of climate change in loess-palaeosol sequences.

The main hypotheses have been proved. Heterogeneity in geochemical, sedimentological and enviromagnetic parameters in the vertical profile at both sites has either been imposed on originally-homogeneous compositions or is a direct reflection of climatic events such as variation in wind strength. Those patterns of heterogeneity correlate, and can be correlated with the known patterns and chronology of Weichselian climate change in the western Europe/North Atlantic region on a range of scales from the local to hemispheric.

The study re-emphasises the value of grain size indices, based on detailed grain size analysis, as a proxy for variation in mean wind strength and in accumulation rates. They show large-magnitude change which can be correlated in detail with the GRIP record.

Weathering effects on both carbonate and silicate minerals are unambiguous at the scale of glacial/interglacial climate change. However, at the interstadial scale, a combination of factors acts to reduce the resolution of the available record. These factors include low accumulation rates during periods of strong interstadials, which results in homogeneous weathering, and high accumulation rates during periods of weaker interstadials, which dilutes the effects of pedogenic alteration. Both of these factors combine to reduce the stadial/interstadial resolution of the weathering record. In addition, carbonate mobility can act to overwrite previous evidence of change whilst silicate

minerals remain relatively unweathered during weaker (and briefer) interstadials, either because the ubiquitous carbonate content buffers weathering reactions or because reaction rates remain slow under these conditions of minor climatic amelioration.

This study concludes that climatically-controlled geochemical variation is present in the loess-palaeosol sequences at the study sites, induced by carbonate and silicate weathering. Carbonate weathering is a reliable indication of major pedogenic episodes but its detailed interpretation is tempered by carbonate mobility. Silicate weathering occurs at lower intensity than carbonate weathering but is a permanent record since silicates are not subject to reprecipitation under these conditions. It can, therefore, identify periods of weathering that have been obscured in the carbonate record by reprecipitation. As a proxy for climatic amelioration, the CIA is directly comparable with the organic carbon record in sensitivity and magnitude. Since organic carbon may be destroyed by, for example, oxidation, it is possible that the CIA could preserve evidence of climatic amelioration when that parallel record has been lost.

Under conditions of moderate or high loess accumulation rates, it is possible to identify periods of minimal weathering that can be equated to climatic minima and periods of increased weathering that can be equated to major interstadials. With the support of a well-resolved site chronology, it would be possible to use the CIA and carbonate profiles to identify at least the main climatic trends without reference to any other proxy. However, this would be a very 'broad brush' treatment of a complex and detailed record. Chemostratigraphy is not a replacement for those other proxies, it complements them and provides additional evidence upon which climatic reconstructions can be made, with an equivalent resolution.

8.6 Future work

This study has applied detailed and fine-resolution analysis of grain size, carbonate content, loss-on-ignition, enviromagnetic and geochemical characteristics to these two western European loess-palaeosol sites. One significant problem remains – is there or is there not Eltville tephra present at the top of the Harmignies profile and at 5 m depth at Metternich? Sample material remains available and this is considered to be a priority task, particularly for Harmignies where positive tephra identification would resolve the Haesaerts/van Vliet-Lanoë conflict. Apart from that, no further work is planned for these sites.

Reference list

Adamiec, G. & Aitken, M.J. (1998). Dose rate conversion factors: new data. *Ancient TL*, **16**, 37-50.

Aide, M & Smith-Aide, C. (2003). Assessing soil genesis by rare-earth elemental analysis. *Soil Science Journal of America*, **67**, 1470-76.

Aitken, M.J. (1985). *Thermoluminescence dating*. Academic Press, London.

Aitken, M.J. (1990). *Science-based Dating in Archaeology*. Longman, London

Allen, P.A. (1997). *Earth Surface Processes*. Boston, Blackwell Science, 404 p.

Alley, R.B., Anandakrishnan, S., Jung, P. & Clough, A. (2001). Stochastic resonance in the North Atlantic: Further Insights. In Seidov, D., Haupt, B.J. and Maslin, M. (eds). The Oceans and Rapid Climate Change: Past, Present and Future. *Geophysical Monograph*, **16**, 57-68.

Alley, R.B., Meese, D.A., Shuman, C.A., Gow, A.J. Taylor, K.C. Grootes, P.M., White, J.W.C., Ram, M., Waddington, E.D., Mayewski, P.A. & Zielinski, G.A. (1993). Abrupt increase in Greenland snow accumulation at the end of the Younger Dryas event. *Nature*, **362**, 527-529.

Alley, R.B. & MacAyeal, D.R. (1994). Ice-rafted debris associated with binge-purge oscillations of the Laurentide ice sheet. *Paleoceanography*, **9**, 503-511.

An Z., Kukla G., Porter S. & Xiao J. (1991a). Magnetic susceptibility evidence of monsoon variation on the loess plateau of China during the last 130,000 years. *Quaternary Research*, **36**, 29-36.

An, Z., Kukla, G., Porter, S. & Xiao, J. (1991b). Late Quaternary dust flow on the Chinese Loess Plateau. *Catena*, **18**, 125-132.

An, Z., Liu, T., Lu, Y., Porter, S.C., Kukla, G., Wu, X., & Hua, Y. (1990). The long-term paleomonsoon variation recorded by the loess-paleosol sequence in central China. *Quaternary International,* **8**, 91-95.

Anonymous. (2005). Thorium: index of properties. Cited 4.4.2005. Available at World Wide Web, URL:
< http://www.webelements.com/webelements/elements/text/Th/index.html>

Antoine, P., Catt, J., Lautridou, J-P. & Sommé, J. (2003). The loess and coversands of northern France and southern England. *Journal of Quaternary Science*, **18**(3-4), 309-318.

Assalay, A.M., Rogers, C.D.F., Smalley, I.J. & Jefferson, I.F. (1998). Silt, 2-62 μm, 9-4Φ. *Earth-Science Reviews*, **45**, 61-88.

Baak, A.I. (1936). *Regional petrology of the southern North Sea*. Dissertation (unpbl), University of Leiden. Quoted by De Ploey (1964) (q.v.)

Bagnold, R. (1941). *The Physics of Blown Sand and Desert Dunes*, Methuen, London.

Balescu, S. (1988). *Apports de la thermoluminescence à la stratigraphie et à la sédimentologie des loess Saaliens du NW de l'Europe* [trans: Application of thermoluminescence to the stratigraphy and sedimentology of Saalian loess of NW Europe]. Thesis, unpblished. Universite Libre de Bruxelles, Faculte des Sciences.

Banerjee, S.K. (1971). Decay of marine magnetic anomalies by ferrous ion diffusion. *Nature: Physical Science* **229**, 181–183.

Barron, E.J. (1985). Explanations of the Tertiary global cooling trend. *Palaeogeogeography, Palaeoclimatology, Palaeoccology*, **50**, 45-61.

Barth M.G., McDonough W.F. & Rudnick R.L. (2000). Tracking the budget of Nb and Ta in the continental crust. *Chemical Geology,* **165**(3–4), 197–213.

Bartlett, W.H.C. (1832). Experiments on the expansion and contraction of building stones by variations in temperature. *American Journal of Science*, **22**, 136–140.

Bastin, B. (1969). Premiers resultants de l'analyse pollinique des loess en Belgique [trans: Initial results of pollen analysis in Belgium loess]. *Bulletin de l'Association Française pour l'etude du Quarternaire.* **1**, 3-11.

Bastin, B. (1970). La chronostratigraphie du Wurm en Belgique a la lumiere de la palynologie des loess et limons [trans; The chronostratigraphy of the Wurmian in Belgium shown by palynology of loess and silts]. *Extrait des Annales de la Société Géologique de Belgique.* **93**, 545-580.

Beaty, C. (1978). Ice ages and continental drift. *New Scientist*, **80**, 776-777.

Begét, J.E. (1996). Tephrochronology and palaeoclimatology of the last interglacial cycle recorded in Alaskan loess deposits. *Quaternary International*, **34-36**, 121-126.

Begét, J.E. Stone, D.B. & Hawkins, D.B. (1990). Palaeoclimatic forcing of magnetic susceptibility variations in Alaskan loess during the late Quaternary. *Geology*, **18**, 40-43.

Bengtsson, L. & Enell, M. (1986). Chemical analysis. *In* Berglund, B.E. (ed.), *Handbook of Holocene Palaeoecology and Palaeohydrology*. John Wiley and Sons, Ltd, Chichester, 423-451.

Bennett, K.D., Whittingham, G & Edwards, K. (1994). Recent plant nomenclature changes and pollen morphology in the British Isles, *Quaternary Newsletter*, **73**, 1-6.

Berner, R.A. & Holdren, G.R. Jr. (1977). Mechanism of feldspar weathering: some observational evidence. *Geology*, **5**.6, 369–372.

Berger, G.W., Mulherm, P.J. & Huntley, D.J. (1980). Isolation of silt-sized quartz from sediments. *Ancient TL*, **11**, 147-152.

Bernet, M., Brandon, M.T., Garver, J.I. & Molitor, B. (2004). Downstream changes of Alpine zircon fission-track ages in the Rhône and Rhine rivers. *Journal of Sedimentary Research*, **74**. 1, 82–94.

Bhatia,M.R. & Taylor, S.R. (1981). Trace-element geochemistry and sedimentary provinces: a study from Tasman Geosyncline, Australia. *Chemical Geology*, **33**, 115–125.

Bibus, E., Bludau, W., Bross, C. & Rähle, W. (1996). Der Altwurm- und Rißabschnitt im Profil Mainz-Wiesenau und die Eigenschaften der Mosbacher Humuszonen [trans: The early Wurmian and late Riss in the Mainz-Wiesenau profile and the characteristics of the Mosbach humic zones. *Frankfurter Geowissen-schafteliche Arbeiten,* **20, 21-52.**

Bidart, S. (1996). Sedimentological study of aeolian soil parent materials in the Rio Grande basin, Buenos Aires Province, Argentina. *Catena,* **27,** 191-207.

Birkeland, P.W. (1999). *Soils and geomorphology.* Oxford University Press.

Biscaye, P.E., Grousset, F.E., Revel, M., Van der Gaast, S., Zielinski, Vaars, A & Kukla, G. (1997). Asian provenance of glacial dust (stage 2) in the Greenland Ice Sheet Project 2 ice core, Summit, Greenland, *Journal of Geophysical Research,* **102** (C12), 26765–26781.

Blakemore, R.P. (1982). Magnetotactic Bacteria. *Annual Review of Microbiology 1982,* 217-238.

Bloemendal, J., King, J.W., Hall, F.R. & Doh, S-J. (1992). Rock magnetism of Late Neogene and Pleistocene deep-sea sediments: Relationship to sediment·source, diagenetic processes and sediment lithology. *Journal of Geophysical Research,* **97,** 4361–4375.

Blott, S.L. & Pye, K. (2001). GRADISTAT: a grain size distribution and statistics package for the analysis of unconsolidated sediments. *Earth Surface Processes and Landforms,* **26,** 1237-1248.

Blum, M.D., Guccione, M.J., Wysocki, D.A., Robnett, P.C. & Rutledge, E.M.(2000). Late Pleistocene evolution of the lower Mississippi River valley, southern Missouri to Arkansas. *Geological Society of America Bulletin,* **112.2,** 221-235.

Busenberg E. & Plummer L.N. (1989). Thermodynamics of magnesian calcite solid–solutions at 25°C and 1 atm total pressure. *Geochim. Cosmochim. Acta.* **53,** 1189-1208.

Bogaard, van den P. (1995). Quaternary volcanism. *Field Guide Excursion A18,* INQUA 24th International Congress.

Boenigk, W. & Frechen, M. (2001). The loess record in sections at Koblenz-Metternich and Tönchesberg in the Middle Rhine area. *Quaternary International*, **76-77**, 201-209.

Boenigk, W., Frechen, M, & Schweitzer, U. (1999). Mikromorphologishe Charakterisierung der Deckschnikten vom Kärlich und Koblenz-Metternich. *Mainzer Geowissenschaftliche Mitteilungen*, **28**, 111-142.

Boenigk, W., Frechen, M, & Weidenfeller, M. (1994). Die mittel- und oberpleistozäne Deckschichtenfolge im Naturschutzgebeit 'Eiszeitlichtes Lößprofil' in Koblenz-Metternich. *Mainzer Geowissenschaftliche Mitteilungen*, **23**, 287-320.

Bond, G., Broecker, W., Johnsen, S., McManus, J., Labeyrie, L., Jouzel, J. & Bonani, G. (1993). Correlations between climate records from North Atlantic sediments and Greenland ice. *Nature*, **365**, 143-147.

Bond, G & Lotti, R. (1995). Iceberg discharges into the North Atlantic on millennial time scales during the Last Glaciation. *Science*, **267**,1005-1010.

Bond, G., Kromer, B., Beer, J., Muscheler, R., Evans, M.N., Showers, W., Hoffmann, S., Lotti-Bond, R., Hajdas, I. & Bonani, G. (2001). Persistent solar influence on North Atlantic climate during the Holocene. *Science*, **294**, 2130-2136.

Bory, A.J-M., Biscaye, P.E., Svensson, A. & Grousset, F.E. (2002). Seasonal variability in the origin of recent atmospheric mineral dust at NorthGRIP, Greenland. *Earth and Planetary Science Letters*, **196**: 3-4, 123-134.

Boss, C.B. & Fredeen, K.J. (1999). *Concepts, instrumentation and techniques in inductively couple plasma optical emission spectrometry*. Perkin-Elmer Corp, USA.

Bøtter-Jensen, L., Bular, E. Duller, G.A.T. & Murray, A.S. (2000). Advances in luminescence instrument systems. *Radiation Measurements*, **32**, 523-528.

Bøtter-Jensen, L., Mejdahl, V. & Murray, A.S., (1999). New light on OSL. *Quaternary Science reviews (Quaternary Geochronology)*, **18**, 303-310.

Bourillet, J-F., Reynaud, J-Y., Baltzer, A. & Zaragosi, S. (2003). The 'Fleuve Manche': the submarine sedimentary features from the outer shelf to the deep-sea fans. *Journal of Quaternary Science*, **18**(3-4) 261–282

Broecker, W. S. (1994). Massive iceberg discharges as triggers for global climate change, *Nature*, **372**, 421.

Broecker, W.S., Bond, G., Klas, M, Bonani, G & Wolfi, W. (1990). A salt oscillator in the glacial Atlantic? *Palaeoceanography*, **5**, 469-477.

Butler, R.F. (1982). Magnetic mineralogy of continental deposits, San Juan Basin, New Mexico, and Clark's Fork Basin, Wyoming, *Journal of Geophysical Research,* **87**, 7843-7852.

Butler R.F. & Banerjee S.K. (1975). Theoretical single-domain grain size range in magnetite and titano-magnetite. *Journal of Geophysical Research,* **80**, 4049–4058.

Caitcheon, G. (1998). *The Application of Environmental Magnetism to Sediment Source Tracing: a New Approach.* CSIRO Land and Water Technical Report Nr 21/98. Cited 22.11.2004, available at World Wide Web URL:
<http://www.clw.csiro.au/publications/technical98/tr21-98.pdf>

Campbell, I.D., Campbell, C., Apps, M.J., Rutter, N.W. & Bush, A.B.G. (1998). Late Holocene ~1500-year periodicities and their implications. *Geology*, **26**, 471-473.

Catt JA. (1978). The contribution of loess to soils in lowland Britain. In: *The Effect of Man on the Landscape: the Lowland Zone*, Limbrey S, Evans JG (eds). Research Report 21, Council for British Archaeology: Oxford; 12–20.

Catt, J.A. (1985). Soil particle size distribution and mineralogy as indicators of pedogenic and geomorphic history: examples from the loessial soils of England and Wales. In Richards, K.S., Arnett R.R. & S. Ellis, S., (eds), *Geomorphology and soils*, 202–218. London. George Allen and Unwin

Catt, J.A. (1991). Soils as indicators of Quaternary climatic change in mid-latitude regions. *Geoderma,* **51**, 167-187.

Catt, J.A. (1996). The Loess of Britain: Distribution, Stratigraphy and Origin. *INQUA/ISSS Paleopedology Commission Newsletter* 12, May 1996. Cited 21.7.2004, available at World Wide Web URL:
<http://fadr.msu.ru/inqua/nl-archive/nl-12/toc.html>

Catt, J.A. & Staines, S.J. (1982). Loess in Cornwall. *Proceedings of the Ussher Society*, **5**, 368-375.

Chambers, F. (2005). Personal communication.

Chang, Q., Mishima, T., Yabuli, S, Takahashi, Y & Shimizu, H. (2000). Sr and Nd isotope ratios and REE abundances of moraines in the mountain areas surrounding the Taklimakan Desert, NW China. *Geochemical Journal*, **34**, 407 to 427.

Chen, F.H., Bloemendal, J., Wang, J.M., Li, J.J. & Oldfield, F. (1996). High-resolution multi-proxy climate records from Chinese loess: evidence for rapid climatic change over the last 75 kyr. *Palaeogeography, Palaeoclimatology, Palaeoecology*, **130**, 323-335.

Chen, J., An, Z., Liu, L.W., Ji, J.F., Yang, J.D. & Chen, Y. (2001). Variations in chemical composition of the aeolian dust in Chinese loess plateau over the past 2.5 ma. and chemical weathering in Asia continent. *Science in China*, **31**, 136-145.

Chlachula, J., Evans, M.E. & Rutter, N.W. (1998). A magnetic investigation of a Late Quaternary loess/palaeosol record in Siberia. *Geophysical Journal International*, **132.1**, 128-132.

Cilek, V. (2001). The loess deposits of the Bohemian Massif: silt provenance, palaeometeorology and loessification processes. *Quaternary International*, **76-77**, 123-128.

Clapperton, C. (1993). *Quaternary geology and geomorphology of South America*. Elsevier Science Publishers B.V., Amsterdam.

Clark, P.U., Alley, R.B. & Pollard, D. (1999). Northern Hemisphere Ice-Sheet Influences on Global Climate Change. *Science*, **286**, 1104-1111.

Claquin, T., Roelandt, C., Kohfeld, K.E., Harrison, S.P., Tegen, I., Prentice, I.C., Balkanski, Y., Bergametti, G., Hansson, M., Mahowald, N., Rodhe, H. & Schulz, M. (2003). Radiative forcing of climate by ice-age atmospheric dust. *Climate Dynamics*, **20**, 193–202.

COHMAP members (1988). Climatic changes of the last 18,000 years: observations and model simulations, *Science,* **241**, 1043-1051.

Colman, S.M. (1982). *Chemical weathering of basalts and andesites: Evidence from weathering rinds*. U.S. Geological Survey Professional Paper 1246. U. S. Gov. Print. Office, Washington, DC.

Coplen, T.B. (1996). New guidelines for reporting stable hydrogen, carbon, and oxygen isotope-ratio data. *Geochimica et Cosmochimica Acta*, **60**, 3359-3360.

Croudace, I.W. (1980). A possible error source in silicate wet-chemistry caused by insoluble fluorides. Chemical Geology, **31**, 153-155.

Crowley, T. (2000). Causes of climate change over the past 1000 years. *Science*, **289**, 270-277.

Currey, B.B. & Follmer, L.R. (1992). The last interglacial-glacial transition in Illinois: 123-25 ka. In: The last interglacial-glacial transition in North America. (eds: Clark, P.U. & Lea, P.D.). *Geological Society of America Special Paper 270*, 71-88.

Dansgaard, W., Johnsen, S.J., Clausen, H.B. & Gunderstrun, N. (1973). Stable isotope glaciology. *Meddelelser om Gronland*, **197**, 1-53.

Dansgaard, W., Johnsen, S.J., Clausen, H.B. & Langway, C.C. Jr. (1971). Climatic record revealed by the Camp Century ice core. In: Late Cenozoic Glacial Ages (ed. Turekian, K.K.), pp.37-56, New Haven: Yale University Press.

Dansgaard, W., Johnsen, S.J., Clausen, H.B., Dahl-Jensen, D., Gundestrup, N., Hammer, C.U. & Oeschger, H. (1984). North Atlantic climatic oscillations revealed by deep Greenland ice cores. *Climate Processes and Climate Sensitivity, Geophysical Monograph, American Geophysical Union* **29**, 288-298.

Dansgaard, W., Johnson, S.J., Clausen, H.B., Dahl-Jensen, D., Gunderstrup, N.S., Hammer, C.U., Hvidberg, C.S., Steffensen, J.P., Sveinbjörndottir, A.E., Jouzel, J. & Bond, G. (1993). Evidence for general instability of past climate from a 250-kyr ice-core record. *Nature*, **364**, 218-220.

De Boer, C.B. (1999). Rock-Magnetic studies on Hematite, Maghemite and igneous/ metamorphic Rocks (PhD thesis, Utrecht University), *Geologica Ultraicctina*, **177**, *254 pp.*

De Ploey, J. (1964). *Contribution à la connaissance des dépôts du Plèistocéne Supéricur en Basse Belgique.* In: Dylik, J., Kondracki, J.,& Krajewski, S. (eds). Report of the VIth International Congress on Quaternary (INQUA), Vol IV.

Dean, W.E. Jnr. (1974). Determination of carbonate and organic matter in calcareous sediments and sedimentary rocks by loss on ignition: comparison with other methods. *Journal of Sedimentary Petrology*, **44**, 242-248

Dearing, J.A., Dann, R.J.L., Hay, K., Lees, J.A., Loveland, P.J., Maher, B.A., O'Grady, K. (1996). Frequency dependent susceptibility measurements of environmental materials. *Geophysics Journal International*, **124**, 228-240.

Derbyshire, E. (1995). Aeolian sediments in the Quaternary record: An introduction. *Quaternary Science Reviews*, **14**, 641-643.

Derbyshire, E, Kemp, R.A. & Meng, X. (1997). Climate change, loess and palaeosols; proxy measures and resolution in North China. *Journal of the Geological Society of London*, **154**, 793-805.

Diao, G. & Wen, Q. (1999). Mobility sequence of chemical elements during loess weathering-pedogenesis, Weinan, Shaanxi Province, China. *Chinese Journal of Geochemistry,* **18**.4, 327-332.

Ding, Z., Liu, T., Rutter, N. W., Yu, Z., Guo, Z. & Zhu, R. (1995). Ice-volume forcing of East Asian winter monsoon variations in the past 800,000 years. *Quaternary Research*, **44**, 149–159.

Ding, Z.L., Sun, J.M, Yang, S.L. & Liu, T.S. (1998). Preliminary magneto-stratigraphy of a thick eolian red clay-loess sequence at Lingtai, the Chinese Loess Plateau. *Geophysical Research Letters*, **25**.8, 1225–1228

Ding, Z.L., Sun., J.M., Yang, S.L. & Liu, T.S. (2001). Geochemistry of the Pliocene red clay formation in the Chinese Loess Plateau and implications for its origin, source provenance and palaeoclimate change. *Geochimica et Cosmochimica Acta*, **65**.5, 901-913.

Ding, Z.L., Rutter, N.W. & Liu, T. (1993). Pedostratigraphy of Chinese loess deposits and climatic cycles in the last 2.5 Ma. *Catena* **20**, 73–91.

Doeglas, D.J. (1949). Loess: an eolian product. *Journal of Sedimentary Petrology*, **19**:3, 112-117.

Drummond, C.N., Patterson, W.P. & Walker, J.C.G. (1995). Climatic forcing of carbon-oxygen isotopic covariance in temperature-region marl lakes, *Geology*, **23**, 1031-1034.

Elkibbi, M & Rial, J.A. (2001). An outsider's review of the astronomical theory of the climate: is the eccentricity-driven insolation the main driver of the ice ages? *Earth-Science Reviews*, **56**, 161–177.

Emiliani, D. (1954). Depth habitats of some species of pelagic foraminifera as indicated by oxygen isotope ratios. *American Journal of Science*, **252**, 149-158.

Emiliani, C. (1955). Pleistocene temperatures. *Journal of Geology*, **63**, 538-578.

Emiliani, C. (1972). Quaternary Hypsithermals. *Quaternary Research*, **3**, 270-273.

Erickson, J. (1990). *Ice Ages: Past and Future.* TAB Books, Blue Ridge Summit, PA.

Evans, M.E. (2001). Magnetoclimatology of aeolian sediments. *Geophysical Journal International*, **144**:2, 495-497.

Evans, M.E. & Heller, F. (2001). Magnetism of loess-palaeosol sequences: recent developments. *Earth-Science Reviews*, **54**, 129-144.

Evans, M.E. & Heller, F. (2003). *Environmental Magnetism: Principles and Applications of Enviromagnetics*. Academic Press, Elsevier Science, Amsterdam.

Fairbanks, R.G. (1989). A 17,000-year glacio-eustatic sea level record: Influence of glacial melting rates on the Younger Dryas event and deep-ocean circulation. *Nature*, **342**, 637-641.

Farrell, J.W., Pedersen, T.F., Calvert, S.E. & Nielsen, B., (1995). Glacial-interglacial changes in nutrient utilization in the equatorial Pacific Ocean. *Nature*, **377**, 515–517.

Fine, P., Singer, M.J., La Ven, R., Verosub, K., Southard, R.J. (1989). Role of pedogenesis in the distribution of magnetic susceptibility in two Californian chronosequences. *Geoderma*, **44**, 287-306.

Fine, P.,Singer, M.J., Verosub, K.L. & TenPas, J. (1993). New evidence for the origin of ferrimagnetic minerals in loess from China, *Soil Science Society of America Journal*, **57**, 1537-1542.

Flint, R.F. (1971). *Glacial and Quaternary Geology*. John Wiley and Sons, Inc. New York, 892pp.

Folk, R.L. & Ward, W.C. (1957). Brasos River: a study in the significance of grain size parameters. *Journal of Sedimentary Petrology*, **27**, 3-26.

Follmer, L.R. (1983). Sangamon and Winsconsian pedogenesis in the Mid-western United States. In: Late Quaternary Environments of the United States, Vol. I, the Late Pleistocene, (eds: Wright, H.E. & Porter, S.C.). p138-144. Univ. of Minnesota Press, Minneapolis.

Food and Agriculture Organisation of the United Nations (1998). *World reference base for soil resources*. FAO, ISRIC and ISSS, Rome.

Forster, T. & Heller, F., (1997). Magnetic enhancement paths in loess sediments from Tajikistan, China and Hungary. *Geophysical Research Letters*, **24**, 17-20.

Frechen, M., Boenigk, W. & Wiedenfeller, M. (1995). Chronostratigraphie des 'Eiszeitlichen Lößprofils' in Koblenz-Metternich. *Mainzer Geowissenschaftliche Mitteilungen*, **24**, 155-180.

Frechen, M., Horváth, E. & Gábris, G. (1997). Geochronology of Middle and Upper Pleistocene loess sections in Hungary. *Quaternary Research*, **48**, 291-312.

Frechen, M., Oches, E.A. & Kohfeld, K.E. (2003). Loess in Europe – mass accumulation rates during the Last Glacial Period. *Quaternary Science Reviews*, **22**, 1835-1857.

Frechen, M., Schweitzer, U. & Zander, A. (1996). Improvements in sample preparation for the fine grain technique. *Ancient TL*, **14**, 15-17.

Frechen, M., van Vliet-Lanoë, B. and van den Haute, P. (2001). The Upper Pleistocene loess record at Harmignies/Belgium – high resolution terrestrial record of climate forcing. *Palaeogeography, Palaeoclimatology, Palaeoecology*, **173**, 175-195.

Friedman, G.M. & Sanders, J.E. (1978). *Principles of sedimentology*. John Wiley and Sons, Inc. New York.

Funk. J.A., von Dobeneck, T. & Reitz, A. (2004). Integrated rock magnetic and geochemical quantification of redoxomorphic iron mineral diagenesis in Late Quaternary sediments from the equatorial Atlantic. In: Wefer, G., Mulitza, S. & Ratmeyer, V. (eds), 2004, *The South Atlantic in the Late Quaternary: Reconstruction of Material Budgets and Current Systems*. Springer-Verlag, Berlin Heidelberg New York Tokyo, pp 237-260.

Fuhrer, K., Neftel, A., Anklin, M. & Maggi, V. (1993). Continuous measurements of hydrogen peroxide, formaldehyde, calcium and ammonium concentrations along the new GRIP ice core from Summit, Central Greenland. *Atmosphere and Environment*, **12**, 1873-1880.

Galbraith, R.F., Roberts, R.G., Laslett, G.M., Yoshida, H. & Olley, J.M. (1999). Optical dating of single and multiple grains of quartz from Jinmium rock shelter, Northern Australia: Part I, Experimental design and statistical models. *Archaeometry*, **41**, 338–364.

Gale, S.J. & Hoare, P.G. (1991). *Quaternary Sediments: Petrographic methods for the study of unlithified rocks*. Belhaven Press, London.

Gallet, S., John, B. M., and Toril, M. (1996). Geochemical characterization of the Luochuan loess–paleosol sequence, China, and paleoclimatic implications. *Chemical Geology* **133,** 67–88.

Gallet, S., Jahn. B-M., Vliet-Lanoë, B. van, Dia, A. & Rossello, E. (1998). Loess geochemistry and its implications for particle origin and composition of the upper continental crust. *Earth and Planetary Science Letters*, **156, 157-172.**

Gillette, D.A. (1992). Are Changes in Dust Sedimentation to Polar Regions a Sign of Dust Production Due to a Climatic Sensitive Variable or More Efficient Atmospheric Transport? *In* Schwartz, S.E and Slinn, W.G.N. (eds.), *Precipitation Scavenging and Atmosphere-Surface Exchange Processses*, Vol. 3 pp. 1719-1732. Hemisphere Publishing Corp., Taylor & Francis Group, Washington.

Gillette, D. A., Blifford, I.H.D. & Fryrear, D.W. (1974). The influence of wind velocity on the size distributions of aerosols generated by the wind erosion of soils. *Journal of Geophysical Research,* **79 (27),** 4068–4075.

Grahmann, R. (1932). Der Löss in Europa [trans: Loess in Europe]. *Gesellschaft für Erdkunde zu Leipzig Mitteilungen*, 5–24.

Grimley, D.A., Follmer, L.R. & McKay, E.D. (1998). Magnetic susceptibility and mineral zonation controlled by provenance in loess along the Illinois and Central Mississippi river valleys. *Quaternary Research*, **49,** 24-36.

Grootes, P.M., Stuiver, M., White, J.W.C., Johnson, S. & Jouzel, J. (1993). Comparison of oxygen isotope records from the GISP2 and GRIP Greenland ice cores. *Nature*, **366, 552-554.**

Gross, G.A., Gower, C.F. & Lefebure, D.V. (1998). Magmatic Ti-Fe±V oxide deposits. *Geological Fieldwork 1997*, British Columbia Ministry of Employment and Investment, Paper 1998-1, pages 24J-1 to 24J-3. Cited 16/2/2005, available at World Wide Web URL:

<http://www.em.gov.bc.ca/Mining/Geolsurv/MetallicMinerals/MineralDepositProfiles/profiles/m04.htm>

Green, J.R. & Margerison, D. (1978). *Statistical treatment of experimental data*. Elsevier Scientific, New York.

GRIP Members (1993). Climate instability during the last interglacial period recorded in the GRIP ice core. *Nature*, **364**, 203-207.

Gullentops, F. (1954). Contribution á la chronologie du Pleistocène et des formes de relief en Belgique. *Memoires de l'Institute Géologique de l'Université de Louvain*, **118**, 223-240.

Gullentops, F. (1981). About the climate of the last glaciation in NW Europe. In '*Symposium on Quaternary Climatic Variations*', Université catholique Louvrain, 22.

Haase, K.M., Goldschmidt, B & Garbe-Schonberg, C.D. (2004). Petrogenesis of Tertiary continental intra-plate lavas from the Westerwald region, Germany. *Journal of Petrology*, **45**.5, 883-905.

Haesaerts, P. (1973). Contribution à la stratigraphie des dépôts du Pléistocène Supérieur du bassin de la Haine. [trans: Contribution to the stratigraphy of Upper Pleistocene deposition in the Haine basin]. Doctoral Thesis (in French), unpublished. Free University of Brussels.

Haesaerts, P., Juvigné, E, Kuyl, O, Mücher, H. & Roebroeks, W. (1981). Compte rendu de l'excursion du 12 Juin 1981, en Hesbaye et au Limbourg Nèederlandais, consacrée a la chronostratigraphie de loess du Pléistocène Supérieur. [trans: Account of the 12 June 1981 trip to Hesbaye and to Dutch Limbourg, to examine the chronostratigraphy of the Upper Pleistocene loess]. *Annales de la Societé Géologique de Belgique*, **104**, 223-240.

Heasaerts, P., Mestdagh, H. & Bosquet, D. (1999). The sequence of Remicourt, (Hesbaye, Belgium): New insights on the pedo- and chronostratigraphy of the Rocourt Soil. *Geologica Belgica*, **2/3**, 5-27.

Haesaerts, P. & van Vliet, B. (1973). Evolution d'un permafrost dans les limons du Dernier Glaciation à Harmignies [trans: The development of a permafrost in last-Glacial Harmignies silt]. *Bulletin Association Francaişe pour L'etude du Quatrenaire,* **3,** 151-164.

Haesaerts, P. & van Vliet-Lanoë, B., (1974). Comte rendu de l'excursion du 25 Mai consacrée à la stratigraphie des limons aux environs de Mons [trans: Account of the 25 May trip to examine the stratigraphy of silts in the Mons region.]. *Annals de Societé Géologique de Belgique,* **97,** 105-137.

Hahn, C. (1969). Mineralogisch-sedimentpetrographische Untersuchungen an den Flussbettsanden im Einzugsbereich des *Alpenrheins* [trans: Mineralogical/ sedimentological/petrographic investigation of fluvial sediments in the catchment area of the alpine Rhine]. *Eclog. geol. Helv.* **62**(1), 227- 78.

Hall, M.J. (1988). Comparison of Spectrex laser particle counter with Coulter counter and pipette sizing methods. *Geological Society of America Bulletin,* **20**:24.

Hammer, C.U. (1980). Acidity of polar ice cores in relation to absolute dating, vulcanism, radio-echoes. *Journal of Glaciology,* **25**(93), 359-372.

Hammer, C.U. (1984). Traces of Icelandic eruptions in the Greenland Ice Sheet. *Jokull,* **34,** 51-65.

Hammer, C. U., Clausen H. B. Dansgaard, W., Gundestrup, N, Johnsen, S.J. & Reeh, N. (1978). Dating of Greenland ice cores by flow models, isotopes, volcanic debris and continental dust. *Journal of Glaciology*. **20**(82), 3-26.

Hammer, C.U., Clausen, H.B., Dansgaard, W., Neftel, A., Kristinsdóttir, P. & Johnson, E. (1985). Continuous Impurity Analysis along the Dye 3 Deep Core. In Langway, C.C., Oeschger, H & Dansgaard, W (eds). Greenland Ice Core: Geophysics, Geochemistry and the Environment: *American Geophysical Union Monograph,* **33,** 77-84.

Hansel, A.K. & Johnson, W.H. (1996). Wedon and Mason Groups: Lithostratigraphic reclassification of deposits of the Winsconsin Episode, Lake Michigan Lobe Area. *Illinois State Geological Survey Bulletin,* **104**.

Haq, B., Hardenbol, J. & Vail, P.R. (1987). Chronology of fluctuating sea levels since the Triassic. *Science,* **235,** 1156-1167.

Hardcastle, I. (1890). On the Timaru loess as a climatic register. *Transactions of the New Zealand Institute,* **23,** 324-332.

Harris, S.E. & Mix, A.C., (1999). Pleistocene precipitation balance in the Amazon Basin recorded in deep-sea sediments. *Quaternary Research,* **51,** 14-26.

Hatté, C., Antoine, P, Fortugne, M. Lang, A, Rousseau, D-D. & Zöller, L. (2001). $\delta^{13}C$ of loess organic matter as a potential proxy for palaeoprecipitation. *Quaternary Research,* **55,** 33–38.

Hatté, C., Pessenda, L.C., Fortugne, M., Zöller, L., Antoine, P. & Rousseau, D. (1999). *^{14}C AMS dating of loess organic matter of Nussloch loess sequence (Rhine Valley, Germany).* Loessfest, 1999. University of Bonn, Germany.

Hatté, C., Pessenda, L.C., Lang, A. & Paterne, M. (2001). Development of an accurate and reliable ^{14}C chronology for loess sequences, Application to the loess sequence of Nussloch (Rhine Valley, Germany). *Radiocarbon,* **43,** 611-618.

Hayden, F.V. (1858). Explanations of a second edition of a geological map of Nebraska and Kansas, based upon information obtained in an expedition to the Black Hills. *Proceedings of the Academy of Natural Sciences of Philadelphia* 139-158.

Hays, J.D., Imbrie, J. & Shackleton, N. J. (1976) Variations in the Earth's Orbit: Pacemaker of the Ice Ages. *Science.* **194,** 1121-1132.

Heinrich, H. (1988). Origin and consequences of cyclic ice rafting in the northeast Atlantic Ocean during the last 130,000 years. *Quaternary Research,* **29,** 142-152.

Heller, F & Liu, T.S. (1982). Magnetostratigraphical dating of loess deposits in China. *Nature,* **300,** 431-433.

Heller, F & Liu, T.S. (1984). Magnetism of Chinese loess deposits. *Geophysical Journal, Royal Astronomical Society,* **77,** 121-141.

Heller, F & Liu, T.S., (1986). Palaeoclimate and sedimentary history from magnetic susceptibility of loess in China. *Geophysical Research Letters*, **13**, 1169-1172.

Heider, F., Zitselsberger, A, & Fabian, K. (1996). Magnetic susceptibility and remanent coercive force in grown magnetite crystals from 0.1 μm to 6 mm. *Phys. Earth Planet. Int.* **93**, 239-256.

Heiri, O., Lotter, A.F. & Lemke, G. (2001). Loss on ignition as a method for estimating organic and carbonate content in sediments: reproducibility and comparability of results. *Journal of Palaeolimnology* **25**, 101-110.

Heslop, D., Langereis, C.G. & Dekkers, M.J. (2000). A new astronomical timescale for the loess deposits of Northern China. *Earth and Planetary Science Letters*, **184**, 125-139.

Hinnov, L.A. & Park, J.J. (1999). Strategies for assessing Early-Middle (Pliensbachian-Aalenian) Jurassic cyclochronologies. *Philosophical Transactions of the Royal Society of London,* **357**, 1831-1859.

Honda, M. & Shimuzu, H. (1998). Geochemical, mineralogical and sedimentological studies on the Taklimakan Desert sands. *Sedimentology*, **45**, 1125-1143.

Hounslow, M.W. & Morton, A.C. (2004). Evaluation of sediment provenance using magnetic mineral inclusions in clastic silicates: comparison with heavy mineral analysis. *Sedimentary Geology*, **171**, 13-36.

Huijzer, B. & Vandenberghe, J. (1998). Climatic reconstruction of the Weichselian Pleniglacial in northwestern and central Europe. *Journal of Quaternary Science*, **13.5**, 391-417.

Huisman, D.J. & Kiden, P. (1997) A geochemical record of Late Cenozoic sedimentation history in the southern Netherlands. *Geologie en Mijnbouw (Geology and Mining)* **76.4**, 277-291.

Huisman, D.J., Klaver, G.T., Veldkamp, A & van Os, B.J.H. (2000). Geochemical compositional changes at the Pliocene-Pleistocene transition in fluviodeltaic deposits in the

Tegelen-Reuver area (southeastern Netherlands). *International Journal of Earth Sciences*, **89**.1, 154-169.

Huntley, D.J., Godfrey-Smith, D.I. and Thewalt, M.L.W. (1985). Optical dating of sediments. *Nature*, **313**, 105-107.

Hus, J.J & Geeraerts, R. (1999). Palaeomagnetic and rock magnetic properties of loess/palaeosol sequences in Belgium. *Geologica Belgica*, **2** (1-2), 89-97.

Hütt, G., Jaek, I. & Tchonka, J. (1988). Optical dating: K-feldspars optical response stimulation spectra. *Quaternary Science Reviews*, **7**, 381-386.

Iishi, T, Isobe, I., Misuta, K., Kanai, Y., Matsuhisa, Y., Mizota, C., Qian, Y., Terashima, S & Okumura, K. (1995). Study of the formation process and sedimentary environment of surface geological features in desertic areas of China, with special reference to the characteristics and origin of eolian sediments. *Bulletin of the Geological Survey of Japan*, **46**, 651-685.

Ikinger, A. & Schirmer, W. (eds.) (2002). Loess units and solcomplexes in the Niederrhein and Maas area. *Terra Nostra*, **1**.

Imbrie, J. (1982). Astronomical theory of the Pleistocene ice ages: a brief historical review. *Icarus*, **50**, 408– 422.

Imbrie, J., Hays, J.D., Martinson, D.G., McIntyre, A., Mix, A.C., Morley, J. J., Paces, N. G., Prell, W. L. & Shackleton, N. J. (1984). The orbital theory of Pleistocene climate: Support from a revised chronology of the marine $\delta^{18}O$ record. In: A. Berger (ed.) *Milankovitch and Climate,* Part *I*, 269-305, D. Reidel, Norwell, Mass.

International Climate Change Taskforce (2005). *Meeting the Climate Challenge.* The Institute for Public Policy Research, London.

Iriondo, M. (1994). The Quaternary of Ecuador. *Quaternary International*, **21**, 101-112.

Iriondo, M. & Kröhling, D. (2004). "New" types of loess, not related to glaciation. Int. Workshop HWK Delmenhorst 15-18 April 2004. Cited 21.9.2004, available at World Wide Web URL:
<http://www.pangaea.de/Projects/PASSED/Downloads/iriondo_kroehling.pdf>

Jackson, M.L., Sayin, M. & Clayton, R.N. (1976). Hexafluorosilicic acid reagent modification for quartz isolation. *Soil Science of America Journal*, **40**, 958-960.

Jahn, B.M., Gallet, S. and Han, J. (2001). Geochemistry of the Xining, Xifeng and Jixian sections, Loess Plateau of China: eolian dust provenance and paleosol evolution during the last 140 ka. *Chemical Geology*, **178**, 71-94.

Jansen, E., Bleil, U., Henrich, R., Kringstad, L. & Slettemark, B. (1988). Palaeoenvironmental changes in the Norwegian Sea and the northeast Atlantic during the last 2.8 m.y.: Deep Sea Drilling Project/Ocean Drilling Project sites 610, 642, 643 and 644. *Palaeoceanography*, **3**, 563-581.

Jefferson, I.F., Evstatiev, D., Karastanev, D., Mavlyanova, N.G. & Smalley, I.J. (2003). Engineering geology of loess and loess-like deposits: a commentary on the Russian literature. *Engineering Geology*, **68**, 333-351.

Jenny H. (1941). *Factors of Soil Formation*. McGraw-Hill, New York.

Johnsen, S.J., Clausen, H.B., Dansgard, W, Fuhrer, K., Gundestrup, N, Hammer, C. U., Ivensen, P., Jouzel, J., Stauffer, B. & Steffensen, J. P. (1992). Irregular glacial interstadials recorded in a new Greenland ice core. *Nature*, **359**, 311-313.

Johnsen, S.J., Dahl-Jensen, D., Dansgaard, W., Gundestrup, N. S. (1995). Greenland temperatures derived from GRIP borehole and ice core isotope profiles. *Tellus series*, **B47**, 624-629.

Juvigné, E & Moors, C. (1995). Geochimie et minerologie du loess de moyenne Belgique oriental [trans: Geochemistry and mineralogy of eastern central Belgian loess]. *Quaestiones Geographicae*, Special Issue **4**, 125-132.

Kasse, C. (1997). Cold-climate aeolian sand-sheet formation in north-western Europe (c. 14-12.4 ka): a response to permafrost degradation and increased aridity. *Permafrost and Periglacial Processes*, **8**.3, 295-311.

Kemp, R.A. (2001). Pedogenic modification of loess: significance for palaeoclimatic reconstructions. *Earth-Science Reviews*, **54**:1-3, 145-156.

Kemp, R.A. & Derbyshire, E. (1998). The loess soils of China as records of climatic change. *European Journal of Soil Science*, **49**, 525-539.

Kemp, R.A. & Zárate, M.A. (2000). Pliocene pedosedimantary cycles in the southern Pampas, Argentina. *Sedimentology*, **47**, 3-14.

Kennedy, G.C. & Knopf, L. (1960). Dating by thermoluminescence. *Archaeology*, **13**, 147-148.

King, J.W., Banerjee, S.K., Marvin, J.A. & Ozdemir, O. (1982). A comparison of different magnetic methods for determining the relative grain size of magnetite in natural materials: some results from lake sediments. *Earth and Planetary Science Letters*, **59**, 404–419.

Kletetschka, G. & Bannerjee, S.K. (1995). Magnetic stratigraphy of Chinese loess as a record of natural fires. *Geophysical Research Letters*, **22**, 1341-43.

Konert, M. & Vandenberghe, J. (1997). Comparison of laser grain size analysis with pipette and sieve analysis: a solution for the underestimation of the clay fraction. *Sedimentology* **44** (3), 523-535.

Kruiver, P.P. & Passier, H.F. (2001). Coercivity analysis of magnetic phases in sapropel S1 related to variations in redox conditions, including an investigation of the S ratio. *Geochemistry, Geophysics, Geosystems: an electronic journal of the earth science*, **2**, Paper number 2001GC000181. Cited 21 November 2004, available at WorldWide Web URL: < http://www.agu.org/journals/gc/

Kukla, G. (1987). Loess stratigraphy in central China. *Quaternary Science Reviews*, **6**, 191–219.

Kukla, G., (2000). The last interglacial, *Science*, **287**, 987-989.

Kukla, G & An, Z.S. (1989). Loess stratigraphy in central China. *Palaeogeography, Palaeoclimatology and Palaeoecology*, **72**, 203-225.

Kukla, G., An, Z.S., Melice, J.L., Gavin, J & Xiao, J.L., (1990). Magnetic susceptibility record of Chinese loess. *Transactions, Royal Society of Edinburgh, Earth Sciences*. **81**, 263-288.

Kukla, G., Heller, F., Liu, X. M., Xu, T. C. & An, Z.S. (1988). Pleistocene climates in China dated by magnetic susceptibility. *Geology*, **16**, 811-814.

Kukla, G. & Kocí, A. (1972). End of the Last Interglacial in the Loess Record. *Quaternary Research* **2**, 374-83.

Kukla, G. & Matthews, R. (1972). When Will the Present Interglacial End? *Science* **178**, 190-91.

Kukla, G, Matthews, R. & Mitchell, J.M. (1972). The end of the present interglacial. *Quaternary Research*, **2**, 261- 269.

Lambeck, K. & Chappell, J. (2001). Sea level change through the last glacial cycle. *Science* **292**, 679–686.

Lambeck, K., Y. Yokoyama, Y. & Purcell, T. (2002). Into and out of the Last Glacial Maximum: sea-level change during Oxygen Isotope Stages 3 and 2. *Quaternary Science Reviews*, **21**, 343-360.

Lang, A., Bork, H-R., Mäckel, R., Preston, N., Wunderlich, J & Dikau, R. (2003). Changes in sediment flux and storage within a fluvial system: some examples from the Rhine catchment. *Hydrological Processes*, **17**, 3321–3334.

Lautridou, J.P. (1985). Le cycle périglaciaire Pléistocène en Europe du Nord-Ouest et plus particulièrement en Normandie [trans: The Pleistocene periglacial cycle in northwest Europe, particularly Normandy]. These Doctoral, Etat Univ. Caen, Caen, 908pp.

Lautridou, J.P. (1990). A propos des relations entre les formations marines Pléistocène et les loess normands [trans: Concerning the relationship between Pleistocene marine formations and Normandy loess].. *Revue Archeologique de l'Oest, Supplement 2*. 41-44.

Le Borgne, E. (1955). Susceptibilite magnetique anormale du sol superficial [trans: Anomalous magnetic susceptibility in topsoils]. *Annales de Geophysique*, **11**, 399-419.

Lebret, P.& Lautridou, J-P. (1991). The loess of West Europe. *Geojournal*, **24**.2, 151-156.

Lericolais, G., Auffret, J.P., Bourillet, J.F. (2003). The Quaternary Channel River: seismic stratigraphy of its palaeo-valleys and deeps. *Journal of Quaternary Science*, **18**, 245–260.

Leuschner, D.C. & Sirocko, F. (2000). The low-latitude monsoon climate during Dansgaard-Oeschger cycles and Heinrich Events. *Quaternary Science Reviews*, **19**, 243-254.

Linell, K.A. & Tedrow, J.C.F. (1981). Soil and permafrost surveys in the Arctic. Clarendon Press, Oxford, 279p.

Lisiecki, L.E. & Raymo, M.E. (2005). A Pliocene-Pleistocene stack of 57 globally distributed benthic $\delta^{18}O$ records. *Palaeoceanography*, **20**. In press. Cited 16.3.2005, available at World Wide Web URL:
<http://www.geo.brown.edu/geopeople/grads/lisiecki/LisieckiRaymo2005.pdf>

Liu, Q., Banerjee, S.K., Jackson, M.J., Deng, C, Pan, Y. & Zhu, R. (2005). Inter-profile correlation of the Chinese loess-palaeosol sequences during Marine Oxygen Isotope Stage 5 and indications of pedogenesis. *Quaternary Science Reviews*, **24**:1-2, 195-210.

Liu, T. S. (1991). *Loess, Environment and Global Changes*. Beijing, Science Press, (in Chinese).

Liu, T.S. (1966). *Composition and texture of loess*. Science Press, Beijing, 132p.

Liu, T.S., An, Z. S., Yuan, B & Han, J. (1985). The loess-palaeosol sequence in China and climatic history. *Episodes*, 8, 21-27.

Liu, T. S., Zhang, S. & Han, J. (1986). Stratigraphy and paleoenvironmental changes in the loess of central China. *Quaternary Science Reviews*, **5**, 489–495.

Liu, X.M., Hesse, P. & Rolph, T. (1999). Origin of maghaemite in Chinese loess deposits: aeolian or pedogenic? *Physics of Earth and Planetary Interiors*, **112**, 191–201.

Liu, X.M., Hesse, P., Begét, J. & Rolph, T. (2001). Pedogenic destruction of ferrimagnetics in Alaskan loess deposits. *Australian Journal of Soil Research*, **39.1**, 99-115.

Loizeau, J.L., Arbouille, D., Santiago, S. & Vernet, J.P. (1994). Evaluation of wide-range laser diffraction grain size analyser for use with sediments. *Sedimentology*, **41**, 353–361.

Lorenz, E.N. (1972). *Predictability - does the flap of a butterfly's wings in Brazil set off a tornado in Texas?* The American Association for the Advancement of Science, Washington, D.C. In: Lorenz, E.N. (1993), *The Essence of Chaos*. U.C.L. Press, London.

Lorenz, E.N. (1991). Chaos, spontaneous climatic variations and detection of the greenhouse effect. In: Schlesinger, M.E. (ed.), (1991), *Greenhouse-Gas-Induced Climate Change: A Critical Appraisal of Simulations and Observations*, Elsevier, Amsterdam, 445-453.

Lorius C, Jouzel, J., Ritz, C., Merlivat, L & Barkov, N. (1985). A 150,000-year climatic record from Antarctic ice. *Nature* **316**(6209), 591-596.

Loutre, M.F. & Berger, A. (2000). Future climatic changes: are we entering an exceptionally long interglacial? *Climatic Change*, **46**, 61-90.

Loutre, M.F. & Berger, A. (2003). Marine Isotope Stage 11 as an analogue for the present interglacial. *Global and Planetary Change*, **36**, 209-217.

Lovley, D.R., Stolz, J.F., Nord, G.L. & Phillips, E.J.P. (1987). Anaerobic production of magnetite by a dissimilatory iron-reducing microorganism. *Nature*, **330**, 252-254.

Lowe, J.J. (2001). Climatic oscillations during the last glacial cycle – nature, causes and the case for synchronous effects. *Biology and Environment: Proceedings of the Royal Irish Academy*, **101B**.1-2, 19-33.

Lowrie, W. (1990). Identification of ferromagnetic minerals in a rock by coercivity and unblocking temperature properties. *Geophysical Research Letters*, **17**, 159-162.

Lu, H., Zhang, F., Xiaodong Liu X, & Duce, R.A. (2004). Periodicities of palaeoclimatic variations recorded by loess-paleosol sequences in China *Quaternary Science Reviews*, **23**, 1891-1900.

Lyell, C. (1834). Observation on the loamy deposit called 'loess' of the basin of the Rhine. *Edinburg New Philosophical Journal*, **17**, 118-120.

Mader, D. (1982). Aeolian sands in continental red beds of the Middle Buntsandstein (Lower Triassic) at the western margin of the German Basin. *Sedimentary Geology*, **31**, 191-230.

Maher, B.A. (1986). Characterisation of soils by mineral magnetic measurements. *Physics of the Earth and Planetary Interiors*, **42**, 76-92.

Maher, B.A. (1988). Magnetic properties of modern soils and Quaternary loessic palaeosols: palaeoclimatic implications. *Palaeogeography, Palaeoclimatology, Palaeoecology*, **137**, 25-54.

Maher, B. (1999). Comments on "Origin of the magnetic susceptibility signal in Chinese loess". *Quaternary Science Reviews*, **18**, 865-869.

Maher, B.A. & Thompson, R. (1988). The formation of ultrafine magnetite in soils. *Nature*, **336**, 368-370.

Maher, B.A. & Thompson, R. (1991). Mineral magnetic record of the Chinese loess and palaeosols. *Geology*, **19**, 3-6.

Maher, B.A. & Thompson, R. (1992). Palaeoclimatic significance of the mineral magnetic record of the Chinese loess and palaeosols. *Quaternary Research*, **37**, 155-170.

Maher, B.A., & Thompson, R. (1995). Palaeorainfall reconstructions from pedogenic magnetic susceptibility variations in the Chinese loess and palaeosols. *Quaternary Research* **44**, 383–391.

Maher, B.A., Thompson, R. & Hunslow, M.W. (1999). 'Introduction', in Maher, B.A. & Thompson, R. (eds), *Quaternary Climates, Environments and Magnetism*, Cambridge University Press, Cambridge, U.K., pp. 1–48.

Mangerud, J., Anderson, S.T., Berglund, B.E. & Donner, J.J. (1974). Quaternary stratigraphy of Norden, a proposal for terminology and classification. *Boreas*, **4**, 109–128.

Martinson, D.G., Pisias, N.G., Hays, J.D., Imbrie, J., Moore, T.C., Jr. & Shackleton, N.J. (1987). Age dating and the orbital theory of the ice ages: development of a high-resolution 0 to 300,000-year chronostratigraphy. *Quaternary Research*, **27**, 1–29.

Maslin, M.A., Li, X.S., Loutre, M.F. & Berger, A. (1998). The contribution of orbital forcing to the progressive intensification of Northern Hemisphere glaciation. *Quaternary Science Reviews*, **17**, 411-426.

Matsuhisa, Y, Mizota, C., Faure, K & Yibing, Q. (1996). Homogenisation processes of fine particles in the arid regions of western China, inferred from oxygen isotope composition of quartz. *The Todai International Symposium on Cosmochronology and Isotope Geoscience, Abstracts*, 29-32.

Mayewski , P.A. & Bender, M. (1995). The GISP2 ice core record - paleoclimate highlights. *Reviews of Geophysics*. **33**:1. Cited 2.11.2004 at World Wide Web URL: <http://www.agu.org/revgeophys/mayews01/mayews01.html>

McDuff, R. (2001). Marine Geological Processes: phase relationships of proxy variables. University of Washington. Cited 20.10.2004 at World Wide Web URL: <http://www2.ocean.washington.edu/oc540/lec01-26/>

McLennan, S.M. (1989). Rare earth elements in sedimentary rocks: Influence of provenance and sedimentary processes. *Reviews in Mineralogy*, **21**, 169-200.

McManus, J.F. (2004) A great grand-daddy of ice cores. *Nature*, **429**, 611-612.

McTainsh, G.H., Nickling, W.G. & Lynch, A.W. (1997). Dust deposition and particle size in Mali, West Africa. *Catena* **29**, 307–322.

McTainsh, G. & Walker, P.H. (1982). Nature and distribution of Harmattan dust. *Zeitschrift für Geomorphologie*, **26**, 417-436.

Meng, X.M., Derbyshire, E. & Kemp, A. (1997). Origin of the magnetic susceptibility signal in Chinese loess. *Quaternary Science Reviews*, **16**, 833-839.

Meyer, W. & Stets, J. (2002). Pleistocene to Recent tectonics in the Rhenish Massif (Germany). *Netherlands Journal of Geosciences/Geologie en Mijnbouw*, **81.2**, 217-221.

Mie, G. (1908). Beiträge zur Optik truüber Medien, speziell kolloidaler Metallosungen, *Ann. Phys.* **25**, 377–445.

Milankovitch, M. (1920). *Théorie Mathématique des Phénomènes Produits par la Radiation Solaire.* Gauthier-Villars, Paris.

Milankovitch, M. (1941). *Canon of Insolation and the Ice-Age Problem.* Royal Serbian Acad. Sp. Pub. 132, Royal Serbian Academy, Belgrade, Yugoslavia.

Mizutanu, S. and Suwa, K. (1966). Orthoquartzitic sand from the Libyan desert, Egypt. *Journal of Earth Science*, **14**, 137-150.

Moore, K.M & Oches, E.A. (2002). *Aminostratigraphy of the last glacial cycle loess of Europe.* Presented to North-Central Section (36th) and Southeastern Section (51st), GSA Joint Annual Meeting (April 3–5, 2002). Cited 4.3.2005, available at World Wide Web URL:
< http://gsa.confex.com/gsa/2002NC/finalprogram/abstract_32408.htm>

Morrás, H.J.M. (1995). Mineralogy and cation exchange capacity of the fine silt fraction in two soils from the southern Chaco region (Argentina). *Geoderma*, **64**, 281-285.

Morrás, H.J.M. (1999). Geochemical differentiation of Quaternary sediments from the Pampean region based on soil phosphorous contents as detected in the early 20th century. *Quaternary International*, **62**, 57-67.

Morrison, R.B. (1978). Quaternary Soil Stratigraphy - Concepts, Methods and Problems. In *Quaternary Soils*, edited by W.C. Mahaney, pp. 77-108. Geo Abstracts, University of East Anglia, Norwich, England.

Mudelsee, M., & Stattegger, K. (1997). Exploring the structure of the Mid-Pleistocene Revolution with advanced methods of time series analysis. *Geologische Rundschau*, **86**, 499-511.

Muhs, D.R. (1984). Intrinsic thresholds in soil systems. *Physical Geography*, **5**, 99-110.

Muhs, D.R. & Bettis, E.A.III. (2000). Geochemical variations in Peoria loess of western Iowa indicate paleowinds of midcontinental North America during last glaciation. *Quaternary Research*, **53**, 49-61.

Muhs, D.R., Ager, T.A., Bettis, E.A., III, McGeehin, J., Been, J.M., Begét, J.E., Pavich, M.J., Stafford, T.W., Jr., & Stevens, D.S.P. (2003). Stratigraphy and paleoclimatic significance of late Quaternary loess-paleosol sequences of the last interglacial-glacial cycle in central Alaska. *Quaternary Science Reviews*, **22**, 1947-1986.

Muhs, D.R., Bettis, E.A.III, Been, J & McGeehin, J.P. (2001). Impact of climate and parent material on chemical weathering in loess-derived soils of the Mississippi river valley. *Soil Science Society of America Journal*, **65**, 1761-1777.

Muhs, D.R., Bush, C.A., Stewart, K.C., Rowland, T.R., and Crittenden, R.C. (1990). Geochemical evidence of Saharan dust parent material for soils developed on Quaternary limestones of Caribbean and western Atlantic islands. *Quaternary Research*, **33**,157-177.

Muhs, D.R., McGeehin, J.P., Beann, J. & Fisher, E. (2004). Holocene loess deposition and soil formation as competing processes, Matanuska Valley, southern Alaska. *Quaternary Research*, **61**, 265-276.

Muhs, D.R. & Zárate, M. (2001). Late Quaternary aeolian records of the Americas and their palaeoclimatic significance. In: Markgraf, V. (ed.), *Interhemispheric Climate Linkages*, pp183-216. Academic Press.

Murray, A.S. & Olley, J.M. (2002). Precision and accuracy in the optically stimulated luminescence dating of sedimentary quartz: a status review. *Geochronometria*, **21**, 1-16.

Murray, A.S. & Wintle, A. G. (2000). Luminescence dating of quartz using an improved single-aliquot regenerative-dose protocol. *Radiation Measurements*, **32**, 57-73.

Murray, R.W., Miller, D.J. & Kryc, K.A. (2000). Analysis of major and trace elements in rocks, sediments, and interstitial waters by inductively coupled plasma-atomic emission spectrometry (ICP-AES). *ODP Tech. Note,* 29 [Online]. Cited 30.11.2004, available from World Wide Web URL:
<http://www-odp.tamu.edu/publications/tnotes/tn29/INDEX.HTM>.

Nawrocki, J, Wojcik, A & Bogucki, A. (1996). The magnetic susceptibility record in the Polish and western Ukraine loess-palaeosol records conditioned by palaeoclimate. *Boreas*, **25**, 161-189.

Neftel, A., Oeschger, H., Schwander, J., Stauffer, B. & Zumbrunn, R. (1982). Ice core sample measurements give atmospheric CO_2 content during the past 40,000 yr. *Nature* **295**, 220-323.

Nesbitt, H.W., (1979). Mobility and fractionation of rare earth elements during weathering of a granodiorite. *Nature*, **279**, 206-210.

Nesbitt, H.W., Markovis, G. & Price, R.C. (1980). Chemical processes affecting alkaline earths during chemical weathering. *Geochim Cosmochim Acta* **44**: 1659-1666.

Nesbitt, H.W, & Young, G.M. (1982). Early Proterozoic climates and plate motions inferred from major element chemistry of lutites. *Nature*, **299**, 715-717.

Nesbitt, H.W. & Young, G.M. (1984). Prediction of some weathering trends of plutonic and volcanic rocks based on thermodynamic and kinetic considerations. *Geochimica et Cosmochimica Acta* **48**, 1523–1534.

Nesbitt, H.W. & Young, G.M. (1989). Formation and diagenesis of weathering profiles, *Journal of Geology*, **97**, 129–147.

Nesbitt, H.W., Young, G.M., McLennan, S.M. & Keays, R.R. (1996). Effects of chemical weathering and sorting on the petrogenesis of siliciclastic sediments, with implications for provenance studies, *Journal of Geology*, **104**, 525–542.

Nesbitt, H.W., Markovics, G. & Price, R.C. (1980). Chemical processes affecting alkalis and alkaline earths during continental weathering. *Geochimica et Cosmochimica Acta*, **44**. 1659-1666.

NGRIP members (Andersen, K.K., Azuma, N., Barnola, J-M., Bigler, M., Biscaye, P., Caillon, N., Chappellaz, J., Clausen, H.B., .Dahl-Jensen, D H., Fischer, H., Fluckiger, J, Fritzsche, D., Fujii, Y., Goto-Azuma, Y., Grønvold, Y.K., Gundestrup, N.S., Hansson, M., Huber, C., Hvidberg, C.S., Johnsen, S.J., Jonsell, U., Jouzel, J., Kipfstuh, S., Landais, A., Leuenberge, M., Lorrain, R., Masson-Delmotte, V., Miller, H., Motoyama, H., Narita, H., Popp, T., Rasmussen, S.O., Raynaud, D., Rothlisberger, R., Ruth, U., Samyn, D., Schwander, J., Shoji, H., Siggard-Andersen, M-L., Steffensen, J.P., Stocker, T., Sveinbjornsdottir, A.E., Svensson, A., Takata, M., Tison, J-L., Thorsteinsson, Th., Watanabe, O., Wilhelms, F.& White. J.W.C.) (2004). High-resolution record of Northern Hemisphere climate extending into the last interglacial period. *Nature*, **431**, 147-150.

Oches, E.A., & Banerjee, S.K. (1996). Rock magnetic proxies of climate change from loess-paleosol sediments of the Czech Republic. *Studia Geophysica et Geodaetica*, **40**, 287–300.

Oches, E.A., McCoy, W.D., Walther, R, Horvath, E & Markovic, S.B. (2004). *Amino-acid racemization in fossil gastropods from central European loess: Arrhenius parameters, palaeotemperatures and ground-temperature controls*. Presented to GSA 2004 Denver Annual Meeting (November 7–10, 2004). Cited 4.3.2005, available at World Wide Web URL:
<http://gsa.confex.com/gsa/2004AM/finalprogram/abstract_81079.htm>

Oeschger, H. (1985). The contribution of ice core studies to the understanding of environmental processes. Greenland Ice Core: Geophysics, Geochemistry, and the Environment. Langway, C.C., Oeschger, H. & Dansgaard, W., eds. *Geophysical Monograph, American Geophysical Union*, **33**, 9-17.

Oeschger, H., J. Beer, U. Siegenthaler, B. Stauffer, W. Dansgaard, and C.C. Langway, Jr. (1984). Late glacial climate history from ice cores. *Climate Processes and Climate Sensitivity. Geophysical. Monograph, American Geophysical Union*, **29**, 299-306.

Opdyke, N & Channell, J. (1996). *Magnetic Stratigraphy, International Geophysics series, 64*. Academic Press Inc. San Diego, 346pp.

Oppo, D.W., McManus, J.F. & Cullen, J.L. (1998). Abrupt climate events 500,000 to 340,000 years ago: evidence from sub-polar north Atlantic sediments. *Science*, **279**, 1335-1338.

Paillard, D. & Parrenin, F. (2004). The Antarctic ice sheet and the triggering of deglaciations. *Earth and Planetary Science Letters*, **227**:3-4, 263-271.

Pécsi, M. (1968). Loess. In: *The Encyclopaedia of Geomorphology* (ed. Fairbridge, R.W.), pp 674-678. Reinhold, New York.

Pécsi, M. (1990). Loess in not just the accumulation of dust. *Quaternary International*, **7.8**, 1-21.

PerkinElmer (1997). *The Optima 3000 family of Inductively Coupled Plasma Optical Emission Spectrometers*. PerkinElmer Instruments LCC, USA.

PerkinElmer (2000). *Optima 4000 Series: hardware guide*. PerkinElmer Instruments LCC, USA.

Peters, C., & Dekkers, M.J. (2003). Room temperature magnetic parameters as a function of concentration, grain size and mineralogy. *Phys. Chem. Earth*, **28**, 659–667.

Petit, J.R. (1990). Paleoclimatological and chronological implications of the Vostok core dust record. Nature, **343**, 56-58.

Petit, J.R., Briat, M. & Royer, A. (1981). Ice age aerosol content from east Antarctica ice core samples and past wind strength. *Nature*, **293**, 391-394.

Petit, J.R., Jouzel, J., Raynaud, D., Barkov, N.I., Barnola, J-M., Basile, I., Bender, M., Chappellaz, J., Davis, M., Delaygue, G., Delmotte, M., Kotlyakov, V.M., Legrand, M., Lipenkov, V.Y., Lorius, C., Pepin, L., Ritz, C., Saltzman, E. and Stievenard, M. (1999). Climate and atmospheric history of the past 420,000 years from the Vostok ice core, Antarctica. *Nature,* **399**, 429-436.

Porter, S. C., & Zhisheng, A. (1995). Correlation between climate events in the North Atlantic and China during the last glaciation. *Nature*, **375**, 305–308.

Porter, S.C. & An, Z.S. (1995). Correlation between climate events in the North Atlantic and China during the last glaciation. *Nature*, **375**, 305-308.

Potts, P.J., Tindle, A.G. & Webb, P.C. (2000). *Geochemical reference material compositions*. Whittles Publishing, UK.

Powers, M. C. (1953). A new roundness scale for sedimentary particles: *Journal of Sedimentary Petrology*, **23**, 117–119.

Preece, S.J., Westgate, J.A. & Stemper, B.A. (1999). Tephrochronology of late Cenozoic loess at Fairbanks, central Alaska. *Geological Society of America Bulletin,* **111**.1, 71–90.

Prescott, J.R. & Hutton, J.T. (1994). Cosmic ray contributions to dose rates for luminescence and ESR dating: large depths and long-term variations. *Radiation Measurements*, **23**, 497-500.

Prodi, F. & Fea, G. (1979). A case of transport and deposition of Saharan dust over the Italian peninsula and southern Europe. *Journal of Geophysical Research*, **84**, 6951-6960.

Price, J.R. & Vebel, M.A. (2003). Chemical weathering indices applied to weathering profiles developed on heterogeneous felsic metamorphic rocks. *Chemical Geology,* **202**.3, 397-416.

Puchelt, H. (1972). *In* "Handbook of Geochemistry" (Wedepohl, K.H., Ed.), pp. 56B1–56O2. Springer, Berlin.

Pye, K. (1983). Grain surface textures and carbonate content of Late Pleistocene loess from West Germany and Poland. *Journal of Sedimentary Petrology*, **53**.3, 973-980.

Pye, K. (1984). Loess. *Progress in Physical Geography*. **8**, 176-217.

Pye, K. (1987). *Aeolian Dust and Dust Deposition*. Academic Press Inc., London.

Pye, K. (1992). Aeolian dust transport and deposition over Crete and adjacent parts of the Mediterranean Sea. *Earth Surface Processes and Landforms*, **17**(3), 271-288.

Pye, K. (1995). The nature, origin and accumulation of loess. *Quaternary Science Reviews* **14**, 653-667.

Radke, L. F., Hobbs, P. V. & Eltgroth, W. M. (1980). Scavenging of aerosol particles by precipitation. *Journal of Applied Meteorology*, **19**, 715-722.

Ramsay, J.G. (1963). Stratigraphy, structure and metamorphism of the western Alps: *Proceedings of the Geological Association*, **74**, 357-391.

Ramsey, M.H., Potts, P.J., Webb, P.C., Watkins, P., Watson, J.S. & Coles, B.J. (1995). An objective assessment of analytical method precision: comparison of ICP-AES and XRF for the analysis of silicate rocks. *Chemical Geology*, **124**, 1-19.

Rasmussen, T.L., Oppo, D.W., Thomsen, E. & Lehman, S.J. (2003). Deep sea records from the southeast Labrador Sea: Ocean circulation changes and ice-rafting events during the last 160,000 years. *Palaeogeography*, **18**, 1-15.

Raymo, M.E (1991). Geochemical evidence supporting T.C. Chamberlain's theory of glaciation. *Geology*, **19**, 344-347.

Raymo, M.E. & Ruddiman, W.F. (1992). Tectonic forcing of late Cenozoic climate, *Nature* **359**, 117–122.

Raymo, M.E., Ruddiman, W.F. & Frolich, P.N. (1988): Influence of late Cainozoic mountain building on ocean geochemical cycles. *Geology*, **16**, 649-653.

Reichart, G.J., Lourens, L.J. & Zachariasse, W.J. (1998). Temporal variability in the northern Arabian Sea Oxygen Minimum Zone (OMZ) during the last 225,000 years. *Palaoceanography*, **13**, 607-621.

Remy, H. & Paas, W. (1959). Die Löß-profil von Koblenz-Metternich und Moselweiß. *Fortschritte Geologie von Reinland und Westfalen*, **4**, 331-336.

Retellack, G.J. (1990). *Soils of the past. An introduction to Paleopedology*. Unwyn-Hyman, London,

Rial, J.A. , Pielke Sr. R.A., Beniston, M., Claussen, M., Canadell, J., Cox, P., Held, H., de Noblet-Ducudre, N., Prinn, R., Reynolds, J & Salas, J.D. (2004). Nonlinearities, Feedbacks and Critical Thresholds Within the Earth's Climate System. *Climatic Change*, **65.1-2**, p11-38.

Richtofen, von, F. (1882). On the mode of origin of the loess. *Geological Magazine*, **9.2**, 293-305.

Ridgewell, A J., Watson, A.J. & Raymo, M.E. (1999). Is the spectral signature of the 100 kyr glacial cycle consistent with a Milankovitch origin? *Palaeoceanography*, **14.4**, 437-440.

Ritter, J.R.R., Jordan, M., Christensen, U.R., & Achauer, U. (2001). A mantle plume below the Eifel volcanic fields, Germany. *Earth and Planetary Science Letters*, **186**, 7-14.

Roberts, H.M., Muhs, D.R., Wintle, A.G., Duller, G.A.T. & Bettis, E.A. (2003). Unprecedented last-glacial mass accumulation rates determined by luminescence dating of loess from western Nebraska. *Quaternary Research*, **59**, 411–419.

Roberts, H.M., Wintle, A.G., Maher, B.A. & Hu, M. (2001). Holocene sediment-accumulation rates in the western Loess Plateau, China, and a 2500-year record of agricultural activity, revealed by OSL dating. *The Holocene*, **11.4**, 477-483.

Rogers, J.R., Bennett, P.C. & Choi, W.J. (1998). Feldspars as a source of nutrients for microorganisms. *American Mineralogist*, **83**, 1532–1540.

Rohling, E.J., Hayes, A., De Rijk, S., Kroon, D., Zacharasse, W.J. & Eisma, D. (1988). Abrupt cold spells in the northwest Mediterranean. *Paleoceanography*, **13**, 316-322.

Rollinson, H. (1993). *Using Geochemical Data: Evaluation, Presentation, Interpretation.* Longman Scientific & Technical.

Röthlisberger, R., Bigler, M., Hutterli, M., Sommer, S., Stauffer, B., Junghans, H.G. & Wagenbach, D. (2000). Technique for continuous high-resolution analysis of trace substances in firn and ice cores. *Environmental Science and Technology*, **34**, 338-342.

Rousseau, D-D., Antoine, P., Hatté, C., Lang, A., Zöller, L., Fortugne, M., Ben Othman, D., Luck, J.M., Moine, O., Labonne, M., Bentaleb, I & Jolly, D. (2002). Abrupt millennial climatic changes from Nussloch (Germany) Upper Weichselian eolian records during the Last Glaciation. *Quaternary Science Reviews*, **21**, 1577-82.

Rousseau, D-D., Kukla, G., Zöller, L & Hradlilva, J. (1998). Early Weichselian dust storm layer at Achenheim in Alsace, France. *Boreas*, **27**, 200-207.

Rousseau, D-D. & Puisségur, A. (1990). A 350,000-year climatic record from the loess sequence of Achenheim, Alsace, France. *Boreas*, **19**, 200-208.

Ruddiman, W.F. (2005). How did humans first alter global climate? *Scientific American*, March, 46-53. Cited 3.4 2005, available at World Wide Web URL: <http://www.uta.edu/geology/Faculty%20Pages/balsam/Classes/SCIE%203303/Ruddiman%20Sci%20Am%202005.pdf>

Ruddiman, W.F. (2005). Cold climate during the closest Stage 11 analog to recent Millennia. *Quaternary Science Reviews*, **24**:10-11, 1111-1121.

Ruddiman, W.F. & Kutzbach, J.E. 1991. Plateau uplift and climatic change. *Scientific American*, **264**(3), 42-50.

Ruddiman' W.F., Raymo, M & McIntyre, A. (1986). Matuyama 41,000-year cycles: North Atlantic Ocean and northern hemisphere ice sheets. *Earth and Planetary Science Letters*, **80**:1-2, 117-129

Ruddiman, W.F., Vavrus, S.J. & Kutzbach, J.E. (2005). A test of the overdue-glaciation hypothesis. *Quaternary Science Reviews*, **24**:1-2, 1-10.

Ruhe, R.V. (1956). Geomorphic surfaces and the nature of soils. *Soil Science*, **115**, 183-193.

Ruth, U. (2002). Concentration and Size Distribution of Microparticles in the NGRIP Ice Core (Central Greenland) during the Last Glacial Period. Berichte zur Polar- und Meeresforschung, 428,146, Universität Bremen. Cited 20 September 2004, available at URL:
http://www.awi-bremerhaven.de/Publications/Rut2002a_abstract.html

Rutter, N.T., Ding, Z-L., & Liu, T-S. (1991) Comparison of isotope stages 1-61 with the Baoji-type pedostratigraphic section of north-central China. *Canadian Journal of Earth Sciences* **28,** 985-990.

Salm, C. van der, Köhlenderg, L & De Vries, W. (1998). Assessment of weathering rates in Dutch loess and river-clay soils at pH3.5, using laboratory experiments. *Geoderma*, **85,** 41-62.

Sánchez-Goñi, M.F, Turon, J-L., Eynaud, F., Shackleton, N.J. & Cayre, O. (2000). Direct land-sea correlation of the Eemian, and its comparison with the Holocene: a high-resolution palynological record off the Iberian margin. *Geologie et Mijnbouw/Netherlands Journal of Geosciences*, **79**(2/3), 345-354.

Sartori, M., Heller, F., Forster, T., Borkovec, M., Hammann, J. & Vincent, E. (1999). Magnetic properties of loess grain size fractions from the section at Paks (Hungary), *PEPI*, **116**, 53-64.

Sayago, J.M., Collantes, M.M., Karlson, A. & Sanabria, J. (2001). Genesis and distribution of the Late Pleistocene and Holocene loess of Argentina: a regional approximation. *Quaternary International*, **76/77**, 247-257.

Schutz, L., Jaenicke, L. Pictrek, H. (1981). Saharan dust transport over the North Atlantic Ocean. In: *Desert dust: origin, characteristics, and effects on man* (ed. Pewe, T.L.). Geological Society of America Special Paper 186, 87-100.

Severinghaus, J.P. & Brook, E. (1999). Abrupt climate change at the end of the last glacial period inferred from trapped air in polar ice. *Science*, **286**, 930-934.

Shackleton, N. J. (1967). Oxygen isotope analyses and Pleistocene temperatures re-assessed. *Nature*, **215**, 15-17.

Shackleton, N.J. (1969). The last interglacial in marine and terrestrial records. *Proceedings of the Royal Society*, **B174**, 135-154.

Shackleton, N.J., An, Z.S., Dodonove, A.E., Gavin, J., Kukla, G.J., Ranov, V.A., & Zhou, L.P. (1995). Accumulation rate of loess in Tjikistan and China: Relationship with global ice volume cycles. *Quaternary Proceedings*, **4**, 1–14.

Shackleton, N.J., Fairbanks, R.G., Chiu, T & Parrenin, F. (2004). Absolute calibration of the Greenland time scale: implications for Antarctic time scales and for $\delta^{14}C$. *Quaternary Science Reviews*, **23**, 1513-1522.

Shackleton, N.J. & Kennett, J.P. (1975). Palaeo-temperature history of the Cenozoic and the initiation of Antarctic glaciation: Oxygen and carbon isotope analysis in DSDP sites 277, 279 and 281. In: Kennet, J.P. *et al.* (eds.), (1975). *Initial Report of the Deep Sea Drilling Project*, **5**, US Govt. Print. Office, Washington D.C., pp. 743-755.

Shenggao, L. (2000). Lithological factors affecting magnetic susceptibility of subtropical soils, Zhejiang Province, China. *Catena*, **40**, 359-373.

Shi, C., Zhu, R., Glass, B.P., Liu, Q, Zerman, A & Suchy, V. (2003). Climate variations since the last interglacial recorded in Czech loess. Geophysical Research Letters, 30:11, 1562-66.

Siever, R. (1988). *Sand*, New York, pp. 225.

Sugiura, N. (1979). ARM, TRM and magnetic interactions: concentration dependence. *Earth Planet. Sci. Lett.*, **42**, 451–455.

Singer, M.J & Fine, P. (1989). Pedogenic factors affecting magnetic susceptibility of northern California soils. *Soil Science Society of America Journal*, **53**, 1119-1127.

Skogerboe, R.K. & Grant, C.L. (1970). Comments on the definition of the terms sensitivity and detection limit. *Spectroscopy Letters*, **3**, 215-220.

Smalley I .J. (1966). Formation of quartz sand. *Nature*, **211**, 476-479.

Smalley, I..J. (Ed.). (1975), *Loess; lithology and genesis*. Benchmark papers in Geology/26. Dowden, Hutchinson and Ross, Inc., Stroudsburg, Pa.

Smalley, I..J. (1990). Possible formation mechanisms for the modal coarse-silt quartz particles in loess deposits. *Quaternary International*, **7/8**, 23-27.

Smalley, I.J. (1995). Making the material: the formation of silt-sized primary mineral particles for loess deposits. *Quaternary Science Review*, **14**, 645-657.

Smalley, I..J. & Krinsley, D.H. (1978). Loess deposits associated with deserts. *Catena*, **5**, 53-66.

Smalley, I.J. & Leach, J.A. (1978). The origin and distribution of the loess in the Danube Basin and associated regions of east-central Europe—a review. *Sedimentary Geology* **21**, 1–26.

Smalley, I.J., Raj Kumar, K., O'Hara Dhand, K. & Jefferson, I.F. (2004). The formation of quartz silt for terrestrial sediments, particularly loess deposits. *International Workshop HWK, Delmenhorst, 15-18 April 2004*. Cited 29.7.2004, available at World Wide Web URL:
<http://www.pangaea.de/Projects/PASSED/Downloads/smalley_et_al.pdf>

Smith, J. (2001). Geochemical Investigation of Argentinean Loess: Implications for loess provenance and weathering histories. Thesis (unpubl.), Royal Holloway University of London.

Soffer O. & Gamble G. (1990). *The World at 18,000 BP*. Unwin Hyman, London.

Sperazza, M., Moore, J.N. & Hendrix, M.S. (2004). High-resolution particle size analysis of naturally occurring very fine-grained sediment through laser diffractometry. *Journal of Sedimentary Research*, **74.5**, 736-743.

Staverton, (2003), current local aviation meteorological data available at World Wide Web URL:
http://www.travel-island.com/cgi-bin/metar/metar.pl?icao=EGBJ

Steffenson, J.P. (1997). The size distribution of microparticles from selected segments of the Greenland ice core project core representing different climatic periods. *Journal of Geophysical Research*, **102**, 26755-26763.

Stirling, C.H., Lee, D-C., Christensen, J.N. & Halliday, A. N. (2000). High precision in-situ ^{238}U-^{238}U-^{230}Th isotopic analysis using laser ablation multiple collector ICPMS. *Geochimica et Cosmochimica Acta*, **64**, 3737-3750.

Stocker, T. F., Wright, D.G. & Mysak, L.A. (1992). A zonally averaged, coupled ocean–atmosphere model for paleoclimate studies. *J. Climate*, **5**, 773–797.

Stuiver, M. & Quay, P.D. (1980). Changes in atmospheric Carbon-14 contributed to a variable sun. *Science*, **207**, 11-19.

Sugiura, N. (1979). ARM, TRM and magnetic interactions: concentration dependence. *Earth and Planetary Science Letters*, **42**, 451-455.

Sun, D, Bloemendal, J., Rea, D.K., Vandenberghe, J., Jiang, F., An, Z & Su, R.. (2002). Grain-size distribution function of polymodal sediments in hydraulic and aeolian environments and numerical partitioning of the sedimentary components. *Sedimentary Geology*, **152**, 263-277.

Sun, J. (2002). Provenance of loess material and formation of loess deposits on the Chinese Loess Plateau. *Earth Planetary Science Letters*, **203**, 845-849.

Svensson, A., Biscaye, P.E. & Grousset, F.E. (2000). Characterization of late glacial continental dust in the Greenland Ice Core Project ice core. *Journal of Geophysical Research*, **105**:D4, 4637-4656.

Swineford, A & Frye, J.C. (1955). Petrographic comparison of some loess samples from western Europe with Kansas loess. *Journal of Sedimentary Research*, **25**.1, 3-23

Tang, Y., Jia, J. & Xie, X., (2003). Records of magnetic properties in Quaternary loess and its palaeoclimatic significance, a brief review. *Quaternary International*, **108**, 33-50.

Tauxe, L., Bertram, H.N. & Seberino, C. (2002). Physical interpretation of hysteresis loops: Micromagnetic modeling of fine particle magnetite. *Geochemistry, Geophysics, Geosystems: an electronic journal of the Earth Sciences*. 3:10. Cited 7.12.2004, available at World Wide Web URL:
< http://magician.ucsd.edu/~ltauxe/CV/pdfs/tauxe02.pdf>

Tauxe, L, Herbert, T., Shackleton, N.J. & Kok, Y.S. (1996). Astronomical calibration of the Matuyama–Brunhes boundary: Consequences for magnetic remanence acquisition in marine carbonates and the Asian loess sequences. *Earth and Planetary Science Letters* **140**, 133–146.

Taylor, S.R. & McLennan, S.M. (1985). The continental crust; its composition and evolution. *Blackwell, Oxford. 312.*

Taylor, S.R., McLennan, S.M. & McCulloch, M.T., (1983). Geochemistry of loess, continental crustal composition and crustal model ages *Geochimica et Cosmochimica Acta*, **47**, 1897-1905.

Tedrow, J.C.F. (1977). *Soils of the Polar Landscapes*. Rutgers, the State University of New Jersey. 637 pp.

Terhorst, B., Appel, E. & Werner, A. (2001). Palaeopedology and magnetic susceptibility of a loess-palaeosol sequence in southwest Germany. *Quaternary International.* **76/77**, 321-240.

Teruggi, M.E. (1957). The nature and origin of Argentine loess. *Journal of Sedimentary Petrology*, **27**, 322-332.

Thompson, L. G. & Mosley-Thompson, E. (1981). Microparticle concentration variations linked with climatic change - evidence from polar ice cores. *Science* **212**(4496), 812-815.

Thompson, M. & Walsh, J.N. (1989). *A Handbook of Inductively Coupled Plasma Spectrometry*. Blackie: London, U.K.

Thompson, R. & Oldfield, F. (1986). *Environmental Magnetism*, Allen and Unwin, London.

Toms, P.S., King, M., Zárate, M.A., Kemp, R.A. & Foit, F.F. Jr. (2004). Geochemical characterisation, correlation and optical dating of tephra in alluvial sequences of central western Argentina. *Quaternary Research*, **62**, 60-75.

Totland, M., Jarvis, I & Jarvis, K.E. (1992). An assessment of dissolution techniques for the analysis of geological samples by plasma spectrometry. *Chemical Geology*, **95**, 35-62.

Tsoar, H. & Pye, K. (1987). Dust transport and the question of desert loess formation. *Sedimentology*, **34**, 139-153.

Van Andel, T.H. & Tzedakis, P.C. (1996). Palaeolithic landscapes of Europe and environs, 150,000 - 25,000 years ago. *Quaternary Science Reviews* **15**, 481-500.

Van den Haute, P., Vancraeynest, L. & de Corte, F. (1998). The Late Pleistocene loess deposits and palaeosols of eastern Belgium: new TL age determinations. *Journal of Quaternary Science*, **13**.5, 487-497.

Van der Vlerk, I.M. & Florschütz, F. (1950). *Nederland in het IJstijdvak.* De Haan, Utrecht: 289 pp.

Van Kolfschoten, T. & Gibbard, P.L. (2000). The Eemian – local sequences, global perspectives: Introduction. *Geologie en Mijnbouw/Netherlands Journal of Geosciences*, **79** (2/3): 129-133.

Van Velzen, A.J. & Dekkers, M.J. (1999). Low-temperature oxidation of magnetite in loess-palaeosol sequences: a correlation of rock magnetic parameters. *Studia Geophysica et Geodetica*, **43**, 357-374.

Van Vliet, B. (1975). *Bijdrage tot de paleopedolgie van boven Pleistoceen, voornamelijk in het bekken van de Haine.* [trans: A contribution to the palaeopedology of the upper Pleistocene, mainly in the Haine Basin]. Doctoral Thesis, unpublished. Rijksuniversiteit Gent.

Van Vliet-Lanoë, B. (1989). Dynamics and extent of the Weichselian permafrost in western Europe (Stages 5e to 1). *Quaternary International*, **3-4**, 109-114.

Van Vliet-Lanoë, B. (1990). The genesis and age of the argillic horizon in Weichselian loess of northwestern Europe. *Quaternary International* **5**, 49-56.

Van Vliet-Lanoë, B. (1992). La niveau à langues de Kesselt: horizon repère de la stratigraphie du Weichsélien supérieur europeén: signification paléo-enviromentale et paléo-climatique. *Memoires Societé Géologique de France*, **160**, 35-55.

Van Vliet-Lanoe B. (1998). Frost and soils: implications for paleosols, paleoclimates and stratigraphy. *Catena*, **34**, 157-183.

Vandenberghe, J., An, Zhisheng, Nugteren, G., Lu, H and van Huissteden, J. (1997). New absolute time scale for the Quaternary climate in the Chinese loess region by grain-size analysis. *Geology*, **25**.1, 35-38.

Vandenberghe, J., Huijzer, A.S., Mücher, H, & Laan, W. (1998). Short climatic oscillations in a western European loess sequence (Kesselt, Belgium). *Journal of Quaternary Science*, **13**, 471-485.

Vandenberghe, J., Mommersteeg, H. & Edelman, D. (1993). Lithogenesis and geomorphological processes of the Pleistocene deposits at Belvédère. *Mededelingen-Rijks Geologische Dienst*, **47**, 7-14.

Velbel M.A. (1985). Geochemical mass balances and weathering rates in forested watersheds of the southern Blue Ridge. *American Journal of Science*, **285**, 904–930

Velichko, A.A. (1990). Loess-paleosol formation on the Russian Plain. *Quaternary International* **7/8**, 103–114.

Verosub, K.L., Fine, P., Singer, M.J. & TenPas, J. (1993). Pedogenesis and paleoclimate: interpretation of the magnetic susceptibility record of Chinese loess-paleosol sequences. *Geology*, **21**.11, 1011–1014.

Verosub, K.L. & Roberts, A. (1995). Environmental magnetism: past, present and future. *Journal of Geophysical Research B: Solid Earth*, **100**(B2), 2175-2192.

Vidal, L., Schneider, R.R., Marchal, O., Bickert, T., Stocker, T.F. & Wefer, G. (1999). Link between the North and South Atlantic during the Heinrich events of the last glacial period. *Climate Dynamics*, **15**, 909-919.

Vidic, N.J. & Verosub, K.L. (1999). Magnetic properties of soils of the Ljubljana Basin chronosequence, Slovenia. *Chinese Science Bulletin*, **44** (Suppl 1), 75-80.

Virlet D'Aoust, P.T. (1857). Observations sur un terrain d'origine meteorique ou de transport aerien qui existe au Mexique et sur le phenomene des trombes de poussiere auquelil doit principalement son origine [trans: Observations on a land surface of meteoric or aerial transport origin in Mexico and on the phenomenon of the dust formations to which it mainly owes its origin]. *Geol. Soc. France*, Full. 2d, Ser. 2, 129–139.

Von Leonhard, K.C. (1823/24). Charakteristik der Felsarten. Vol. 3. J. Engelmann Verlag, Heidelberg.

Walsh, J.N., (1992). Use of multiple internal standards for high-precision, routine analysis of geological samples by inductively-coupled plasma atomic emission spectrometry. *Chemical Geology*, **95**, 113-121.

Watkins, P.J. & Nolan, J. (1992). Determination of rare-earth elements, yttrium, scandium and hafnium using cation-exchange separation and inductively-coupled plasma - atomic emission spectrometry. *Chem. Geol.*, **95**, 131-139.

Welch, J.E. & Hale, I.M. (1987). Pleistocene loess in Kansas – status, present problems and future considerations. *In*: Johnson, W.C. (ed.). *Quaternary environments of Kansas: Kansas Geological Survey Guidebook*, Series 3, 67-84.

Welch, S.A. & McPhail, D.C. (2003). Mobility of major and trace elements during biologically-mediated weathering of granite. *In*: Roach, I.C. (ed.). *Advances in Regolith*, 437-440. Cooperative Research Centre for Landscape Environments and Mineral Exploration.

Weniger, G.C. (1990). *Germany at 18,000 BP.* Ch.9 p.172-178 in; Soffer O. & Gamble G. (1990) (q.v.).

Wentworth, C.K. (1922). A scale of grade and class terms for clastic sediments. *Journal of Geology*, **30**, 377-392.

West. R. (1978). *Quaternary Geology and Biology*, Cambridge University Press, Cambridge UK.

Westgate, J.A., Preece, S.J., Kotler, E & Hall, S. (2000). Dawson tephra: a prominent stratigraphic marker of Late Wisconsinan age in west-central Yukon, Canada. *Canadian Journal of Earth Science*, **37**(4), 621-627.

Westgate, A., Stemper, B.A. & Péwé, T.L. (1990). A 3 m.y. record of Pliocene–Pleistocene loess in interior Alaska. *Geology* **18**.9, 858–861.

Williams, E.L., Walter, L.M., Ku, T.C.W., Budai, J.M. & Kling, G.W. (2003). The weathering of silicate minerals in the glaciated mid-continent US: results from natural and experimental field studies. Geological Society of America, *Abstracts with Programs*, 35.6, 104.

Williams, M.A.J., Dunkerley, D.L., De Deckker, P., Kershaw, A.P. & Stokes, T.J. (1993). *Quaternary Environments*. Routledge, Chapman and Hall, Inc., New York, NY.

Wilson, M.J. (2004). Weathering of the primary rock-forming minerals: processes, products and rates. *Clay Minerals*, **39**, 233-266.

Wintle, A.G. (1973). Anomalous fading of thermoluminescence in mineral samples. *Nature*, **245**, 143-144.

Wintle, A.G. (1981). Thermoluminescence dating of Late Devensian loesses in southern England. *Nature*, **289**, 479-480.

Wintle, A.G. (1997). Luminescence dating: laboratory procedures and protocols. *Radiation Measurements*, **27**, 769-817.

Wintle A.G. & Catt J.A. (1985). Thermoluminescence dating of soils developed in Late Devensian loess at Pegwell Bay, Kent. *Journal of Soil Science* **36**, 293-298.

Wintle A.G. & Huntley, D.J. (1982). Thermoluminescence dating of sediments. *Quaternary Science Reviews*, **1**, 31-53.

Wolf-Welling, T.C.W., Thiede, J., Myhre, A.M. & Leg 151 Shipboard Scientific party. (1995). Bulk sediment parameter and coarse fraction analysis: Palaeoceanographic implications of Fram Strait sites 908 and 909, ODP leg 151 (NAAG), *EOS Transactions* **76**(17), supplement 166.

Woldstedt, P. (1950). *Norddeutschland und angrenzende Gebiete im Eiszeitalter.* Koechler, Stuttgart: 464 pp.

Worm, H-U., (1999). Time-dependent IRM: a new technique for magnetic granulometry. *Geophysical Research Letters*, **26**.16, 2557-2560.

Xiao, J.L.,An, Z.S., Liu, T.S., Inouchi, Y., Kumai, H., Yoshikawa, S. & Kondo, Y. (1999). East Asian monsoon variation during the last 130,000 years: Evidence from the Loess Plateau of central China and Lake Biwa of Japan, *Quaternary Science Reviews*, **18**, 147–157.

Xiao, J., Porter, S.C., An, Z., Kumai, H. & Yoshikawa, S. (1995). Grain size of quartz as an indicator of winter monsoon strength on the Loess Plateau of central China during the last 130,000 yr. *Quaternary Research*, **43**, 22-29.

Xie, Q., Chen, T., Xu, H., Xu, X, Chen, J, Ji, J. & Lu, H. (2004). Characteristics and genesis of maghemite in loess-palaeosol sequences of China. *Paper 108-13, 2004 Denver Annual meeting of the Geological Society of America*. Cited 2.12.2004, available at World Wide Web URL:

<http://gsa.confex.com/gsa/2004AM/finalprogram/abstract_77176.htm>

Yang, S.Y., Li, C.X., Yang, D.Y. & Li, X.S. (2004). Chemical weathering of the loess deposits in the lower Changjiang valley, China, and palaeoclimatic implications. *Quaternary International*, **117**, 27-34.

Yokoyama, Y., Lambeck, K., De Decker, P., Johnson, P & Fifield, L.K. (2000). Timing of the Last Glacial Maximum from observed sea-level minima. *Nature*, **406**, 713-716.

Zack, T., von Eynatten, H. & Kronz, A. (2004). Rutile geochemistry and its potential use in quantitative provenance studies. In press: *Sedimentary Geology*.

Zachos, J.C., Paganini, M., Sloan, L, Thomas, E & Billups, K. (2001). Trends, rhythms and aberrations in global climate 65 Ma to present. *Science*, **292**, 686-693.

Zárate, M.A. (2003). Loess of southern South America. *Quaternary Science Reviews*, **22**, 1987-2006.

Zender, C.S., Bian, H, & Newman, D. (2002). The mineral 'Dust Entrainment And Deposition' (DEAD) model: Description and 1990s dust climatology. *Journal of Geophysical Research*, **108** (D14), 4416-20.

Zhou, L-P., Oldfield, F., Wintle, A.G., Robinson, S & Wang, J.T. (1990). Partly pedogenic origin of magnetite variations in Chinese loess. *Nature*, **346**(6286), 737-739.

Zhu, R., Kazansky, A., Matasova, G., Guo, B., Zykina, V, Petrovsky, E. and Jordanova, N. (2000). Rock-magnetic investigation of Siberian loess and its implications. *Chinese Science Bulletin*, **45**, 2192-2197.

Zhu, R., Matasova, G., Kazansky, A., Zykina, V, and Sun, J.M. (2003). Rock magnetic record of the last glacial-interglacial cycle from the Kurchal loess section, southern Siberia. *Geophysical Research International*, **2**, 335-343.

Zimmerman, D.W. (1971). Thermoluminescence dating using fine grains from pottery. *Archeometry*, **13**, 29-52.